Las Vegas Carbon Source Apportionment Study

Final Report

December 28, 2004

PREPARED BY

Mark C. Green
M.-C. Oliver Chang
Judith C. Chow
Hampden Kuhns
L.-W. Antony Chen
Nicholas Nussbaum
Djordje Nikolic
Pat Arnott
Suresh Kumar NK
Vicken Etyemezian

Contact: oliver.chang@dri.edu
Desert Research Institute
755 East Flamingo Road
Las Vegas, NV 89119

Report Prepared for:

Dennis Ransel
Clark County Department of Air Quality Management
500 South Grand Central Parkway
P.O. Box 551741
Las Vegas, NV 89155-1741

Table of Contents

LIST OF TABLES

LIST OF FIGURES

1. INTRODUCTION

In 2002, Desert Research Institute (DRI) completed the Las Vegas Valley Visibility and $PM_{2.5}$ Study (Green et al., 2002). The major objectives of this study were to:

- Characterize the level of fine particulate matter ($PM_{2.5}$) and its chemical composition at urban, suburban, and background (transport) sites for the Las Vegas Valley.
- Determine background levels of $PM_{2.5}$ chemical components transported into the Las Vegas Valley.
- * Estimate chemical component contributions to haze (i.e., sulfate [$SO_4^{=}$], nitrate [NO_3^{-}], carbonaceous compounds, and crustal material).
- Estimate relative contributions of locally generated haze and transported haze.

The results showed that haze and $PM_{2.5}$ levels at the urban site (East Charleston) were much higher than the suburban (Palo Verde) and background (Jean) sites. This effect was most pronounced during winter stagnation conditions. The suburban site was influenced by local sources, but its levels of haze and $PM_{2.5}$ were closer to those of the background site than those of the urban site. At the urban site, haze and $PM_{2.5}$ were highest in winter; at the background site, haze and $PM_{2.5}$ tended to be lower in winter. Contributions to $PM_{2.5}$ by major chemical components at East Charleston by sampling day are shown in Figure 1-1. Note the predominance of carbonaceous compounds (organic compounds [OMC] and elemental carbon [EC]) and crustal (soil) material.

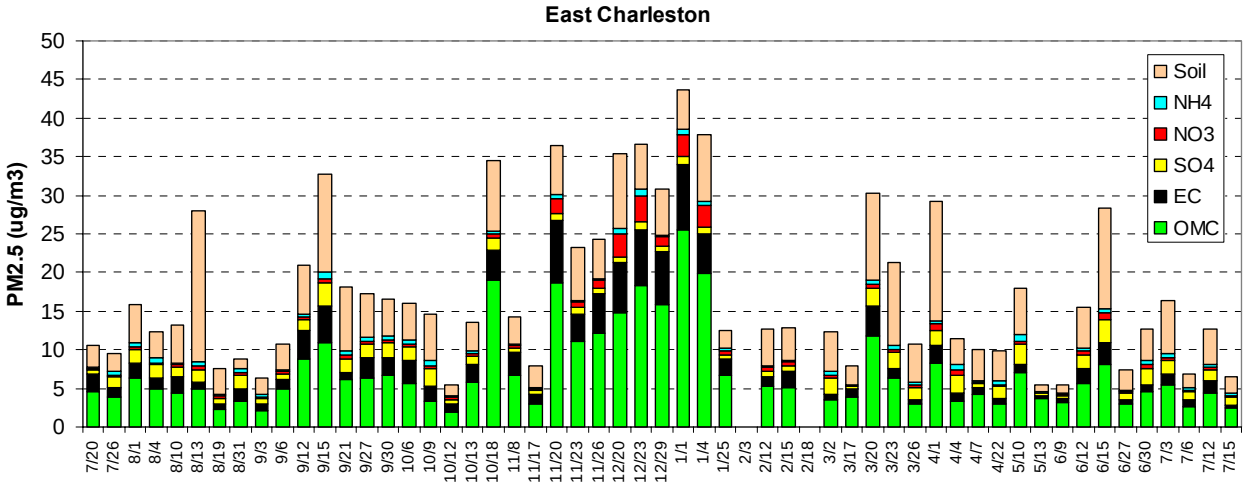

Figure 1-1. Chemical component contributions to $PM_{2.5}$ at the East Charleston site, July 2000 – July 2001.

Background sources outside the valley were estimated to contribute about two-thirds of the $PM_{2.5}$ and a little over one-half of the haze at the suburban Palo Verde site, on

average. At the urban East Charleston site, over three-quarters of the $PM_{2.5}$ and haze were caused by local (Las Vegas urban area) sources. The local and background contributions to haze at the east Charleston site are shown for each chemical component in Figure 1-2. The major components are OMC, EC, sulfates, nitrate, fine soil, and coarse mass (mainly crustal or dust). The fine soil and coarse mass components are mainly due to disturbed land, construction activity, and road dust.

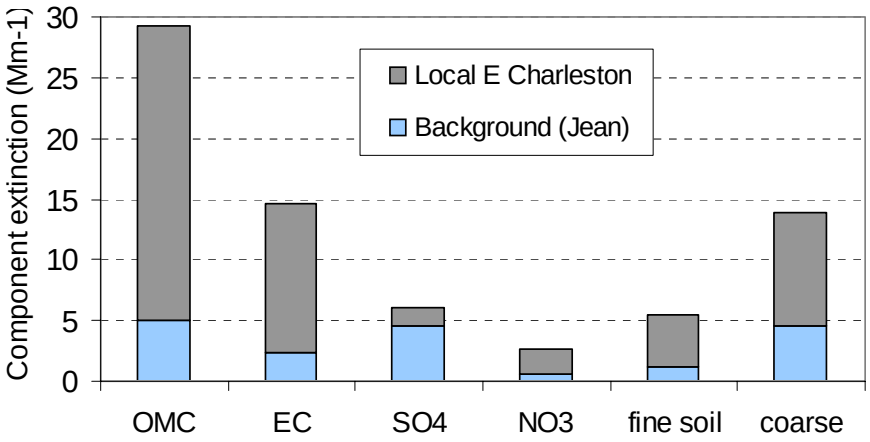

Figure 1-2. Local and background contributions to haze at East Charleston by chemical component.

Most of the increase in $PM_{2.5}$ and haze over the background level is due to particles containing organic carbon (OC), EC, and crustal material. At the East Charleston site, OC and EC compounds account for over half of the $PM_{2.5}$ mass and about 60% of the haze. Crustal material was estimated to contribute 25% of the $PM_{2.5}$ and 27% of the haze at East Charleston.

The Clark County Department of Air Quality Management (CCDAQM) funded this study to better understand source category contributions to carbonaceous compounds in the urban core. Based upon studies elsewhere, and general knowledge of sources and activity levels within the valley, the following source types are expected to be significant contributors to fine carbonaceous compounds and haze:

- Gasoline vehicles
- On-road diesel vehicles
- Non-road diesel engines (e.g., construction equipment)

Sources expected to be of lesser importance, but of some significance at certain times and locations, are:

- Wood burning (locally in winter, some forest fire smoke transported into the valley in summer)
- Meat cooking

A primary objective of the study is to determine the relative contributions of on-road and non-road diesel vehicles, and of gasoline vehicles, in order to help determine if control measures are needed and, if so, which types could be implemented to reduce haze.

The study includes:

- A collection of source profiles representing gasoline and diesel sources in the valley.
- A contrast of emission factors and compositions between warm and cool weather and between non-oxygenated and oxygenated gasoline.
- Summer and winter fuel-based emission factors of carbon monoxide (CO), nitric oxide (NO), nitrogen dioxide (NO_2), ammonia (NH_3), sulfur dioxide (SO_2), and total hydrocarbon (THC) for on-road gasoline and diesel vehicles.
- The collection and analysis of additional $PM_{2.5}$ samples at four sites in the urban core during 12 days in January 2003.
- High time-resolution measurements of OC and EC, light absorption, light scattering, CO, and NO2 at the East Charleston site.
- Organic speciation of particulate samples.
- Use of receptor modeling techniques to apportion carbon to gasoline vehicles, diesel vehicles, meat cooking, and wood smoke.
- Use of high time-resolution data and site-to-site variability in conjunction with receptor modeling results in a weight-of-evidence assessment.

Section 2 describes the measurement program for ambient sampling, source measurement technology, and principles and approaches for the Chemical Mass Balance (CMB) source apportionment model. Database and data validation are in Section 3. Section 4 discusses the data of 24-hour ambient samples and diurnal patterns of OC/EC, light absorption (b_{abs}), and light scattering at the East Charleston site. Section 5 presents the emission factors of emission sources of on-road gasoline vehicles, on-road diesel vehicles, and non-road diesel engines in the program. Section 6 discusses the source apportionment results based on ambient results and source profiles. Section 7, the conclusion of this study, suggests additional work, and references are found in Section 8. The Appendices contain source emission profiles obtained in this program and profiles from other studies used in the CMB source apportionment study.

2. AMBIENT MEASUREMENT NETWORK AND SOURCE CHARACTERIZATION

2.1 *Ambient Site Description*

A wintertime mini-intensive $PM_{2.5}$ speciation study was conducted at four locations: City Center (CC), J.D. Smith Elementary School (JD), Orr Middle School (OR), and East Charleston (MS). The locations of the sites are shown in Figure 2-1. Table 2-1 provides the street address and elevation of the sites and the pollutants monitored by the CCDAQM. The MS site is located about 50 meters (m) north of East Charleston Street, a secondary thoroughfare. Businesses along East Charleston include a Mexican restaurant, which is east of the site; apartment buildings and detached houses are north of the site. The CC site is in a residential area northeast of downtown Las Vegas, immediately northeast of the intersection of US-95 and I-15. It is also approximately 5 m below US-95, which is elevated in the area near the monitoring site (see Figure 2-2). A commercial area is located to the south, across I-515. The JD site is adjacent to J.D. Smith Elementary School, which is in a residential area. The OR site is on the property of Orr Middle School. The immediate vicinity is residential, although a large shopping center (The Boulevard Mall) is approximately 400 m to the west.

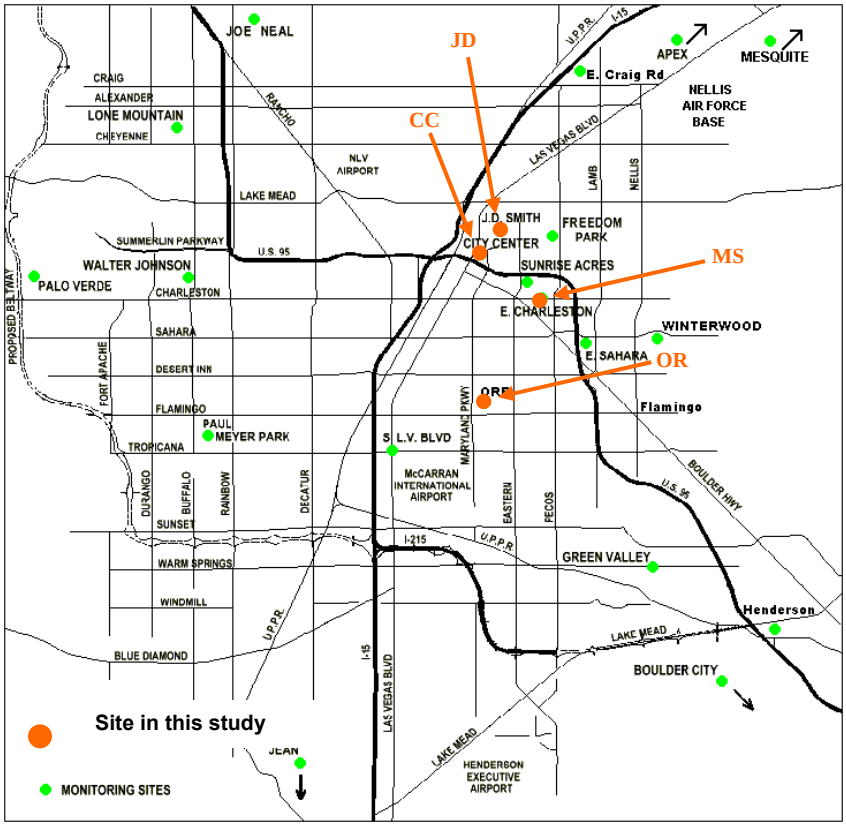

Figure 2-1. Ambient air monitoring locations during the winter mini-intensive study (not to scale). CC = City Center; JD = J.D. Smith Elementary School; OR = ORR Middle School; MS = East Charleston

Table 2-1. Descriptions of ambient monitoring sites in this study.

Site Name and Location	UTM Coordinates (Zone 11)	Elevation above Mean Sea Level (MSL)	Site Description
Orr Middle School (OR) 1562 E. Katie Ave. Las Vegas	36.120 N 155.130 W	597m	An urban/residential site in eastern Las Vegas. The site is located on the west side of Orr Middle School. North of the site is a community center park. The immediate vicinity is residential. A large shopping center (The Boulevard Mall) is located approximately 400 m to the west of the site.
J. D. Smith Elementary School (JD) 1301B E. Tonopah Ave. Las Vegas	36.191 N 115.123 W	570m	An urban/residential site in north-eastern Las Vegas. The site is adjacent to J.D. Smith Elementary School. The site is on a field covered with grass. The immediate vicinity is residential.
City Center (CC) 559 North 7th St. Las Vegas	36.174 N 115.136 W	619m	An urban/commercial site in northern Las Vegas. This site is approximately 100 m north of Freeway 515, which links Las Vegas to Southeastern Clark County (Henderson and Boulder City), and 100 m west of North Las Vegas Boulevard. The site is located on a gravel and dirt lot. The area is residential. The site is approximately 5 m below I-515, which is elevated in the area of the monitoring site, so an impact from vehicle emissions would be expected.
East Charleston (MS) 2801 E. Charleston Blvd., Las Vegas	36.159 N 115.110 W	567 m	An urban/commercial/residential site in eastern Las Vegas. The site is approximately 40 m north of East Charleston St., a moderately-to-heavily traveled thoroughfare, and adjacent to a Mexican fast-food restaurant to the east. The area is designated as being in non-attainment for carbon monoxide (CO), although exceedences have not been recorded recently. It is expected to have among the highest $PM_{2.5}$ levels in the Las Vegas Valley. About 15 m to the north of the Southern Nevada Air Quality Study (SNAQS) site is a Clark County Department of Air Quality Monitoring (CCDAQM) site.

Figure 2-2. View of City Center (CC) monitoring site with elevated US-95 visible in background.

At all four sites, two types of filter samplers were used: 1) a sampler to measure $PM_{2.5}$ mass and concentrations of elements, ions, and carbonaceous compounds; and 2) a sampler specifically designed for sampling and analysis of organic aerosols. Both samplers operated for 24-hour intervals and constituted the major data sources for source attribution (receptor modeling). Samples were collected during periods of light winds, stable conditions, and observed levels of haze. The schedule for filter samplers is shown in Table 2-2.

Table 2-2. The overall sample collection schedule for winter mini-intensive study, January 2003.

OR	JD	CC	MS
1/3/2003		1/3/2003	1/3/2003
1/4/2003	1/4/2003	1/4/2003	1/4/2003
1/5/2003	1/5/2003	1/5/2003	
1/12/2003	1/12/2003	1/12/2003	1/12/2003
1/13/2003	1/13/2003	1/13/2003	1/13/2003
1/14/2003	1/14/2003	1/14/2003	1/14/2003
1/20/2003	1/20/2003	1/20/2003	1/20/2003
1/21/2003	1/21/2003	1/21/2003	1/21/2003
1/22/2003	1/22/2003	1/22/2003	1/22/2003
1/23/2003	1/23/2003	1/23/2003	1/23/2003
1/24/2003	1/24/2003	1/24/2003	1/24/2003
1/25/2003	1/25/2003	1/25/2003	1/25/2003

Instruments for higher time resolution are listed in Table 2-3. At the MS site, additional instruments included:

- Aethalometers for EC
- Sunset Laboratory Carbon Aerosol Analysis Field Instrument with 90-minute time resolution for OC and EC particulate (PM) concentrations
- Photoacoustic instrument for light absorption, with data processed to 30-minute averages

Table 2-3. Air quality measurement acquired during the winter mini-intensive study.

	Orr Middle School (OR)	**J.D. Smith Elementary School (JD)**	**City Center (CC)**	**East Charleston (MS)**
$PM_{2.5}$ mass, chemistry [a]	DRI	DRI	DRI	DRI
Organic chemistry [a]	DRI	DRI	DRI	DRI
Aethalometer	n/a	DRI	DRI	DRI
Photoacoustic instrument	n/a	n/a	n/a	DRI
Near real-time Sunset carbon analyzer	n/a	n/a	n/a	DRI
Ozone (O_3)	n/a	CCDQMA	CCDQMA	n/a
Portable carbon dioxide (CO_2) analyzer	n/a	n/a	n/a	DRI
Carbon monoxide (CO)	CCDQMA	CCDQMA	CCDQMA	CCDQMA (nearby at Sunrise Acres)
PM_{10}	CCDQMA		CCDQMA	CCDQMA
$PM_{2.5}$			CCDQMA	CCDQMA
Met One Meteorological data	CCDQMA	CCDQMA	n/a	CCDQMA

[a] 24-hour-average (midnight to midnight) $PM_{2.5}$ measurements were acquired in January 2003 based on projected meteorological conditions of calm wind and stagnant air.
[b] 5-minute-average black carbon measurement was acquired with a Magee 7-wavelength aethalometer.

2.2 *Ambient Measurements*

2.2.1 Time integrated $PM_{2.5}$ mass and chemistry

2.2.1.1 Sequential gas sampler (SGS)

DRI sequential gas samplers (SGS), shown schematically in Figure 2-3, were used at the four study sites. Each SGS was equipped with a Sensidyne/Bendix 240 cyclone to sample $PM_{2.5}$ at a flow rate of 113 L/min. The SGS was configured to take two simultaneous samples (i.e., Teflon-membrane/citric acid impregnated cellulose fiber and quartz-fiber/sodium chloride impregnated cellulose fiber filter packs) at 20 L/min through each sampling port. The remaining 73 L/min required for the 113 L/min total inlet flow was drawn through a makeup air sampling port inside the plenum. A vacuum pump drew air through the paired filter packs when the valves were open. The flow rate was controlled by maintaining constant pressure across a valve with a differential pressure regulator.

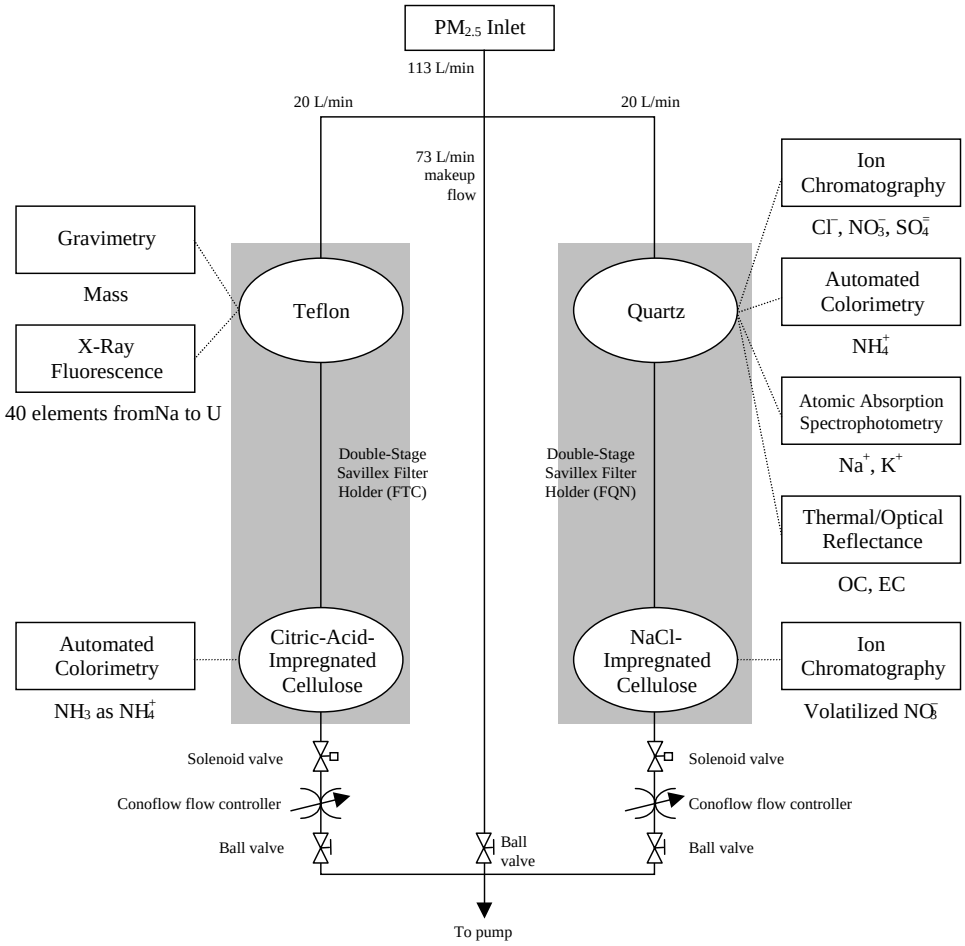

Figure 2-3. $PM_{2.5}$ sequential gas sampler (SGS) configuration for the study.

Twenty-four-hour (midnight to midnight) filter pack samples were acquired in January 2003, based on the projection of stagnant meteorological conditions, by SGS for $PM_{2.5}$ mass and chemistry at all four sites.

The filters were loaded into perfluoroalkoxy (PFA) Teflon filter holders at DRI's Environmental Analysis Facility (EAF) in Reno, NV. Each filter holder has a tapered extender section (called a receptacle) that mates to the sampler plenum by means of an O-ring and a retainer ring. As shown in Figure 2-3, the Teflon-membrane filter collected particles for mass analysis by gravimetry and elemental analysis (40 elements, including Na, Mg, Al, Si, P, S, Cl, K, Ca, Ti, V, Cr, Mn, Fe, Co, Ni, Cu, Zn, Ga, As, Se, Br, Rb, Sr, Y, Zr, Mo, Pd, Ag, Cd, In, Sn, Sb, Ba, La, Au, Hg, Tl, Pb, and U) by x-ray fluorescence (XRF) (Watson et al., 1999). The citric acid impregnated backup filter on a separate stage behind the Teflon-membrane filter was used to acquire volatilized organic PM. The deposit on the quartz-fiber filter was analyzed for chloride (Cl^-), NO_3^-, and $SO_4^=$ by ion chromatography; for ammonium (NH_4^+) by automated colorimetry; for water-soluble sodium (Na^+) and potassium (K^+) by atomic absorption spectrophotometry; and for OC and EC by thermal/optical reflectance (TOR) (Chow et al., 1993, 2001).

2.2.1.2 Semi-volatile organic compound (SVOC) sampler

SVOC samples were transferred through a Bendix Cyclone to remove particles larger than 2.5 µm prior to collection. The samples were collected using a filter followed by an adsorbent cartridge. The media used for collection of semi-volatile organic compounds (SVOCs) were as follows:

- Pallflex (Putnam, CT) T60A20 102-mm TIFG filters
- PUF (polyurethane foam) sheets, purchased from E.R. Carpenter Company Inc. (Richmond, CA) and cut into 2-inch diameter plugs
- XAD-4 resin (20-60 mesh) purchased from Aldrich Chemical Company, Inc. (Milwaukee, WI)

The flow through the sampler was set prior to sample collection by placing a calibrated rotameter on the inlet and setting the position of the needle valve to achieve the desired flow rate of 113 L/min. The samples were isotopically spiked, extracted in dichloromethane, and concentrated prior to analysis. Sample extracts were analyzed for the electron impact (EI) gas chromatography/mass spectrometry (GC/MS) technique using a Hewlett-Packard 5890 GC equipped with a model 7673A Automatic Sampler interfaced to a model 5970B Mass Selective Detector (MSD). To assist in the unique identification of individual compounds, selected samples were analyzed by combined gas chromatography/Fourier Transform Infrared/mass spectrometry (GC/IRD/MSD) techniques (i.e., using the Fourier transform infrared [FTIR] detector to aid mass spectrometric identification). Quantification of polycyclic aromatic hydrocarbons (PAHs) and other compounds of interest was obtained by multiple ion detection (MID).

2.2.2 Continuous measurements

2.2.2.1 Aethalometer

Magee Scientific 7-wavelength (350, 450, 571, 590, 660, 880, and 950 nm) aethalometers were used to measure light absorption (b_{abs}). The aethalometer measures changes in transmission of light through a paper tape onto which air is sampled. The calculated light absorption is then converted to a "black carbon" concentration by using a wavelength-dependent absorption coefficient (10 m^2/g at 550 nm). The aerosol is collected on an area of a fibrous filter at a moderate face velocity (Hansen, 1999). The aethalometers collected 5-minute continuous data. Each aethalometer was connected to an external pump at flow rates of 5.0 L/min. Each aethalometer stored measurement data on floppy disks and used the aethalometer's internal computer as a backup system for data collection. The resulting database was queried and sorted for light absorption computations and the results were placed into Excel for further analysis and control.

2.2.2.2 Photoacoustic instrument

The photoacoustic instrument is a fundamental measurement of b_{abs} for particles suspended in their natural environment. A photoacoustic instrument detects the absorption of a laser beam by aerosol placed in its acoustic resonator. The laser power is modulated at the acoustic resonant frequency of the resonator. Light-absorbing aerosol components (i.e., black carbon [BC]) convert laser beam power to an acoustic pressure wave through heating accompanied by gas expansion. The acoustic resonator amplifies this pressure wave by its quality (Q) factor. A microphone detects the acoustic signal, which provides a measure of light absorption (Arnott et al., 1999).

The photoacoustic principle is more than a century old, having been discovered by Alexander Graham Bell, but until recently it has been impractical to implement for the low levels in ambient air. Photoacoustic instruments have measured high concentrations in engine exhaust for more than two decades (Faxvog and Roessler, 1979 1982; Truex and Anderson, 1979; Killinger et al., 1980; Japar and Szkarlat, 1981a, 1981b; Japar et al., 1982, 1984; Roessler, 1982, 1984). The particle mass absorption efficiency is independent of particle size for particle diameters smaller than the wavelength of light (Killinger et al., 1980). Therefore, a measurement of b_{abs} can be translated into a BC or EC concentration with an appropriate mass absorption efficiency, independent of particle size. The large dynamic range of the photoacoustic instrument makes it suitable to measure b_{abs} over a wide range of EC concentrations in source and ambient samples (Moosmüller et al., 2001a, 2001b). In this study, the photoacoustic instrument was used to measure only b_{abs}, with absorption efficiencies for each measurement system achieved by the division of the photoacoustic b_{abs} by method-specific EC and BC mass concentrations.

2.2.2.3 Sunset Laboratory Carbon Aerosol Analysis Field Instrument

The Sunset Laboratory Carbon Aerosol Analysis Field Instrument is a semi-continuous instrument that provides time-resolved OC/EC analysis using the NIOSH Method 5040

thermal decomposition protocol. A quartz-fiber filter punch is mounted in the instrument, and samples are collected for the desired time period. Once the collection is complete, the oven is purged with helium (He). The oven temperature is increased stepwise to 870 °C, thermally desorbing organic compounds and pyrolysis products into a manganese dioxide (MnO_2) oxidizing oven. As the carbon fractions flow through the MnO_2 oven they are quantitatively converted to carbon dioxide (CO_2) gas. The CO_2 is swept out of the oxidizing oven in the He stream and measured directly by a self-contained non-dispersive infrared (NDIR) detector system. A second temperature ramp is initiated in the He/O_2 gas stream and any EC is oxidized off the filter and into the oxidizing oven. The EC is then detected in the same manner as the OC. A fixed volume loop is used to inject an external standard at the end of every analysis. This external standard data is incorporated into every data package and is used along with the known carbon concentration in the loop to calculate the analytical results.

The pyrolysis-induced error for EC is corrected by focusing a tuned diode laser through the sample chamber so that the laser passes through a mounted filter. Initial absorbance of the modulated laser is recorded. As the temperature ramp proceeds, a data system monitors the laser absorbance continuously. Any charring of the OC results in an increase in laser absorbance. After the initial temperature ramp, when the He is switched to a He/O_2 mixture, all the EC is oxidized off and the laser absorbance is reduced to the background level. When the resulting NDIR data are reviewed with an overlay of laser absorbance, the point in the second phase oxidizing ramp at which the laser absorbance equals the initial absorbance is the split point. Any EC detected before this point is said to have been formed pyrolytically by charring of the OC. This carbon is subtracted from EC observed during the oxidizing phase of the analysis and is assigned as OC. The primary assumption, for this correction, is that the particulate-bound EC and the pyrolytically formed EC have the same absorption efficiency.

2.3 *Source Emission Measurement*

The following section describes the site and study design for the three proposed carbon sources—1) on-road gasoline vehicles, 2) on-road diesel vehicles, and 3) non-road diesel engines—for which the DRI In-Plume Sampling System was deployed. These source samples were collected during the summer and winter due to different fuel standard requirements. The summer samples were collected during August 20-23, 2003, for on-road gasoline and diesel vehicles; the winter samples were collected during December 8-12, 2003, for all three source types.

2.3.1 Site description

2.3.1.1 Emissions of on-road gasoline vehicles

For on-road gasoline vehicle emissions, the In-Plume Sampling System was set up approximately 15 m southwest of the intersection of Flamingo Road and Swenson Road. The location is about 3 km east of the Las Vegas Strip and the traffic is dominated by local gasoline vehicles. Vehicles turned right or left from Flamingo Road to Swenson Road at speeds of 20–50 km/hr with slight acceleration. Average vehicle counts were 8–

12 vehicles per lane per minute. There was no observable difference in vehicle counts between rush hours (7–9 a.m. and 4–6 p.m.) and noon. Two to three samples were collected daily from 7 a.m. to 7 p.m.

2.3.1.2 Emissions of on-road diesel vehicles

The North Regional Transportation Commission (RTC) bus depot in Las Vegas is one of two parking and maintenance yards for public transportation buses serving Clark County. Approximately 250–280 buses return to the North RTC bus depot for overnight parking after the last service route at night and depart for their first service route in the morning. More than 85% of the buses leave the bus yard between 3:30 and 5:45 a.m. daily. Prior to leaving the bus yard, the drivers are handed documents to be signed off at the security gate. Thus, each bus decelerated, stopped, idled, and accelerated, the time for which ranged from 10 to 30 seconds. The DRI In-Plume Sampling System was set up at the security gate and the inlet was supported by a 3 m long PVC tube, as shown in Figure 2-4. The inlet of the sampling system was approximately 3–5 m away from the bus tailpipe, where the exhaust plume was fully mixed with ambient air. Each filter sampling period was approximately 30–45 minutes, depending on the frequency of bus traffic.

Figure 2-4. Sampling of on-road diesel vehicles at RTC bus depot, Las Vegas, NV.

2.3.1.3 Emissions of non-road diesel engines

Non-road diesel engine emission measurements were conducted on December 12, 2003, at Ahern Rentals, 1785 West Bonanza Road, Las Vegas, NV. Five samples were collected from 21 different types of non-road diesel engines. Details of the engine types, make, model number, and applications are listed in Table 2-4.

Each diesel engine was brought to the trailer where the DRI In-Plume Sampling System was located. The engines were operated from cold start to an rpm level that they would reach during typical use, as shown in Figure 2-5. For example, the forklift unit lifted an air compressor, as shown in Figure 2-5(a), which increased the engine load. The inlet of the in-plume system was approximately 1.5 m away from the exhaust pipes, where the exhaust was cooled and mixed with ambient air, yet were not too diluted (i.e., carbon dioxide [CO_2] was detectable). The sampling duration was based on the filter mass loading projected by the TSI DustTrak.

Table 2-4. List of non-road diesel engines used for emissions from non-road engines on December 12, 2003.

Type	Manufacture	Model Number	Application	Filter ID (hh:mm–hh:mm)
Backhoe Skiploader	CAT	416C	Digging/loading	VSFT/VSFQ023 (7:44 – 8:03 am)
Backhoe Skiploader	CASE	50L	Digging/loading	VSFT/VSFQ023 (7:44 – 8:03 am)
Backhoe Skiploader	DEERE	310E	Digging/loading	VSFT/VSFQ023 (7:44 – 8:03 am)
Bulldozer/Compactor	CAT	CP-323	Bulldozing/ Compacting	VSFT/VSFQ026 (08:14-08:41 am)
Ditch Witch	Trencher	3700	Trenching	VSFT/VSFQ026 (08:14-08:41 am)
Roller	CAT	n/a	Roller	VSFT/VSFQ026 (08:14-08:41 am)
Bobcat*	Ingersoll Rand	453	Digging/ loading	VSFT/VSFQ026 (08:14-08:41 am)
Scraper	Kubota	B2710	Leveling/ loading	VSFT/VSFQ026 (08:14-08:41 am)
Bobcat	Ingersoll Rand	763	Digging/loading	VSFT/VSFQ026 (08:14 – 08:41 am) / VSFT/VSFQ028 (08:50 – 09:15 am)
Compressor	I/R	185	Compressing air	VSFT/VSFQ028 (08:50 – 09:15 am)
Night Light	Allmard	6330	Generating lights	VSFT/VSFQ028 (08:50 – 09:15 am)
Arc Welder	Lincon	Classic III D (220A)	Welding	VSFT/VSFQ028 (08:50 – 09:15 am)
Generator	Denvo MQ Power	DGA7055JU(70 kW)	Power generating	VSFT/VSFQ028 (08:50 – 09:15 am)
Backhoe/ Skiploader	Kubota	BX22	Digging/loading	VSFT/VSFQ030 (09:24 – 10:05 am)
Road Grader / Ripper**	CAT	140H	Grading	VSFT/VSFQ030 (09:24 - 10:05 am)
Roller	Sakai	SW900	Rolling	VSFT/VSFQ030 (09:24 – 10:05 am)
Road Grader	CAT	14H	Grading	VSFT/VSFQ030 (09:24 – 10:05 am) / VSFT/VSFQ032 (10:17 – 10:55 am)
Backhoe	Hitachi	EX370	Digging	VSFT/VSFQ032 (10:17 – 10:55 am)
Compactor	Wacker Corp.	RT560	Compacting	VSFT/VSFQ032 (10:17 – 10:55 am)
Forklift	Terex	TH1056C	Lifting	VSFT/VSFQ032 (10:17 – 10:55 am)
Bobcat	ScatTrak	200D	Digging/loading	VSFT/VSFQ032 (10:17 – 10:55 am)

* Exhaust was collected on both VSTF/VSTQ026 and VSTF/VSTQ028
** Exhaust was collected on both VSTF/VSTQ030 and VSTF/VSTQ032
n/a: Not available

a)

b)

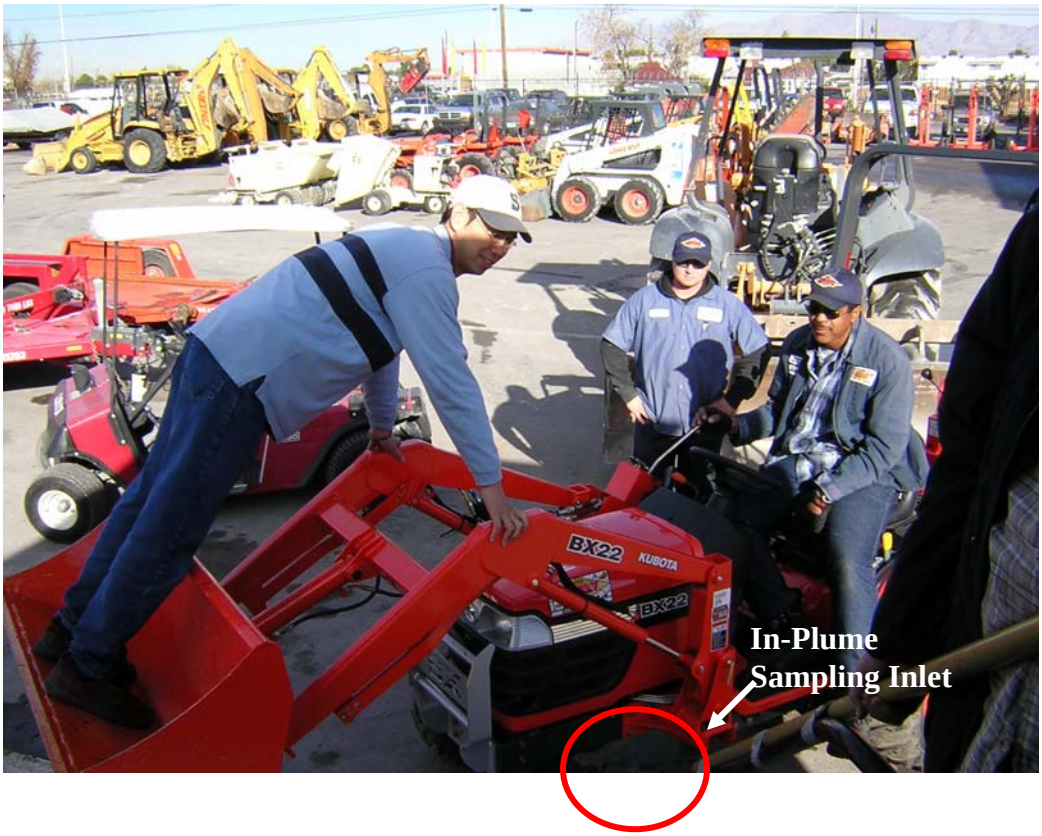

Figure 2-5. Non-road diesel engines mimic field operation by (a) lifting a power generator and (b) lifting a weight of 160 pounds. (Circle indicates sample collection point.)

2.3.2 Measurement technologies: DRI In-Plume Sampling System

The In-Plume Sampling System was developed at DRI to measure concentrations of gaseous and PM emissions from combustion sources. Using a carbon mass balance approach, fuel-based emission factors (in grams of pollutant per kg fuel burned) can be calculated from the simultaneous measurements of gases and particles provided by the system (Pokharel et al., 2002; Moosmüller et al., 2003). The sampling inlet is placed near a source plume cooled and diluted with ambient air. Since emissions of pollutants are referenced to the total carbon emitted (i.e., CO_2 + CO + HC), it is not necessary to capture the entire plume to obtain an emission factor. The In-Plume Sampling System has the following advantages: 1) the emission factors at specific conditions can be estimated in a short time if real-time measurements of pollutants are available in the system, and 2) emission factors for sources in the real world can be estimated with parameters that can affect source emissions. For example, emission factors for motor vehicle exhaust in the fleet can be estimated by deploying the system roadside to collect partial plumes from passing vehicles, which vary by year, make, model, type, and speed.

Figure 2-6 shows a schematic of the In-Plume Sampling System and Table 2-5 describes the instrumentation used. Gaseous emissions are measured with an FTIR spectrometer equipped with a ducted gas cell to permit fast response times (1.5 s) over a 10 m optical path. Particles are measured using a combination of real-time and integrated techniques including TSI DustTraks, an Electronic Low Pressure Impactor (ELPI), and filter-based sampling methods. The sampling system is field transportable. Instruments are mounted on two hand carts for easy offloading and positioning near the plume. The In-Plume system uses a time-integrated filter-based PM sampling system for chemical speciation. Teflon-coated Bendix 240 cyclones are used to remove particles greater than a specified aerodynamic diameter from the sample flow prior to $PM_{2.5}$ sample collection. $PM_{2.5}$ 50% cutpoints for the Bendix 240 cyclone were achieved by running the sample flows at 113 L/min. Sample flows, temperature, and gauge pressure behind each filter pack are monitored by TSI Series 4102 mass flow meters. These data are logged on a field computer. The operator can adjust the flow control valves over the sampling period to maintain the appropriate particle size cut for each filter.

The sampling system was configured to collect gas and particle measurements close to exhaust pipes for on-road gasoline vehicles. A cable protector designed to prevent vehicles from damaging extension cords across roads was fitted with a sampling line, and a 2.54 cm inlet hole was drilled in the middle of the cable protector to draw air into the sampling system from the center of the traffic lane. The inlet line was then connected to a plenum and redirected to numerous sampling instruments. Tests with this configuration indicated that CO_2 could be measured above background (>600 ppm) for vehicles traveling at speeds of less than 50 km/hr. Optimal sampling occurred when the plume was not dispersed over a long distance (i.e., slow vehicle speed).

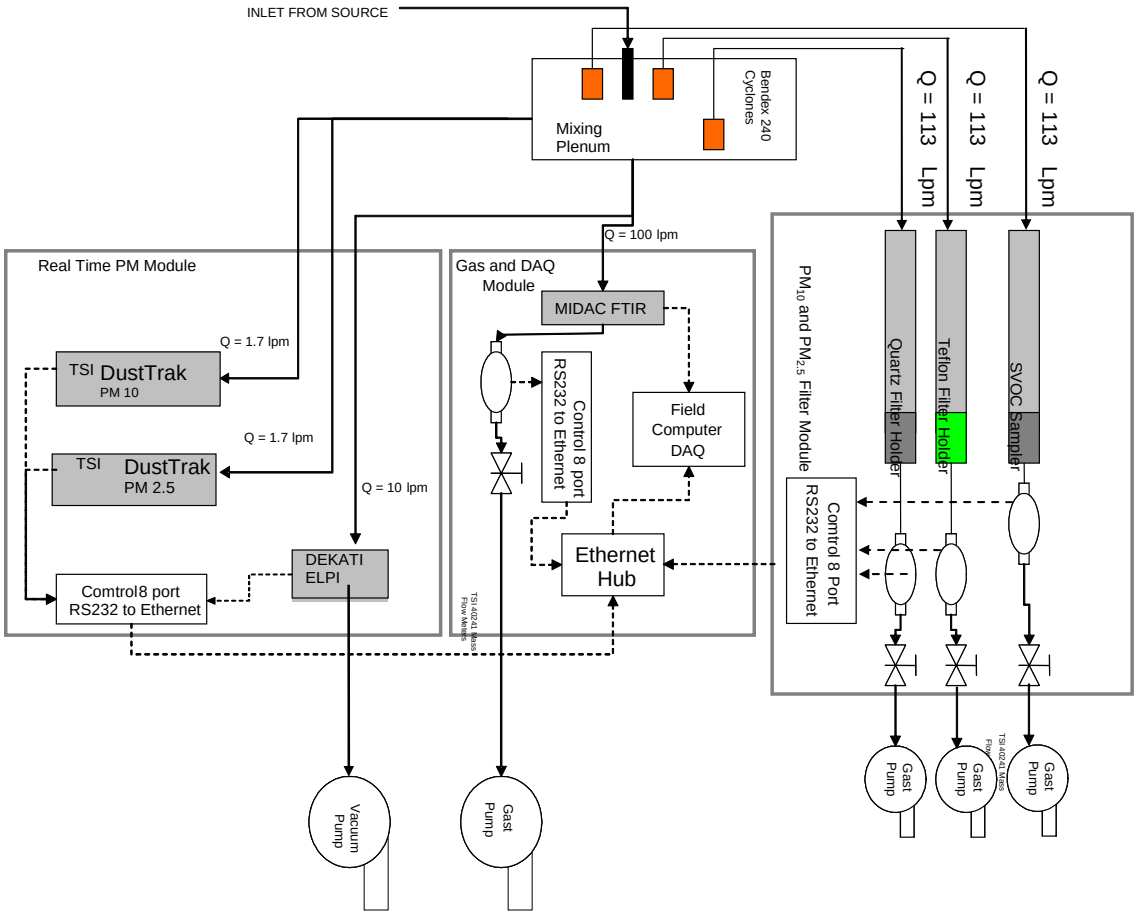

Figure 2-6. Schematic of DRI In-Plume Sampling System.

Table 2-5. Instrumentation of the DRI In-Plume Sampling System.

Instrument	Measurement	Method	Response Time (s)
Midac I-Series FTIR	Molecular gas species concentration	Dispersive IR	1.5
Dekati Electronic Low Pressure Impactor (10 lpm)	Aerodynamic number size distribution of particles	Current dissipation arising from deposition of charged particles to impactor substrates	5
TSI DustTrak	Particle mass	780 nm laser light scattering of particle stream at 90 degrees	1
PTFE/Quartz filter sampler	Mass and chemical composition of particles and gases	Collection and analysis of exposed filters	>1000
TSI 4043 Mass Flow Meters	Mass flow through filter	Hot wire anemometer	<1
SVOC sampler	Semi-volatize Organic Compounds in both particle and gas phases	Timing intervals of wheel strikes on road tubes across lane	>1000

2.3.3 Instrument Descriptions

2.3.3.1 Fourier Transform Infrared (FTIR) Spectrometer

A Midac FTIR spectrometer was used to measure infrared exhaust absorption spectra at a frequency of one scan per 1.5 s. The instrument uses a Michelson interferometer with a mercury-cadmium-tellurium (MCT) liquid nitrogen cooled detector. Measured species, wave number regions, calibration ranges, and typical concentrations are listed for 10 gases in Table 2-6.

Calibration spectra were created using U.S. Environmental Protection Agency (EPA) certified gases diluted with ultra-pure nitrogen using an Environics gas dilution system. A custom ducted gas cell with a 10 m folded optical path length was designed to facilitate rapid air changes in the 2 liter analytical volume. Typical flow rates through the gas cell are 100 L/min. The FTIR is referenced with ambient air in the field. As a result, gas concentrations are measured as the difference from the ambient air. For example, a typical vehicle pass over the road level inlet at 20 km/hr results in a 7 s CO_2 peak with an average concentration of 150 ppm above ambient air.

Table 2-6. Gases analyzed using classical least squares analysis of infrared spectra from FTIR.

Species	Reference Region (cm^{-1})		Average measured gaseous concentration (ppm) in In-Plume	Uncertainty Standard Error (ppm)	Calibration Range (ppm)	
	Lower υ_1	Lower υ_2				
CO_2	723.00	750.00	150	17	100	4730
CO	2133.31	2142.20	1.93	0.05	1.0	1005
NH_3	955.55	976.14	0.04	0.01	1.0	110
NO	1873.00	1878.50	0.12	0.13	0.2	20
	1880.60	1883.80				
	1898.60	1901.30				
	1926.00	1932.00				
	1934.60	1939.90				
H_2O	1200.00	1300.00	93	27	5.0	5294
C_4H_{10}	3041.30	2825.64	0.04	0.05	1.0	100
C_6H_{14}	3029.79	2817.96	0.06	0.04	0.2	200
C_2H_4	957.97	936.57	0.00	0.08	0.5	20
NO_2	1584.00	1588.70	0.00	0.11	0.2	20
	1597.50	1600.20				
	1604.30	1605.90				
	1610.60	1613.80				
SO_2	1112.50	1120.30	0.00	0.14	1.0	100
	1123.40	1134.00				
	1138.60	1148.10				
	1153.60	1164.00				
	1166.60	1172.50				
	1176.60	1185.10				
	1188.00	1197.20				
	1199.90	1209.00				
	1226.90	1235.70				

2.3.3.2 Electrical Low Pressure Impactor (ELPI)

The ELPI (Dekati Instruments, Finland) uses a unipolar corona charger to impart a positive charge to the measured aerosol. The particles then travel through a cascade impactor and are deposited on 1 of 12 substrates (0.030 µm to 9.6 µm) based on their aerodynamic diameter. The substrates are electrically isolated with Teflon supports and the accumulating charge on each of the substrates is measured by an array of electrometers. The measured current on each of the stages is proportional to the number of particles depositing on the stage. The ELPI measures the number concentration of particles based on their aerodynamic size at a frequency of 1 Hz.

Van Gulijk et al. (2001) investigated the performance of the ELPI through controlled tests on a diesel soot aerosol. Scanning electron microscopy (SEM) analysis of the impactor stages indicated that the fractal structure of the aerosol quickly formed mounds on the impactor substrates, resulting in a dynamic shift in the impactor cut sizes. Subsequent analyses (van Gulijk et al., 2003) found that the use of oiled sintered stages on the impactor extended the sampling capacity of the ELPI by more than a factor of 50 by wicking particles away from the impact area. For this study, the ELPI was operated using oiled sintered substrates followed by a filter stage.

The mass of particles collected on the filter stage is negligible (<0.01%) with respect to the larger stages. However, the abundance of these nanoparticles in the sample stream can cause a bias in the measurement of coarse particles. The corona charger imparts a positive charge to all particles passing through the impactor. While most particles deposit onto the substrates due to inertial forces, a fraction of the smallest particles diffuse to all impactor surfaces and deposit their charge. The charge deposited to the upper stages of the impactor by nanoparticles is substantially larger than the charge deposited by coarse aerosol particles. Marjamäki et al. (2002) developed an algorithm to use the number concentration of particles collected on the filter stage to estimate the diffusion of particles to the upper stages of the impactor. This algorithm was applied to all ELPI measurements to reduce the coarse particle artifact in the dataset.

Previous studies of tailpipe exhaust show that more than 90% of exhaust particles are less than 1 µm in size (Brown et al., 2000; Kleeman et al., 2000). In contrast, road dust emissions are predominantly associated with particles larger than 1 µm (Kuhns et al., 2001). Converting the number size distribution produced by the ELPI to a mass size distribution requires assumptions about the shape and density of particles depositing on each stage. In addition, measurements of diesel exhaust size distributions (assuming unit density particles) indicate that the coarse particle correction algorithm may not be entirely correct for nanoparticles that deposit a charge on the upper stages while passing through the filter stage. Shi et al. (2000) divided the mass of particles collected on a filter by the volume (assuming spherical particles) deposited on ELPI stages 1–8 (0.030 to 1.090 µm) to obtain a density for particles emitted from a diesel engine. Repeated measurements under different engine speeds and loads indicated that particle density ranged from 0.25 to 0.75 g/cm^3. In an earlier study, Kittelson et al. (1978) measured particle densities from a diesel engine between 0.8 g/cm^3 and 2.0 g/cm^3. Therefore, ELPI should be used as semi-quantitative method for PM.

2.3.3.3 DustTrak

The TSI DustTrak nephelometer measures particle scattering at a wavelength of 780 nm in a cone of scattering angles near 90 degrees. PM_{10} and $PM_{2.5}$ aerodynamic size cut inlets may be installed upstream of the analytical chamber to limit the size of measured aerosol particles. The DustTrak has a flow rate of 1.7 L/min and is calibrated using National Institute of Standards and Technology (NIST) Arizona Road Dust. The calibration material is lightly absorbing with a median diameter of approximately 2 µm. The instrument is most sensitive to non-absorbing particles with diameters on the same length scale as the light source (0.78 µm). The sensitivity is reduced for particles of other sizes. Exhaust particles have a DustTrak mass scattering efficiency similar to the calibration aerosol despite their difference in size and index of refraction. As a result, the DustTrak provides reasonable (within a factor of 2) measurements of aerosol mass for both exhaust and dust particles. In an evaluation of the DustTrak and other real-time instruments, Moosmüller et al. (2001) determined that the DustTrak provided a useful fast response measurement of particle concentration. Accurate real-time measurements of PM mass are possible if the DustTrak is calibrated with filter-based measurements.

2.3.3.4 Filter media and filter pack configuration

Lippman (1989), Lee and Ramamurthi (1993), Watson and Chow (1993, 1994), and Chow (1995) evaluated substrates for different sampling and analyses. The configurations of filter sampling used in the In-Plume Sampling System include: 1) polyolefin-ringed Teflon membranes (Gelman [Ann Arbor, MI], 2.0 µm pore size [#R2PJ047] for mass and elemental analysis) followed by a pre-fired quartz-fiber filter (Pallflex [#2500QAT-UP]) to quantify volatilized carbon; 2) a pre-fired quartz-fiber filter for soluble ions (Cl^-, NO_3^-, $SO_4^=$, and NH_4^+) and carbon analyses followed by a cellulose-fiber filter (Whatman 31ET) impregnated with citric acid to collect gaseous ammonia (NH_3).

Teflon-membrane filters are individually light-checked for the absence of holes and flaws. Teflon-membrane filters are placed in Petri dishes for equilibration in a controlled environment (temperature 21.5 ± 1.5 °C and relative humidity 35 ± 5%) for at least three weeks before gravimetric determination. Quartz-fiber filters are prefired at 900 °C for six hours and stored under refrigeration. Whatman cellulose-fiber filters are impregnated with citric acid and stored under refrigeration. Two filters out of each batch of 100 are analyzed to determine that elemental background levels are within 2 times the detection limits. If the limits are exceeded, the batch is rejected. Blank quartz-fiber filters are heated for at least three hours at 900 °C to remove organic artifacts. Two filters from each batch of 100 are acceptance tested for Cl^-, NO_3^-, $SO_4^=$, NH_4^+, OC, and EC, and NH_3. Levels cannot exceed 1 µg/filter or the batch is rejected. After acceptance testing, the filters are refrigerated in sealed bags until sampling.

2.3.3.5 $PM_{2.5}$ filter samplers and flowmeters

The exhaust sample stream was split after air was sampled through the inlet. One stream went to the real-time instrumentation (FTIR, ELPI, and TSI DustTraks) and the other

entered a filter sampling plenum. Air was drawn from the plenum through a parallel array of Bendix 240 cyclones. The sample air then passed through Nuclepore filter holders with 47 mm quartz-fiber and Teflon filters. The cyclones were operated at 113 L/Min to achieve 2.5 µm size cuts. Each filter was monitored at 1 Hz with a digital mass flow meter to facilitate accurate volume determination.

2.3.3.6 Data acquisition system

Data from the flow meters, FTIR, DustTraks, and ELPI were logged in real time through serial ports into Ethernet hubs on each cart. The hubs were each linked to an Ethernet switch and data was logged and displayed in real time using a portable computer. When operating multiple instruments, the use of real-time displays increases data recovery because the user can monitor the status of all instruments from a single location. The data acquisition system assigns a common time stamp to all measurements to ensure that 1 Hz data are synchronized.

2.4 *Source Apportionment Modeling*

The overall objectives of this study's components are: 1) to validate the application of the chemical mass balance (CMB) receptor model (Watson et al., 1990a; 1990b); 2) to apportion measured $PM_{2.5}$ primary emission source categories aerosol and secondary aerosols; and 3) to apportion measured carbonaceous compounds in $PM_{2.5}$ to primary emissions source categories. The data used for this modeling are the ambient chemical compositions and the chemical source profiles with their related uncertainty estimates. This is one of the most important analysis tasks associated with the Las Vegas Carbon Source Apportionment study. A more detailed explanation of the activities involved is given in the following sub-sections.

2.4.1 CMB Receptor Model for Source Apportionment

Receptor models use the chemical and physical characteristics of gases and particles measured at source and receptor to identify their sources and quantify their contributions. The characteristics used for these purposes must be such that: 1) they are present in different proportions in different source emissions; 2) the proportions remain relative, constant from each source type; and 3) changes in the proportions between source and receptors are negligible or can be accounted for.

CMB is the most widely used model in the United States, especially in the west. It has also gained acceptance and application throughout the world. The CMB consists of a least-squared solution to a set of linear equations which express each receptor concentration of a chemical species as a linear sum of products of source profile species and source contributions. The source profile species (i.e., the fractional amount of the species in the emissions from each source type) and the captor concentrations, each with realistic uncertainty estimates, serve as input data to the CMB model. The output consists of the contributions from each source to the total ambient aerosol mass as well as to individual chemical species concentrations. The model calculates values for contributions from each source and the uncertainties of those values. Input data uncertainties are used

both to weight the relative importance of the input data to the model solution and to estimate uncertainties of the source contributions.

CMB 8.0 software currently in use applies the same effective variance solution developed and tested in CMB 7.0 by Watson et al. (1984) because: 1) it calculates realistic uncertainties of source contributions from both the source and receptor uncertainties; and 2) chemical species measured more precisely in both source and receptor samples are given greater influence in the solution than are less precisely measured species. CMB 8.0 uses a Microsoft Windows-based interface and is more user friendly than CMB 7.0.

Watson (1979) observed that individual source with similar source profiles, such as different soils and road dusts, would yield unreliable strength estimates if used in the same CMB. Henry (1982, 1984) proposed a quantitative method of identifying this interference between similar source compositions, which is known as "collinearity." Henry's (1982) "singular value decomposition" defines an "estimable space in which resolvable sources should like." The source types that do not fall into this estimable space are collinear, or too similar to be resolved from a combination of one or more of the source types which do lie within the estimable space. Henry (1982, 1984) further proposed that linear combinations of source contributions resulting from collinear source compositions would be more representative of the summed contributions of these sources. Analytical measures of collinearity and Henry's (1994) linear combination method are available in the EPA/DRI Version 7.0 of the CMB model (Watson et al 1990a). CMB 8.0 makes the collinearity measures proposed by Henry (1992) more transparent to identify the degree of collinearity.

2.4.2 Applicability and Validation of CMB

The CMB modeling procedure requires: 1) identification of the contributing source types; 2) selection of chemical species to be included; 3) estimation of the fractions of each chemical species contained in each source type (i.e., the source compositions); 4) estimation of the uncertainties of both ambient concentrations and source compositions; and 5) solution of the CMB equations. These procedures are described in an application and validation protocol (Watson et al., 1991) and consist of seven steps: 1) determination of model applicability; 2) estimation of initial source contributions; 3) examination of model outputs and performance measures; 4) identification of deviations from model assumptions; 5) identification and correction of model input errors; 6) verification of the consistency and stability of source contribution estimates; and 7) evaluation of the results of the CMB analysis with respect to other $PM_{2.5}$ source assessment methods.

CMB receptor model source apportionment activities are shown in Figure 2-7(a-b) and include:

Test CMB Model Applicability. The requirements for CMB model applicability are as follows: 1) a sufficient number of receptor samples are taken with an accepted method to represent the different levels of $PM_{2.5}$ concentrations and the composition of the $PM_{2.5}$ in different locations; 2) samples are analyzed for chemical species which are also present in source emissions; 3) potential source contributors have been identified and chemically

characterized; and 4) the number of non-collinear source types is less than the number of measured species. The sampling and analysis described in other parts of this study have been specifically designed to obtain this type of receptor measurement needed as model inputs. Sufficient sampling locations, sampling durations, and sampling periods have been designed to characterize $PM_{2.5}$ in the study region.

Perform Initial Source Contribution Estimates. The winter ambient samples are submitted to rigorous CMB analyses to determine which source profiles best fit the data. These same samples are used as examples for sensitivity testing as described below. Profiles measured in Las Vegas Valley and those acquired from other source apportionment studies are applied to ambient measurements for comparisons of source contribution estimates. As a result of these initial source contribution estimates, the number of profiles used in the majority of CMB analyses is reduced to a manageable subset which can justifiably represent the contributions to receptor chemical concentrations. The initial CMB provides a framework for conducting individual CMBs on remaining samples at all sites. Each CMB source apportionment for all chemically speciated samples is calculated independently, with addition, deletion, or substitution of profiles after examination of the CMB performance measures as explained below.

Examine Model Outputs and Performance Measures. Watson et al. (1991) defined several performance measures which are examined with each CMB to eliminate many combinations of profiles from further consideration. There may be several profiles which attain the performance measure target values. When this is the case, it is necessary to group these individual sources into source types which are not specific to individual source. Evaluation of several different profile combinations are made for every $PM_{2.5}$ sample. Frequency distributions are created to show how often different profiles were used, the typical values of performance measures, and the absolute and relative uncertainty estimates for each source type.

Evaluate Deviations from Model Assumptions. The basic assumptions of the CMB model (Watson, 1979) are as follows: 1) compositions of source emissions are constant over the period of ambient and source sampling; 2) chemical species do not react with each other (i.e., they add linearly); 3) all sources with a potential for significantly contributing to the receptor have been identified and have had their emissions characterized; 4) the source compositions are linearly independent of each other; 5) the number of sources or source categories is less than or equal to the number of chemical species; and 6) measurement uncertainties are random, uncorrelated, and normally distributed. The effects of deviations from these assumptions should be evaluated as part of each receptor modeling study. Lowenthal et al. (1992) illustrated several of these tests, which are performed while making initial source contribution estimates. These tests include:

- Source profile sensitivity tests. Several different profiles representing different source types are applied, and the source apportionments derived from them are compared to evaluate sensitivity.
- Species sensitivity tests. Key marker species are added to and dropped from the CMB fit and the source contributions estimates will be compared. These tests demonstrate the robustness of the modeling system and the extent to which certain

source types depend on accurate source and receptor measurement of single marker species.

- Randomized uncertainty tests. Test data set are constructed by randomly modified measured data in proportion to their stated uncertainties. Averages and standard deviations of the source contributions derived from these data sets will be calculated and compared with the source contribution estimates from a single run to evaluate the error propagation characteristics of the CMB model in the circumstance.

Identification and Correction of Model Input Errors. CMB modeling has been found to be a useful data validation tool. It often identifies inconsistencies in chemical ratios and size fractions or between the sums of species and mass measurements. Discrepancies in performance measures, especially comparisons between calculated and measured concentrations, are investigated by consulting the field and laboratory logs. In certain cases, re-analysis of existing samples is recommended.

Verification of the Consistency and Stability of Source Contribution Estimates. Several of the activities described above examine consistency and stability in detail for several cases. Abbreviated versions of these tests are applied to every interactive CMB on every sample. An average of five different configurations of source profiles and ambient fitting species are usually examined for each CMB source apportionment. Notes are made of samples with significant inconsistencies and instabilities, and these are summarized to accompany the quantitative source apportionments.

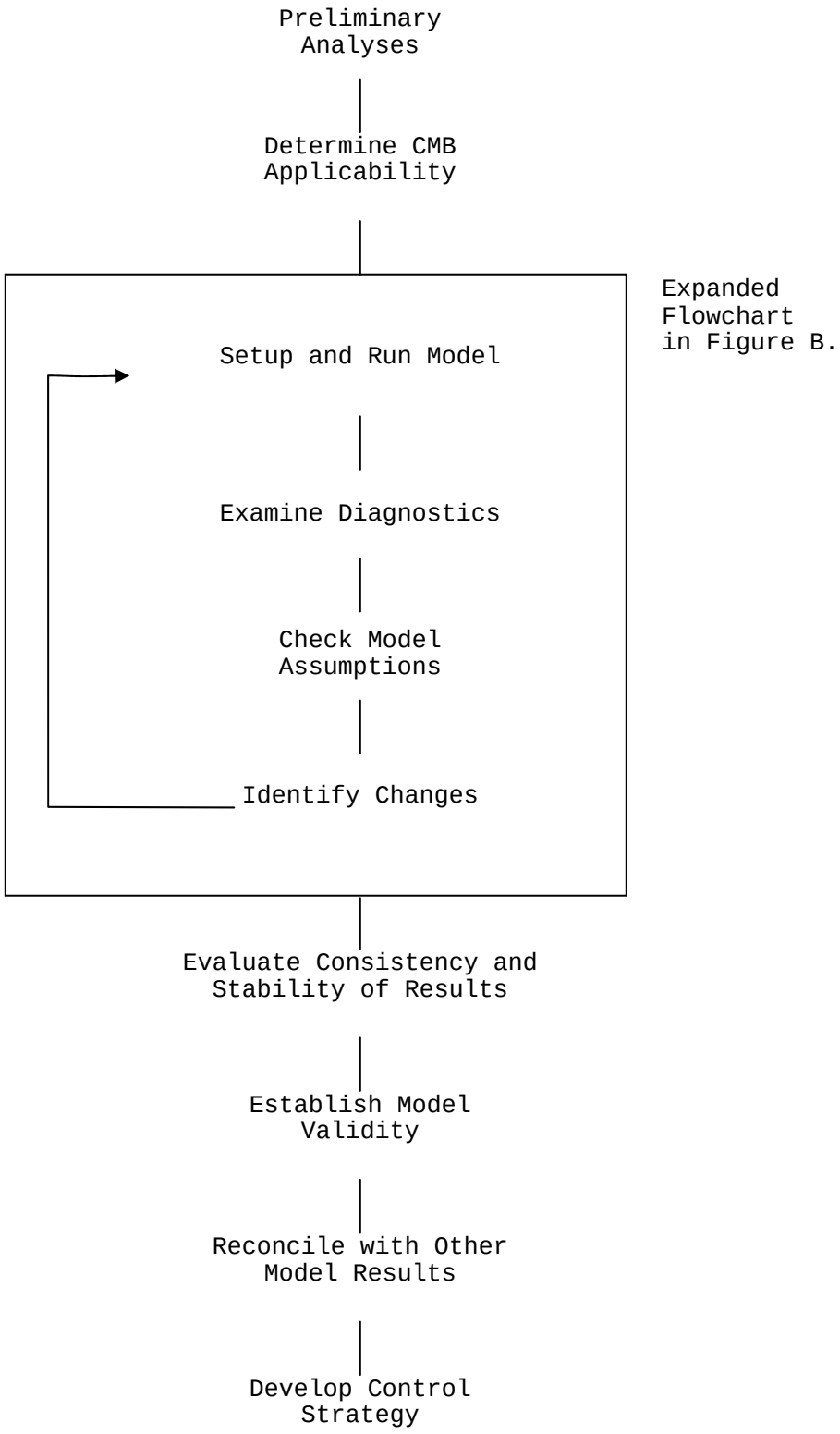

Figure 2-7(a). CMB application and validation flowchart.

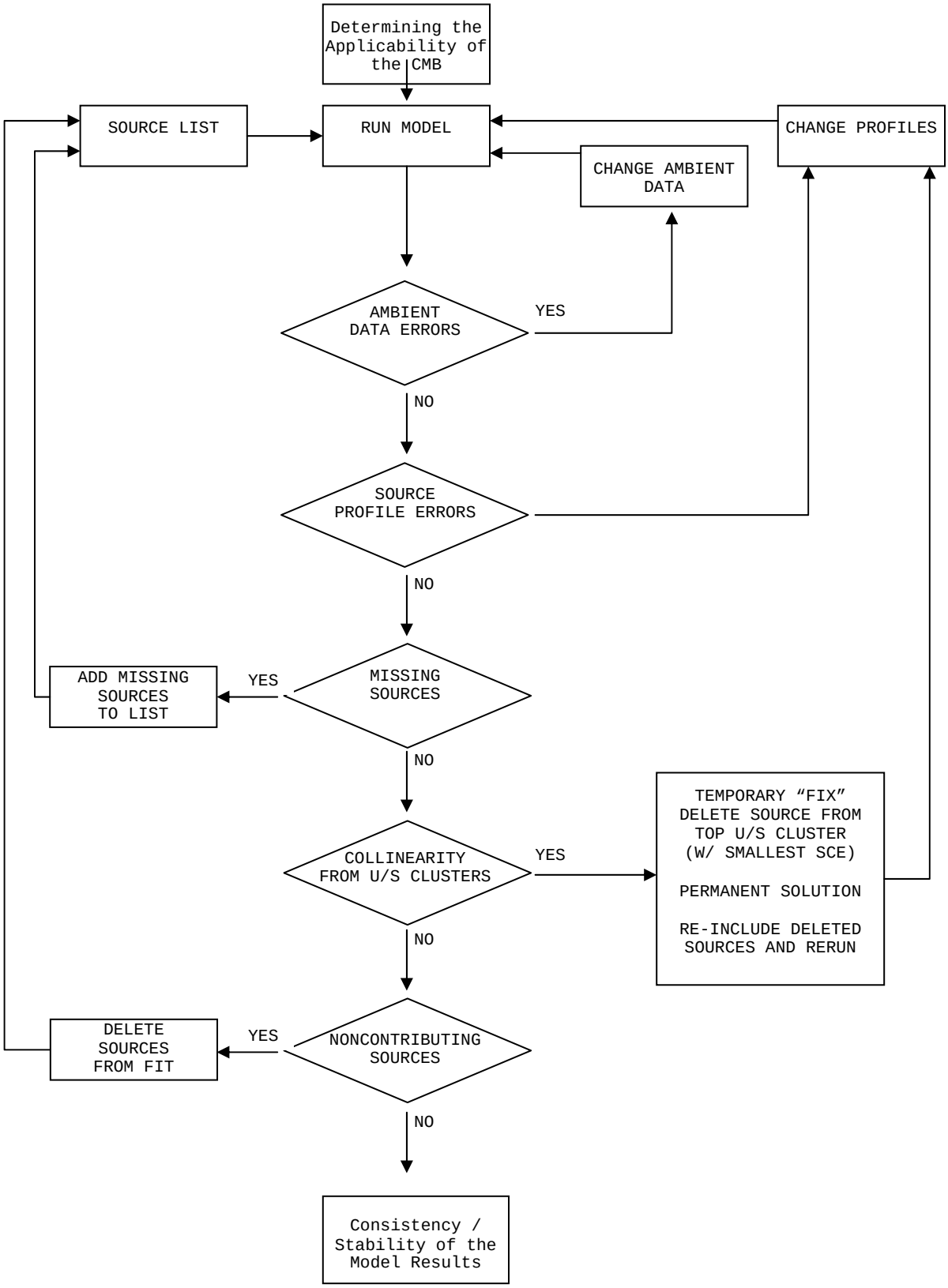

Figure 2-7(b). Flowchart for problem identification and correction.

2.4.3 Model data output and evaluation

The model provides three primary outputs. These are: 1) contribution estimates (to ambient concentrations) of the sources or source categories which are included in the fit (SCE); 2) the standard errors of these source contribution estimates (STDEER); and 3) the species concentrations calculated from the fit (CALC). These three statistics can be used to evaluate how well the model's calculated species concentrations "fit" or match the ambient measurements for these species. These are: 1) the percent of total mass explained by the fit (%MASS, target 100% ± 20%); 2) R-SQUARE (target 0.8 to 1); and 3) CHI-SQUARES (target 0.0 to 4.0). Generally, it is desirable to obtain a good "fit" of the data and obtain SCEs that have STDEER that are low, relative to the size of SCE.

3. DATABASE AND DATA VALIDATION

This section evaluates the precision, accuracy, and validity of Las Vegas Valley Carbon Apportionment (LASCA) aerosol measurements. Numerous air quality studies have been conducted over the past decade, but the data are often not available or applicable to data analysis and modeling because the databases lack documentation with regard to sampling and analysis methods, quality control/quality assurance procedures, accuracy specifications, precision calculations, and data validity. Lioy et al. (1980), Chow and Watson (1989), Watson and Chow (1992), and Chow and Watson (1994) summarize the requirements, limitations, and current availability of ambient and source databases in the United States. The LASCA data sets intend to meet these requirements. The data files for these studies have the following attributes:

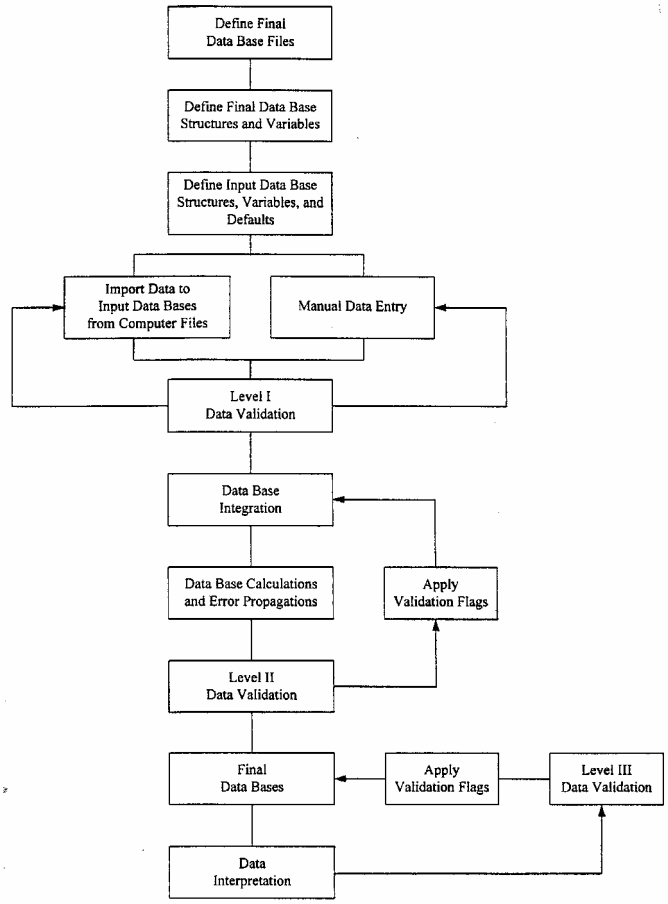

Figure 3-1. Flow diagram of the database management system.

- They contain the ambient observables needed to assess source and receptor relationships.
- They are available in a well-documented, computerized form accessible by personal computers and over the Internet.
- Measurement methods, locations, and schedules are documented.
- Precision and accuracy estimates are reported.
- Validation flags are assigned.

This section introduces the features, data structures, and contents of the LASCA data archive. The approach that was followed to obtain the final data files is illustrated in Figure 3-1. Detailed data processing and data validation procedures are documented in Section 3.2. These data are available on floppy diskettes in Microsoft Excel format for convenient distribution to data users. The file extension identifies the file type according to the following definitions:

- TXT = ASCII text file
- DOC = Microsoft Word document
- XLS = Microsoft Excel spreadsheet

The assembled aerosol database for filter pack measurements taken during LASCA is fully described by the file “LASCAFLDNAME.XLS” (see Table 3-1) which documents variable names, descriptions, and measurement units.

Table 3-1. Variable names, descriptions, and measurement units in the assembled aerosol database for filter pack measurements taken during the study.

Field Code	Description	Measurement Unit
SITE	Sampling site	
DATE	Sampling date	
SIZE	Sample particle size cut	µm
STRTHHMM	Sample start time	
STOPHHMM	Sample end time	
TID	Teflon filter pack ID	
QID	Quartz filter pack ID	
TFFLG	Teflon filter pack field flag	
QFFLG	Quartz filter pack field flag	
MSGF	Gravimetry analysis flag	
NHCF	Ammonia analysis flag	
HNIF	Volatilized nitrate analysis flag	
ANIF	Anion analysis flag	
N4CF	Ammonium analysis flag	
KPAF	Soluble potassium analysis flag	
OETF	Carbon analysis flag	
ELXF	XRF analysis flag	
TVOC	Teflon filter volume	m^3
TVOU	Teflon filter volume uncertainty	m^3
QVOC	Quartz filter volume	m^3
QVOU	Quartz filter volume uncertainty	m^3
MSGC	Mass concentration	$\mu g/m^3$
MSGU	Mass concentration uncertainty	$\mu g/m^3$
NHCC	NH3 concentration	$\mu g/m^3$
NHCU	NH3 concentration uncertainty	$\mu g/m^3$
HNIC	Volatilized nitrate concentration	$\mu g/m^3$
HNIU	Volatilized nitrate concentration uncertainty	$\mu g/m^3$
CLIC	Chloride concentration	$\mu g/m^3$
CLIU	Chloride concentration uncertainty	$\mu g/m^3$
N3IC	Nitrate concentration	$\mu g/m^3$
N3IU	Nitrate concentration uncertainty	$\mu g/m^3$
S4IC	Sulfate concentration	$\mu g/m^3$
S4IU	Sulfate concentration uncertainty	$\mu g/m^3$
N4CC	Ammonium concentration	$\mu g/m^3$
N4CU	Ammonium concentration uncertainty	$\mu g/m^3$
KPAC	Soluble Potassium concentration	$\mu g/m^3$
KPAU	Soluble Potassium concentration uncertainty	$\mu g/m^3$
OCTC	Organic Carbon concentration	$\mu g/m^3$
OCTU	Organic Carbon concentration uncertainty	$\mu g/m^3$
ECTC	Elemental Carbon concentration	$\mu g/m^3$
ECTU	Elemental Carbon concentration uncertainty	$\mu g/m^3$

Table 3-1. (continued)

Field Code	Description	Measurement Unit
TCTC	Total Carbon concentration	$\mu g/m^3$
TCTU	Total Carbon concentration uncertainty	$\mu g/m^3$
NAXC	Sodium concentration	$\mu g/m^3$
NAXU	Sodium concentration uncertainty	$\mu g/m^3$
MGXC	Magnesium concentration	$\mu g/m^3$
MGXU	Magnesium concentration uncertainty	$\mu g/m^3$
ALXC	Aluminum concentration	$\mu g/m^3$
ALXU	Aluminum concentration uncertainty	$\mu g/m^3$
SIXC	Silicon concentration	$\mu g/m^3$
SIXU	Silicon concentration uncertainty	$\mu g/m^3$
PHXC	Phosphorous concentration	$\mu g/m^3$
PHXU	Phosphorous concentration uncertainty	$\mu g/m^3$
SUXC	Sulfur concentration	$\mu g/m^3$
SUXU	Sulfur concentration uncertainty	$\mu g/m^3$
CLXC	Chlorine concentration	$\mu g/m^3$
CLXU	Chlorine concentration uncertainty	$\mu g/m^3$
KPXC	Potassium concentration	$\mu g/m^3$
KPXU	Potassium concentration uncertainty	$\mu g/m^3$
CAXC	Calcium concentration	$\mu g/m^3$
CAXU	Calcium concentration uncertainty	$\mu g/m^3$
TIXC	Titanium concentration	$\mu g/m^3$
TIXU	Titanium concentration uncertainty	$\mu g/m^3$
VAXC	Vanadium concentration	$\mu g/m^3$
VAXU	Vanadium concentration uncertainty	$\mu g/m^3$
CRXC	Chromium concentration	$\mu g/m^3$
CRXU	Chromium concentration uncertainty	$\mu g/m^3$
MNXC	Manganese concentration	$\mu g/m^3$
MNXU	Manganese concentration uncertainty	$\mu g/m^3$
FEXC	Iron concentration	$\mu g/m^3$
FEXU	Iron concentration uncertainty	$\mu g/m^3$
COXC	Cobalt concentration	$\mu g/m^3$
COXU	Cobalt concentration uncertainty	$\mu g/m^3$
NIXC	Nickel concentration	$\mu g/m^3$
NIXU	Nickel concentration uncertainty	$\mu g/m^3$
CUXC	Copper concentration	$\mu g/m^3$
CUXU	Copper concentration uncertainty	$\mu g/m^3$
ZNXC	Zinc concentration	$\mu g/m^3$
ZNXU	Zinc concentration uncertainty	$\mu g/m^3$
GAXC	Gallium concentration	$\mu g/m^3$
GAXU	Gallium concentration uncertainty	$\mu g/m^3$
ASXC	Arsenic concentration	$\mu g/m^3$
ASXU	Arsenic concentration uncertainty	$\mu g/m^3$

Table 3-1. (continued)

Field Code	Description	Measurement Unit
SEXC	Selenium concentration	µg/m^3
SEXU	Selenium concentration uncertainty	µg/m^3
BRXC	Bromine concentration	µg/m^3
BRXU	Bromine concentration uncertainty	µg/m^3
RBXC	Rubidium concentration	µg/m^3
RBXU	Rubidium concentration uncertainty	µg/m^3
SRXC	Strontium concentration	µg/m^3
SRXU	Strontium concentration uncertainty	µg/m^3
YTXC	Yttrium concentration	µg/m^3
YTXU	Yttrium concentration uncertainty	µg/m^3
ZRXC	Zirconium concentration	µg/m^3
ZRXU	Zirconium concentration uncertainty	µg/m^3
MOXC	Molybdenum concentration	µg/m^3
MOXU	Molybdenum concentration uncertainty	µg/m^3
PDXC	Palladium concentration	µg/m^3
PDXU	Palladium concentration uncertainty	µg/m^3
AGXC	Silver concentration	µg/m^3
AGXU	Silver concentration uncertainty	µg/m^3
CDXC	Cadmium concentration	µg/m^3
CDXU	Cadmium concentration uncertainty	µg/m^3
INXC	Indium concentration	µg/m^3
INXU	Indium concentration uncertainty	µg/m^3
SNXC	Tin concentration	µg/m^3
SNXU	Tin concentration uncertainty	µg/m^3
SBXC	Antimony concentration	µg/m^3
SBXU	Antimony concentration uncertainty	µg/m^3
BAXC	Barium concentration	µg/m^3
BAXU	Barium concentration uncertainty	µg/m^3
LAXC	Lanthanum concentration	µg/m^3
LAXU	Lanthanum concentration uncertainty	µg/m^3
AUXC	Gold concentration	µg/m^3
AUXU	Gold concentration uncertainty	µg/m^3
HGXC	Mercury concentration	µg/m^3
HGXU	Mercury concentration uncertainty	µg/m^3
TLXC	Thallium concentration	µg/m^3
TLXU	Thallium concentration uncertainty	µg/m^3
PBXC	Lead concentration	µg/m^3
PBXU	Lead concentration uncertainty	µg/m^3
URXC	Uranium concentration	µg/m^3
URXU	Uranium concentration uncertainty	µg/m^3
COMMENT	Sampling and/or analysis comments	

3.1 *Database Structures and Features*

The raw LASCA data was processed with Microsoft FoxPro 2.6 for Windows (Micrsosoft Corp., 1994), a commercially available relational database management system. FoxPro can handle 256 fields of up to 4,000 characters per record and up to one billion records per file. This system can be implemented on most IBM PC-compatible desktop computers. The data base files (*.DBF) can also be read directly into a variety of popular statistical, plotting, data base, and spreadsheet programs without having to use any specific conversion software. After processing, the final LASCA data was converted from FoxPro to Microsoft Excel format for reporting purposes.

In FoxPro, one of five field types (character, date, numerical, logical, or memo) was assigned to each observable. Sampling sites and particle size fractions are defined as "Character" fields, sampling dates are defined as "Date" fields, and measured data are defined as "Numeric" fields. "Logical" fields are used to represent a "yes" or "no" value applied to a variable, and "Memo" fields accommodate large blocks of textual information and are used to document the data validation results.

Data contained in different XBase files can be linked by indexing on and relating to common attributes in each file. Sampling site, sampling hour, sampling period, particle size, and sampling substrate IDs are, typically, the common fields among various data files that can be used to relate data in one file to the corresponding data in another file.

To assemble the final data files, information was merged from many data files derived from field monitoring and laboratory analyses by relating information on the common fields cited above.

3.2 *Measurement and Analytical Specifications*

Every measurement consists of: 1) a value; 2) a precision; 3) an accuracy; and 4) a validity (Hidy, 1985; Watson et al., 1989, 1995). The measurement methods described in this volume are used to obtain the value. Performance testing via regular submission of standards, blank analysis, and replicate analysis are used to estimate precision. These precisions are reported in the data files described in Section 3.1 so that they can be propagated through air quality models and used to evaluate how well different values compare with one another. The submission and evaluation of independent standards through quality audits are used to estimate accuracy. Validity applies both to the measurement method and to each measurement taken with that method. The validity of each measurement is indicated by appropriate flagging within the database, while the validity of the methods has been evaluated in this study by tests described in Section 3.4.

3.2.1 Definitions of measurement attributes

The precision, accuracy, and validity of the LASCA aerosol measurements are defined as follows (Chow et al., 1993):

- A measurement is an observation at a specific time and place which possesses: 1) value – the center of the measurement interval; 2) precision – the width of the

measurement interval; 3) accuracy – the difference between measured and reference values; and 4) validity – the compliance with assumptions made in the measurement method.

- A measurement method is the combination of equipment, reagents, and procedures which provide the value of a measurement. The full description of the measurement method requires substantial documentation. For example, two methods may use the same sampling systems and the same analysis systems. These are not identical methods, however, if one performs acceptance testing on filter media and the other does not. Seemingly minor differences between methods can result in major differences between measurement values.

- Measurement method validity is the identification of measurement method assumptions, the quantification of effects of deviations from those assumptions, the evaluation that deviations are within reasonable tolerances for the specific application, and the creation of procedures to quantify and minimize those deviations during a specific application. A substantial effort was expended during LASCA to establish the validity of measurement methods, especially for the measurements of EC, babs, and particle nitrate.

- Sample validation is accomplished by procedures that identify deviations from measurement assumptions and the assignment of flags to individual measurements for potential deviations from assumptions.

- The comparability and equivalence of sampling and analysis methods are established by the comparison of values and precisions for the same measurement obtained by different measurement methods. Inter-laboratory and intra-laboratory comparisons are usually made to establish this comparability. Simultaneous measurements of the same observable are considered equivalent when more than 90% of the values differ by no more than the sum of two one-sigma precision intervals for each measurement.

- Completeness measures how many environmental measurements with specified values, precisions, accuracies, and validities were obtained out of the total number attainable. It measures the practicability of applying the selected measurement processes throughout the measurement period. Databases which have excellent precision, accuracy, and validity may be of little use if they contain so many missing values that data interpretation is impossible.

A database with numerous data points, such as the one used in this study, requires detailed documentation of precision, accuracy, and validity of the measurements. This section addresses the procedures followed to define these quantities and presents the results of those procedures.

3.2.2 Definitions of measurement precision

Measurement precisions were propagated from precisions of the volumetric measurements, the chemical composition measurements, and the field blank variability using the methods of Bevington (1969) and Watson et al. (1995). The following equations calculated the precision associated with filter-based measurements:

$$C_i = (M_i - B_i)/V \quad (3\text{-}1)$$

$$V = F \times t \quad (3\text{-}2)$$

$$B_i = \frac{1}{n}\sum_{j=1}^{n} B_{ij} \quad \text{for } B_i > \sigma_{Bi} \quad (3\text{-}3)$$

$$B_i = 0 \quad \text{for } B_i \le \sigma_{Bi} \quad (3\text{-}4)$$

$$\sigma_{Bi} = STD_{Bi} = \left[\frac{1}{n-1}\sum_{j=1}^{n}(B_{ij} - B_i)^2\right]^{1/2} \quad \text{for } STD_{Bi} > SIG_{Bi} \quad (3\text{-}5)$$

$$\sigma_{Bi} = SIG_{Bi} = \left[\frac{1}{n}\sum_{j=1}^{n}(\sigma_{Bij})^2\right]^{1/2} \quad \text{for } STD_{Bi} \le SIG_{4Bi} \quad (3\text{-}6)$$

$$\sigma_{Ci} = \left[\frac{\sigma_{Mi}^2 + \sigma_{Bi}^2}{V^2} + \frac{\sigma_V^2 (M_i - B_i)^2}{V^4}\right]^{1/2} \quad (3\text{-}7)$$

$$\sigma_{RMS_i} = \left(\frac{1}{n}\sum_{j=1}^{n}\sigma_{Ci}^2\right)^{1/2} \quad (3\text{-}8)$$

$$\sigma_V/V = 0.05 \quad (3\text{-}9)$$

where:

B_i = average amount of species i on field blanks
B_{ij} = the amount of species i found on field blank j
C_i = the ambient concentration of species i
F = flow rate throughout sampling period
M_i = amount of species i on the substrate
M_{ijf} = amount of species i on sample j from original analysis
M_{ijr} = amount of species i on sample j from replicate analysis
n = total number of samples in the sum
SIG_{Bi} = the root mean square error (RMSE), the square root of the averaged sum of the squared of σ_{Bij}.
STD_{Bi} = standard deviation of the blank
σ_{Bi} = blank precision for species i
σ_{Bij} = precision of the species i found on field blank j
σ_{Ci} = propagated precision for the concentration of species i
σ_{Mi} = precision of amount of species i on the substrate
σ_{RMS_i} = root mean square precision for species i
σ_V = precision of sample volume
t = sample duration
V = volume of air sampled

Dynamic field blanks were periodically placed in each sampling system without air being drawn through them to estimate the magnitude of passive deposition for the period of time which filter packs remained in a sampler (typically 24 hours). No statistically significant inter-site differences in field blank concentrations were found for any species after removal of outliers (i.e., concentration exceeding three times the standard deviations of the field blanks). The average field blank concentrations (with outliers removed) were calculated for each species on each substrate (e.g., Teflon-membrane, quartz-fiber), irrespective of the sites.

3.2.3 Analytical specifications

Blank precisions (σ_{Bi}) are defined as the higher value of the standard deviation of the blank measurements, STD_{Bi}, or the square root of the averaged squared uncertainties of the blank concentrations, SIG_{Bi}. If the average blank for a species was less than its precision, the blank was set to zero (as shown in Equation 3-4). The precisions (σ_{Mi}) for XRF analysis were determined from counting statistics unique to each sample. Hence, the σ_{Mi} is a function of the energy-specific peak area, the background, and the area under the baseline.

3.3 *Quality Assurance*

Quality control (QC) and quality auditing establish the precision, accuracy, and validity of measured values. Quality assurance (QA) integrates QC, quality auditing, measurement method validation, and sample validation into the measurement process. The results of quality assurance are data values with specified precisions, accuracies, and validities.

Field blanks were acquired and replicate analyses were performed for ~10% of all ambient samples. Quality audits of sample flow rates were conducted at the beginning, middle, and end of the study period, and these audits determined that flow rates were within ±10% of specifications. Data were submitted to three levels of data validation (Chow et al., 1994; Watson et al., 2001). Detailed data validation processes are documented in the following subsections.

3.4 *Data Validation*

Data acquired from the study was submitted to three data validation levels:

- Level 0 sample validation: designates data as they come off the instrument. This process ascertains that the field or laboratory instrument is functioning properly.
- Level I sample validation: 1) flags samples when significant deviations from measurement assumptions have occurred, 2) verifies computer file entries against data sheets, 3) eliminates values for measurements that are known to be invalid because of instrument malfunctions, 4) replaces data from a backup data acquisition system in the event of failure of the primary system, and 5) adjusts values for quantifiable calibration or interference biases.

- Level II sample validation applies consistency tests to the assembled data based on known physical relationships between variables.
- Level III sample validation is part of the data interpretation process. The first assumption upon finding a measurement which is inconsistent with physical expectations is that the unusual value is due to a measurement error. If, upon tracing the path of the measurement, nothing unusual is found, the value can be assumed to be a valid result of an environmental cause. Unusual values are identified during the data interpretation process as: 1) extreme values, 2) values which would otherwise normally track the values of other variables in a time series, and 3) values for observables which would normally follow a qualitatively predictable spatial or temporal pattern.

Level I validation flags and comments are included with each data record in the data base as documented in Section 3.2. Level II validation tests and results are described in the following subsections.

Level II tests evaluate the chemical data for internal consistency. In this study, Level II data validations were made for: 1) reconstructed mass versus measured mass, 2) physical consistency, and 3) adsorption of gaseous organic carbon onto a quartz-fiber filter. Correlations and linear regression statistics were computed and scatter plots prepared to examine the data.

3.4.1 Sum of chemical species versus mass

Major PM components were used to reconstruct PM mass, including: 1) geological material, which is estimated as 1.89*Al+2.14*Si+1.4*Ca+1.43*Fe to account for unmeasured oxides; 2) organic matter (1.4*OC) to account for unmeasured hydrogen and oxygen; 3) soot (EC); 4) $SO_4^{=}$; 5) NO_3^{-}; 6) NH_4^{+}; 7) noncrustal trace elements (sum of elements measured by XRF other than Al, Si, Ca, and Fe); and 8) unidentified mass (difference between measured mass and the sum of the major components).

Figure 3-2(a-b) shows that high correlations ($r^2 > 0.9$) were found between reconstructed and measured mass at all four sites. Compositing them, the slope of reconstructed mass to measured mass is 0.945, yet the average ratio of reconstructed mass to measured mass shown is 1.29. A large intercept of 5.14 $\mu g/m^3$ suggests the sampling artifact resulted from significant adsorption of volatile organic species onto the quartz filter. This is usually more pronounced when the ambient $PM_{2.5}$ mass fraction is low but organic compound concentration is high during long sampling periods. The positive sampling artifact of organic compound adsorption onto a quartz-fiber filter could be reduced by subtracting with organic compounds determined by backup filter. The comparison of reconstructed mass with subtraction from the backup filter and measured mass shows a slope of 0.92 and reduced intercept of 2.79 $\mu g/m^3$. The average ratio of reconstructed mass (with backup filter subtraction) to measured mass can be reduced to 1.11.

a)

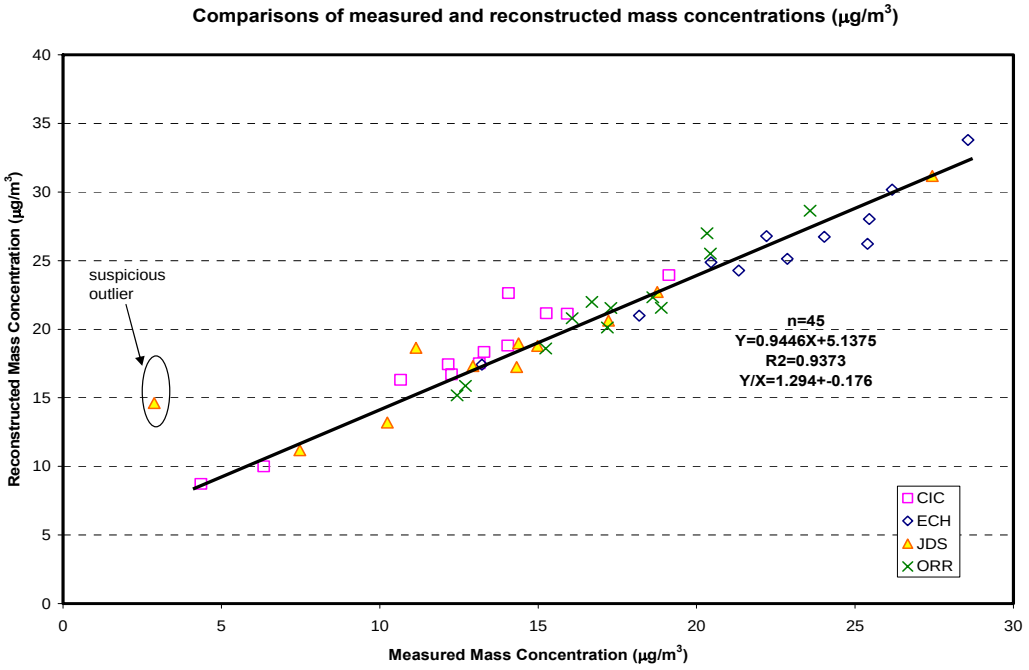

b)

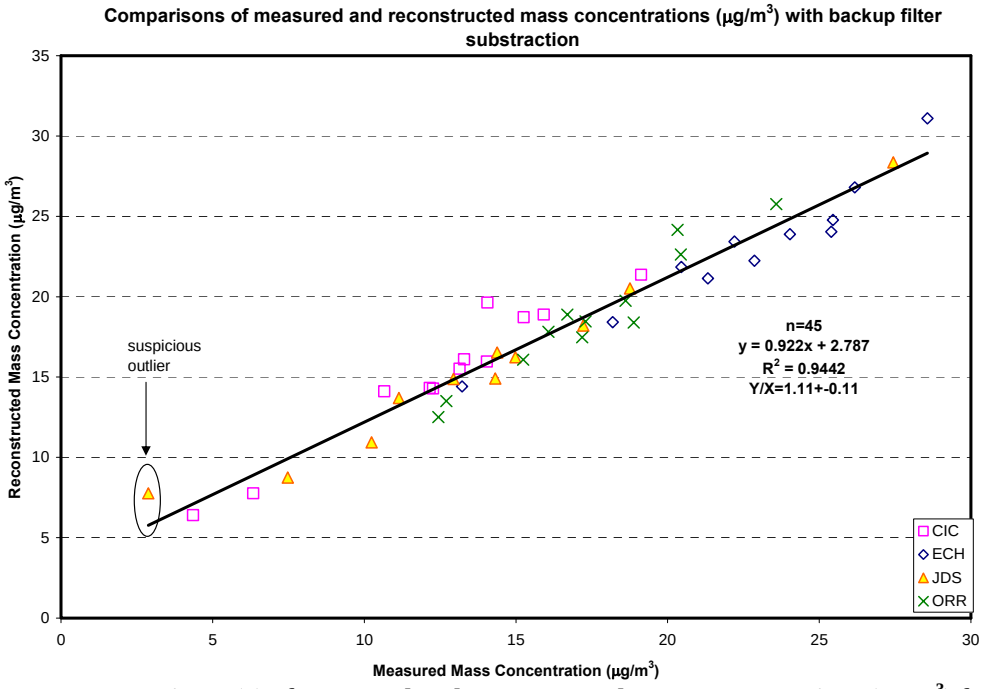

Figure 3-2. Comparisons (a) of measured and reconstructed mass concentrations (µg/m^3) for all sites in the winter intensive study and comparisons (b) of measured and reconstructed mass concentrations (µg/m^3) with backup organic compound subtraction for all sites in the winter intensive study.

3.4.2 Physical consistency

The compositions of chemical species concentrations measured by different chemical analysis methods were examined. Physical consistency was tested for: 1) $SO_4^=$ versus total sulfur (S), 2) Cl^- versus chlorine (Cl), and 3) K^+ versus total potassium (K). An outlier was found on the sample collected at JD on 1/12/2003, which is excluded from statistical analysis and comparison in the following section. These results were compared with results from the previous Las Vegas Valley Visibility and $PM_{2.5}$ study in 2000.

3.4.2.1 Sulfate ($SO_4^=$) versus total sulfur (S)

$SO_4^=$ was measured by IC analysis on quartz-fiber filters, and S was measured by XRF analysis on Teflon-membrane filters. The ratio of $SO_4^=$ to S should equal 3:1 if all of the S were present as $SO_4^=$. Figure 3-3 shows scatter plots of $SO_4^=$ versus S concentrations at the four sites. The average $SO_4^=$/S ratio was 2.46 ± 0.16, slightly below the 3-to-1 line. The regression statistics give a slope of 2.5534 with negligible intercept of -0.0187 µg/m^3 with a good correlation ($r^2 > 0.95$). The average $SO_4^=$/S ratio in this study is very close to the annual average (slope of 2.8423, average Y/X = 2.7208) found in the previous visibility and $PM_{2.5}$ study. This suggests that there have not been significant changes in the $SO_4^=$/S sources in the Las Vegas Valley.

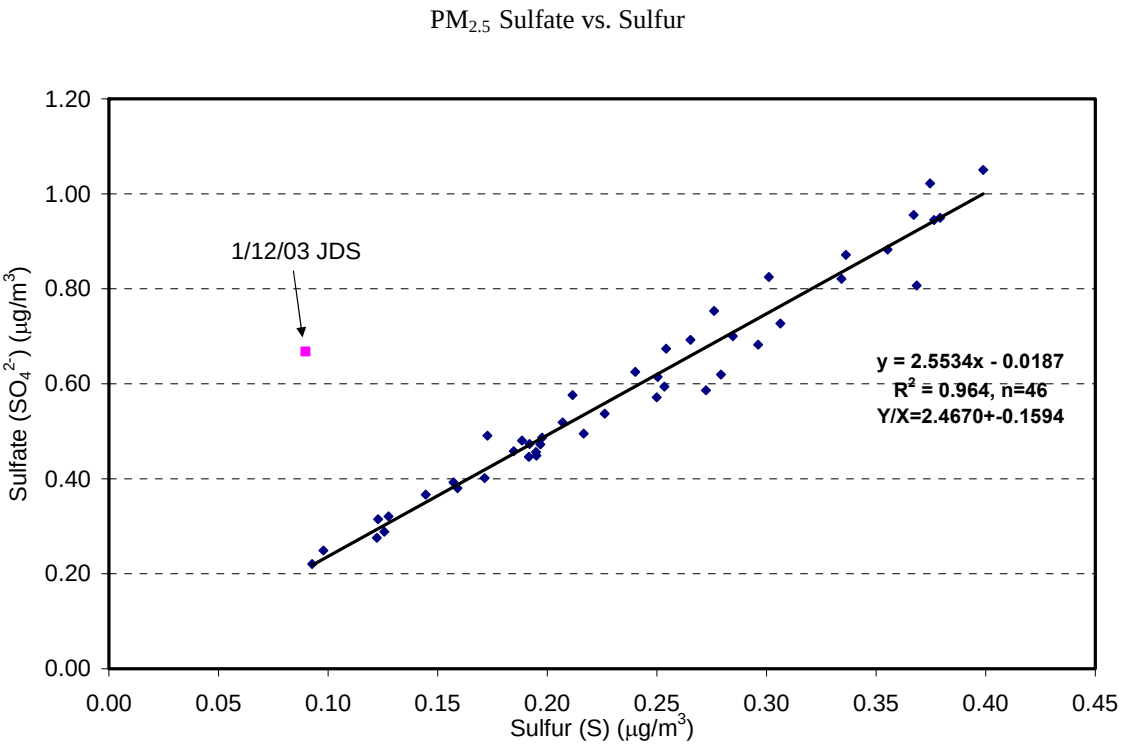

Figure 3-3. Scatter plot of sulfate versus sulfur concentrations at the four sites.

3.4.2.2 Chloride (Cl^-) versus Chlorine (Cl)

Cl^- was measured by IC on quartz-fiber filter, and Cl was measured by XRF on Teflon-membrane filters. Because Cl^- is the water-soluble portion of Cl, the Cl^--to-Cl ratio is expected to be less than unity. Figure 3-4 shows that the $PM_{2.5}$ Cl^- concentrations during this study were below 0.3µg/m^3 with high relative uncertainties, but there were moderate-high correlations (r^2 = 0.87) between $PM_{2.5}$ Cl^- and Cl measurements. The uncertainty of Cl^- measurements were higher at low concentrations because its elution peak in gas chromatographic analysis is close to the distilled water dip which, in turn, shifts the baseline of the chromatogram (Chow and Watson, 1999). In addition, Cl collected on the Teflon filter may be lost through volatilization because XRF analysis is conducted in a vacuum chamber. Such losses are especially apparent when Cl concentrations are low.

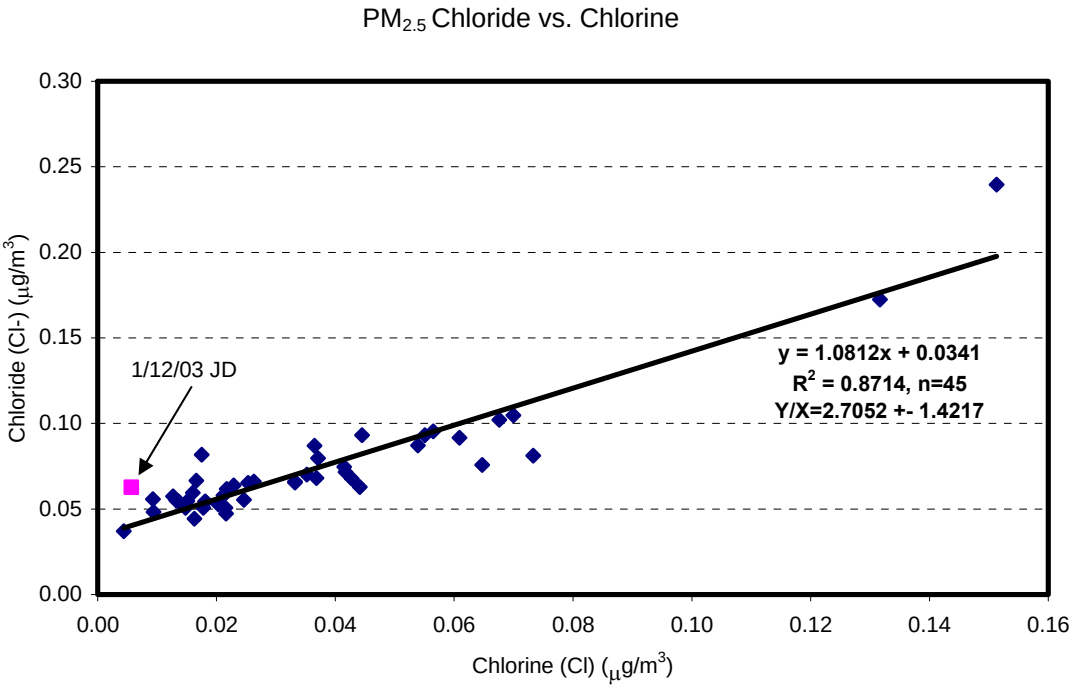

Figure 3-4. $PM_{2.5}$ chloride versus chlorine concentrations.

3.4.2.3 Soluble potassium (K^+) versus total potassium (K)

K^+ was measured by atomic adsorption spectrophotometry (AAS) analysis on quartz-fiber filters, and K was measured by XRF on Teflon-membrane filters. Figure 3-5 displays the scatter plot of $PM_{2.5}$ K^+ versus K concentrations. The K concentrations were low (<0.30µg/m^3), and associated with large uncertainty. Yet, the regression statistics show high-moderate correlations (r^2 = 0.89) between K^+ and K. The average K^+/K ratio is 0.6756, which is slightly higher than the annual average K^+/K ratio (Y/X=0.5569) from 7/10/2000 to 7/21/2001.

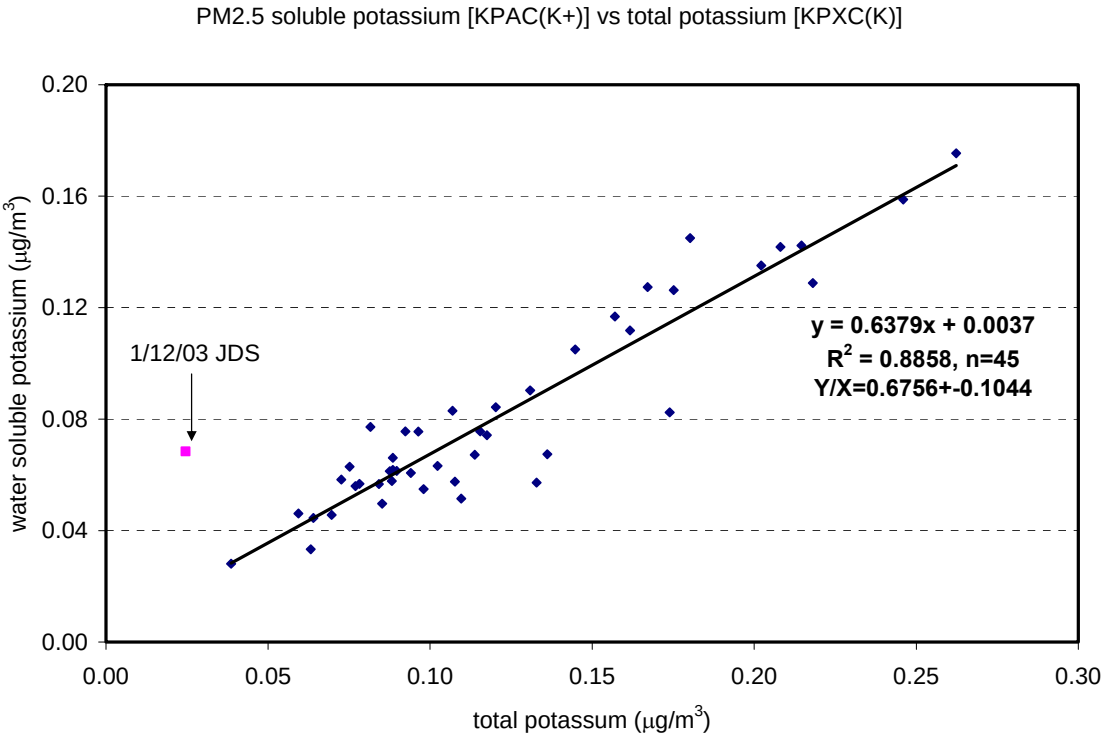

Figure 3-5. Scatter plot of $PM_{2.5}$ water-soluble potassium versus potassium concentrations.

3.4.3 Adsorption of gaseous OC on quartz-fiber filters

Certain organic compounds in suspended particles maintain a gas/particle equilibrium with their environments similar to the situation for ammonium nitrate. Previous studies have found that either some volatile organic compounds (VOCs) evaporate from a filter (negative artifact) during sampling or that some gaseous organic species are adsorbed (positive artifact) on quartz-fiber filters (Eatough et al., 1990; McDow and Huntziker, 1990; Tang et al. 1994; Turpin et al, 1994)

Several denuding and backup filter sampling systems have been applied to evaluate these artifacts. Eatough et al. (1990) and Tang et al. (1994) concluded that desorption of organic gasses from particles on the front quartz-fiber filter was the dominant sampling artifact (negative artifact), while Turpin et al. (1994) concluded that adsorption of organic gases by the quartz-fiber filter was the dominant sampling artifact (positive artifact) for OC. Turpin et al. (1994) recommended that a backup quartz-fiber filter behind the front Teflon-membrane filter (as shown in Figure 2-3 for the $PM_{2.5}$ sequential gas sampler configuration) be used to estimate the amount of organic gases which might absorb onto the backup quartz-fiber filter was dependent upon the source mixture in the atmosphere. Either a non-absorbing filter medium needs to be developed, or complex denuding and absorbent backup sampling systems need to be applied to improve the accuracy of OC measurements.

Figure 3-6 compares the ratio of OC measured on the backup quartz-fiber filter behind the front Teflon-membrane filter with the sum of $PM_{2.5}$ particulate OC measured on the front quartz-fiber filter (which sampled alongside this filter pack) plus the OC measured

on the backup quartz-fiber filter. The plot shows that at all sites, the OC concentrations on the backup filter ranged from 11% to 42% of the total organic carbon (TOC, sum of OC from the front and backup filter). Most of the elevated concentrations of artifact OC on the backup filters were associated with lower (<10 µg/m^3) $PM_{2.5}$ mass concentrations. As $PM_{2.5}$ mass concentrations exceeded 12µg/m^3, the artifact of OC decreased to less than 25% of the total organic carbon. However, the artifact of OC was never less than 10% of the total organic carbon during this study period.

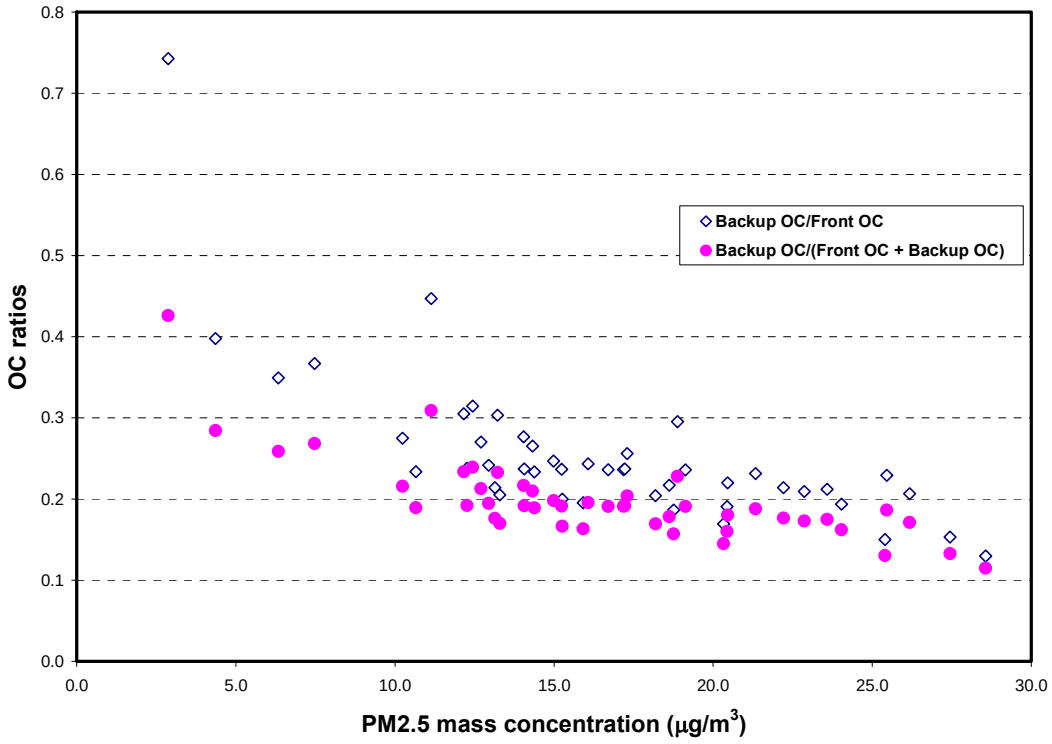

Figure 3-6. Relationship between the ratio of: 1) backup to total filter, and 2) backup to front filter organic carbon (OC) as a function of $PM_{2.5}$ mass at the four sites during the Las Vegas Carbon Source Apportionment Study.

The relationship between the ratio of backup to front filter organic carbon as a function of $PM_{2.5}$ mass is also displayed in Figure 3-6 as well. The ratios were slightly higher than backup to total filter OC, yet fairly consistent. The differences between the ratios of backup to front filter OC and backup to total filter OC decrease as $PM_{2.5}$ mass concentrations increase. Relatively larger adsorption of OC at lower $PM_{2.5}$ concentrations suggests that particles provided additional adsorption sites on the front filter, especially in a cleaner environment (Chow et al, 1996). In addition, as $PM_{2.5}$ at these sites is dominated by carbonaceous compounds, the results agree with theory that volatilization losses decrease as OC concentration in particle phase increases. A similar relationship was found between backup/front filter OC and $PM_{2.5}$ mass during the 1990 SJVAQS/AUSPEX summer study (Chow et al., 1998) and 1995 IMS95 fall and winter study. The positive artifact due to adsorption of OC can explain the higher intercept of comparing reconstructed mass and measured mass in Section 3.4.1.

3.5 *Data Processing for In-Plume Sampling System*

3.5.1 Calculation of fuel based emission factor

After sampling, all data were downloaded from the field computer to a data server. The ELPI, DustTrak, traffic counter, and flow meter data were imported into a relational database and constant time offsets were added to each dataset to synchronize the occurrence of concentration peaks.

The FTIR spectra were processed using the Autoquant Pro version 4 package. Concentrations were calculated using a classical least squares fit of the data. These data were then processed using linear interpolation to fit the 0.66 Hz dataset to coincide with the other 1 Hz datasets. The FTIR 1 Hz dataset was imported into the relational database and joined to the other data based on time. The master table of all measurements was then exported and processed to identify peaks in the CO_2 signal.

Fuel-based emission factors were calculated from the background subtracted average peak concentrations. Using the carbon mass balance technique described by Moosmüller et al. (2003) and Fraser et al. (1998), the fuel-based emission factors were calculated as:

$$EF_P = CMF_{fuel} \frac{C_P}{C_{CO_2}\left(\frac{M_C}{M_{CO_2}}\right) + C_{CO}\left(\frac{M_C}{M_{CO}}\right)} \tag{3-10}$$

where EF_P is the emission factor of pollutant P in g pollutant per g fuel, CMF_{fuel} is the carbon mass fraction of the fuel (typically 85% to 88% for gasoline and diesel, and 45% to 50% for wood fuel), C_i is the mass concentration of species i in grams per cubic meter, and M_i is the molecular (or atomic) weight of species i in grams per mole.

The start and stop points of the CO_2 peaks were used to integrate the pollutant concentrations. To ensure a high signal-to-noise ratio, peaks with integrated CO_2 concentrations of less than 1000 ppm were discarded. A CO_2 peak exists when CO_2 is above the background by more than 3 standard errors of the CO_2 measurement. The background is defined as the 15th percentile value of the CO_2 over a 100 s window centered on the measurement. This process provides an unambiguous peak definition while compensating for low frequency drift in the background CO_2 measurement.

Background concentrations, which are defined as the pollutant concentrations corresponding to the 15th percentile CO_2 value of the 100 s window, were subtracted from the average peak pollutant concentrations. The exhaust concentrations of each species were calculated as the instantaneous signal measured during each peak minus the average of the points in the 100 s window that are not associated with CO_2 peaks.

3.5.2 Example of the calculation of fuel-based emission factors: motor vehicle exhaust at Lake Tahoe, NV

In order to determine fuel-based emission factors, the exhaust portion of each ambient measurement must be extracted from the background concentration. A simple peak

finding algorithm is applied to determine when a peak is present. Since CO_2 is the dominant species in vehicle exhaust, the peak finding algorithm is applied to CO_2 to determine the beginning and ending points of each peak.

The simplest form of peak finder compares a measurement with a threshold value to determine if the point is significantly above background. For roadside measurements of CO_2, the background concentration can vary by 50 ppm or more over the course of a day. These variations may be associated with atmospheric mixing of combustion emissions close to the ground and vegetative respiration that consumes CO_2. To account for the low frequency changes in background concentration, the CO_2 data are filtered by subtracting the 15th percentile value from a moving 100 s window (i.e., 50 s ahead and 50 s behind) surrounding each data point. The choice of the percentile value and the size of the window are arbitrary and should be based on how frequently the inlet is sampling a plume. If no plumes are present, the background would be defined at the 50th percentile or median concentration. In dense traffic areas, this percentile is likely to reflect CO_2 concentrations impacted by vehicle exhaust and a lower percentile value should be used. The size of the moving window should be sufficiently larger than the duration of the individual peaks so that the 15th percentile value will be representative of a point that is not influenced by exhaust plumes.

Figure 3-7 shows the time series of the mid-road CO_2 measurements between 14:35 and 14:40 PDT on 7/26/03 at the southeast corner of the intersection of Country Club and Lakeshore in Tahoe, NV. The CO_2 gas concentrations are referenced to ambient concentrations at the beginning of the sampling period. For periods where there is no apparent exhaust peak (i.e., 14:37:25 PDT to 14:37:45 PDT and 14:38:40 PDT to 14:39:00 PDT), the moving 15th percentile background appears to pass through the middle of these background data points.

The lower panel of Figure 3-7 shows the background (i.e., moving 15th percentile value of 100 s window) subtracted from the raw CO_2 signal. This signal is then compared with the analytical uncertainty (i.e., standard error) of the CO_2 measurement. If the background subtracted signal is more than 3 times the uncertainty, then the data point is defined as part of a peak. If the next data point is also greater than 3 times, then the uncertainty is associated with the same peak. To ensure that the peak is sufficiently large to calculate a meaningful fuel-based emission factor, the time integrated CO_2 peak must be more than 1000 ppm s. In many instances, plumes from passing vehicles are insufficient to meet this criteria and these results are not included in average emission factor calculations.

The sensitivity of CO_2 peak integral to the choice of the percentile background value can be assessed with the data in Figure 3-7. The peak that begins at 14:36:12 PDT and ends at 14:36:19 PDT is 7 s long and has an integral of 1366 ppm s using the 15th percentile 100 s window as background. If the 5th percentile or 25th percentile background had been used, the integrated values of the peak would have been 1282 ppm s (-9%) or 1422 ppm s (+4%), respectively. Thus, the choice of background percentile may introduce <10% uncertainty into the emission factor calculations.

Figure 3-8 shows a time series of concentration data measured by the sampling system. With a traffic density of ~200 vehicles per hour per lane, many of the identified plumes represent the emissions of more than one vehicle traveling close together. The lower panel of Figure 3-8 is the CO_2 time series. The segments identified as single peaks using the algorithm described above are shaded black.

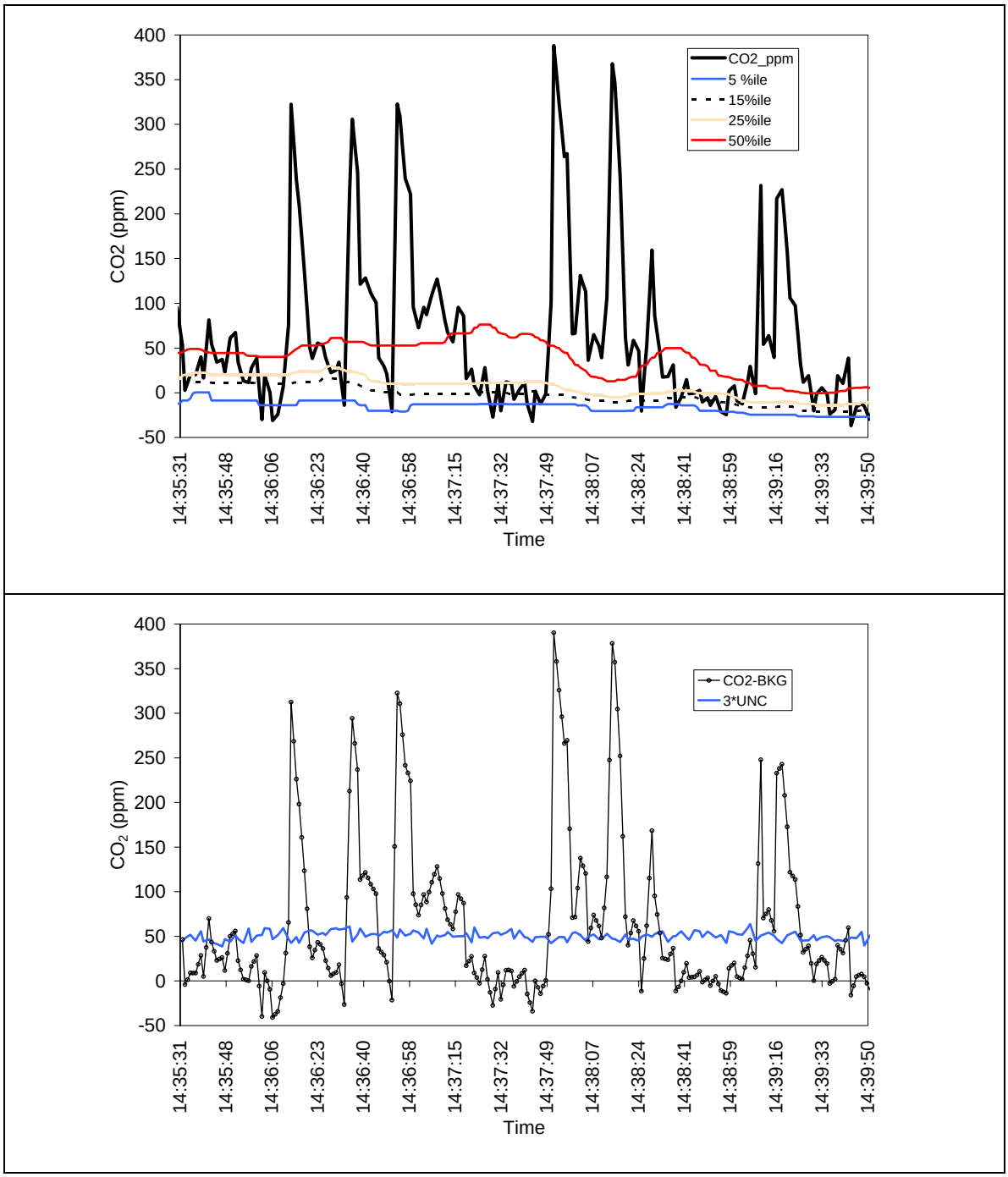

Figure 3-7. Upper panel shows the raw CO_2 concentration with the moving 100 s window percentile baselines. The time series shows that the CO_2 baseline decrease by ~20 ppm over the period and that the 15th percentile baseline best fits the non-plume points. The lower panel shows the CO_2

concentration with the 15th percentile value subtracted (line with marker points). The blue line is 3 times the analytical uncertainty of the CO_2 measurement.

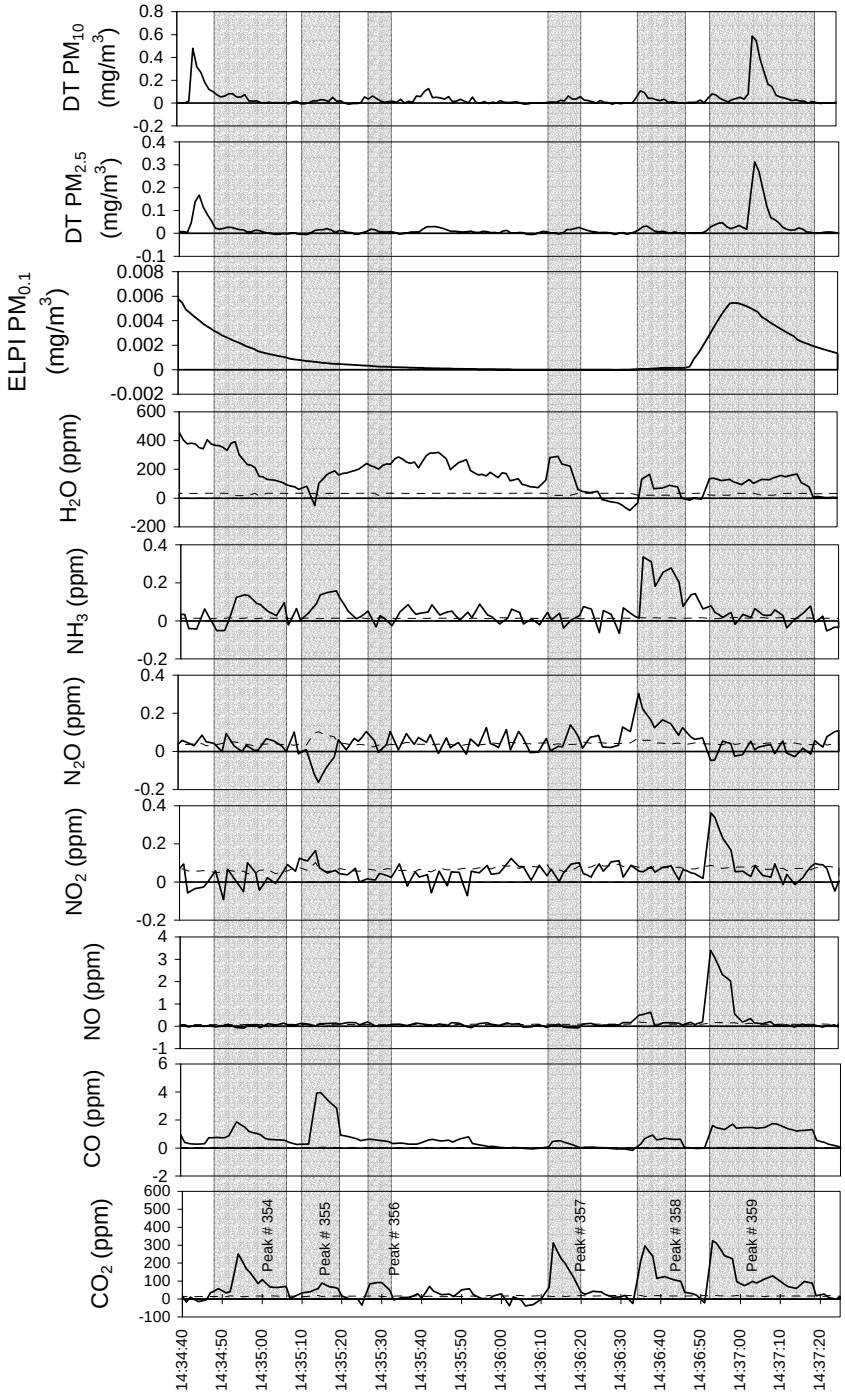

Figure 3-8. Concentration time series of CO_2, CO, NO, NO_2, N_2O, NH_3, H_2O, and PM measured by ELPI and DustTraks. The shaded areas are periods when the measured plume is linked to the passage of one or more vehicles. The dotted black line represents the analytical uncertainty of the gaseous measurements.

The time series show very different chemical profiles for each of the plumes. Plume 355 not only has the lowest integrated CO_2 concentration, but also has the highest CO concentration, indicating a higher fuel-based CO emission factor than the other plumes in Figure 3-8. Plume 359 shows features that indicate mixing of two or more exhaust plumes. The first 10 s of the plume show elevated levels of NO and NO_2, and these levels decrease in the latter 20 s of the plume, although CO_2 and CO remain above background. This composition of plume 359 is very different from plume 358, which shows elevated N_2O and NH_3 concentrations. These species likely represent the emissions from a vehicle with a three-way catalytic converter that is reducing thermal NO_x beyond N_2 and O_2 to create NH_3.

Particle emissions show similar variability between vehicles. The mass of particles (assuming spheres) with aerodynamic diameter below 0.1 μm are shown in the upper panel of Figure 3-8. During this experiment, ELPI was operated with the electrometers set to their largest detectable range (400,000 fA). This resulted in a very sensitive measurement. However, the time scales of the measurements were on the order of 20 s. As a result, the ELPI was able to detect fresh ultrafine emissions from the vehicles, but the time response was too slow to link these concentrations to individual plumes. In later experiments, the ELPI was operated at a range of 10,000 fA, and plumes from individual vehicles were distinguishable. The TSI DustTrak has a fast 1 Hz time response. The time series of the DustTraks operating with a 2.5 μm and 10 μm inlets are shown below the ELPI time series in Figure 3-8. A PM_{10} and $PM_{2.5}$ peak was observed during the middle of plume 359. This peak does not appear to be associated with the same vehicle that created the NO peak. The first peak in the DustTrak time series appears to precede the CO_2 peak. These elevated levels may be due to exhaust or road dust from a vehicle passing in the opposite direction.

Emission factors for all species measured and their propagated uncertainties are shown in Table 3-2. To ensure sufficient plume densities for each peak, valid CO_2 peaks were required to have integrated plume values of more than 1000 ppm s. Peaks 355 and 356 had integrated values of ~500 ppm s, resulting in larger emission factor uncertainties. The detection limit of the In-Plume Sampling System is affected by both the variability of the ambient background and the detection sensitivity of the instruments used. The measurement of water appears to be influenced by the background concentrations. Although the FTIR can measure propane hexane, ethylene, formaldehyde, SO_2, and other species found in exhaust, the levels typically observed in the exhaust are lower than can be detected.

Table 3-2. Emission factor results for vehicles associated with individual plumes.

Peak Number	354	357	358	359
Vehicles	Volkswagen Car Dodge Car	Lincoln Car	GMC PU Toyota Car	GMC PU Ford PU Ford SUV
CO_2 * Plume Duration (ppm s)	1645	1366	1771	3257
Species	**Emission Factors (g/kg fuel)**	**Emission Factors (g/kg fuel)**	**Emission Factors (g/kg fuel)**	**Emission Factors (g/kg fuel)**
CO	15.8 ± 3.0	0.3 ± 0.4	4.2 ± 0.8	19.0 ± 2.8
NO	-1.1 ± 1.9	-1.3 ± 2.1	3.0 ± 2.0	12.0 ± 2.7
NO_2	-1.1 ± 2.0	0.4 ± 1.5	0.5 ± 1.9	1.4 ± 2.0
N_2O	-0.7 ± 1.5	0.1 ± 0.8	2.6 ± 1.2	-1.2 ± 1.1
H_2O	2703 ± 925	917 ± 1217	-1493 ± 502	-542 ± 551
Formaldehyde	-1.5 ± 2.5	-0.3 ± 1.5	0.0 ± 1.6	0.2 ± 1.8
Hexane	-2.9 ± 2.4	-1.9 ± 3.0	-5.5 ± 2.9	-1.0 ± 2.3
Propane	-0.9 ± 2.2	-0.4 ± 1.5	-0.4 ± 1.7	0.0 ± 1.8
NH_3	0.4 ± 0.2	-0.1 ± 0.2	1.6 ± 0.3	0.0 ± 0.2
Ethylene	-0.5 ± 0.5	0.0 ± 0.3	-0.1 ± 0.4	0.3 ± 0.4
SO_2	-0.8 ± 8.0	4.3 ± 7.2	-4.5 ± 5.1	1.2 ± 5.7
$PM_{2.5}$ (DustTrak)	0.03	-0.02	-0.02	0.73
PM_{10} (DustTrak)	0.29	-0.07	0.06	1.13

Figure 3-9 shows the measured volume size distributions normalized to the total volume of particles collected on stages 1 through 10 (particles less than 2.3 µm aerodynamic diameter) for samples collected with the elevated and road-level inlets. Both size distributions show a large increase in particle volume on Stages 9 and 10 (0.98 µm to 2.3 µm) accounting for more than 40% of the total particle volume. For experiments using the road-level inlet, some enhancement in particle concentrations on the upper stages of the impactor is to be expected because road dust was sampled along with the exhaust. This is not the case with the elevated inlet, where vehicles (i.e., buses) are stopped or traveling at speeds of less than 10 km/hr and soil concentrations are less than 10% of the $PM_{2.5}$ mass. The increase in particle concentrations on Stages 9 and higher appears to be an artifact of sampling fresh exhaust with large number concentrations of nucleating particles and not an indication of coarse particles.

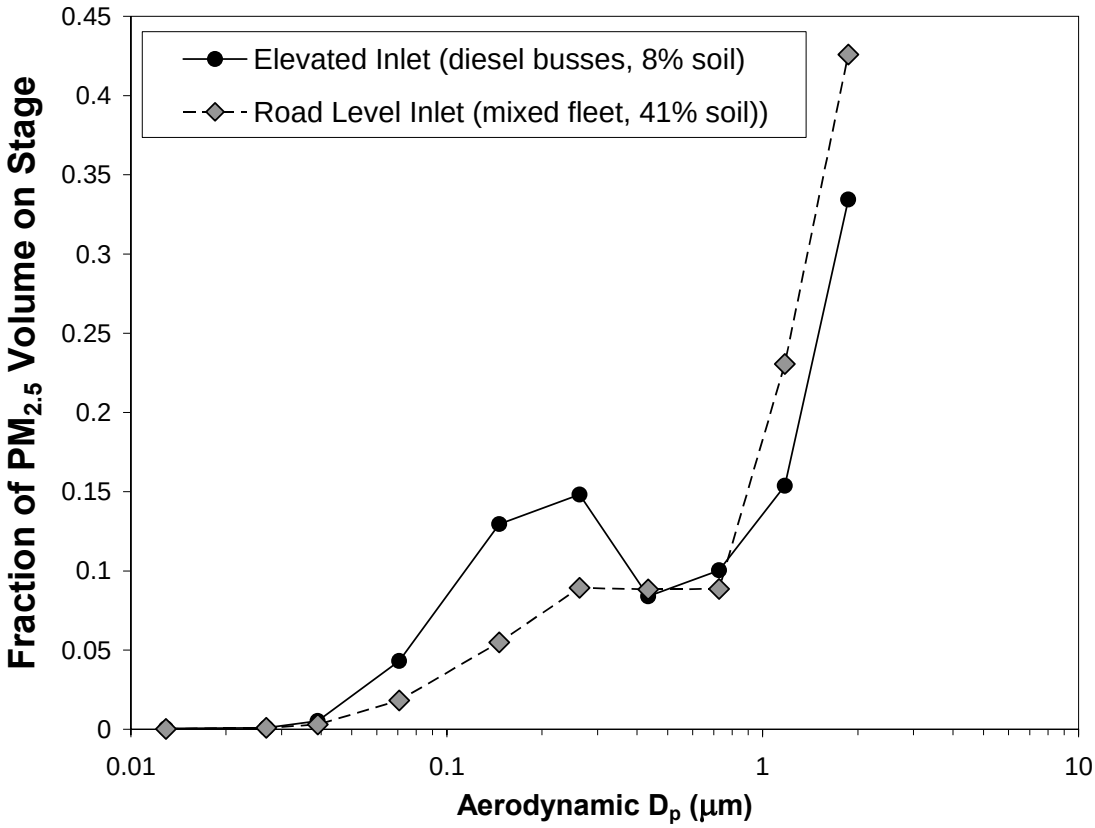

Figure 3-9. ELPI size distributions of exhaust samples measured using elevated and ground level inlets.

The bulk density of particles was calculated by dividing the particle volume on stages 10 and below (assuming spherical particles) by the mass of $PM_{2.5}$ measured using a filter sampler. The calculated particle densities are shown in Figure 3-10. Densities range from 0.5 to 1.5 g/cm^3. The inter-sample variability is larger than the density differences between diesel exhaust (black columns) and exhaust from the mixed fleet (gray columns).

DustTraks were operated in parallel with the ELPI and after the sample stream passed through the optical path of the FTIR on the In-Plume Sampling System. Figure 3-11 compares DustTrak PM concentrations with filter-based PM concentrations for PM_{10} and $PM_{2.5}$. The correlation coefficient for the relationship between the DustTrak signal and PM_{10} ($r^2 = 0.85$) is much stronger than the PM_{10} correlation ($r^2 = 0.31$). Nevertheless, emission factors estimated by ELPI and DustTrak provide a range of true emission factors and variabilities.

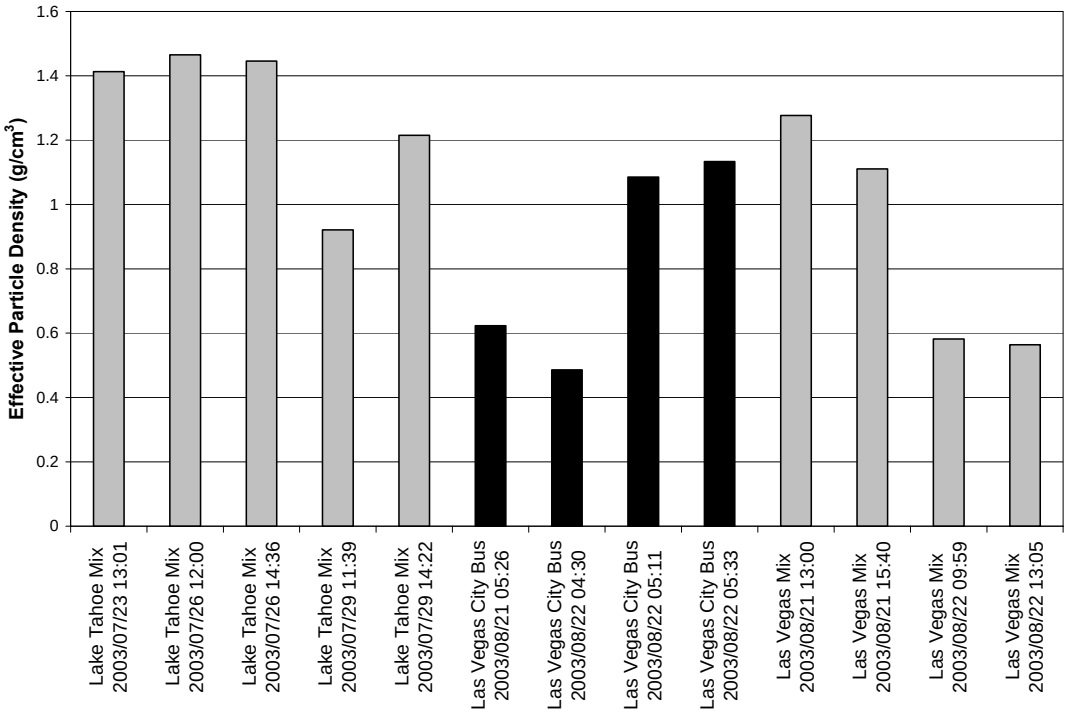

Figure 3-10. Particle densities inferred from ELPI and $PM_{2.5}$ filter-based measurements. The black columns are samples corresponding exclusively to diesel exhaust and ~10% road dust. The gray columns are samples from a mixed fleet of both gasoline and diesel vehicles collected at road level and composed of 41% road dust.

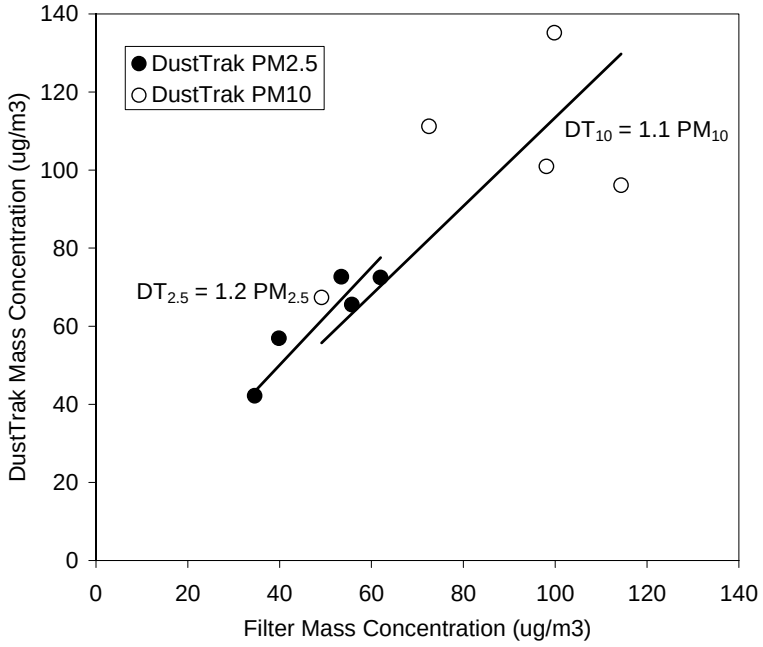

Figure 3-11. Comparison of DustTrak PM with filter-based PM. Data represents five sampling periods from a mixed fleet of vehicles operating in Lake Tahoe. The road level inlet was used to collect the samples.

4. CHEMICAL SPECIATION AND SPATIAL DISTRIBUTION OF PARTICULATES IN AMBIENT MEASUREMENT

The mini-intensive winter study consisted of 10-12 days of 24-hour aerosol measurement at each of the four locations—MS, JD, OR, and CC—during January 2003. Detailed site descriptions are summarized in Table 2-1. This section examines the spatial distributions of $PM_{2.5}$ and its chemical components during this study.

4.1 *Meteorological conditions in Las Vegas Valley for the winter mini-intensive ambient samplers*

The weather conditions in Las Vegas Valley during the winter intensive ambient sample collection are shown in Figure 4-1. The maxima, minima, and average dew point; temperature; relative humidity; barometric pressure; and wind speed of each day are listed in Table 4-1. There was no precipitation during these sampling collection periods. The average 24-hour ambient temperature ranged from 10.5 to 13 °C; the daily minimum was 5.0 °C and the maximum was 22.8 °C. A slightly higher 24-hour-average temperature was 15.6 °C on January 25, 2003. The relative humidity was 20% to 60% and the dew point was less than 2 °C. The mean wind speed was 5 km/hour—a mild to calm south/southwest prevailing wind—but a prevailing east wind was observed on January 5, 2003, when the high mean wind velocity was 16 km/hour.

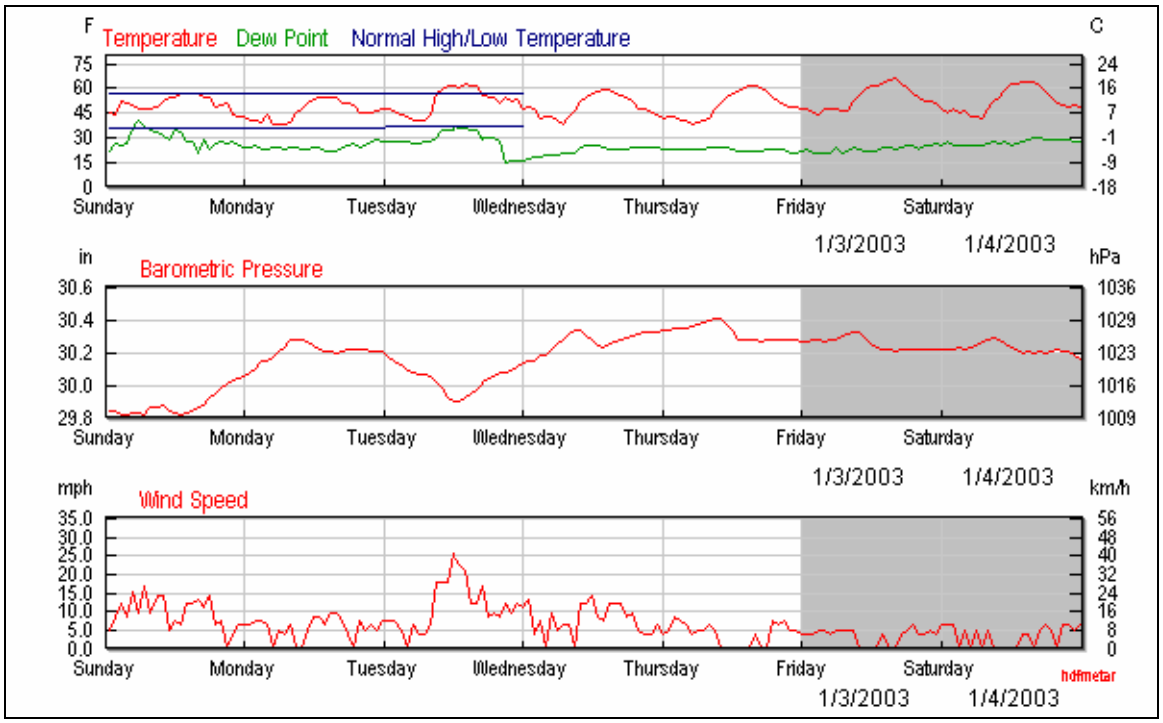

Figure 4-1. Meteorological conditions in Las Vegas Valley during January 2003 winter mini-intensive study.

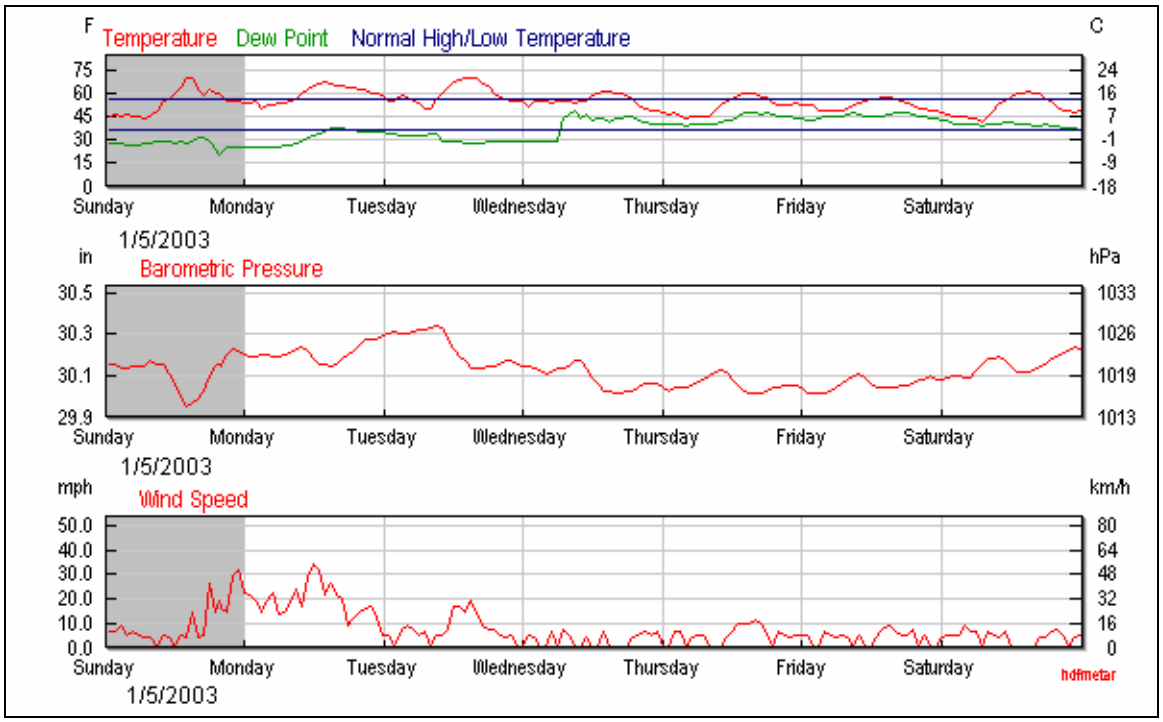

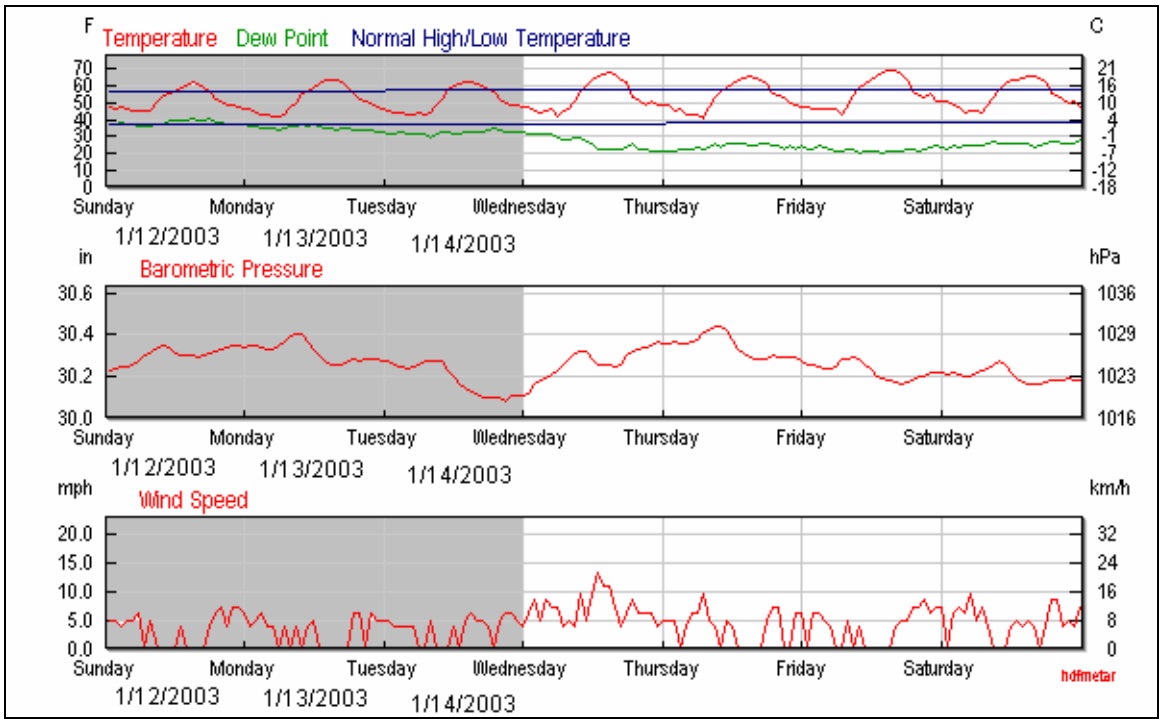

Figure 4-1 (continued).

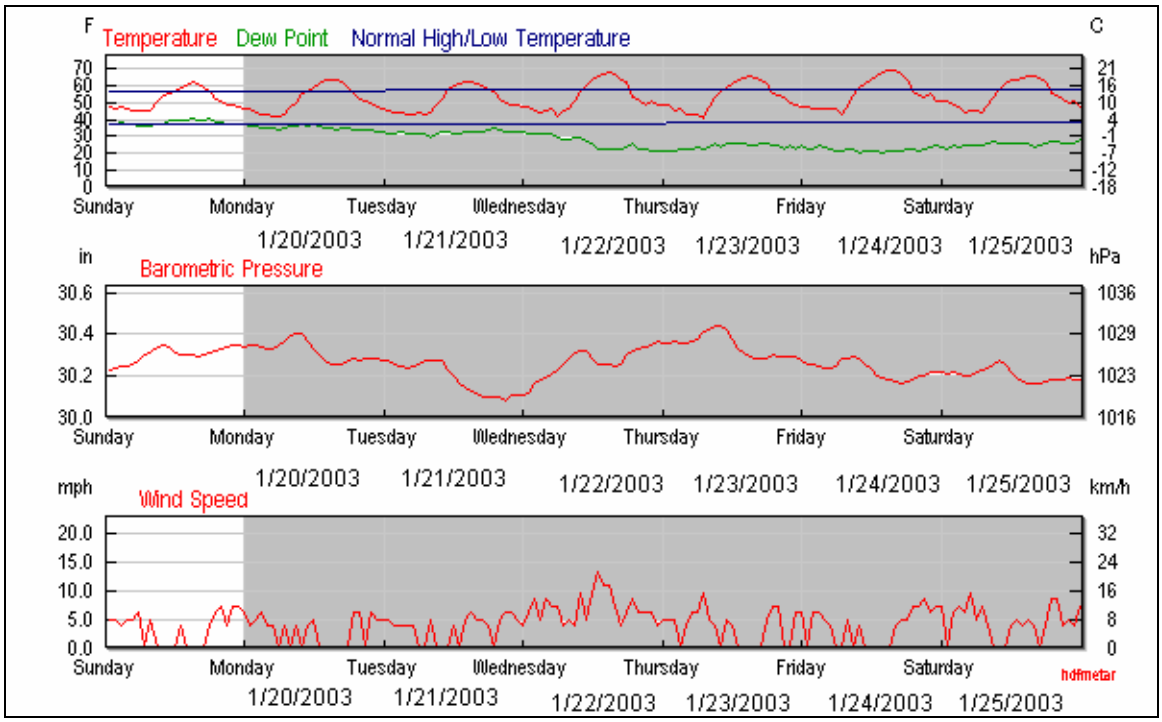

Figure 4-1 (continued).

Table 4-1. The meteorological conditions in Las Vegas Valley for ambient sample collection.

DATE	Temperature (°C)			Dew Point (°C)			Relative Humidity (%)			Pressure (hPa)			Wind Speed(km/h)	
(PST ZONE)	Max	Mean	Min	Max	Mean	Min	Max	Mean	Min	Max	Mean	Min	Max	Mean
1/3/2003	18.3	12.2	5.6	-3.9	-6.7	-7.2	40	30	19	1027	1025	1023	14.4	4.8
1/4/2003	17.2	11.1	5.0	-1.7	-3.9	-4.4	51	37	23	1026	1024	1021	14.4	4.8
1/5/2003	21.7	13.9	6.1	-0.6	-2.8	-7.2	53	37	20	1024	1019	1014	60.8	16.0
1/12/2003	16.1	11.1	6.1	3.9	2.2	1.7	71	57	42	1028	1026	1024	12.8	4.8
1/13/2003	17.2	11.1	5.0	2.2	1.7	0.0	76	55	34	1029	1027	1025	12.8	4.8
1/14/2003	16.1	10.6	5.0	1.1	-0.6	-2.2	67	50	32	1025	1022	1018	12.8	4.8
1/20/2003	16.7	11.1	5.0	-1.7	-3.9	-4.4	51	39	27	1023	1020	1018	12.8	4.8
1/21/2003	16.7	10.6	4.4	2.8	-1.1	-2.2	62	49	36	1023	1020	1018	14.4	8.0
1/22/2003	17.8	11.7	5.0	2.2	0.6	-0.6	67	52	36	1028	1025	1023	12.8	4.8
1/23/2003	17.8	12.8	7.8	2.2	1.7	-1.1	61	46	31	1025	1022	1018	16.0	4.8
1/24/2003	20.6	13.3	5.6	-1.1	-1.7	-2.8	53	37	21	1021	1020	1018	14.4	6.4
1/25/2003	22.8	15.6	7.8	1.1	-1.1	-1.7	50	38	25	1025	1022	1019	33.6	11.2

4.2 *Spatial distributions of 24-hour $PM_{2.5}$ mass and chemical compositions during the winter mini-intensive study*

4.2.1 Statistical summary of $PM_{2.5}$ mass and chemical concentrations

Table 4-2(a-d) presents averages, standard deviations, maxima, and minima for the SGS $PM_{2.5}$ chemical concentrations measured at these four sites during January 2003. Contributions to $PM_{2.5}$ mass by major chemical components by sampling day and sampling site are shown in Figure 4-2(a-d). Since the samples were collected during periods of calm wind and stagnant air conditions, the averaged concentrations were expected to be higher than the average of January 2003.

The highest $PM_{2.5}$ mass concentration was 23.58 ± 1.19 μg/m^3 at OR on 1/23/2003, 27.44 ± 1.38 μg/m^3 at JD on 1/4/2003, 19.13 ± 0.96 μg/m^3 at CC on 1/23/2003, and 28.57 ± 1.43 μg/m^3 at MS on 1/3/2003. The average $PM_{2.5}$ concentration was 17.46 ± 3.21 μg/m^3 at OR, 13.80 ± 6.36 μg/m^3 at JD, 12.55 ± 4.01 μg/m^3 at CC, and 22.54 ± 4.24 μg/m^3 at MS. The $PM_{2.5}$ mass concentrations at these four compliance monitoring sites during this study were all below the federal 24-hour National Ambient Air Quality Standard (NAAQS) standard of 65μg/m^3. At MS site, the average $PM_{2.5}$ concentration was 40% higher than the average annual $PM_{2.5}$ concentration from 7/20/00 to 7/21/01. This is due to the study design, which targeted sample collection during periods that simulated an "air pollution episode" in the valley.

The most abundant (>1 μg/m^3) chemical species in $PM_{2.5}$ were nitrate and OC and EC, the latter of which comprised more than 80% of the averaged $PM_{2.5}$ mass, except for 74% at MS. $PM_{2.5}$ OC is the single largest component of $PM_{2.5}$ mass. The average OC concentration was highest at MS (10.4 ± 1.9 μg/m^3), followed by OR (8.61 ± 1.71 μg/m^3), JD (7.48 ± 2.12 μg/m^3), and CC (7.13 ± 1.47 μg/m^3). The highest OC concentration of 13.1 ± 0.94 μg/m^3 was observed at JD on 1/4/2003. The average EC concentration was highest at MS (4.42 ± 1.02 μg/m^3), followed by OR (3.57 ± 0.88 μg/m^3), CC (3.49 ± 1.06 μg/m^3), and JD (3.23 ± 0.88 μg/m^3). The highest EC concentration of 5.88 ± 0.48μg/m^3 was observed at MS on 1/22/2003. The third-largest component in $PM_{2.5}$ is nitrate, the levels of which were similar across all four sites. The average nitrate concentrations were slightly higher at OR (1.95 ± 1.31 μg/m^3) and were lowest at JD (1.69 ± 1.15 μg/m^3). Nitrate concentrations were similar at CC (1.86 ± 1.21 μg/m^3) and MS (1.84 ± 0.9 μg/m^3).

Table 4-2(a). Statistical summary of $PM_{2.5}$ mass and chemical compositions (µg/m^3) acquired at Orr Middle School (OR) in January 2003 winter mini-intensive study.

	average	stdev	No. in average	Minimum	Maximum	Date with Maximum
Mass	17.46	3.21	12	12.44	23.58	1/23/2003
OC1 BK	0.54	0.27	12	0.23	0.90	1/20/2003
OC2 BK	0.51	0.07	12	0.41	0.61	1/13/2003
OC3 BK	0.69	0.16	12	0.48	0.91	1/13/2003
OC4 BK	0.18	0.01	12	0.16	0.20	1/13/2003
OP BK	0.09	0.04	12	0.00	0.15	1/21/2003
OC BK	2.01	0.18	12	1.68	2.26	1/22/2003
EC1 BK	0.04	0.03	12	0.00	0.08	1/23/2003
EC2 BK	0.08	0.02	12	0.05	0.12	1/23/2003
EC3 BK	0.01	0.02	12	0.00	0.05	1/25/2003
EC BK	0.04	0.05	12	0.00	0.12	1/25/2003
TC BK	2.05	0.19	12	1.68	2.29	1/20/2003
Chloride	0.07	0.02	12	0.05	0.10	1/21/2003
Nitrate	1.95	1.31	12	0.37	5.33	1/23/2003
Sulfate	0.66	0.22	12	0.45	1.02	1/23/2003
Ammonium	0.68	0.43	12	0.15	1.73	1/23/2003
Ammonia	0.06	0.01	12	0.04	0.09	1/5/2003
Soluble Potassium	0.07	0.02	12	0.05	0.14	1/4/2003
O1TC	1.17	0.42	12	0.43	1.81	1/14/2003
O2TC	1.92	0.43	12	1.22	2.47	1/3/2003
O3TC	3.61	1.05	12	2.27	5.75	1/3/2003
O4TC	1.87	0.48	12	1.34	2.88	1/3/2003
OPTC	0.04	0.08	12	0.00	0.22	1/25/2003
OCTC	8.61	1.71	12	6.10	11.94	1/3/2003
E1TC	2.96	0.85	12	1.49	4.03	1/23/2003
E2TC	0.60	0.16	12	0.38	0.98	1/13/2003
E3TC	0.05	0.04	12	0.00	0.13	1/13/2003
ECTC	3.57	0.88	12	1.82	4.66	1/23/2003
TCTC	12.18	2.37	12	7.91	16.04	1/3/2003
Sodium	0.05	0.07	12	0.00	0.25	1/3/2003
Magnesium	0.07	0.04	12	0.00	0.14	1/25/2003
Aluminum	0.07	0.02	12	0.02	0.10	1/25/2003
Silicon	0.35	0.13	12	0.15	0.63	1/5/2003
Phosphorus	0.00	0.00	12	0.00	0.00	1/4/2003
Sulfur	0.27	0.08	12	0.19	0.38	1/22/2003
Chlorine	0.04	0.02	12	0.02	0.07	1/21/2003
Potassium	0.12	0.03	12	0.09	0.20	1/4/2003
Calcium	0.67	0.26	12	0.23	1.09	1/5/2003
Titanium	0.01	0.01	12	0.00	0.02	1/5/2003
Vanadium	0.00	0.00	12	0.00	0.00	1/5/2003
Chromium	0.00	0.00	12	0.00	0.01	1/25/2003
Manganese	0.01	0.00	12	0.00	0.01	1/20/2003
Iron	0.37	0.06	12	0.23	0.46	1/24/2003
Cobalt	0.00	0.00	12	0.00	0.00	1/24/2003
Nickel	0.00	0.00	12	0.00	0.00	1/13/2003
Copper	0.01	0.00	12	0.01	0.02	1/21/2003
Zinc	0.03	0.01	12	0.01	0.04	1/3/2003
Gallium	0.00	0.00	12	0.00	0.00	1/5/2003
Arsenic	0.00	0.00	12	0.00	0.00	1/23/2003
Selenium	0.00	0.00	12	0.00	0.00	1/14/2003
Bromine	0.00	0.00	12	0.00	0.01	1/23/2003
Rubidium	0.00	0.00	12	0.00	0.00	1/21/2003
Strontium	0.01	0.01	12	0.00	0.02	1/4/2003
Yttrium	0.00	0.00	12	0.00	0.00	1/3/2003
Zirconium	0.00	0.00	12	0.00	0.00	1/4/2003
Molybdenum	0.00	0.00	12	0.00	0.00	1/14/2003
Palladium	0.00	0.00	12	0.00	0.00	1/24/2003
Silver	0.00	0.00	12	0.00	0.00	1/23/2003
Cadmium	0.00	0.00	12	0.00	0.00	1/23/2003
Indium	0.00	0.00	12	0.00	0.00	1/13/2003
Tin	0.00	0.00	12	0.00	0.00	1/21/2003
Antimony	0.00	0.00	12	0.00	0.01	1/3/2003
Barium	0.03	0.01	12	0.02	0.04	1/25/2003
Lanthanum	0.01	0.01	12	0.00	0.02	1/20/2003
Gold	0.00	0.00	12	0.00	0.00	1/3/2003
Mercury	0.00	0.00	12	0.00	0.00	1/13/2003
Thallium	0.00	0.00	12	0.00	0.00	1/3/2003
Lead	0.01	0.00	12	0.00	0.01	1/22/2003
Uranium	0.00	0.00	12	0.00	0.00	1/14/2003

Table 4-2(b). Statistical summary of $PM_{2.5}$ mass and chemical compositions (μg/m^3) acquired at J.D. Smith Elementary School (JD) in January 2003 winter mini-intensive study.

	average	stdev	No. in average	Minimum	Maximum	Date with Maximum
Mass	13.80	6.36	11	2.88	27.44	1/4/2003
OC1 BK	0.37	0.12	11	0.21	0.55	1/12/2003
OC2 BK	0.54	0.17	11	0.40	0.89	1/12/2003
OC3 BK	0.99	0.58	11	0.63	2.54	1/12/2003
OC4 BK	0.23	0.21	11	0.11	0.78	1/12/2003
OP BK	0.05	0.04	11	0.00	0.13	1/12/2003
OC BK	2.19	1.05	11	1.57	4.89	1/12/2003
EC1 BK	0.21	0.47	11	0.00	1.45	1/12/2003
EC2 BK	0.17	0.28	11	0.03	0.91	1/13/2003
EC3 BK	0.01	0.02	11	0.00	0.05	1/12/2003
EC BK	0.33	0.69	11	0.00	1.82	1/12/2003
TC BK	2.52	1.73	11	1.57	6.71	1/12/2003
Chloride	0.07	0.06	11	0.05	0.24	1/4/2003
Nitrate	1.69	1.15	11	0.26	4.39	1/4/2003
Sulfate	0.52	0.19	11	0.28	0.87	1/22/2003
Ammonium	0.64	0.36	11	0.16	1.39	1/4/2003
Ammonia	0.05	0.01	11	0.03	0.06	1/4/2003
Soluble Potassium	0.06	0.02	11	0.03	0.13	1/4/2003
O1TC	0.88	0.31	11	0.42	1.61	1/4/2003
O2TC	1.55	0.39	11	1.07	2.23	1/4/2003
O3TC	3.49	1.09	11	2.12	6.30	1/4/2003
O4TC	1.52	0.57	11	0.86	2.94	1/4/2003
OPTC	0.04	0.06	11	0.00	0.17	1/21/2003
OCTC	7.48	2.12	11	4.72	13.10	1/4/2003
E1TC	2.40	0.70	11	1.04	3.23	1/4/2003
E2TC	0.83	0.35	11	0.40	1.51	1/23/2003
E3TC	0.04	0.02	11	0.02	0.08	1/14/2003
ECTC	3.23	0.88	11	1.88	4.40	1/23/2003
TCTC	10.71	2.71	11	6.66	16.75	1/4/2003
Sodium	0.04	0.05	11	0.00	0.15	1/5/2003
Magnesium	0.06	0.03	11	0.00	0.10	1/24/2003
Aluminum	0.06	0.02	11	0.02	0.11	1/4/2003
Silicon	0.26	0.10	11	0.04	0.36	1/23/2003
Phosphorus	0.00	0.00	11	0.00	0.01	1/13/2003
Sulfur	0.20	0.08	11	0.09	0.34	1/22/2003
Chlorine	0.03	0.04	11	0.01	0.15	1/4/2003
Potassium	0.09	0.04	11	0.02	0.17	1/4/2003
Calcium	0.54	0.21	11	0.07	0.78	1/23/2003
Titanium	0.01	0.00	11	0.00	0.01	1/20/2003
Vanadium	0.00	0.00	11	0.00	0.00	1/20/2003
Chromium	0.00	0.00	11	0.00	0.01	1/25/2003
Manganese	0.00	0.00	11	0.00	0.01	1/20/2003
Iron	0.26	0.10	11	0.05	0.41	1/20/2003
Cobalt	0.00	0.00	11	0.00	0.00	1/4/2003
Nickel	0.00	0.00	11	0.00	0.00	1/5/2003
Copper	0.01	0.01	11	0.00	0.02	1/4/2003
Zinc	0.02	0.01	11	0.00	0.04	1/23/2003
Gallium	0.00	0.00	11	0.00	0.00	1/14/2003
Arsenic	0.00	0.00	11	0.00	0.00	1/20/2003
Selenium	0.00	0.00	11	0.00	0.00	1/14/2003
Bromine	0.00	0.00	11	0.00	0.00	1/4/2003
Rubidium	0.00	0.00	11	0.00	0.00	1/20/2003
Strontium	0.00	0.00	11	0.00	0.00	1/23/2003
Yttrium	0.00	0.00	11	0.00	0.00	1/5/2003
Zirconium	0.00	0.00	11	0.00	0.00	1/4/2003
Molybdenum	0.00	0.00	11	0.00	0.00	1/13/2003
Palladium	0.00	0.00	11	0.00	0.00	1/4/2003
Silver	0.00	0.00	11	0.00	0.00	1/4/2003
Cadmium	0.00	0.00	11	0.00	0.00	1/25/2003
Indium	0.00	0.00	11	0.00	0.00	1/23/2003
Tin	0.00	0.00	11	0.00	0.00	1/4/2003
Antimony	0.00	0.00	11	0.00	0.00	1/4/2003
Barium	0.02	0.01	11	0.01	0.04	1/4/2003
Lanthanum	0.00	0.01	11	0.00	0.01	1/12/2003
Gold	0.00	0.00	11	0.00	0.00	1/5/2003
Mercury	0.00	0.00	11	0.00	0.00	1/12/2003
Thallium	0.00	0.00	11	0.00	0.00	1/22/2003
Lead	0.01	0.01	11	0.00	0.02	1/4/2003
Uranium	0.00	0.00	11	0.00	0.00	1/23/2003

Table 4-2(c). Statistical summary of $PM_{2.5}$ mass and chemical compositions (μg/m^3) acquired at City Center (CC) in January 2003 winter mini-intensive study.

	average	stdev	No. in average	Minimum	Maximum	Date with Maximum
Mass	12.55	4.01	12	4.36	19.13	1/23/2003
OC1 BK	0.49	0.12	12	0.38	0.73	1/23/2003
OC2 BK	0.42	0.05	12	0.33	0.51	1/22/2003
OC3 BK	0.66	0.14	12	0.43	0.88	1/22/2003
OC4 BK	0.17	0.03	12	0.12	0.21	1/3/2003
OP BK	0.04	0.03	12	0.00	0.09	1/22/2003
OC BK	1.76	0.25	12	1.43	2.23	1/20/2003
EC1 BK	0.03	0.02	12	0.00	0.09	1/23/2003
EC2 BK	0.05	0.02	12	0.03	0.10	1/22/2003
EC3 BK	0.00	0.01	12	0.00	0.02	1/22/2003
EC BK	0.04	0.04	12	0.00	0.15	1/23/2003
TC BK	1.81	0.26	12	1.46	2.26	1/20/2003
Chloride	0.06	0.01	12	0.04	0.08	1/5/2003
Nitrate	1.86	1.21	12	0.22	4.31	1/23/2003
Sulfate	0.49	0.21	12	0.22	0.82	1/22/2003
Ammonium	0.72	0.40	12	0.16	1.50	1/23/2003
Ammonia	0.03	0.00	12	0.02	0.04	1/23/2003
Soluble Potassium	0.06	0.01	12	0.03	0.08	1/12/2003
O1TC	1.30	0.33	12	0.76	1.94	1/23/2003
O2TC	1.33	0.32	12	0.77	1.89	1/23/2003
O3TC	3.00	0.83	12	1.28	3.92	1/3/2003
O4TC	1.31	0.54	12	0.61	2.80	1/22/2003
OPTC	0.19	0.12	12	0.00	0.38	1/12/2003
OCTC	7.13	1.47	12	4.17	9.06	1/22/2003
E1TC	2.62	0.90	12	0.84	4.09	1/23/2003
E2TC	1.02	0.37	12	0.63	1.95	1/22/2003
E3TC	0.04	0.01	12	0.02	0.06	1/24/2003
ECTC	3.49	1.06	12	1.48	5.00	1/23/2003
TCTC	10.63	2.45	12	5.65	13.30	1/3/2003
Sodium	0.02	0.03	12	0.00	0.07	1/13/2003
Magnesium	0.04	0.02	12	0.00	0.08	1/5/2003
Aluminum	0.03	0.01	12	0.02	0.04	1/20/2003
Silicon	0.13	0.04	12	0.06	0.19	1/3/2003
Phosphorus	0.00	0.00	12	0.00	0.00	1/20/2003
Sulfur	0.19	0.08	12	0.09	0.31	1/23/2003
Chlorine	0.02	0.01	12	0.00	0.04	1/3/2003
Potassium	0.08	0.02	12	0.04	0.10	1/3/2003
Calcium	0.26	0.09	12	0.10	0.42	1/3/2003
Titanium	0.00	0.00	12	0.00	0.01	1/4/2003
Vanadium	0.00	0.00	12	0.00	0.00	1/4/2003
Chromium	0.00	0.00	12	0.00	0.00	1/25/2003
Manganese	0.00	0.00	12	0.00	0.01	1/14/2003
Iron	0.19	0.05	12	0.10	0.29	1/3/2003
Cobalt	0.00	0.00	12	0.00	0.00	1/3/2003
Nickel	0.00	0.00	12	0.00	0.00	1/14/2003
Copper	0.01	0.00	12	0.00	0.01	1/3/2003
Zinc	0.02	0.01	12	0.01	0.03	1/23/2003
Gallium	0.00	0.00	12	0.00	0.00	1/3/2003
Arsenic	0.00	0.00	12	0.00	0.00	1/12/2003
Selenium	0.00	0.00	12	0.00	0.00	1/22/2003
Bromine	0.00	0.00	12	0.00	0.01	1/23/2003
Rubidium	0.00	0.00	12	0.00	0.00	1/4/2003
Strontium	0.00	0.00	12	0.00	0.01	1/3/2003
Yttrium	0.00	0.00	12	0.00	0.00	1/13/2003
Zirconium	0.00	0.00	12	0.00	0.00	1/3/2003
Molybdenum	0.00	0.00	12	0.00	0.00	1/3/2003
Palladium	0.00	0.00	12	0.00	0.00	1/21/2003
Silver	0.00	0.00	12	0.00	0.00	1/20/2003
Cadmium	0.00	0.00	12	0.00	0.00	1/20/2003
Indium	0.00	0.00	12	0.00	0.00	1/25/2003
Tin	0.00	0.00	12	0.00	0.00	1/21/2003
Antimony	0.00	0.00	12	0.00	0.01	1/3/2003
Barium	0.02	0.01	12	0.01	0.03	1/3/2003
Lanthanum	0.00	0.00	12	0.00	0.01	1/21/2003
Gold	0.00	0.00	12	0.00	0.00	1/5/2003
Mercury	0.00	0.00	12	0.00	0.00	1/20/2003
Thallium	0.00	0.00	12	0.00	0.00	1/5/2003
Lead	0.00	0.00	12	0.00	0.01	1/23/2003
Uranium	0.00	0.00	12	0.00	0.00	1/5/2003

Table 4-2(d). Statistical summary of $PM_{2.5}$ mass and chemical compositions ($\mu g/m^3$) acquired at East Charleston (MS) in the January 2003 winter mini-intensive study.

	average	stdev	No. in average	Minimum	Maximum	Date with Maximum
Mass	22.54	4.24	11	13.22	28.57	1/3/2003
OC1 BK	0.70	0.20	11	0.45	0.98	1/21/2003
OC2 BK	0.46	0.07	11	0.29	0.56	1/23/2003
OC3 BK	0.70	0.21	11	0.48	1.11	1/23/2003
OC4 BK	0.20	0.03	11	0.16	0.27	1/13/2003
OP BK	0.05	0.05	11	0.00	0.13	1/22/2003
OC BK	2.10	0.26	11	1.56	2.41	1/23/2003
EC1 BK	0.07	0.05	11	0.01	0.13	1/12/2003
EC2 BK	0.10	0.03	11	0.06	0.15	1/13/2003
EC3 BK	0.01	0.01	11	0.00	0.02	1/13/2003
EC BK	0.13	0.11	11	0.00	0.30	1/13/2003
TC BK	2.23	0.26	11	1.69	2.71	1/13/2003
Chloride	0.09	0.03	11	0.06	0.17	1/3/2003
Nitrate	1.84	0.90	11	0.44	3.96	1/23/2003
Sulfate	0.71	0.19	11	0.46	1.05	1/22/2003
Ammonium	0.65	0.31	11	0.20	1.34	1/23/2003
Ammonia	0.08	0.02	11	0.05	0.10	1/4/2003
Soluble Potassium	0.13	0.03	11	0.07	0.18	1/4/2003
O1TC	1.81	0.44	11	0.70	2.34	1/13/2003
O2TC	2.15	0.46	11	1.31	2.84	1/13/2003
O3TC	4.23	1.04	11	3.49	6.82	1/3/2003
O4TC	2.16	0.57	11	1.47	3.49	1/3/2003
OPTC	0.05	0.11	11	0.00	0.34	1/12/2003
OCTC	10.40	1.90	11	7.07	14.84	1/3/2003
E1TC	3.96	0.97	11	1.73	5.20	1/13/2003
E2TC	0.48	0.12	11	0.23	0.68	1/22/2003
E3TC	0.04	0.01	11	0.00	0.05	1/21/2003
ECTC	4.42	1.02	11	2.30	5.88	1/22/2003
TCTC	14.82	2.49	11	9.37	19.21	1/3/2003
Sodium	0.03	0.05	11	0.00	0.15	1/14/2003
Magnesium	0.11	0.03	11	0.06	0.16	1/3/2003
Aluminum	0.08	0.02	11	0.05	0.12	1/3/2003
Silicon	0.48	0.14	11	0.23	0.67	1/3/2003
Phosphorus	0.00	0.00	11	0.00	0.01	1/20/2003
Sulfur	0.28	0.08	11	0.18	0.40	1/22/2003
Chlorine	0.06	0.03	11	0.04	0.13	1/3/2003
Potassium	0.19	0.04	11	0.14	0.26	1/4/2003
Calcium	0.96	0.33	11	0.38	1.41	1/3/2003
Titanium	0.01	0.00	11	0.00	0.02	1/3/2003
Vanadium	0.00	0.00	11	0.00	0.00	1/12/2003
Chromium	0.01	0.01	11	0.00	0.03	1/25/2003
Manganese	0.01	0.00	11	0.00	0.01	1/20/2003
Iron	0.48	0.12	11	0.29	0.71	1/20/2003
Cobalt	0.00	0.00	11	0.00	0.00	1/20/2003
Nickel	0.00	0.00	11	0.00	0.00	1/20/2003
Copper	0.01	0.01	11	0.01	0.02	1/20/2003
Zinc	0.03	0.01	11	0.02	0.05	1/3/2003
Gallium	0.00	0.00	11	0.00	0.00	1/12/2003
Arsenic	0.00	0.00	11	0.00	0.00	1/20/2003
Selenium	0.00	0.00	11	0.00	0.00	1/12/2003
Bromine	0.00	0.00	11	0.00	0.01	1/23/2003
Rubidium	0.00	0.00	11	0.00	0.00	1/4/2003
Strontium	0.01	0.00	11	0.00	0.01	1/24/2003
Yttrium	0.00	0.00	11	0.00	0.00	1/13/2003
Zirconium	0.00	0.00	11	0.00	0.00	1/3/2003
Molybdenum	0.00	0.00	11	0.00	0.00	1/3/2003
Palladium	0.00	0.00	11	0.00	0.00	1/24/2003
Silver	0.00	0.00	11	0.00	0.00	1/21/2003
Cadmium	0.00	0.00	11	0.00	0.00	1/21/2003
Indium	0.00	0.00	11	0.00	0.00	1/14/2003
Tin	0.00	0.00	11	0.00	0.00	1/3/2003
Antimony	0.00	0.00	11	0.00	0.01	1/3/2003
Barium	0.04	0.01	11	0.02	0.06	1/20/2003
Lanthanum	0.01	0.00	11	0.00	0.01	1/25/2003
Gold	0.00	0.00	11	0.00	0.00	1/25/2003
Mercury	0.00	0.00	11	0.00	0.00	1/12/2003
Thallium	0.00	0.00	11	0.00	0.00	1/21/2003
Lead	0.01	0.00	11	0.00	0.01	1/3/2003
Uranium	0.00	0.00	11	0.00	0.00	1/24/2003

4.3 *Spatial Variation of $PM_{2.5}$ Mass and Chemical Compositions*

Figure 4-2(a-d) shows the day-by-day contributions of each major components to $PM_{2.5}$ at each site. Figure 4-3(a-d) shows the fractional contribution of each major chemical components each day to $PM_{2.5}$. The daily $PM_{2.5}$ concentration at MS was the highest among all four sites, except that the $PM_{2.5}$ concentration was highest at JD on 1/4/2003. The daily $PM_{2.5}$ mass concentrations were similar in CC and JD and were generally lower among the four sites. $PM_{2.5}$ concentration at MS was 5% to 25% higher than OR and was 20% to 50% higher than CC and JD. Similar spatial trend is found for organic matter and EC. Geological material concentration at MS is found to be 2.5 to 3.5 times higher than in CC, which suggests that contribution from geological material to $PM_{2.5}$ is more local impact.

Comparing the relative contribution of chemical species at each location (Figure 4-4) shows that total carbonaceous compounds (OM + EC) have the highest contribution to $PM_{2.5}$ mass in CC, and are relatively consistent from day to day. Geological material has the least contribution to $PM_{2.5}$ mass at CC than at the other three sites. This suggests that $PM_{2.5}$ concentration at CC is more dominated by emission sources with carbonaceous compounds than at other three sites.

4.3.1 Spatial distribution of EC to OC ratios

The EC/OC ratios at the ambient samples can be used to evaluate the impact of various sources. Diesel engine exhaust has a higher EC/OC ratio (usually greater than 1), which is significantly different from other sources, including wood burning, gasoline exhaust, road dust, vegetative detritus, and coal combustion. Fuel oil is an exception. The EC concentration alone implicates the importance of diesel when other sources are insignificant. The average 24-hour EC/OC ratios in Figure 4-4 are usually less than 0.5. The largest averaged EC/OC ratio was found to be 0.49 at CC, and the daily EC/OC ratio is generally higher than at the other tree sites. This observation agrees with the fact that CC is close to the freeway and is affected by diesel vehicles.

a)

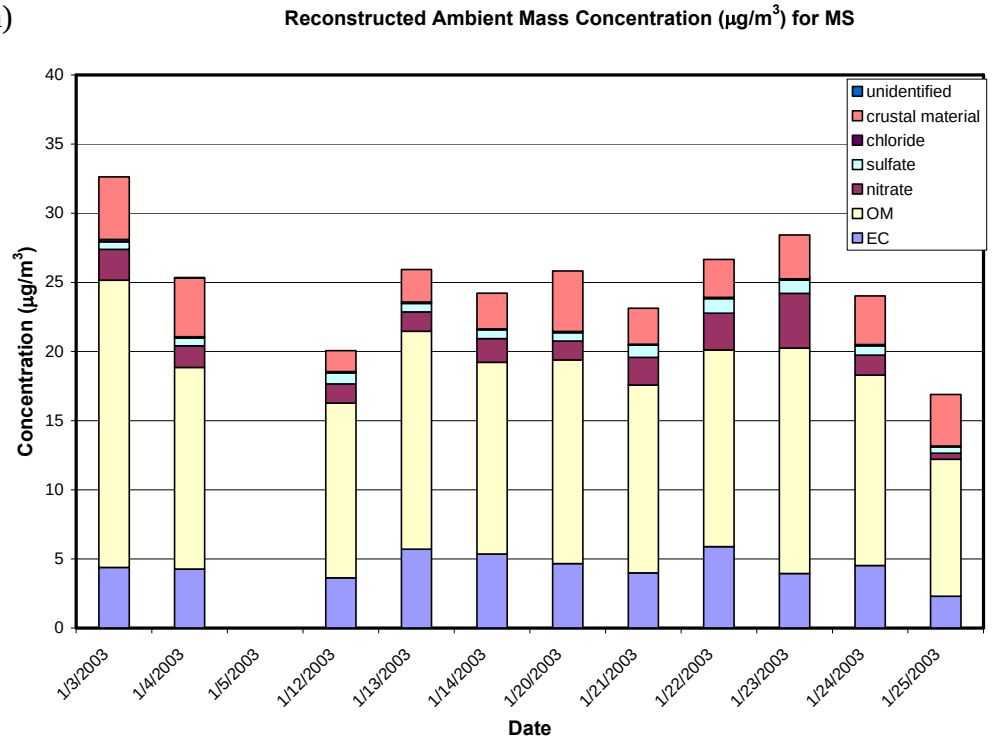
Reconstructed Ambient Mass Concentration (µg/m3) for MS
unidentified
crustal material
chloride
sulfate
nitrate
OM
EC
Concentration (µg/m3)
0
5
10
15
20
25
30
35
40
1/3/2003
1/4/2003
1/5/2003
1/12/2003
1/13/2003
1/14/2003
1/20/2003
1/21/2003
1/22/2003
1/23/2003
1/24/2003
1/25/2003
Date

b)

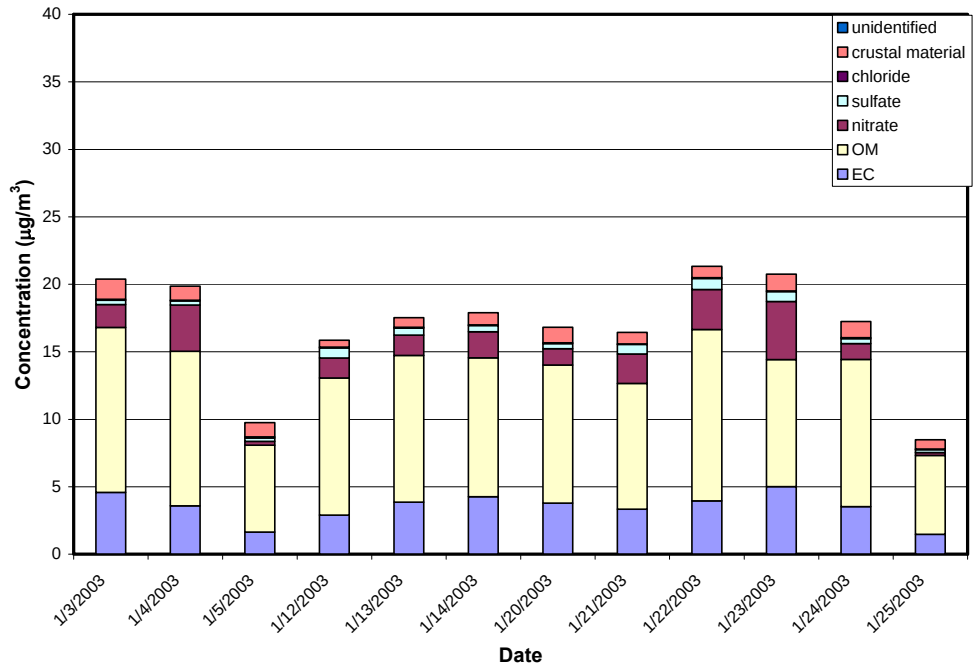
Reconstructed Ambient Mass Concentration (µg/m3) for CC
unidentified
crustal material
chloride
sulfate
nitrate
OM
EC
Concentration (µg/m3)
0
5
10
15
20
25
30
35
40
1/3/2003
1/4/2003
1/5/2003
1/12/2003
1/13/2003
1/14/2003
1/20/2003
1/21/2003
1/22/2003
1/23/2003
1/24/2003
1/25/2003
Date

c)

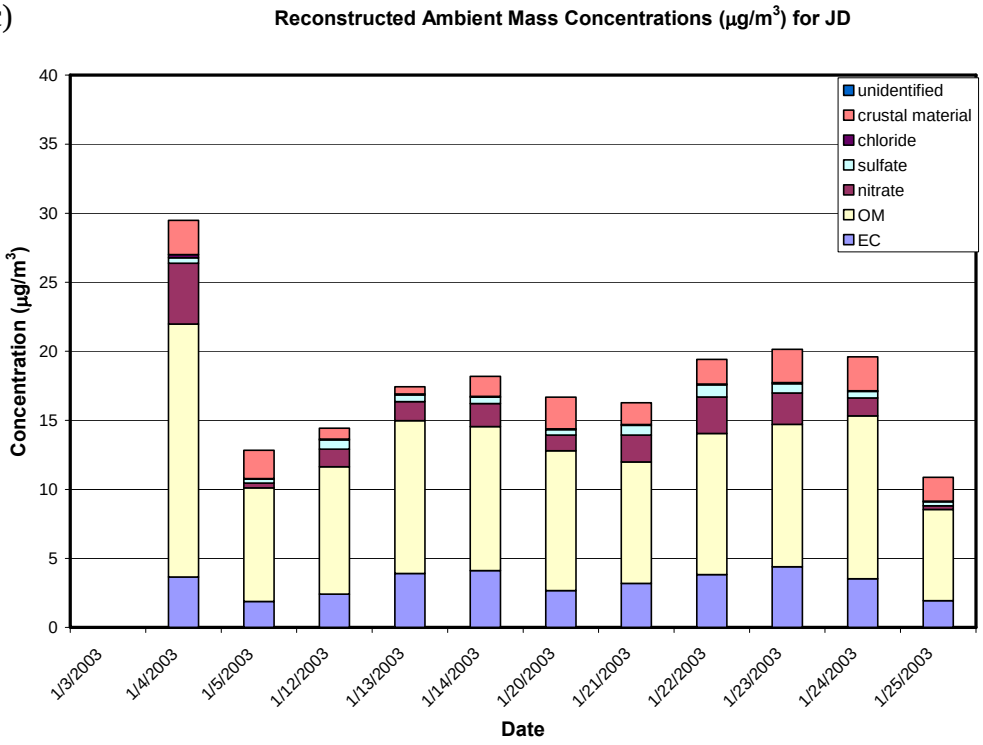

d)

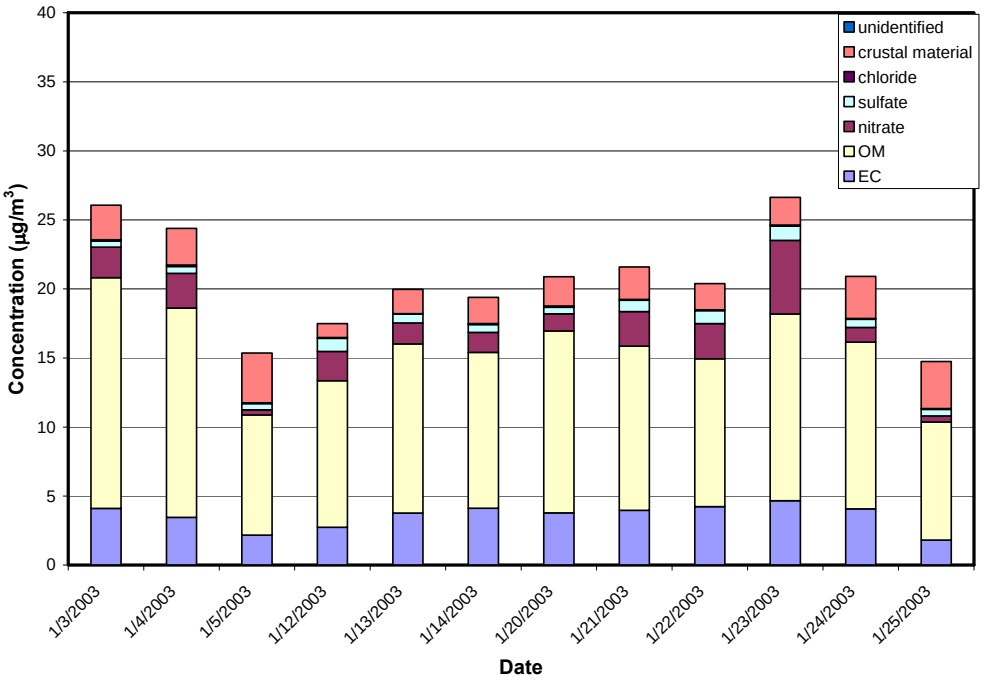

Figure 4-2. Time series plots of contribution of each major chemical components to reconstructed $PM_{2.5}$ mass at a) East Charleston (MS), b) City Center (CC), c) J.D. Smith School (JD), and d) Orr Middle School (OR).

a)

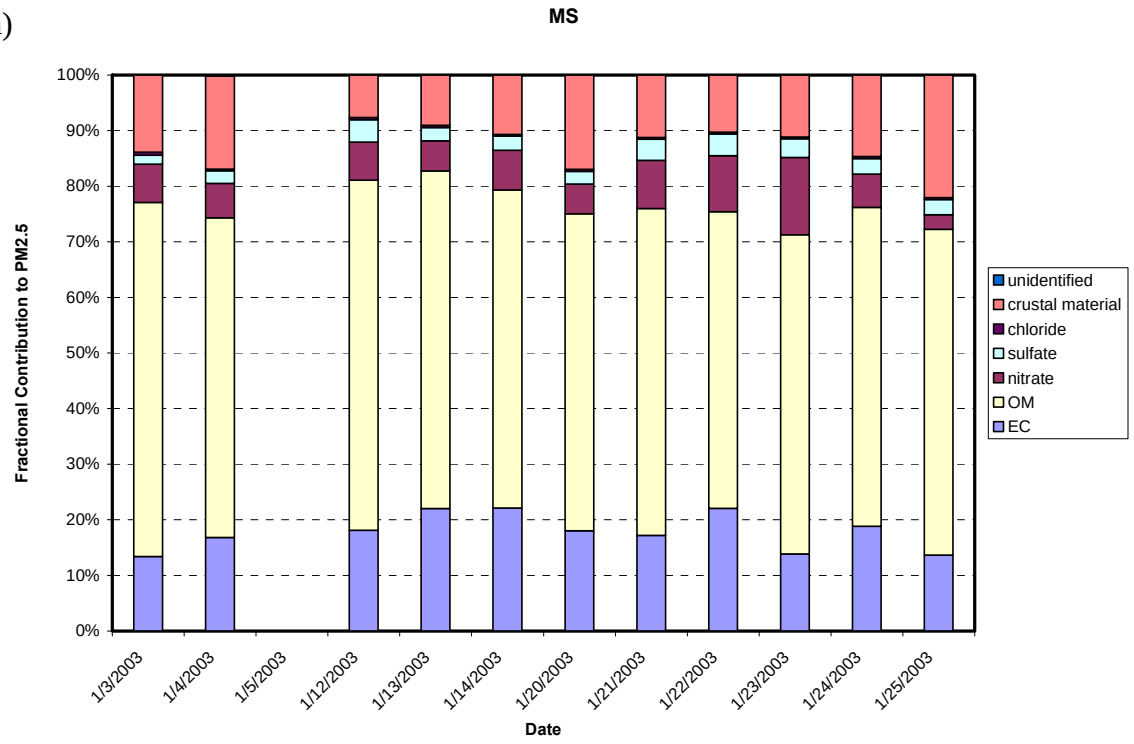
MS
Fractional Contribution to PM2.5
100%
90%
80%
70%
60%
50%
40%
30%
20%
10%
0%
1/3/2003
1/4/2003
1/5/2003
1/12/2003
1/13/2003
1/14/2003
1/20/2003
1/21/2003
1/22/2003
1/23/2003
1/24/2003
1/25/2003
Date
unidentified
crustal material
chloride
sulfate
nitrate
OM
EC

b)

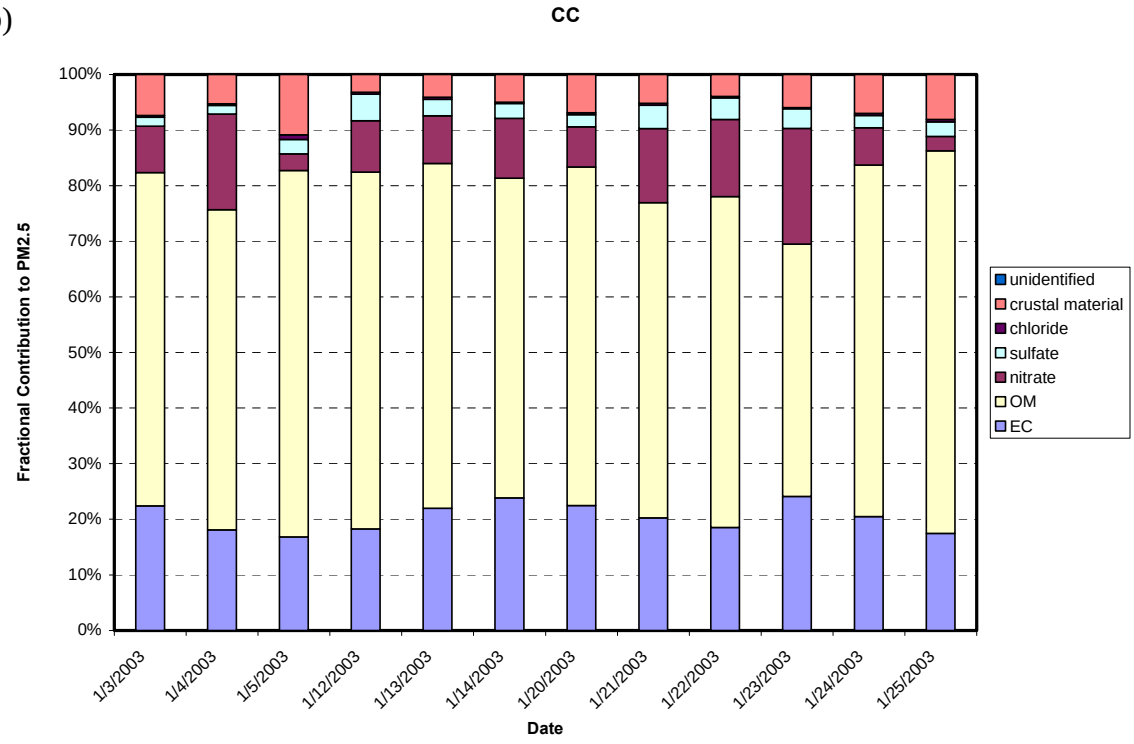
CC
Fractional Contribution to PM2.5
100%
90%
80%
70%
60%
50%
40%
30%
20%
10%
0%
1/3/2003
1/4/2003
1/5/2003
1/12/2003
1/13/2003
1/14/2003
1/20/2003
1/21/2003
1/22/2003
1/23/2003
1/24/2003
1/25/2003
Date
unidentified
crustal material
chloride
sulfate
nitrate
OM
EC

c)

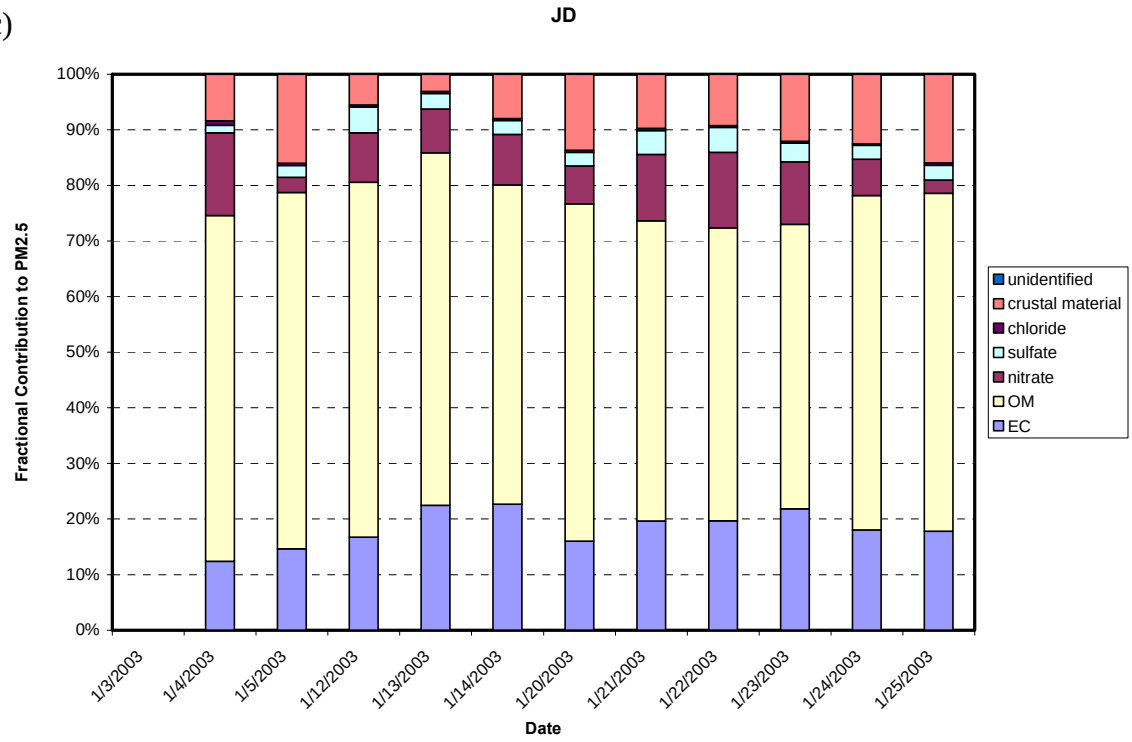

d)

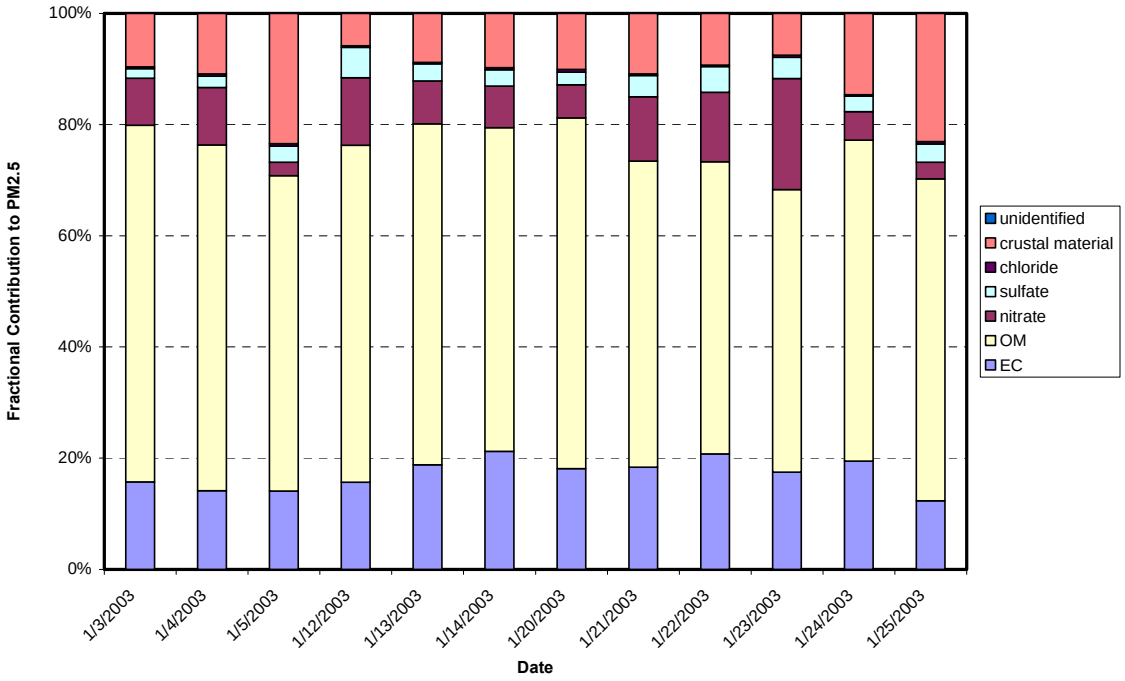

Figure 4-3. Time series plots of fractional contribution of each major chemical components to $PM_{2.5}$ mass a) East Charleston (MS); b) City Center (CC), c) J.D. Smith School (JD), and d) Orr School (OR).

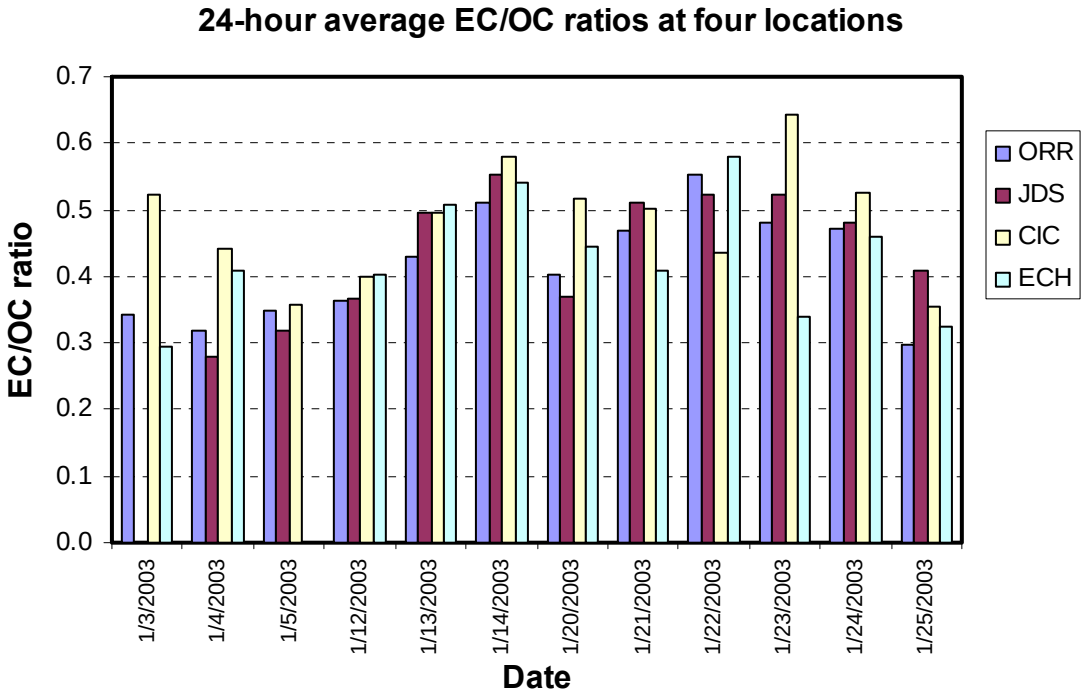

Figure 4-4. Twenty-four-hour average EC/OC ratio for winter intensive study at four locations.

The ratios of hopanes (H) + steranes (S) to OC implicate the relative importance of automobile emissions to OC. In addition, it has been found that diesel-powered and gasoline-powered vehicles emit H + S and EC in different rates. Gasoline-powered vehicles are an important source of H + S but are minor contributors to EC, while diesel-powered vehicles are an important source of both EC and H + S. The daily median (H + S) to OC ratios and (H + S) to EC ratios are shown in Figure 4-5(a-b), in which the error bars are the 5th and 95th percentiles of the calculated ratios during the study for each location. Although the median H + S to OC and H + S to EC ratios were higher at JD and CC than at OR and MS, the range of the ratios for each location suggests little difference among these sites. Carbonaceous emissions are probably contributed by local motor vehicles.

(a) H+S to OC ratios

(b) H+S to EC ratios

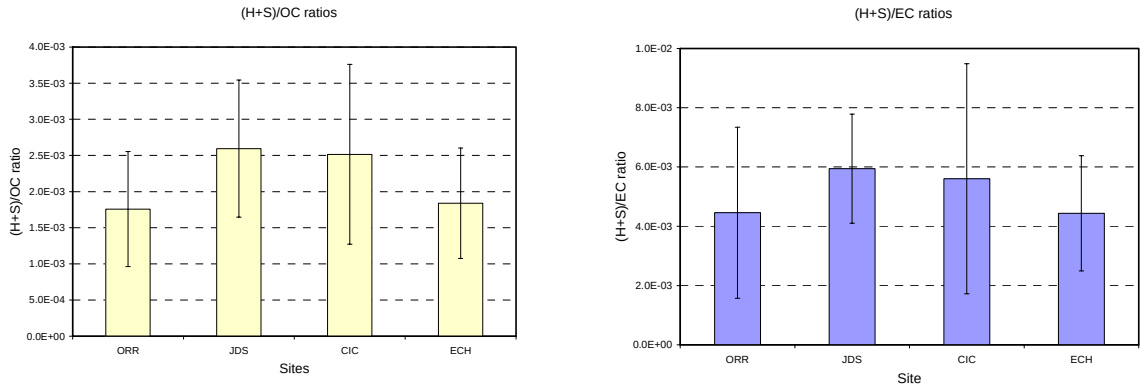

Figure 4-5. H + S to EC and H + S to OC ratios for the four sites during the winter intensive study.

4.4 *Spatial Variations Organic Tracers in Ambient Winter Intensive Study*

Organic tracers that are often used to identify different emissions source are PAHs, hopanes and steranes, levoglucosan, and cholesterol. PAHs are the products of incomplete combustion from variable sources, such as fossil fuel combustion and biomass burning. Hopanes (H) and steranes (S) can be used as molecular tracers for the fine PM emitted from motor vehicles. They can be found in diesel fuel, and are present in the lubricating oil used by both diesel-powered and gasoline-powered motor vehicles (Cass, 1998). Levoglucosan is a major constituent and is well accepted as a marker of the fine particle emissions from cellulose during biomass burning (Simoneit et al., 1999). Cholesterol usually results from meat cooking. The range of concentrations for total PAHs, H + S, levoglucosan, and cholesterol measured are listed in Table 4-2 and the spatial distributions by sample and site are in Figure 4-6.

Table 4-3. Concentrations of total PAH, total hopanes (H) + steranes (S), and total polar species measured during January 2003.

Site		Total Polar (µg/m3)	Total Hopanes and Steranes (µg/m3)	Total PAH (µg/m3)	Levoglucosan (ng/m3)	Cholesterol (ng/m3)
	average	1.88E+00	1.43E-02	3.63E+00	1.21E+02	1.39E+01
	standard deviation	1.16E+00	4.05E-03	1.36E+00	9.97E+01	1.04E+01
ORR	minimum	3.69E-01	9.52E-03	1.94E+00	0.00E+00	1.89E+00
	maximum	3.61E+00	2.44E-02	6.43E+00	3.00E+02	3.69E+01
	date of maximum	1/4/2003	1/25/2003	1/13/2003	1/4/2003	1/20/2003
	average	1.83E+00	1.86E-02	4.63E+00	2.53E+02	1.28E+01
	standard deviation	8.30E-01	6.68E-03	1.96E+00	1.89E+02	8.76E+00
JDS	minimum	6.47E-01	1.10E-02	2.41E+00	3.71E+00	2.08E+00
	maximum	3.64E+00	3.39E-02	8.90E+00	5.98E+02	2.89E+01
	date of maximum	1/4/2003	1/24/2003	1/24/2003	1/4/2003	1/22/2003
	average	1.97E+00	1.68E-02	3.44E+00	1.14E+02	1.99E+01
	standard deviation	6.01E-01	4.45E-03	1.54E+00	1.21E+02	3.16E+01
CIC	minimum	7.19E-01	1.13E-02	1.55E+00	0.00E+00	1.97E+00
	maximum	2.61E+00	2.57E-02	6.33E+00	3.24E+02	1.02E+02
	date of maximum	1/23/2003	1/25/2003	1/3/2003	1/12/2003	1/21/2003
	average	2.91E+00	2.07E-02	5.86E+00	3.16E+02	1.61E+01
	standard deviation	1.28E+00	4.56E-03	2.61E+00	3.38E+02	8.29E+00
ECH	minimum	8.44E-01	1.58E-02	2.78E+00	0.00E+00	1.99E+00
	maximum	4.86E+00	2.96E-02	1.03E+01	1.06E+03	2.76E+01
	date of maximum	1/4/2003	1/22/2003	1/3/2003	1/4/2003	1/23/2003

4.5 *Organic Tracers*

4.5.1 Polar, hopanes and steranes, and PAHs

The highest average organic tracer concentrations were at MS with 2.91 ± 1.28 µg/m^3 for polar species, $2.07*10^{-2} \pm 4.56*10^{-3}$ µg/m^3 for hopanes and steranes, and 5.86 ± 2.61 µg/m^3 for PAHs. The fact that average organic tracer concentrations are higher at MS than at the three other sites suggests that MS is slightly more impacted by motor vehicle exhausts. The average H + S concentrations measured were $1.86*10^{-2} \pm 6.68*10^{-3}$ µg/m^3 for JD, $1.68*10^{-2} \pm 4.56*10^{-3}$ µg/m^3 for CC, and $1.43*10^{-2} \pm 4.05*10^{-3}$ µg/m^3 for OR.

a)

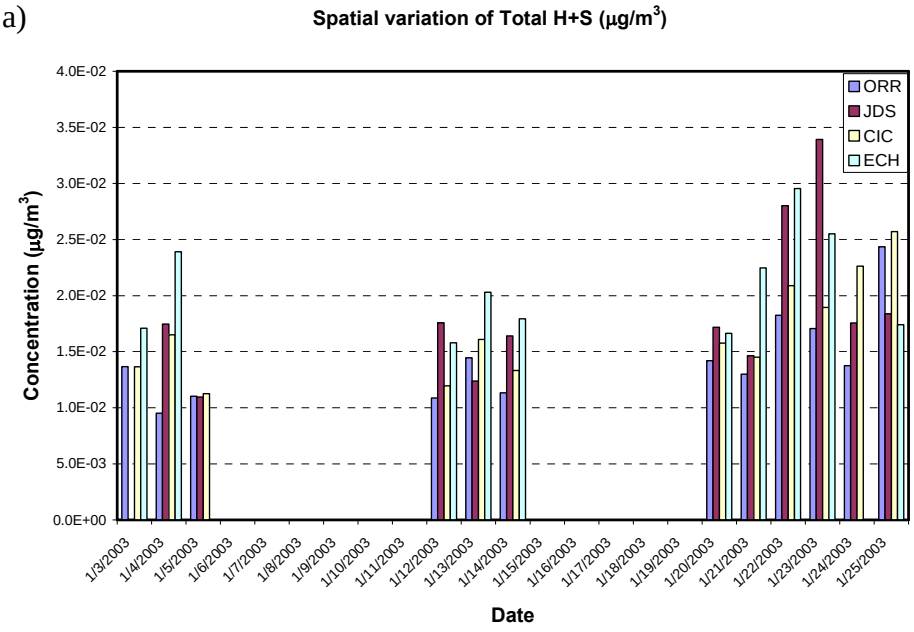

b)

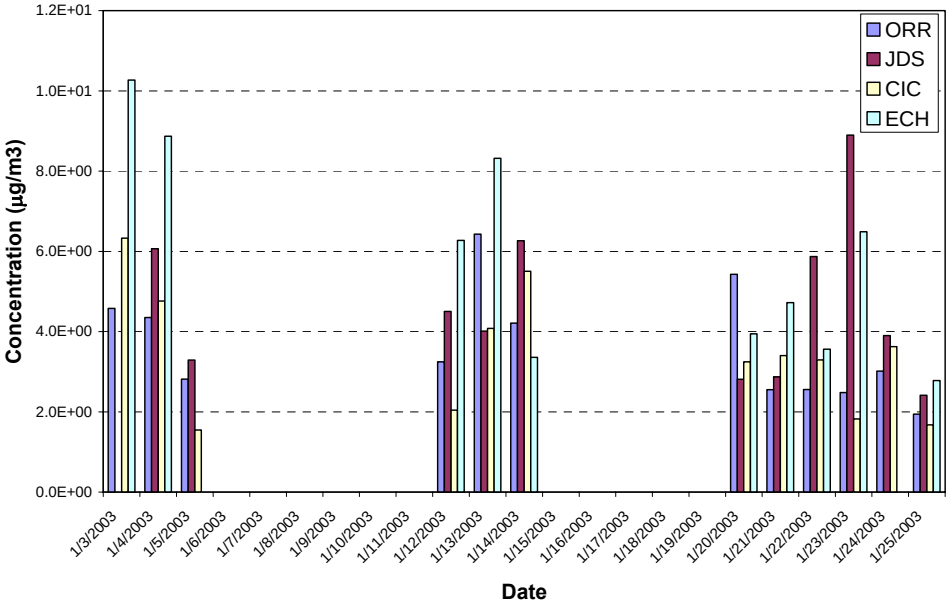

Figure 4-6. Spatial distributions of a) hopanes (H) + steranes (S), and b) polycyclic aromatic hydrocarbon (PAH) concentrations at the four sites during the winter intensive study of January 2003.

4.5.2 Levoglucosan and cholesterol

Levoglucosan is widely used as the major tracer for PM emissions from biomass burning (Simoneit et al, 1999). The distribution of levoglucosan during the winter study is shown in Figure 4-7. The concentrations of levoglucosan range from 80 ng/m^3 to 600 ng/m^3. Higher concentrations of 200–1,060 ng/m^3 were observed at MS. The average levoglucosan concentrations were 121 ± 97 ng/m^3 at OR, 253 ± 189 ng/m^3 at JD, 114 ± 121 ng/m^3 at CC, and 316 ± 338 ng/m^3 at MS.

Cholesterol is the tracer for PM emissions from meat cooking. As shown in Figure 4-7(b), no spatial pattern was observed among these four sites, although the highest cholesterol concentration of $1.02*10^2$ ng/m^3 was observed at CC.

a)

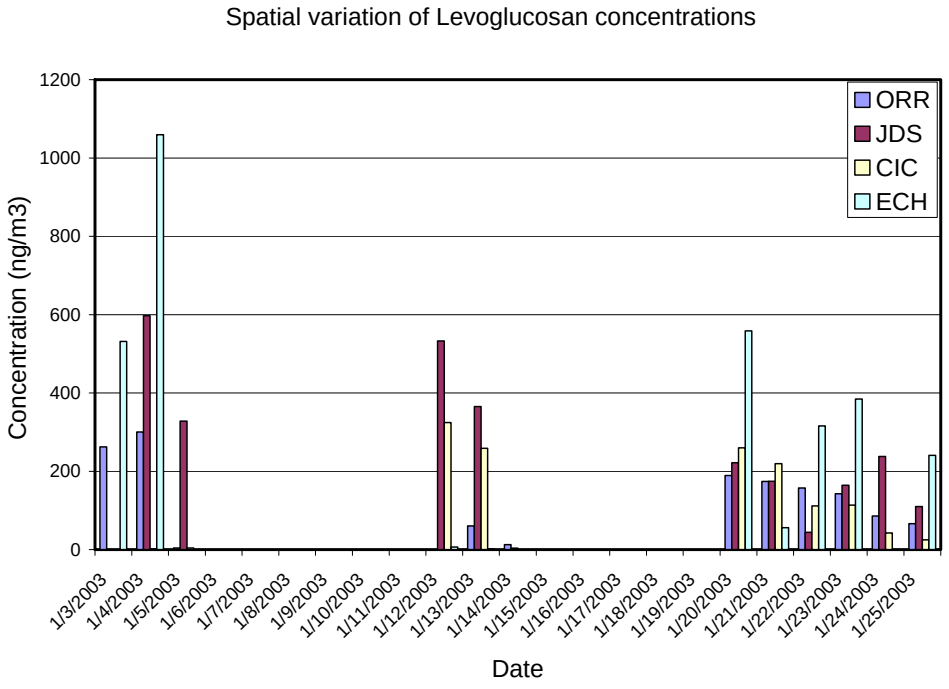

b)

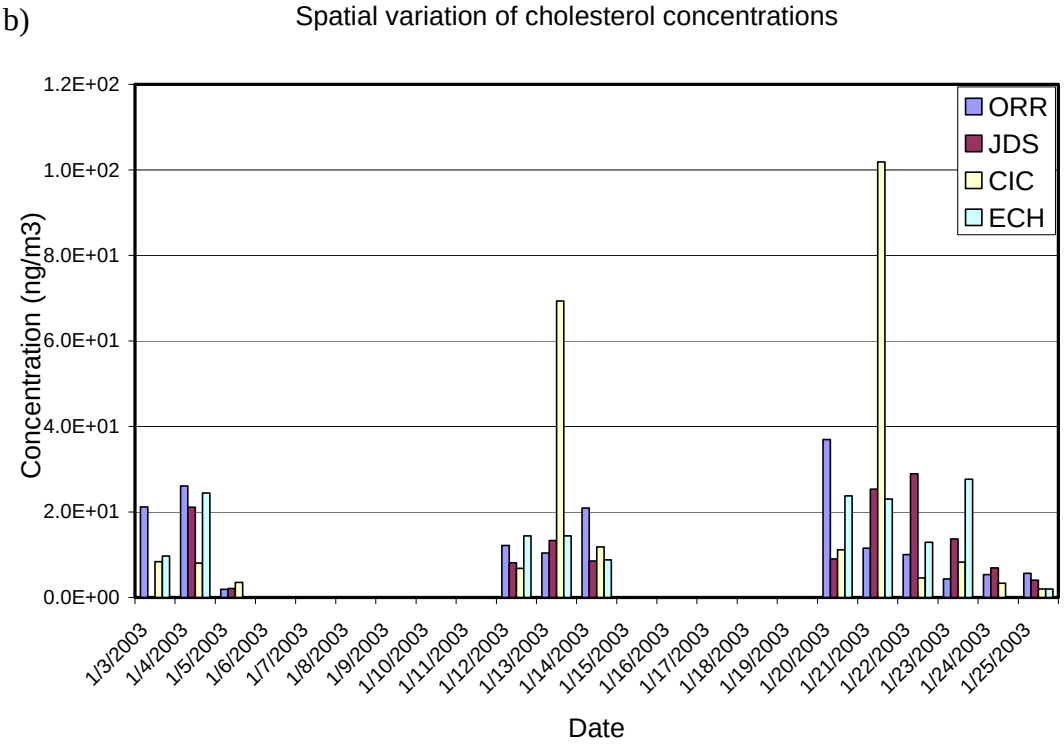

Figure 4-7. Spatial distributions of a) Levoglucosan, and b) cholesterol concentrations at the four sites during the winter intensive study of January 2003.

4.6 *Continuous Ambient Data*

4.6.1 Comparison of aethalometer derived EC concentrations at three sites

Time series plots of hourly averaged aethalometer-derived EC concentrations for the MS, JD, and CC sites are shown in Figure 4-8. The three sites track closely in diurnal and day-to-day patterns.

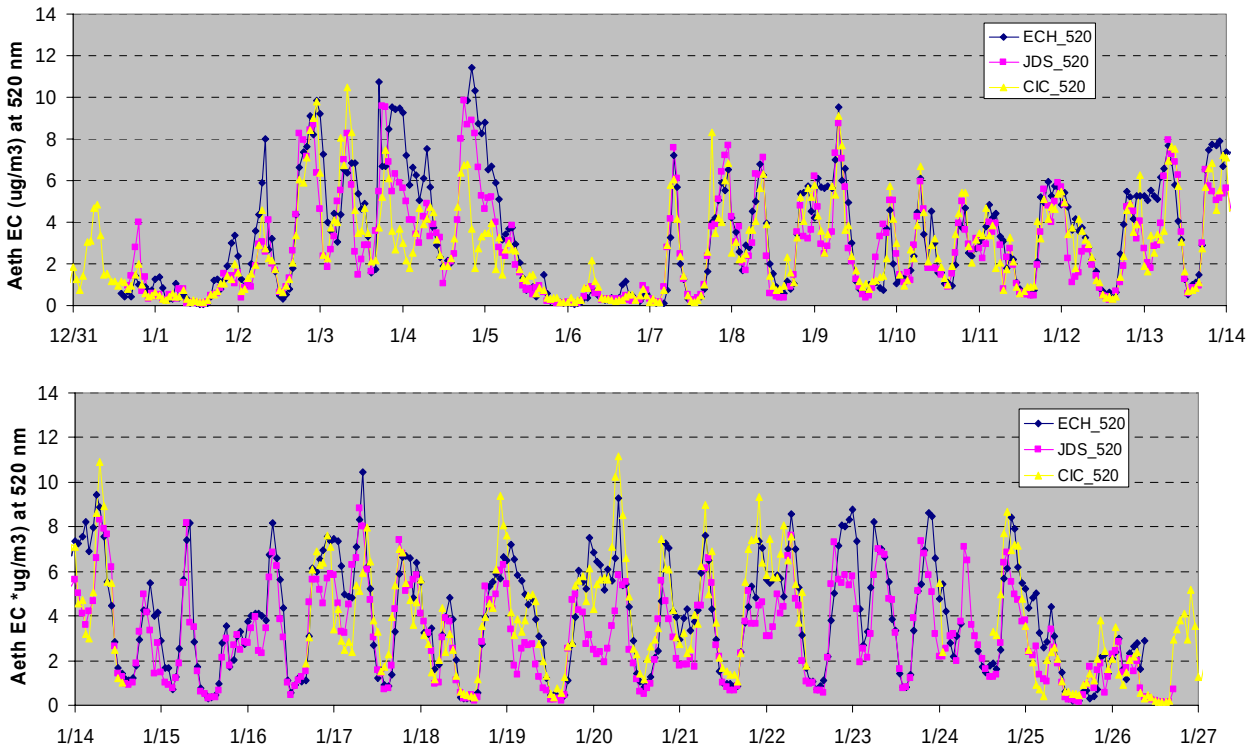

Figure 4-8. Diurnal pattern of aethelometer-derived EC at East Charleston (MS), J.D. Smith Elementary School (JD), and City Center (CC) in January 2003.

Figure 4-9 shows the average diurnal pattern in aethalometer-derived EC at each site for the days that all three sites had complete data. All sites have a pronounced peak for the 7–8 a.m. averaging period and a broad minimum from about noon to 5 p.m. coinciding with a period of maximum mixing. All sites have increasing concentrations in early evening as emissions increase and the mixed layer rapidly decreases after sunset. Concentrations peak at JD and CC about 7–8 p.m., but continue to rise at the MS site through 8–9 p.m. Concentrations at all sites are flat until about midnight, when they begin to decline. The concentrations decline more slowly at MS and the decline is from a higher level; thus EC concentration at the MS site from about 8 p.m. to 5 a.m. is significantly higher than at the other sites. This EC concentration at MS might be explained by more residential wood combustion and contributions from cooking in winter due to the higher population there. The higher BC concentration at CC, in relation to JD, suggests the transportation of BC from US-95.

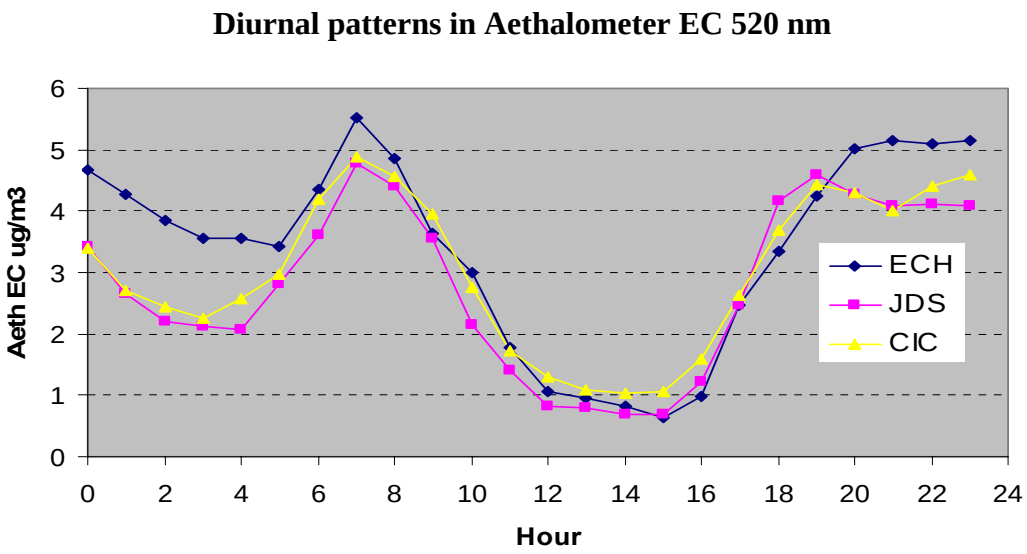

Figure 4-9. Diurnal patterns in aethalometer-derived EC concentrations (µg/m^3) at 520 nm for East Charleston (MS), J.D. Smith Elementary School (JD), and City Center (CC) in January 2003.

Figures 4-10(a-c) are scatterplots of hourly averaged EC concentrations for the three sites. JD and MS are the most highly correlated, with an r^2 of 0.75. The square correlation coefficient or the MS/CC pair is 0.60, and for JD and CC, 0.66. The higher nighttime concentrations at MS show up in the slope of the regression line, which is 0.83 for CC/MS and 0.79 for JD/MS. The slope for the CC/JD pair is essentially 1. This may be explained by the fact that JD is downwind from the CC site, where southwesterly prevailing winds transport vehicle emissions from US-95.

a)

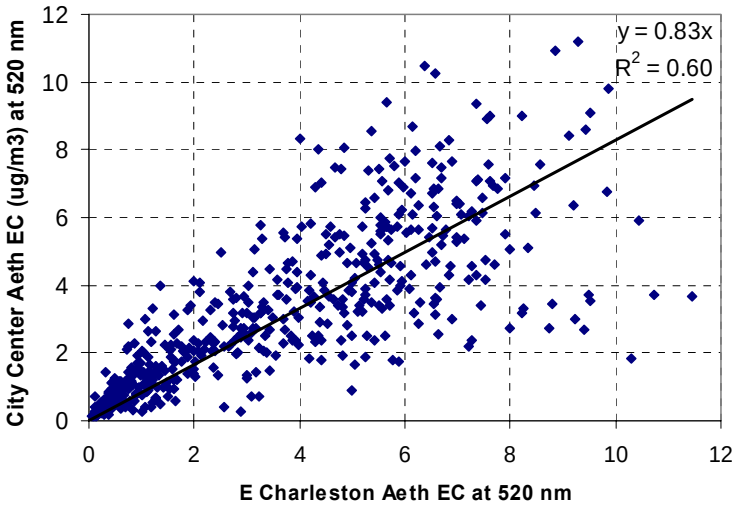

b)

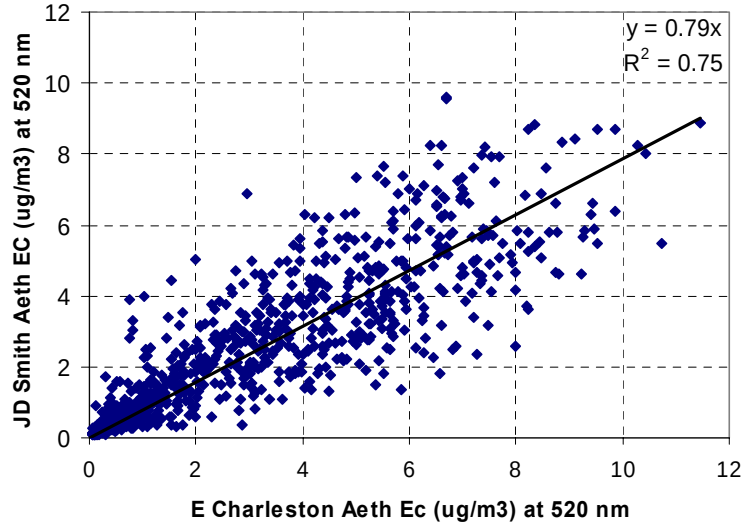

c)

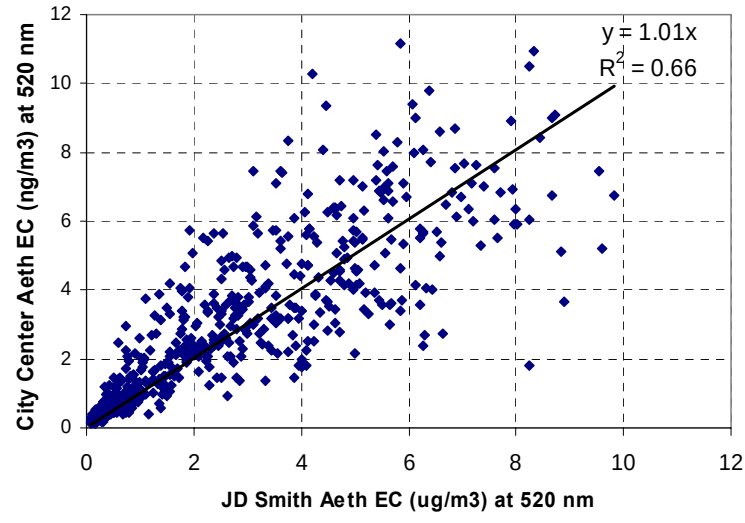

Figure 4-10. Scatterplots of hourly averaged EC concentrations for East Charleston (MS), J.D. Smith Elementary School (JD), and City Center (CC) in January 2003.

4.6.2 Diurnal variations of CO and EC derived from aethalometer at J.D. Smith Elementary School (JD) and City Center (CC)

The diurnal pattern of CO measurements at CC and JD is shown in Figure 4-11. CO is an indicator of incomplete combustion processes. The CO peaks are observed from 6–8 a.m. and decrease as the vertical mixing increases at noon. A second peak from 4–10 p.m. was rather broad; occasionally, two sub-peaks were observed within the second peak at CC. The first CO peak observed in the morning was usually higher than the second peak observed in the evening. This suggests two evening rush hours (based on work schedules) within the valley. CO concentration at JD is generally higher than CC. Considering JD is the relative downwind site of CC, the higher concentrations at JD suggest other emission sources at JD in addition to exhaust from US-95.

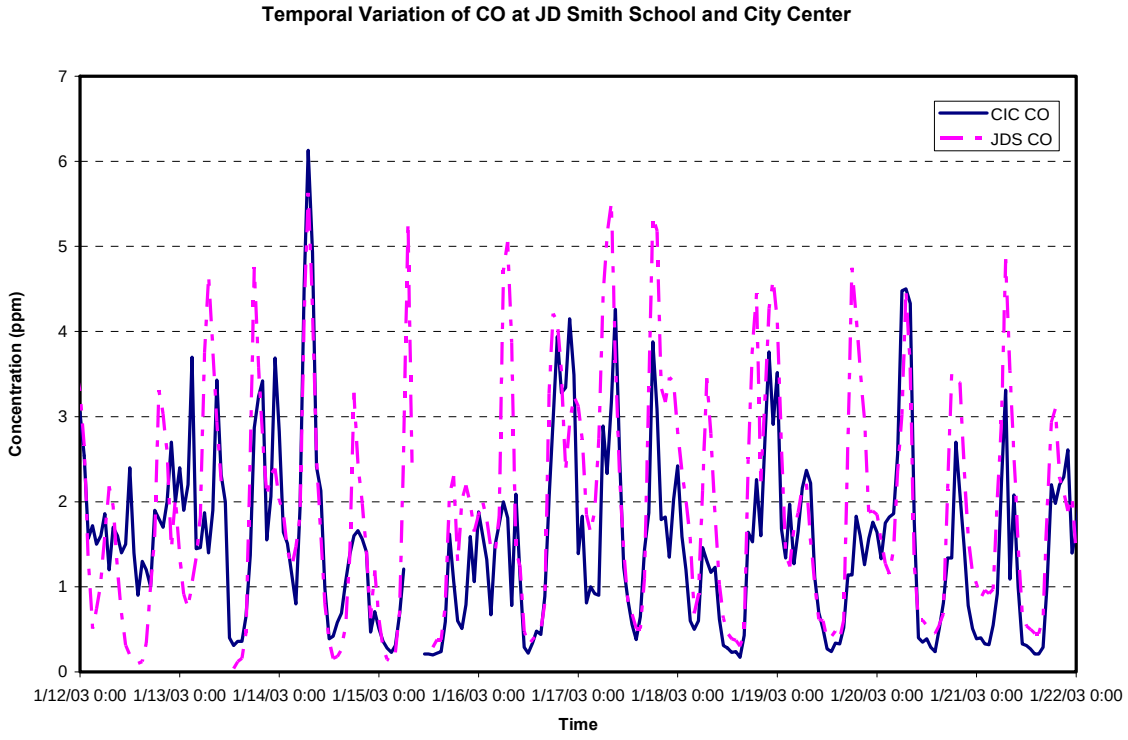

Figure 4-11. Diurnal variations of carbon monoxide at City Center (CC) and J.D. Smith Elementary School.

Comparisons of the diurnal variations between EC and CO concentrations at CC and JD are shown in Figure 4-12. The variations of CO concentrations track EC concentration closely at both the CC and JD sites. The results suggest that the assumption of emission sources from US-95 impacting the "receptor" sites, CC and JD, is very reasonable.

a)

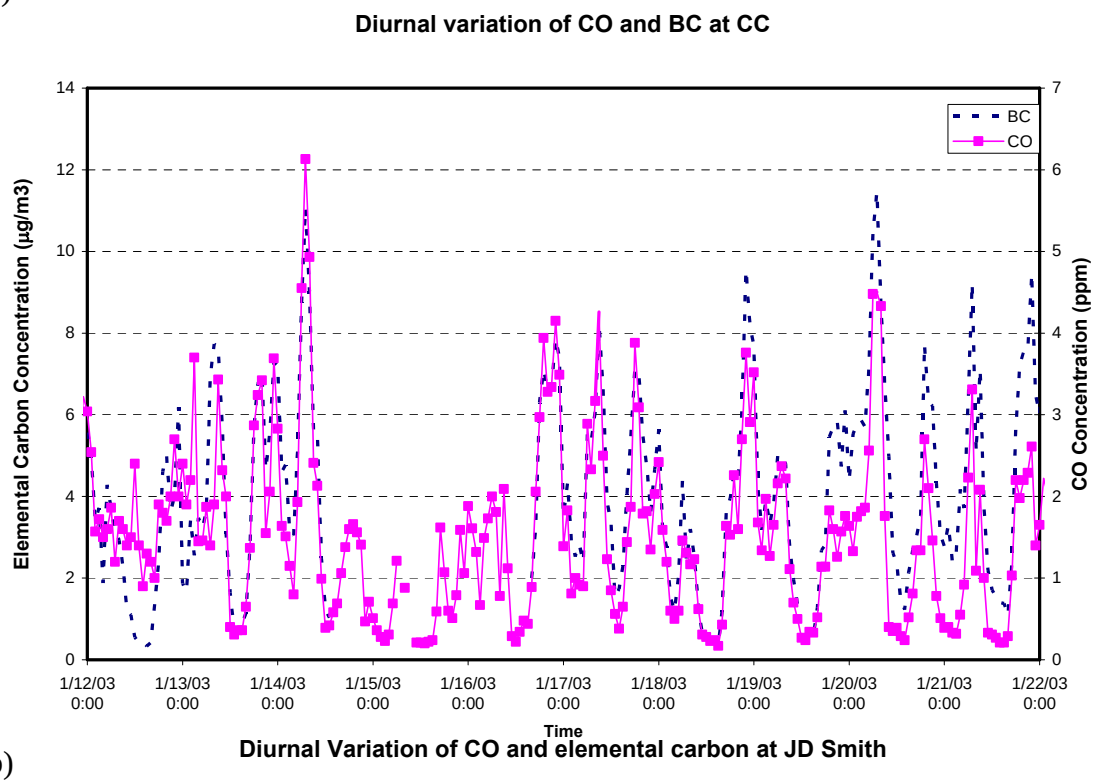

b)

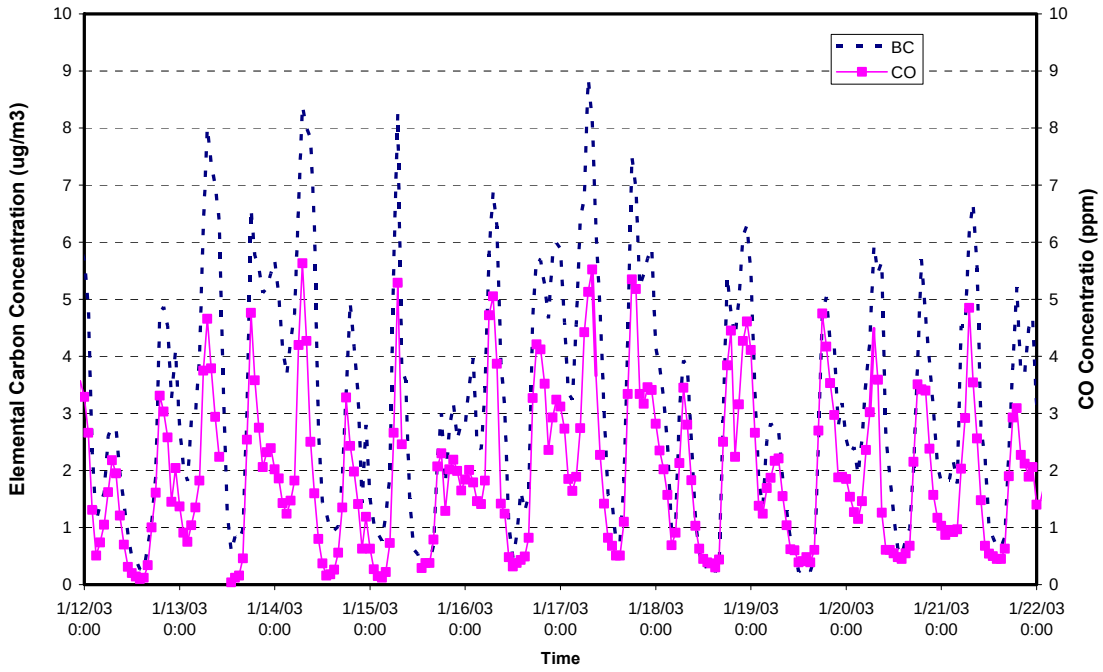

Figure 4-12. Diurnal variations of CO and EC concentrations at (a) City Center, and (b) J.D. Smith Elementary School. (Only 1/12/03–1/22/03 were plotted; similar diurnal patterns were observed on all other dates.)

4.6.3 Diurnal patterns OC, EC, TC at East Charleston (MS)

OC and EC concentrations at East Charleston varied by time of day, as did their relative amounts. Differing ratios of EC/OC (or EC/TC) imply a different mixture of carbon source types.

Figure 4-13 shows the average diurnal pattern in OC, EC, and TC concentrations at MS from January 11 to 28, 2003. The data is from the Sunset Laboratory Carbon Aerosol Analysis Field Instrument, using the IMPROVE temperature protocol.

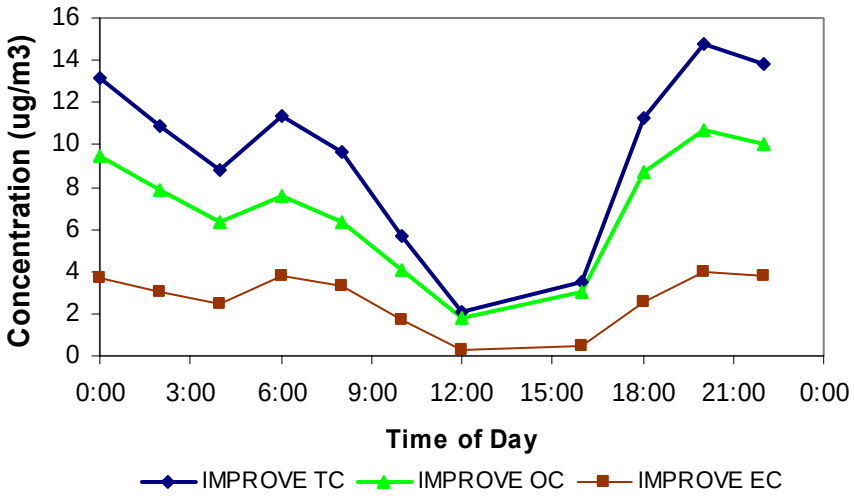

Figure 4-13. Averaged diurnal pattern in OC, EC, and TC at East Charleston (MS), January 11–26, 2003. Samples were collected for 95 minutes, followed by a 25-minute analysis time, except for midday, when samples were collected for three hours. Data is plotted at the beginning of each sample period.

TC and OC show maximum concentrations for the 8:00 to 9:35 p.m. sampling period. Concentrations decline slowly overnight, then a secondary maximum occurs during the 6:00 to 7:30 a.m. period. Concentrations were low during the middle of the day as daytime heating of the ground caused increased vertical mixing of pollutants.

EC concentrations were about the same during mornings and evenings. The ratio of EC to TC was at a maximum in the morning, as shown in Figure 4-14. This suggests that the relative impact of diesel sources or high-emitting gasoline vehicles is greatest this time. Wood smoke was evident during most evenings at the MS site. This may explain the high concentrations of OC during the evenings and the lower ratio of EC/TC compared to morning. The low ratio of EC/TC in midday is thought to be due to the increased mixing in daytime causing more regional than urban influence to be imposed.

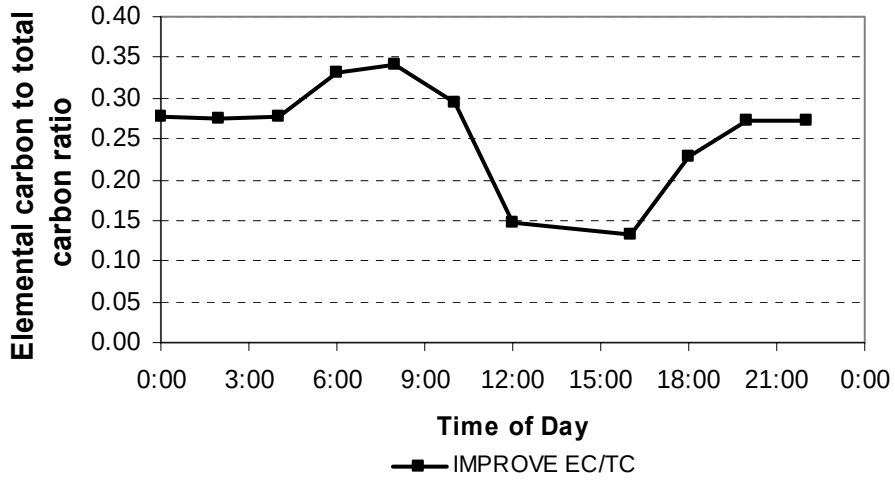

Figure 4-14. Average ratio of EC to TC by time of day at the East Charleston (MS) site. The ratio is computed for the period of January 11-26, 2003. The IMPROVE temperature protocol was used.

4.6.4 Comparison of photoacoustic light absorption with Sunset Laboratory carbon analyzer EC

Photoacoustic light absorption at 532 nm was compared to EC concentrations from the Sunset Laboratory carbon analyzer at MS. The IMPROVE and NIOSH temperature protocols were used to determine the EC concentrations over about a two-week period for each method. Figure 4-15 compares the EC concentration from each method to light absorption from the photoacoustic method. Both methods show the EC highly correlated (r^2 = 0.97-0.98) with light absorption, but the slope is 16.3 m^2g^{-1} for the NIOSH method compared to 11.7 m^2g^{-1} for the IMPROVE temperature method. This implies that IMPROVE method EC (using transmission) is about 40% higher than NIOSH EC. The intercept is thought to be a thermal/optical transmittance (TOT) artifact.

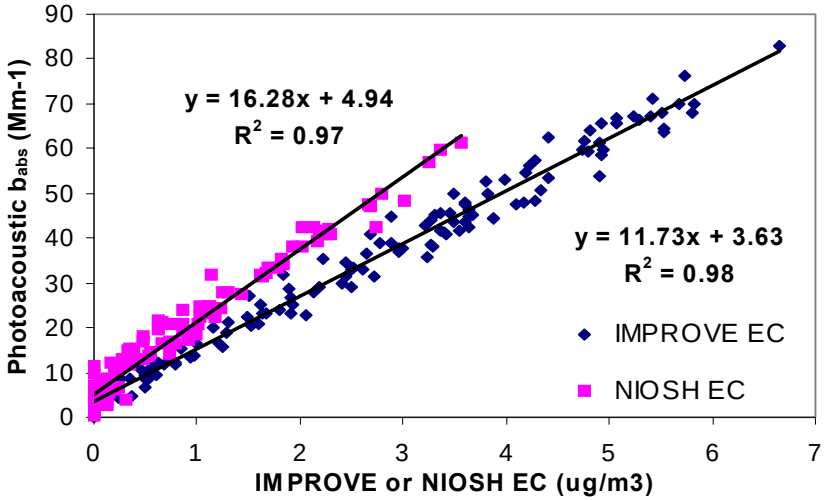

Figure 4-15. Comparison of the IMPROVE and NIOSH EC to photoacoustic light absorption.

4.6.5 Distribution of particle cross-sectional area at East Charleston during January 2003 winter intensive study

CO_2 levels at MS are shown in Figure 4-16. Global background CO_2 is approximately 360 parts per million (ppm). Human-caused CO_2 is mainly due to the combustion of fossil fuels. Figure 4-16 shows that for January 2003, CO_2 levels were substantially elevated above global background for the entire time until January 31, when they began falling to near background levels as a cold front approached and passed through southern Nevada. This continuously elevated CO_2 concentration in January indicated that monitoring site at MS was constantly exposed to the effects of combustion products (i.e., little cleansing of the atmosphere). By early February, more active weather patterns periodically cleansed the atmosphere, as shown by lower and fluctuating CO_2 levels. Because CO_2 was not measured at other sites, the spatial extent of the persistent high concentrations is not known.

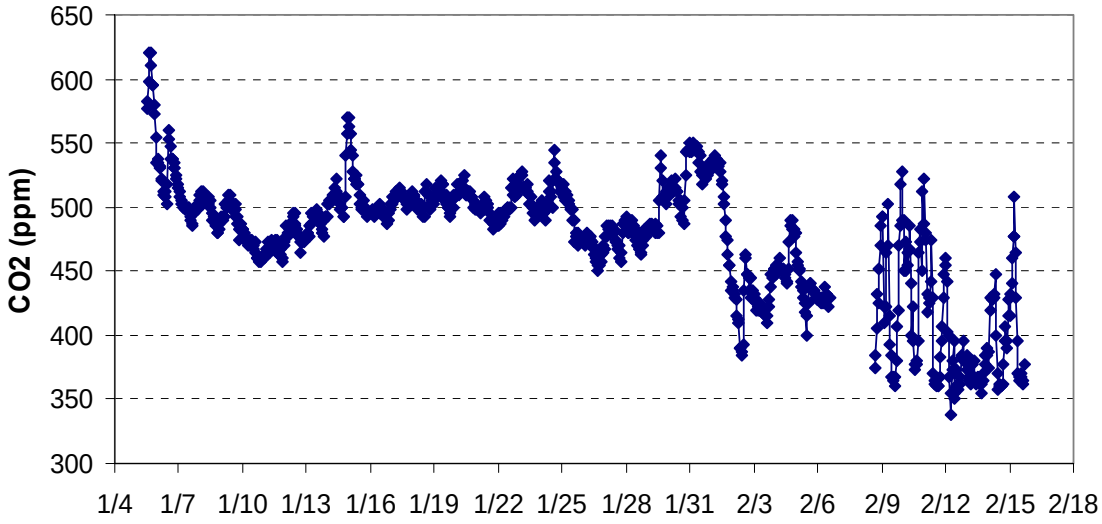

Figure 4-16. Temporal variation of CO_2 (ppm) at East Charleston (MS) during January 2003.

A Climet optical particle counter was operated at the East Charleston site during January 2003 winter intensive study period. The instrument uses measured light scattering of individually sampled particles to assign them to one of 16 particle size bins. The range of detected particle diameter (µm) in the 16 bin are 0.3–0.4, 0.4–0.5, 0.5–0.63, 0.63–0.8, 0.8–1.0, 1.0–1.3, 1.3–1.6, 1.6–2.0, 2.0–2.5, 2.5–3.2, 3.2–4.0, 4.0–5.0, 5.0–6.3, 5.3–8.0, 8.0–10.0, and >10 µm.

The distributions of fractional particle cross-section area by particle diameter are plotted in Figure 4-17, using the averaged measured particle size distributions. The cross-sectional area of particles is closely related with the amount of light scattering (and effect on visibility) by the particles. Thus is it useful to compare the area of particles in different size ranges to estimate their relative effects on haze caused by light scattering.

Figure 4-17 shows the fractional change in particle cross-sectional area within the particle size bin width in dA/dlog(dp), where A is the ratio of total particle cross sectional area within the bin width to total particle cross-sectional area, and dp is the bin width in the particle size range. The distributions of fractional particle cross-sectional area are unitless.

Dual peaks were observed in Figure 4-17 in the smallest bin (0.3–0.4 µm) and at 5.0–6.3 µm. A minimum fractional cross-section area was observed between 1.0 and 2.0 µm. The peak at 0.3–0.4 µm represents primary combustion particle emissions that have been in the atmosphere long enough to grow by coagulation and condensation. Very fresh combustion particles (<10 seconds) would be even smaller ultrafine particles, mostly around 0.05–1.0µm. Particles in the 0.3–0.4 µm size range could also include some secondary sulfate and nitrate particles. The broad larger peak at 5.0–6.3µm includes particle sizes typically associated with crustal material (dust), such as road dust and dust from disturbed land.

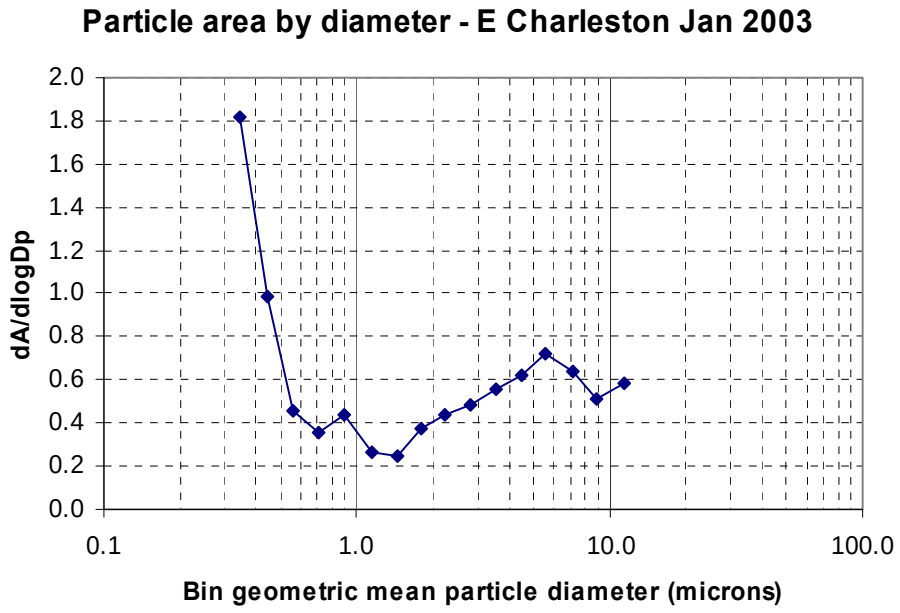

Figure 4-17. Average distribution of fractional particle cross-section area at East Charleston, January 2003.

Table 4-4 and Figure 4-18 show the cumulative particle area as a function of particle size. About 45% of particle area is from particles less than 1.0 μm in diameter. The vast majority of these particles are expected to result from combustion processes or secondary gas-to-particle conversion. About 40% of the particle area is from particles with diameter greater than 2.5 μm. These particles would be expected to result primarily from mechanical processes, such as wind erosion, road dust, mineral processing, etc. Thus, both small and large particles contribute significantly to haze at the East Charleston site. Thus, combustion particles from motor vehicles, wood smoke, and dust are both important in the winter haze at East Charleston.

Table 4-4. Cumulative particle area by particle diameter.

bin maximum diameter	Cumulative area (%)
0.4	22.7
0.5	32.3
0.63	36.8
0.8	40.5
1	44.8
1.3	47.8
1.6	50.1
2	53.7
2.5	57.9
3.2	63.1
4	68.5
5	74.5
6.3	81.8
8	88.4
10	93.4
13	100.0

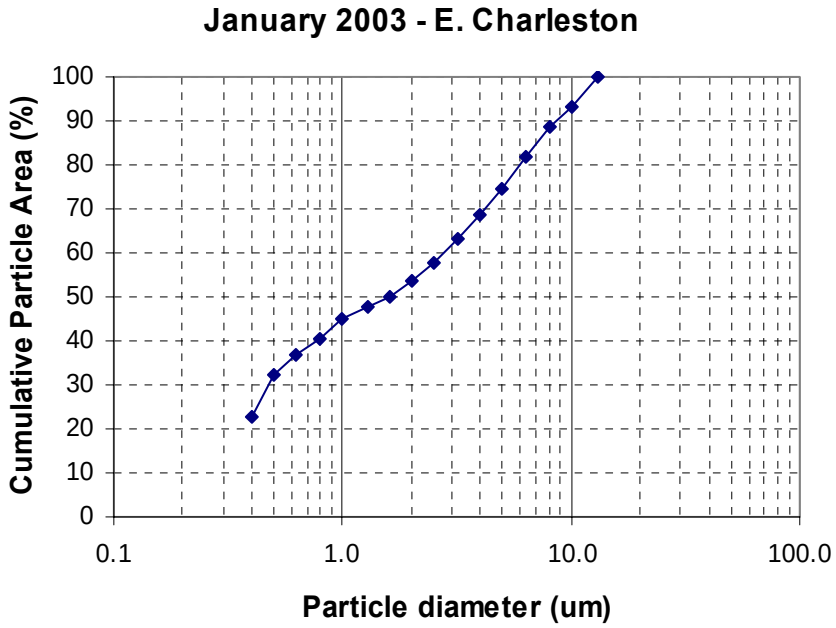

Figure 4-18. Plot of cumulative particle area by particle diameter.

5. EMISSION SOURCE PROFILES

5.1 *Fuel-based Emission Factor*

Emission factors for gaseous species by FTIR measurements were calculated for each filter sampling interval using the method described in Section 2, and the results of average, median, and standard deviations of emission factors are tabulated in Table 5-1. The average and standard deviation of emission factors are based on the emission factor developed from each filter sample within the source type, not from each vehicle. Therefore, average and median emission factors are similar. However, the average emission factor can be driven by high/low emitters. For example, a study with remote sensing conducted in Las Vegas Basin during 2001-2002 found the highest 10% of emitters result in 75–80% skewness regarding higher emission factors for CO. Only peaks with integrated CO_2 of greater than 1000 ppm s are included in the following analysis.

Table 5-1. Fuel-based emission factor by FTIR, both summer and winter, in the Las Vegas Basin.

	Winter									Summer					
	on-road vehicles, mixed fleet, Swenson and Flammingo			on-road diesel bus, North RTC, Las Vegas			non-road diesel engines (AHERN)			on-road vehicles, mixed fleet			on-road diesel bus		
	average	Median	Standard Deviation	average	Median	Standard Deviation	average	Median	Standard Deviation	average	Median	Standard Deviation	average	Median	Standard Deviation
gNH3/kgfuel	0.845	0.837	0.083	0.056	0.043	0.036	0.083	0.097	0.098	0.371	0.369	0.035	0.027	0.045	0.041
gCO2/kgFuel	3024.124	3020.418	14.171	3048.121	3053.512	11.671	3013.294	3019.771	28.561	2999.201	3004.350	13.586	3050.555	3045.806	9.711
gCO/kgFuel	30.127	31.414	8.960	18.173	15.522	6.974	27.537	35.538	11.639	39.390	36.058	7.575	16.994	18.840	5.864
gEthylene/kgFuel	1.117	1.088	0.165	0.214	0.202	0.068	0.634	0.712	0.339	0.766	0.754	0.067	0.122	0.145	0.128
gFormaldehyde/kgFuel	2.270	2.124	0.583	0.448	0.404	0.231	6.402	1.939	4.602	1.719	1.654	0.136	0.263	0.292	0.292
gHexane/kgFuel	1.367	1.468	0.492	0.891	0.693	0.484	4.898	1.138	3.879	3.500	3.352	0.584	0.563	0.654	0.826
gNO/kgFuel	4.535	4.743	0.836	31.419	34.021	2.940	18.595	19.036	6.916	3.292	3.276	0.320	21.537	18.366	3.264
gNO2/kgFuel	1.739	1.799	0.257	2.947	2.897	0.504	8.534	8.266	2.352	1.678	1.638	0.157	0.680	1.271	0.765
gN2O/kgFuel	0.638	0.599	0.364	0.356	0.413	0.236	1.555	0.604	1.202	0.648	0.680	0.151	0.201	0.195	0.029
gPropane/kgFuel	1.446	1.435	0.405	0.195	0.196	0.167	2.799	0.616	2.142	2.719	2.758	0.223	0.337	0.325	0.074
gSO2/kgFuel	7.593	7.028	1.560	0.760	0.576	0.419	2.878	2.298	1.654	6.152	6.141	0.454	0.723	1.019	1.113
gPM2.5 (DustTrak) /kgFuel	0.382	0.321	0.186	0.299	0.266	0.126	1.799	1.930	0.729	0.238	0.221	0.224	0.051	0.005	0.028
gPM0.1(ELPI)/gFuel	0.001	0.001	0.001	0.003	0.003	0.001	0.004	0.005	0.005	0.001	0.001	0.001	0.001	0.001	0.001
gPM1.0(ELPI)/kgFuel	0.080	0.069	0.060	0.241	0.249	0.036	0.507	0.607	0.610	0.114	0.095	0.062	0.367	0.154	0.193
gPM2.5 (ELPI)/kgFuel	0.668	0.392	0.615	0.985	1.028	0.095	2.451	2.863	2.425	0.377	0.373	0.191	0.606	0.277	0.308

5.1.1 CO emission factors

CO has the highest signal-to-noise ratio and is one of the most abundant species in vehicle exhaust for all species measured with the FTIR. For on-road mixed fleet vehicles, the average CO emission factor of 30.127 g CO/kg fuel in winter is 31% less than in summer (39.390 g CO/kg fuel). The reduction of the average CO emission factor in winter mixed fleet on-road vehicles is probably due to the oxygenated gasoline fuel used in wintertime program in Las Vegas Valley, which results in better combustion efficiency. There is no significant difference in the average CO emission factors between winter (18.173g CO/kg fuel) and summer (16.994g CO/kg fuel) on-road diesel vehicles. The average CO emission factor for non-road diesel engines is equivalent to on-road mixed fleet vehicles.

The average CO emission factor for on-road mixed fleet vehicles is within 10% of that of 39–55 g CO/kg fuel recorded in Las Vegas Valley during 2000–2002 using vehicle emission remote sensing systems (VERSS) (Mazzoleni et al., 2004). The slightly lower average CO emission factor in this study may be explained by newer cars from car rental companies in the basin and/or better maintained vehicles. The average CO emission factors based on in-plume methodology and VERSS technologies show excellent agreement.

5.1.2 NH_3 emission factors

Mobile sources of ammonia can be a large fraction of urban NH_3 emission inventories. NH_3 is of interest to air quality regulation because it is a precursor to both ammonium sulfate and ammonium nitrate (NH_4NO_3) secondary aerosols. Although NH_4NO_3 is a relatively small fraction of the total $PM_{2.5}$ mass in the Las Vegas Valley, the analysis of mobile NH_3 emission on an in-use fleet provide a valuable check on the overall quality of the in-plume measurement. NH_3 emissions from vehicles are reaction products generated in the three way catalytic converter (Gillies and Gertler, 2000). The catalytic converter is designed to reduce CO and NO simultaneously via the chemical reaction:

$$2NO + 2CO \rightarrow N_2 + 2CO_2 \qquad (5\text{-}1)$$

When hydrocarbons are present in the exhaust, hydrogen may be produced in the catalytic converter via the reaction:

$$C_nH_{(2n+2)} + 2nH_2O \rightarrow (3n+1)H_2 + nCO_2 \qquad (5\text{-}2)$$

In turn, the hydrogen is then available to initiate a competing reaction with equation 5-2:

$$NO + CO + 1.5H_2 \rightarrow NH_3 + CO_2 \qquad (5\text{-}3)$$

A comparison of the average NH_3 emission factors shows that it is twice as high in winter than in summer for on-road mixed fleet vehicles and on-road diesel vehicles. NH_3 emission factors are 10 times higher for on-road mixed fleet vehicles than for on-road

diesel vehicles, regardless of season. The NH_3 emission factor for non-road diesel engines is 50% higher than that of on-road diesel vehicles.

Unlike NO, CO, and hydrocarbon (HC), studies have shown that high NH_3 emissions may originate from late-model and properly maintained vehicles (Huai et al, 2003). The fleet average NH_3 emission factors measured in Las Vegas Valley are in excellent agreement (<15% difference) with published results from Fraser and Cass (1998) of 0.76 g NH_3/kg fuel, but twice of those from Baum et al. (2001) using remote sensing and Allen et al. (2001) based on tunnel studies.

5.1.3 NO_x and THC emission factors

The oxides of nitrogen (NO_x) emission factor is the sum of NO, nitrous oxide (N_2O), and NO_2 emission factors, and the total hydrocarbon (THC) emission factor is the sum of ethylene, hexane, and propane emission factors. The NO_x emission factor is higher in winter than in summer, probably due to lower temperature and cold starts in winter. The NO_x emission factor for on-road diesel vehicles is four to five times higher than for mixed fleet on-road vehicles. The NO_x emission factor in summer for on-road diesel vehicles is slightly less than 8.4 g NO/kg fuel, as recorded by VERSS. THC emission factor for mixed fleet on-road vehicles is higher than on-road diesel vehicles. THC summer emission factor determined by the in-plume method is slightly higher than THC determined by VERSS. It should be emphasized that the average emission factor represents the emission factor for each type of source and can be biased by either high and/or low emitters during sample collection. There is substantial variation, as can be seen in the standard deviation derived from each type of sample collected during the study.

5.1.4 PM emission factors

PM emission factors for on-road mixed fleet vehicles measured with the In-Plume Sampling System need to be considered within the context of the sampling system. Unlike dynamometer testing, where sampling probes are connected directly to the exhaust pipe of a vehicle, the location of the In-Plume sampling inlet in the middle of the road results in the simultaneous sampling of road dust, brake/tire wear material, and engine exhaust. Chemical analysis of aerosol filter samples collected with the In-Plume Sampling System indicate that as much as 50–60% of the $PM_{2.5}$ is composed of geologic material (i.e., oxides of Fe, Al, Si, Ca, and Ti), and secondary aerosols of ammonium bisulfate ($[NH_4]\cdot HSO_4$) and NH_4NO_3. Analysis of exhaust emissions from dynamometer studies in Denver, CO, indicated that ~88% of exhaust PM_{10} is composed of a combination of OC and EC (Cadle et al., 1999).

A limitation of the system is that for vehicles with bumper-level exhaust pipes, plumes of exhaust are immediately mixed with road dust suspended by the vehicle's tires. Consequently, elevated levels of combustion products (i.e., CO_2, CO, and NO) are accompanied by increased levels of both road dust and exhaust PM. The fraction of resuspended road dust caused by vehicles can be estimated and subtracted by applying CMB with dust source profiles collected in Las Vegas (Chow et al., 1999). Based on

these results, the components of fine road dust and exhaust emission factors can be calculated using the following equations:

$$RoadDustEF_{PM_{2.5.}} = f_{2.5} EF_{PM_{2.5}} \quad (5\text{-}4)$$

$$ExhaustEF_{PM_{2.5}} = (1 - f_{2.5}) EF_{PM_{2.5}} \quad (5\text{-}5)$$

where f_x is the road dust fraction of $PM_{2.5}$ from CMB subtraction analysis. $EF_{PM2.5}$ represents the emission factors of $PM_{2.5}$ as shown in Table 5-1. Road dust PM accounted for 44.51 ± 4.8% of $PM_{2.5}$ mass for winter on-road mixed-fleet vehicles and 63.1% ± 19.0% for summer. Emission factors of PM were estimated by measurements from DustTrak and ELPI. As explained in Section 2.3.3.2, it is more appropriate to use the emission factor of $PM_{1.0}$ than $PM_{2.5}$ when ELPI is used to estimate the $PM_{2.5}$ emission factor. Caution should be exercised when comparing PM emission factors determined by DustTrak and ELPI. The mass estimate by DustTrak is based on light scattering techniques, which are strongly dependent on particle size distribution in the air sample. As mentioned in Section 2.3.3.2, the specific density may be needed for mass estimates by ELPI and the specific density may change depending on emission source. However, emission factors developed by ELPI and DustTrak can provide an estimate of the range of PM emission factors. The largest ELPI $PM_{2.5}$ emission factor is for non-road diesel engine exhaust (0.5 $PM_{1.0}$/kg fuel) and is lowest for on-road mixed fleet vehicles. The ELPI $PM_{2.5}$ emission factors in summer are 50% higher than those in winter for both on-road mixed fleet and diesel vehicles. Emission factors for ultrafine particles (particles with aerodynamic diameters less than 0.1μm) is very low (<0.001 g ultrafine PM/kg fuel), approximately 1% to $PM_{2.5}$.

5.2 *Source $PM_{2.5}$ Chemical Species Composition*

The results of $PM_{2.5}$ chemical speciation for source emission profiles obtained from the In-Plume Sampling System are shown in Figure 5-1(a-e). The data of $PM_{2.5}$ inorganic chemical species and organic species are listed in Appendix A. These profiles result from samples composited from each type of source: four samples of summer mixed fleet on-road vehicle exhausts; four samples of winter on-road mixed fleet vehicle exhausts; four samples of summer on-road diesel bus; four samples of winter on-road diesel bus; and five samples of winter off-road diesel engines.

It is most likely that roadside samples (i.e., mixed fleet on-road vehicles) are affected by vehicle-related resuspended road dust, although the $PM_{2.5}$ inlet in the In-Plume System will reduce the contribution of geological material. Therefore, prior to sample compositing for profiles of summer and winter mixed fleet on-road vehicles, the CMB model was performed to remove remaining contributions of geological material and secondary aerosol in the ambient air background. The source profiles used in CMB were from the DRI source profile database and include: geological profile (composite of GCONS1, GCONS2, GCONS3, GCONS4 and GCONS4, Las Vegas, 1995), bisulfate (AMBSUL), and NO_3^- (AMNIT). Only crustal species (Al, Si, Ca, and Fe), bisulfate, and NO_3^- are used as fitting species. The calculated concentrations of both the fitting and non-fitting species were then subtracted from the original roadside motor vehicle sample

concentrations. The source profile for each sample was calculated and normalized based on residual mass (i.e., the difference between the measured and CMB calculated contribution of mass and chemical species).

It was found that the sum of species is 27% higher for mixed fleet on-road vehicles than the remaining measured mass in summer and 40% higher in winter. This is more likely to be an artifact of the adsorption of volatile organic species onto a quartz filter (carbon) than mass (PTFE filter). Such an adsorption artifact is usually produced in low-temperature OC (i.e., OC1 and OC2) carbon fractions. This is more pronounced for roadside sampling than on-road diesel vehicles and non-road engines because of: 1) the lower PM source concentrations from on-road vehicles; 2) the higher contribution of low molecular weight organic compounds from ambient air; 3) the longer sample collection time; and 4) the different organic compounds emitted from mixed fleet on-road vehicles. After excluding the low-temperature carbon fraction, the sum of species comprises 95% of remaining mass from CMB for the summer roadside profile and 98% for the winter on-road profile.

a)

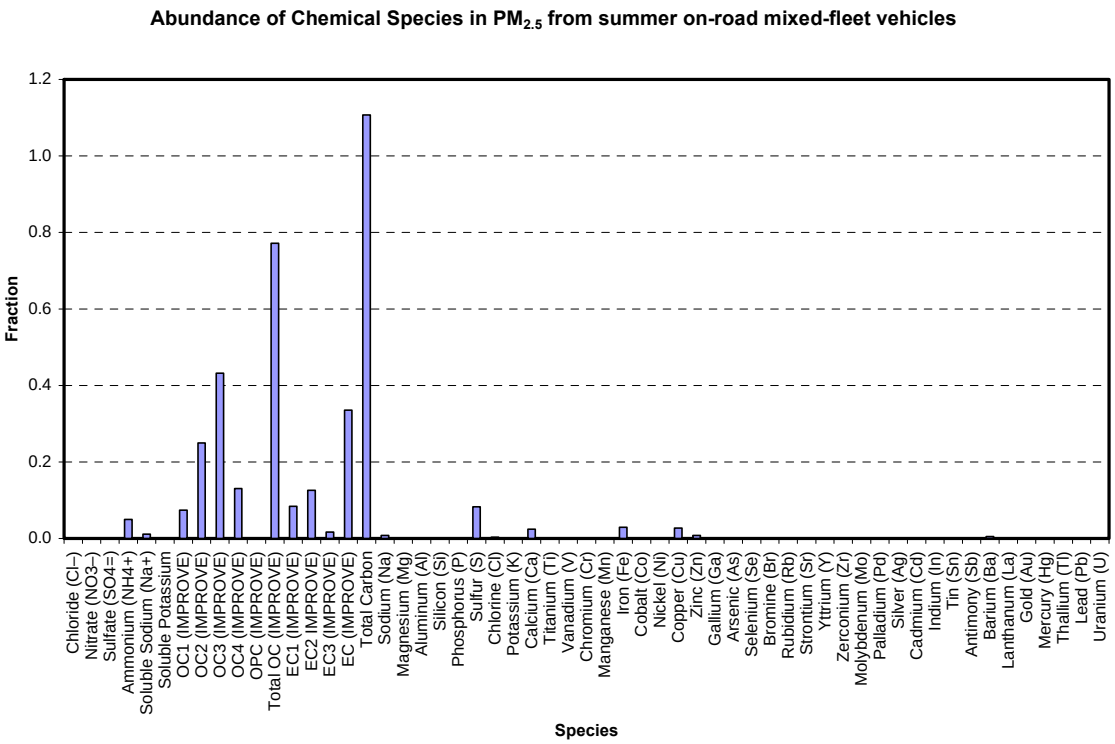
Abundance of Chemical Species in PM2.5 from summer on-road mixed-fleet vehicles
Fraction
1.2
1.0
0.8
0.6
0.4
0.2
0.0
Chloride (Cl-)
Nitrate (NO3-)
Sulfate (SO4=)
Ammonium (NH4+)
Soluble Sodium (Na+)
Soluble Potassium
OC1 (IMPROVE)
OC2 (IMPROVE)
OC3 (IMPROVE)
OC4 (IMPROVE)
OPC (IMPROVE)
Total OC (IMPROVE)
EC1 (IMPROVE)
EC2 IMPROVE)
EC3 (IMPROVE)
EC (IMPROVE)
Total Carbon
Sodium (Na)
Magnesium (Mg)
Aluminum (Al)
Silicon (Si)
Phosphorus (P)
Sulfur (S)
Chlorine (Cl)
Potassium (K)
Calcium (Ca)
Titanium (Ti)
Vanadium (V)
Chromium (Cr)
Manganese (Mn)
Iron (Fe)
Cobalt (Co)
Nickel (Ni)
Copper (Cu)
Zinc (Zn)
Gallium (Ga)
Arsenic (As)
Selenium (Se)
Bromine (Br)
Rubidium (Rb)
Strontium (Sr)
Yttrium (Y)
Zerconium (Zr)
Molybdenum (Mo)
Palladium (Pd)
Silver (Ag)
Cadmium (Cd)
Indium (In)
Tin (Sn)
Antimony (Sb)
Barium (Ba)
Lanthanum (La)
Gold (Au)
Mercury (Hg)
Thallium (Tl)
Lead (Pb)
Uranium (U)
Species

b)

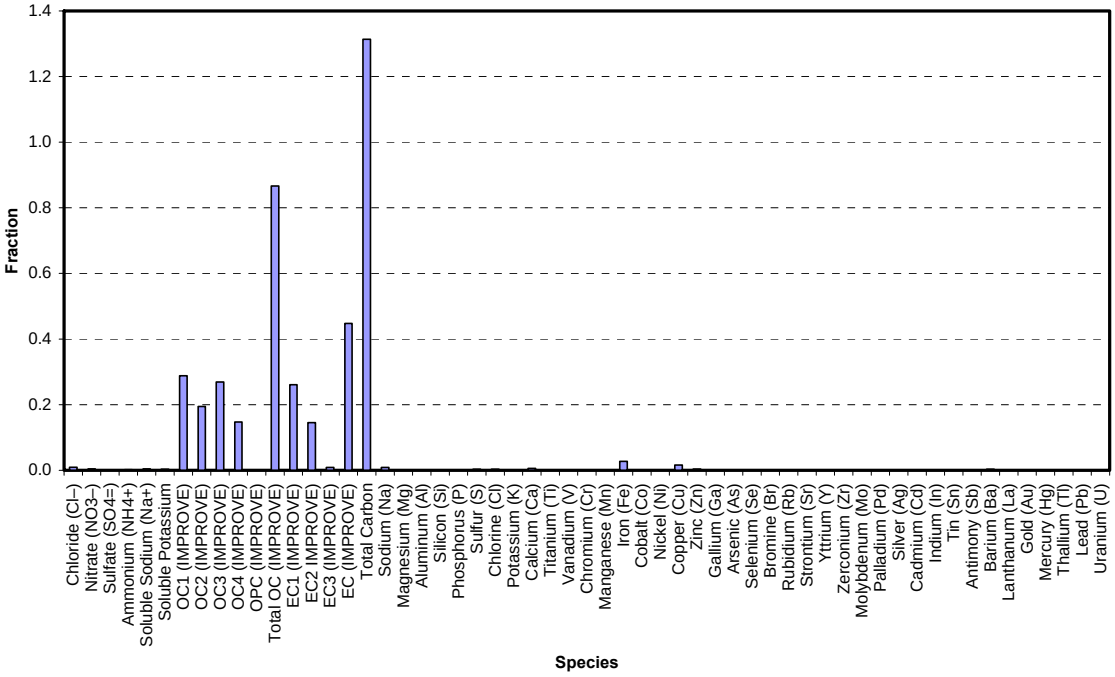
Abundance of Chemical Species in PM2.5 from winter on-road mixed fleet vehicles
Fraction
1.4
1.2
1.0
0.8
0.6
0.4
0.2
0.0
Chloride (Cl-)
Nitrate (NO3-)
Sulfate (SO4=)
Ammonium (NH4+)
Soluble Sodium (Na+)
Soluble Potassium
OC1 (IMPROVE)
OC2 (IMPROVE)
OC3 (IMPROVE)
OC4 (IMPROVE)
OPC (IMPROVE)
Total OC (IMPROVE)
EC1 (IMPROVE)
EC2 IMPROVE)
EC3 (IMPROVE)
EC (IMPROVE)
Total Carbon
Sodium (Na)
Magnesium (Mg)
Aluminum (Al)
Silicon (Si)
Phosphorus (P)
Sulfur (S)
Chlorine (Cl)
Potassium (K)
Calcium (Ca)
Titanium (Ti)
Vanadium (V)
Chromium (Cr)
Manganese (Mn)
Iron (Fe)
Cobalt (Co)
Nickel (Ni)
Copper (Cu)
Zinc (Zn)
Gallium (Ga)
Arsenic (As)
Selenium (Se)
Bromine (Br)
Rubidium (Rb)
Strontium (Sr)
Yttrium (Y)
Zerconium (Zr)
Molybdenum (Mo)
Palladium (Pd)
Silver (Ag)
Cadmium (Cd)
Indium (In)
Tin (Sn)
Antimony (Sb)
Barium (Ba)
Lanthanum (La)
Gold (Au)
Mercury (Hg)
Thallium (Tl)
Lead (Pb)
Uranium (U)
Species

c)

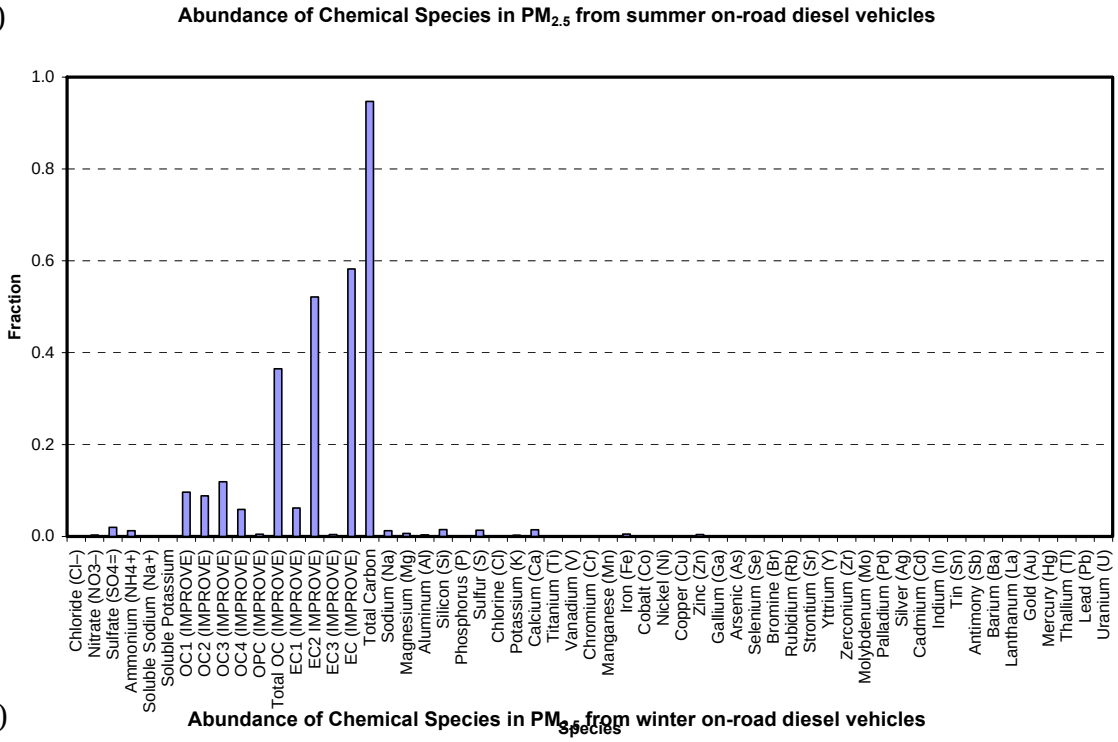
Abundance of Chemical Species in PM2.5 from summer on-road diesel vehicles
Fraction
1.0
0.8
0.6
0.4
0.2
0.0
Chloride (Cl–)
Nitrate (NO3–)
Sulfate (SO4=)
Ammonium (NH4+)
Soluble Sodium (Na+)
Soluble Potassium
OC1 (IMPROVE)
OC2 (IMPROVE)
OC3 (IMPROVE)
OC4 (IMPROVE)
OPC (IMPROVE)
Total OC (IMPROVE)
EC1 (IMPROVE)
EC2 IMPROVE)
EC3 (IMPROVE)
EC (IMPROVE)
Total Carbon
Sodium (Na)
Magnesium (Mg)
Aluminum (Al)
Silicon (Si)
Phosphorus (P)
Sulfur (S)
Chlorine (Cl)
Potassium (K)
Calcium (Ca)
Titanium (Ti)
Vanadium (V)
Chromium (Cr)
Manganese (Mn)
Iron (Fe)
Cobalt (Co)
Nickel (Ni)
Copper (Cu)
Zinc (Zn)
Gallium (Ga)
Arsenic (As)
Selenium (Se)
Bromine (Br)
Rubidium (Rb)
Strontium (Sr)
Yttrium (Y)
Zerconium (Zr)
Molybdenum (Mo)
Palladium (Pd)
Silver (Ag)
Cadmium (Cd)
Indium (In)
Tin (Sn)
Antimony (Sb)
Barium (Ba)
Lanthanum (La)
Gold (Au)
Mercury (Hg)
Thallium (Tl)
Lead (Pb)
Uranium (U)
Species

d)

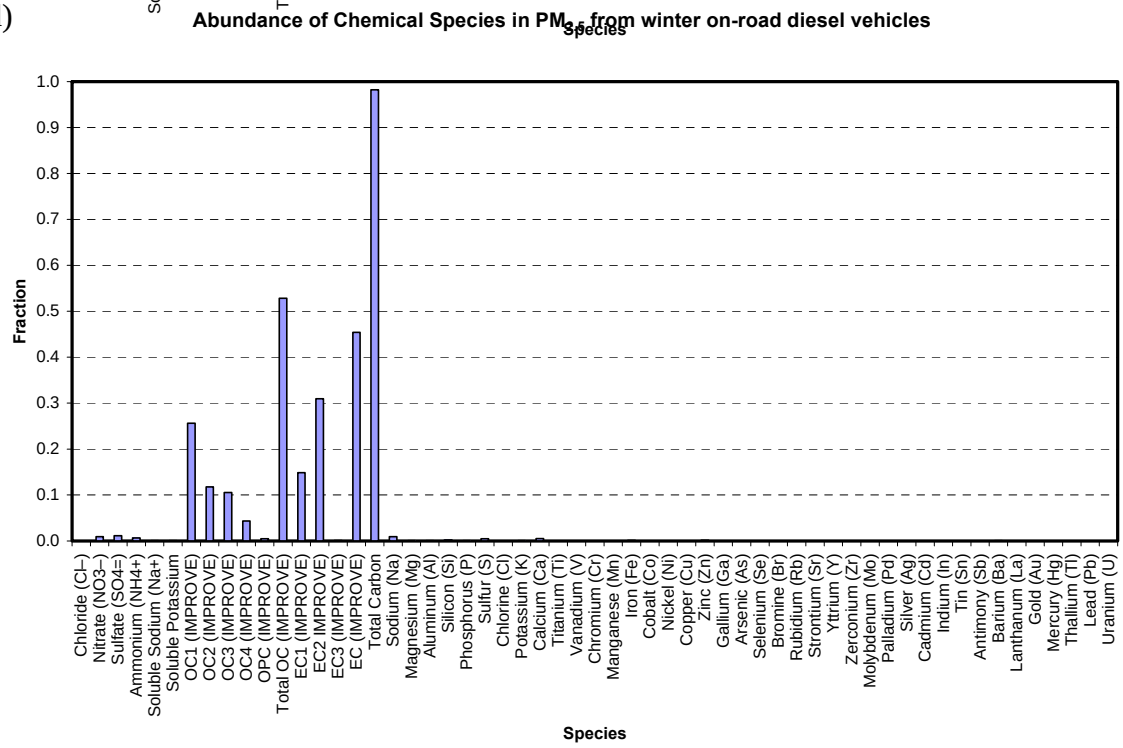
Abundance of Chemical Species in PM2.5 from winter on-road diesel vehicles
Fraction
1.0
0.9
0.8
0.7
0.6
0.5
0.4
0.3
0.2
0.1
0.0
Chloride (Cl–)
Nitrate (NO3–)
Sulfate (SO4=)
Ammonium (NH4+)
Soluble Sodium (Na+)
Soluble Potassium
OC1 (IMPROVE)
OC2 (IMPROVE)
OC3 (IMPROVE)
OC4 (IMPROVE)
OPC (IMPROVE)
Total OC (IMPROVE)
EC1 (IMPROVE)
EC2 IMPROVE)
EC3 (IMPROVE)
EC (IMPROVE)
Total Carbon
Sodium (Na)
Magnesium (Mg)
Aluminum (Al)
Silicon (Si)
Phosphorus (P)
Sulfur (S)
Chlorine (Cl)
Potassium (K)
Calcium (Ca)
Titanium (Ti)
Vanadium (V)
Chromium (Cr)
Manganese (Mn)
Iron (Fe)
Cobalt (Co)
Nickel (Ni)
Copper (Cu)
Zinc (Zn)
Gallium (Ga)
Arsenic (As)
Selenium (Se)
Bromine (Br)
Rubidium (Rb)
Strontium (Sr)
Yttrium (Y)
Zerconium (Zr)
Molybdenum (Mo)
Palladium (Pd)
Silver (Ag)
Cadmium (Cd)
Indium (In)
Tin (Sn)
Antimony (Sb)
Barium (Ba)
Lanthanum (La)
Gold (Au)
Mercury (Hg)
Thallium (Tl)
Lead (Pb)
Uranium (U)
Species

e)

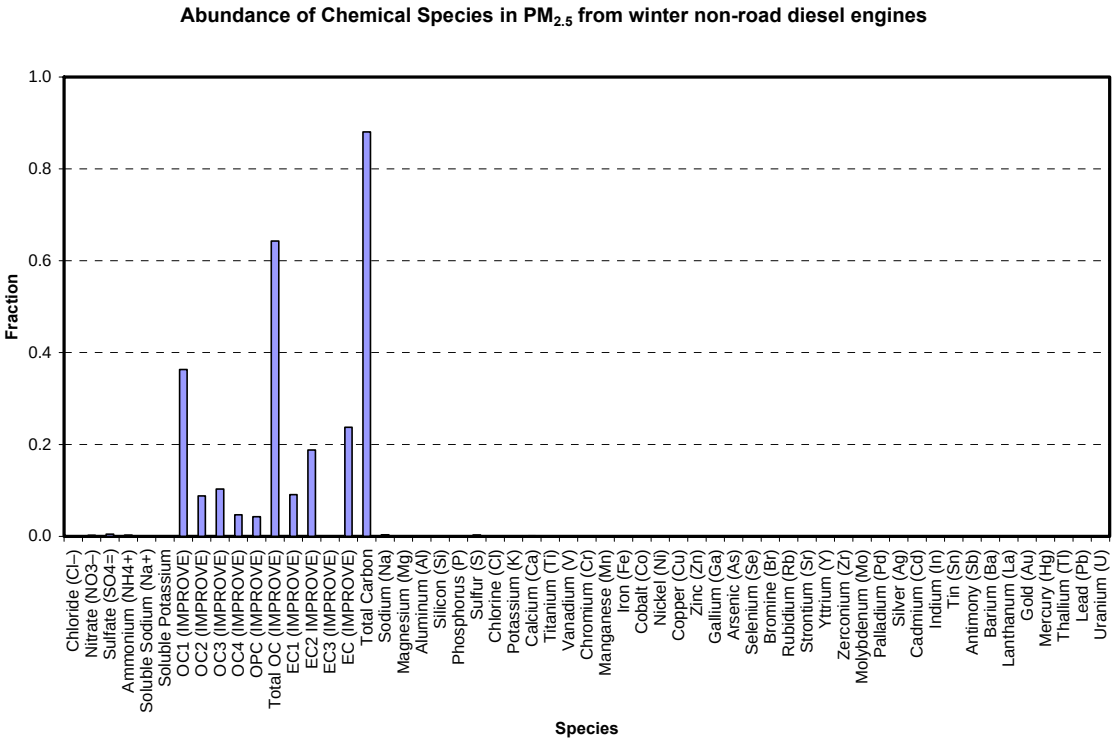

Figure 5-1. Abundance of chemical species in $PM_{2.5}$ from (a) summer on-road mixed fleet vehicles, (b) winter on-road mixed fleet vehicles, (c) summer on-road diesel vehicles, (d) winter on-road diesel vehicles, and (e) winter non-road diesel engines.

The most abundant species for $PM_{2.5}$ chemical speciation profiles are carbonaceous compounds (more than 80%) for all sources. The high-temperature OC (i.e., OC-OC1-OC2) carbon fraction comprises 56% of the mixed fleet on-road vehicle profile in summer and 47% in winter. High-temperature OC comprises 36.5% of $PM_{2.5}$ in summer on-road diesel vehicle profile, 53% in winter on-road diesel vehicles, and 64% in winter non-road diesel engines. The high-temperature OC fraction is substantially lower for both on-road diesel bus profiles for summer (18%) and winter (15%). The high-temperature OC fraction in summer is higher than winter for both mixed fleet on-road vehicles and on-road diesel vehicles.

EC/OC ratios can be used to identify the impact of sources from diesel engines and oil combustion. In general, the EC/OC ratio for diesel exhaust is larger than the unity and is higher than those from on-road gasoline vehicle exhaust. An EC/OC ratio lower than unity was found as well (Gillies and Gertler, 2000). For this study, a comparison was made between EC and the high-temperature OC fraction in source profiles rather than EC/OC, due to potential sampling artifacts mentioned earlier. The EC/high-temperature OC ratio is 0.6 for summer on-road vehicles, 1.09 for winter on-road vehicles, 3.24 for summer on-road diesel vehicles, 3.04 for winter on-road diesel vehicles, and 1.24 for non-road diesel engines. EC/high-temperature OC ratios for on-road diesel vehicle profiles are higher than those for mixed fleet on-road vehicles. Although there is no difference between on-road diesel and non-road diesel fuel compositions in the Las

Vegas Basin, the lower EC/high-temperature OC ratio observed in non-road engines can be attributed to the wide variety of engines tested in the non-road diesel profile and the difference between on-road and non-road diesel engine types.

6. SOURCE CONTRIBUTIONS TO AMBIENT $PM_{2.5}$, ORGANIC CARBON, AND ELEMENTAL CARBON

The overall objectives of this study are: 1) to validate the application of the CMB receptor model (Watson et al., 1990a, 1990b); 2) to apportion measured $PM_{2.5}$ primary emission source categories to aerosol and secondary aerosols; and 3) to apportion measured carbonaceous compound in $PM_{2.5}$ to primary emission source categories.

The source contributions to each chemically speciated sample at each site are presented both in tabular form and in the form of stacked bar error. Average contributions to $PM_{2.5}$ are calculated for the entire study period. Contributions at the different sites are compared and contrasted. The samples with the largest contributions from each source type are identified. A data base is constructed which contains the contribution of each source type to each chemical species. This data base can be used for statistical analysis of source contribution estimates and for detailed integration with other data analysis results in case studies.

The data used for this modeling are the ambient chemical compositions and the chemical source profiles with their related uncertainty estimates. The base input source profiles used in CMB for this study include: 1) paved road dust, 2) secondary NH_4NO_3, 3) secondary $(NH_4)_2SO_4$, 4) residential wood combustion (woodstove with almond) from Lake Tahoe, 5) on-road mixed-fleet vehicles in Las Vegas, and 6) on-road diesel buses. A more detailed explanation of the activities involved is given in the following subsections.

6.1 *Validating Application of CMB model*

6.1.1 Selection of source profiles and fitted species for CMB

Previous emission estimates (Chow et al., 1999) for PM_{10} in the Las Vegas non-attainment area show significant contributions to the PM_{10} mass from paved road dust, unpaved road dust, and construction dust. Construction emission has increased more than 10 times from 1989 to 1995. A large fraction of the geological material, however, is in the coarse particle mode (>2.5 μm in diameter). The major sources of $PM_{2.5}$ also include mobile exhausts (gasoline and diesel), residential wood burning, and stationary sources. In Las Vegas, the stationary sources are not expected to emit substantial primary carbonaceous particles. Gaseous emissions from these point sources, such as NO and SO_2, may be oxidized in the atmosphere, leading to secondary aerosol such as NO_3^- and sulfate ($SO_4^=$). For this study, the focus is on apportioning carbonaceous aerosol in winter, paved road dust, on-road gasoline vehicle emission, on-road diesel vehicle emission, residential wood combustion, secondary $(NH_4)_2SO_4$, and secondary NH_4NO_3 source profiles chosen as the base CMB input. Unpaved road dust and non-road diesel emission profiles are similar to paved road dust and on-road diesel, respectively, in many aspects. They are also used in CMB fitting as part of the sensitivity test.

The species fitted in CMB for this study are listed in Table 6-1 and their abundances (relative to the measured mass) in each profile are presented in Appendix A and Appendix B. Individual and/or composite profiles can be used in CMB. Nevertheless,

composite source profiles are usually preferred since they reflect the source variability in addition to the analytical uncertainty. The number of species used in the fitting determines the model degree of freedom. NO_3^-, SO_4^{2-}, and NH_4^+ are chosen for their secondary aerosol profiles. K^+ is known to be a marker for vegetative burning. OC and EC are present in all combustion sources. Crustal elements—Al, Si, K, Ca, Ti, and Ba—are commonly found in the paved road dust (e.g., Chow et al., 2003). Cl, V, Cr, Mn, Fe, Ni, Cu, Zn, and Pb are also included for their ambient levels, which are typically above the detection limit.

In order to resolve the difference between gasoline and diesel emissions, several organic markers are selected for CMB analysis. Hopanes and steranes are found in diesel fuel and are present in the lubricating oil used by both diesel and gasoline vehicles. Some high molecule weight PAHs, such as benzo(ghi)perylene, indeno(1,2,3-cd)pyrene, and coronene, are unique to gasoline vehicle emission (Rogge et al., 1993). Levoglucosan is a major constituent of the fine emissions from cellulose during biomass burning and has been accepted as a good tracer for biomass burning (Simoneit et al., 1999). It is noted that the abundance of organic markers generally shows larger variability than inorganic/elemental species between individual source profiles from multiple tests, due to the low concentration of organic compounds. This leads to a larger uncertainty associated with organic marker in the composite source profiles and less weighting in CMB. Despite the fact that these organic markers could be good indicators for specific emitters, their emission factors may vary too significantly to impact the overall results of CMB source apportionment.

Table 6-1. Species included in the CMB base trial for the Las Vegas study.

Index	*Abbreviation*	*Fitted*	*Name*	*Marker for*
1	NHCC		Ammonia	
2	CLIC		Chloride	
3	N3IC	*	Nitrate	Secondary
4	S4IC	*	Sulfate	Secondary
5	N4CC	*	Ammonium	Secondary
6	NAAC		Soluble sodium	
7	KPAC	*	Soluble potassium	Vegetative burning
8	O1TC		Organic carbon I (40 – 120°C)	
9	O2TC		Organic carbon II (120 – 250°C)	
10	O3TC		Organic carbon III (250 – 450°C)	
11	O4TC		Organic carbon IV (450 – 550°C)	
12	OPTC		Pyrolyzed organic carbon	
13	OCTC	*	Total organic carbon	Combustion
14	E1TC		Elemental carbon I (550 °C)	
15	E2TC		Elemental carbon II (550 – 700°C)	
16	E3TC		Elemental carbon III (700 – 800°C)	
17	ECTC	*	Total elemental carbon	Combustion, diesel
18	TCTC		Total carbon	
19	NAXC		Sodium	
20	MGXC		Magnesium	
21	ALXC	*	Aluminum	Geological
22	SIXC	*	Silicon	Geological
23	PHXC		Phosphorus	
24	SUXC		Sulfur	
25	CLXC	*	Chlorine	
26	KPXC	*	Potassium	Geological
27	CAXC		Calcium	
28	TIXC	*	Titanium	Geological
29	VAXC	*	Vanadium	Oil Combustion
30	CRXC	*	Chromium	
31	MNXC	*	Manganese	
32	FEXC	*	Iron	Tire Brake
33	COXC		Cobalt	
34	NIXC	*	Nickel	
35	CUXC	*	Copper	
36	ZNXC	*	Zinc	
37	GAXC		Gallium	
38	ASXC		Arsenic	
39	SEXC		Selenium	
40	BRXC		Bromine	
41	RBXC		Rubidium	
42	SRXC		Strontium	
43	YTXC		Yttrium	
44	ZRXC		Zirconium	
45	MOXC		Molybdenum	
46	PDXC		Palladium	
47	AGXC		Silver	
48	CDXC		Cadmium	
49	INXC		Indium	
50	SNXC		Tin	
51	SBXC		Antimony	

52	BAXC	*	Barium	Geological
53	LAXC		Lanthanum	
54	AUXC		Gold	
55	HGXC		Mercury	
56	TLXC		Thallium	
57	PBXC	*	Lead	
58	URXC		Uranium	
59	baanth	*	Benz(a)anthracene (PAH)	
60	bbjkfl		Benzo(b+j+k)fluoranthe (PAH)	
61	bghipe	*	Benzo(ghi)perylene (PAH)	Gasoline
62	bntiop	*	Benzonaphthothiophene (PAH)	
63	chol		cholesterol (POLAR)	Cooking
64	azeac		azelaic acid-TMS (POLAR)	
65	chrysn	*	Chrysene (PAH)	
66	corone	*	Coronene (PAH)	Gasoline
67	fluora	*	Fluoranthene (PAH)	
68	hop19		17a(H),21ß(H)-Hopane	
69	hop21	*	22S-17a(H),21ß(H)-30-Homohopane	Diesel & Gasoline
70	hop22		22R-17a(H),21ß(H)-30-Homohopane	Diesel & Gasoline
71	hop24		22S-17a(H),21ß(H)-30,31-Bishomohopane	Diesel & Gasoline
72	hop25		22R-17a(H),21ß(H)-30,31-Bishomohopane	
73	hop9		C27-tetracyclic terpane	
74	incdpy	*	Indeno[123-cd]pyrene (PAH)	Gasoline
75	pyrene		Pyrene (PAH)	
76	retene		Retene (PAH)	
77	levg	*	Levoglucosan (POLAR)	Vegetative burning

6.2 *Sensitivity Test*

The on-road gasoline, on-road diesel, and non-road diesel profiles (December 2003) were acquired at Las Vegas within one year of the ambient measurements (January 2003). The dust profiles were acquired at various locations in Las Vegas during 1995. The wood combustion profiles, including wood stoves and fireplaces burning hardwood and softwood, were acquired as part of the Lake Tahoe source characterization study. Emission factors may change with time; wood burning emission may be influenced by temperature, relative humidity, air pressure, and other subtle furnace configurations. These variations propagate into the CMB and cause some biases. Even though the base input profiles are selected reasonably, it is important to estimate how sensitive the CMB outputs are to the various input data by carrying out a sensitivity test. The sensitivity test examines the robustness of the base CMB results by running the model with different source profiles, different fitting species, and also for different ambient samples. The ambient sample with highest ambient $PM_{2.5}$ concentration (1/23/2003, $PM_{2.5}$ ~19 $\mu g/m^3$) from the CC site is selected for this test for two reasons: 1) the CC site is next to I-515 and is expected to be more influenced by on-road diesel vehicles than the other three sites; and 2) the dominant source for geological material at CC is likely paved road dust. Table 6-2 lists the alternative source profiles used in the sensitivity test.

Table 6-2. A list of profiles used in the sensitivity test.

Source Type	Source Profiles	Profile Description
Geological	GPVRDC	Composite of 7 paved road dust profiles (Chow et al., 1995)
	GCONSC	Composite of 5 construction dust profiles (Chow et al., 1995)
	GUPRDC	Composite of 2 unpaved road dust profiles (Chow et al., 1995)
Motor Vehicle	OnRGASC	The composite of 4 on-road vehicle emission at Swenson (December 2003)
	OnRGAS2	The second test of on-road vehicle emission at Swenson (December 2003)
	OnRGAS4	The fourth test of on-road vehicle emission at Swenson (December 2003)
	OnRDIE	On-road diesel emission, composite of 4 samples (December 2003)
	OffRDIR	Off-road diesel emission, composite of 5 samples (December 2003)
Residential Wood Combustion	WSALMC	Woodstove fueled with almond (Kuhn et al., 2004)
	WSPINC	Woodstove fueled with pine (Kuhn et al., 2004)
	FPOAKC	Fireplace fueled with oak (Kuhn et al., 2004)
	FPJUNC	Fireplace fueled with juniper (Kuhn et al., 2004)
	WOODST	Composite of two woodstove profiles (Kuhn et al., 2004)
Secondary	AMSUL	Secondary ammonium sulfate
	AMVSUL	Secondary ammonium bisulfate
	AMNIT	Secondary ammonium nitrate

Table 6-3 compares the CMB outputs for various combinations of input source profiles. Three criteria used to evaluate the agreements between model calculation and measurements are: 1) R-square (target = 1), 2) Chi-square (target < 4), and 3) percent of mass (100% ± 20%). Since this study is for carbon apportionment, Percent of TC is also shown as a criterion.

Table 6-3. Sensitivity test for CMB results using alternative source profiles.

CIC (1/23/03)	Base Input	Test 1	Test 2	Test 3	Test 4	Test 5	Test 6	Test 7	Test 8	Test 9	Test 10	Test 11	Test 12
GPVRDC	2.51 ± 0.51			2.51 ± 0.51	2.51 ± 0.24	2.6 ± 0.25	2.45 ± 0.61	2.6 ± 0.54	2.54 ± 0.52	2.93 ± 0.71	2.9 ± 0.7	3.05 ± 0.64	3.07 ± 0.65
GCONSC		2.17 ± 0.47											
GUPRDC			1.87 ± 0.48										
OnRGASC	5.74 ± 1.09	6.27 ± 1.16	6.5 ± 1.17	5.73 ± 1.09			7.53 ± 0.82	6.23 ± 1.01	5.71 ± 1.08	8.92 ± 1.34	8.93 ± 1.34	7.95 ± 1.23	7.99 ± 1.24
OnRGAS2					0.46 ± 0.12								
OnRGAS4						1.69 ± 0.26							
OnRDIE	3.71 ± 1.98	3.41 ± 2.07	3.13 ± 2.09	3.72 ± 1.98	12.53 ± 2.21	9.64 ± 1.85			2.94 ± 3.07	-0.42 ± 3.83	0.26 ± 2.42	1.49 ± 2.24	1.42 ± 2.24
OffRDI								3.91 ± 2.45	1.2 ± 3.5	1 ± 4.48			
WSALMC	2.43 ± 0.85	2.42 ± 0.89	2.49 ± 0.92	2.43 ± 0.85	4.86 ± 0.85	4.51 ± 0.75	2.23 ± 0.91	2.29 ± 0.85	2.39 ± 0.84				
WSPINEC												0.39 ± 0.15	
FPOAKC													
FPJUNC													0.17 ± 0.09
WOODST													
AMSUL	0.87 ± 0.13	0.9 ± 0.13	0.91 ± 0.13		0.73 ± 0.11	0.77 ± 0.11	0.93 ± 0.13	0.9 ± 0.12	0.88 ± 0.13	0.93 ± 0.15	0.92 ± 0.15	0.9 ± 0.14	0.9 ± 0.14
AMBSUL				0.75 ± 0.11									
AMNIT	5.44 ± 0.46	5.43 ± 0.46	5.43 ± 0.46	5.69 ± 0.47	5.37 ± 0.45	5.39 ± 0.45	5.48 ± 0.47	5.47 ± 0.46	5.45 ± 0.46	5.47 ± 0.47	5.47 ± 0.47	5.46 ± 0.47	5.46 ± 0.47
CHI SQUARE	1.86	1.72	1.77	1.87	7.79	7.62	1.37	1.73	1.97	2.34	2.25	1.95	1.98
R SQUARE	0.92	107.7	0.91	0.91	0.75	0.77	0.92	0.92	0.92	0.87	0.87	0.9	0.9
PERP MASS (%)	108.2	107.7	106.3	108.9	138.3	128.7	97.3	111.9	110.4	98.4	96.6	100.6	99.5
PREP TC (%)	98	99	100	98	119	109	87	101	100	99	97	97	98
Fitting Species clusters													
Site													

Table 6-3 (continued)

CIC (1/23/03)	Test 13	Test 14	Test 15	Test 16	Test 17	Test 18	Test 19	Test 20	Test 21	Test 22	Test 23	Test 24	Test 25	Test 26
GPVRDC	2.59 ± 0.49	2.39 ± 0.54	2 ± 0.44	2.6 ± 0.49	4.08 ± 0.76	4.85 ± 0.98	6.03 ± 0.91	7.24 ± 1.23	5.57 ± 0.69	5.96 ± 0.76	3.76 ± 0.41	4.08 ± 0.47	2.62 ± 0.5	3.18 ± 0.64
GCONSC														
GUPRDC														
OnRGASC	5.44 ± 1.05	6.16 ± 1.17	4.65 ± 2.03	5.3 ± 1.04	8.23 ± 1.53	11.79 ± 1.82	8.8 ± 1.71	14.12 ± 2.22	6.26 ± 1.2	7.55 ± 1.25	3.27 ± 0.68	4.43 ± 0.75	5.53 ± 1.05	7.75 ± 1.21
OnRGAS2														
OnRGAS4														
OnRDIE	2.21 ± 1.86	3.02 ± 2.1	5.23 ± 3.15	4.32 ± 1.94	0.27 ± 2.47	-3.52 ± 3.28	0.99 ± 2.76	-4.94 ± 4	3.37 ± 2.11	1.9 ± 2.22	0.19 ± 1.07	-1.02 ± 1.3	2.91 ± 1.97	0.68 ± 2.18
OffRDI														
WSALMC			2.78 ± 1.04	2.3 ± 0.81	3.89 ± 1.26		5.09 ± 1.48		1.46 ± 0.75		1.63 ± 0.55		2.31 ± 0.82	
WSPINEC														
FPOAKC	6.04 ± 1.65													
FPJUNC						0.21 0.12		0.54 ± 0.28		0.27 ± 0.14		0.19 ± 0.1		0.17 ± 0.09
WOODST		4.01 ± 1.6												
AMSUL	0.86 ± 0.12	0.89 ± 0.13	0.86 ± 0.12	0.86 ± 0.12	1.27 ± 0.18	1.32 ± 0.2	1.21 ± 0.18	1.28 ± 0.21	0.74 ± 0.13	0.76 ± 0.13	0.29 ± 0.,05	0.31 ± 0.07	0.88 ± 0.12	0.91 ± 0.14
AMBSUL														
AMNIT	5.45 ± 0.46	5.44 ± 0.46	5.43 ± 0.45	5.44 ± 0.49	6.44 ± 0.55	6.48 ± 0.56	3.18 ± 0.3	3.24 ± 0.33	2.72 ± 0.25	2.74 ± 0.26	0.3 ± 0.049	0.31 ± 0.06	5.45 ± 0.46	5.47 ± 0.47
CHI SQUARE	1.89	1.51	1.82	1.8	1.27	1.47	1.14	1.85	1.3	1.23	2.53	1.98	2.07	2.18
R SQUARE	0.92	0.92	0.92	0.94	0.94	0.91	0.95	0.89	0.94	0.94	0.87	0.87	0.91	0.89
PERP MASS (%)	118.1	114.6	109.7	108.8	102.6	89.6	99.5	84.4	107.3	102.2	126.4	111	103.1	94.9
PREP TC (%)	111	98	99	98	92	90	96	95	101	101	86	84	106	1.06
Fitting Species clusters			No Fe, Mn, and Cu	No organic compounds									OC, EC corrected for backup filter	
Site					ORR (1/23/03)	ORR (1/23/03)	ECH (1/22/03)	ECH (1/22/03)	JDS (1/23/03)	JDS (1/23/03)	JDS (1/25/03)	JDS (1/25/03)		

The base fit (degree of freedom = 24) overestimates the gravimetric mass by ~8% and underestimates the total carbon by ~2% for this sample, both of which are within the uncertainty of measured values. An r^2 of 0.91 indicates that the model explains 91% of the data variation. This model predicts that paved road dust, on-road gasoline, on-road diesel, residential wood combustion, secondary sulfate, and secondary nitrate contribute to 12 ± 3%, 28 ± 5%, 18 ± 9%, 12 ± 4%, 4 ± 1%, and 26 ± 2% of the $PM_{2.5}$ mass, respectively.

Tests 1 and 2 examine the impacts of different geological source profiles on CMB source apportionment results. Either construction or unpaved road dust causes little change in the overall model performance; partitioning between geological, on-road gasoline, and on-road diesel sources do cause change, but generally within the calculated uncertainties of the base fit. Since there is no evidence to justify using construction or unpaved road dust profiles, the paved road dust profile is used hereafter in the CMB analysis. Test 3 demonstrates the minor effect using $[NH_4]\cdot HSO_4$ instead of $(NH_4)_2SO_4$ profiles has. This is partly due to the relatively minor contribution of $SO_4^=$ to $PM_{2.5}$ mass.

Tests 4–8 examine the effect of using alternate mobile emission profiles. Collinearity appears when including both on-road and off-road diesel profiles. These two source subtypes cannot be resolved with the current fitting species. Using an individual source profile rather than the composite one always leads to higher Chi-square values. Tests 9–14 examine the effect of not including wood combustion or using other wood combustion profiles. Fireplaces burning softwood should be more common at Las Vegas Valley in winter than woodstoves burning hardwood. However, the profile of fireplace burning juniper leads to a scenario in which the wood combustion contributes to <1% of $PM_{2.5}$ mass in Test 12. Test 18 and Test 19 also show that this profile leads to model instability. Due to the unavailability of wood burning profiles directly measured at Las Vegas, the profile of wood stove burning almond is used hereafter for a better fit. The selection of woodstove burning almond for CMB in this study suggests only that a similar residential wood combustion profile can be found in Las Vegas Valley, but does not suggest that woodstove burning almond is the only and/or main source of RWC in the valley.

Tests 15 and 16 examine the influence of Fe, Mn, and Cu, as well as organic markers on the model results. Excluding these species cause only minor changes in the CMB apportionment results. This proves the stability of the base fit. Tests 17–24 extrapolate some CMB inputs to the other three sampling sites. Generally, the base input source profiles also explain the observed $PM_{2.5}$ mass and TC for OR, JD, and MS.

In this study, the ambient measurements were achieved using sequential quartz-quartz filters. The backup filter is commonly used for evaluating and adjusting the organic sampling artifacts (Chow and Watson, 2002; Turpin et al., 1994). It has been shown (Section 3.4.3) that subtracting OC on the backup filter from the front filter leads to a better $PM_{2.5}$ mass closure. Tests 25 and 26 examine CMB fitting using front OC subtracted from backup-filter OC. Contribution from on-road diesel is reduced but the others remain almost the same. Although Test 25 shows only a slight difference of source contributions from the base fit, the R-square decreases and Chi-square increases, indicate

less-fitted model results for ambient samples with subtracting backup filters. At the same time, the model overestimates both $PM_{2.5}$ mass and TC by less than 10%.

The base input selected does not present a significant weakness in all of these sensitivity tests. Therefore, it is adopted for the CMB source apportionments for this study. Figure 6-1(a-c) compares the measured and constructed concentrations of $PM_{2.5}$ mass, OC, and EC for the 46 samples. Their agreements are generally within 25%. The biases likely result from three origins: 1) unidentified sources, 2) sampling artifacts, and 3) profile aging. The earlier emission estimates (Chow et al., 1999) and this sensitivity do not suggest a major unidentified source. Watson et al. (2002) demonstrated how the changes in a source profile as it ages in the atmosphere impact the CMB performance. In the urban area, however, the transit time between sources and receptors are relatively short, so that the profile aging is limited. The adsorption of volatile or semi-volatile organic vapors onto a quartz-fiber filter inflates the OC mass. This amount of adsorption varies between ambient and source samples due to different sampling durations, and this influences the CMB fitting for $PM_{2.5}$ mass and OC. Measured and CMB calculated mass are highly correlated at 0.87, 0.87, and 0.77 for $PM_{2.5}$ mass, OC, and EC, respectively.

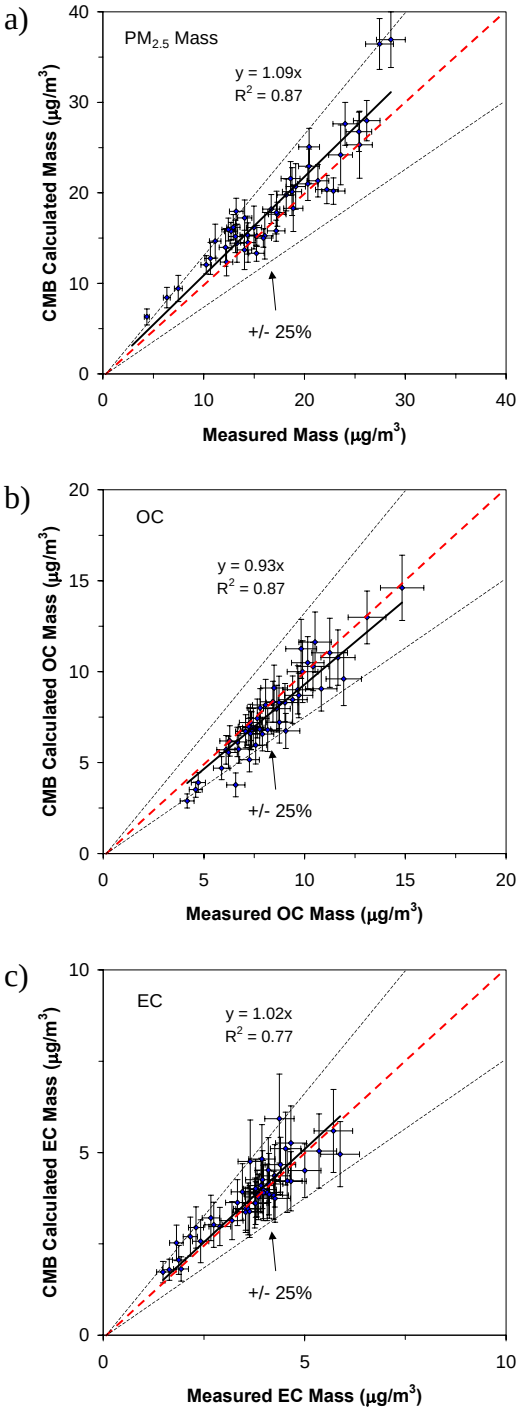

Figure 6-1. Comparisons between measured and CMB calculated (a) $PM_{2.5}$ mass, (b) OC, and (c) EC for the Las Vegas $PM_{2.5}$ Apportionment Study.

6.3 *$PM_{2.5}$ Source Apportionment*

The contribution from the sources to ambient $PM_{2.5}$ concentration with time is presented in Figure 6-2. The OR site is at a moderately populated residential area farther away from downtown than the other three sites. During this study, roughly grouped into three periods—1/3/2003–1/5/2003, 1/12/2003–1/14/2003, and 1/20/2003–1/25/2003—the

source apportionment results for $PM_{2.5}$ at OR is consistent, showing dominant contributions from paved road dust and on-road mixed fleet gasoline vehicles. There is very little contribution from on-road diesel vehicles. The JD and CC sites are northeast of highway US-95 (I-515) and east of I-15. Considering the southeasterly prevailing wind for most of the sampling period, these two sites are expected to be impacted by the mobile emissions from highway traffic. Increased on-road diesel vehicle contribution is observed during the second and third periods at the CC and JD sites. During the third period, the on-road diesel vehicle contribution nearly equals that of on-road mixed fleet vehicles at CC. However, on-road diesel vehicle contribution is very low during the first episode. It is noted that 1/3/2003–1/5/2003 was the extended weekend following New Year's Day (Wednesday), and this may explain the absence of on-road diesel vehicle emissions at the very end of the holiday season. Another feature of the first period is the elevated contribution from wood/vegetative combustion at JD and MS. The $PM_{2.5}$ sample at JD on 1/4/2003 (Saturday) contains much higher K^+, cholesterol, and levoglucosan than 1/5/2003 (Sunday), and the organic mass is about twice as high. This might suggest a special gathering near J.D. Smith Elementary School on 1/4/2003. The MS site is at a densely populated area in Las Vegas. The wood combustion contribution at this site is substantially higher than at the other three sites, accounting for about one-third of the $PM_{2.5}$ mass. Since this site is south of US-95, it does not show a significant impact from highway diesel vehicles.

a)

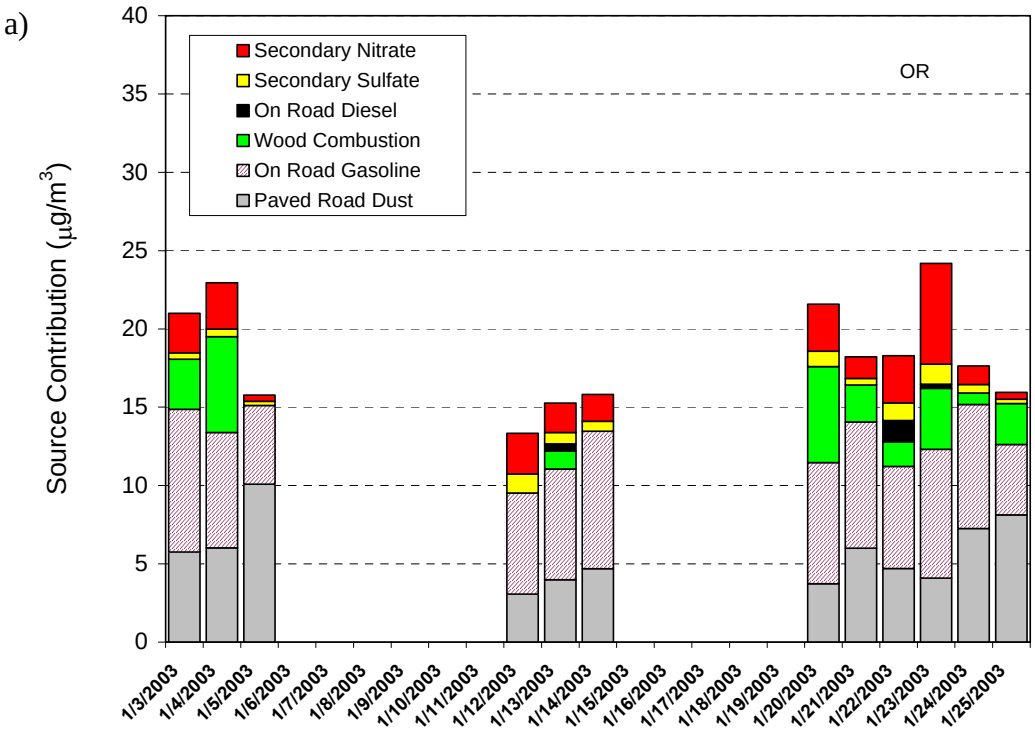
Secondary Nitrate
Secondary Sulfate
On Road Diesel
Wood Combustion
On Road Gasoline
Paved Road Dust
OR
Source Contribution (μg/m3)
0
5
10
15
20
25
30
35
40
1/3/2003
1/4/2003
1/5/2003
1/6/2003
1/7/2003
1/8/2003
1/9/2003
1/10/2003
1/11/2003
1/12/2003
1/13/2003
1/14/2003
1/15/2003
1/16/2003
1/17/2003
1/18/2003
1/19/2003
1/20/2003
1/21/2003
1/22/2003
1/23/2003
1/24/2003
1/25/2003

b)

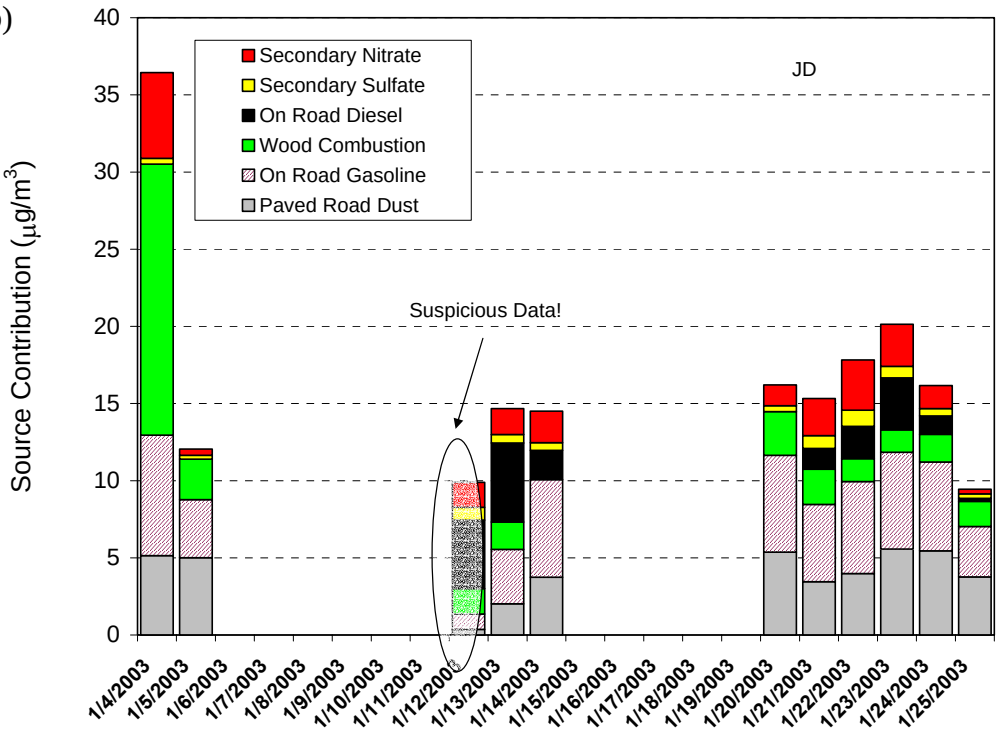
Secondary Nitrate
Secondary Sulfate
On Road Diesel
Wood Combustion
On Road Gasoline
Paved Road Dust
JD
Suspicious Data!
Source Contribution (μg/m3)
0
5
10
15
20
25
30
35
40
1/4/2003
1/5/2003
1/6/2003
1/7/2003
1/8/2003
1/9/2003
1/10/2003
1/11/2003
1/12/2003
1/13/2003
1/14/2003
1/15/2003
1/16/2003
1/17/2003
1/18/2003
1/19/2003
1/20/2003
1/21/2003
1/22/2003
1/23/2003
1/24/2003
1/25/2003

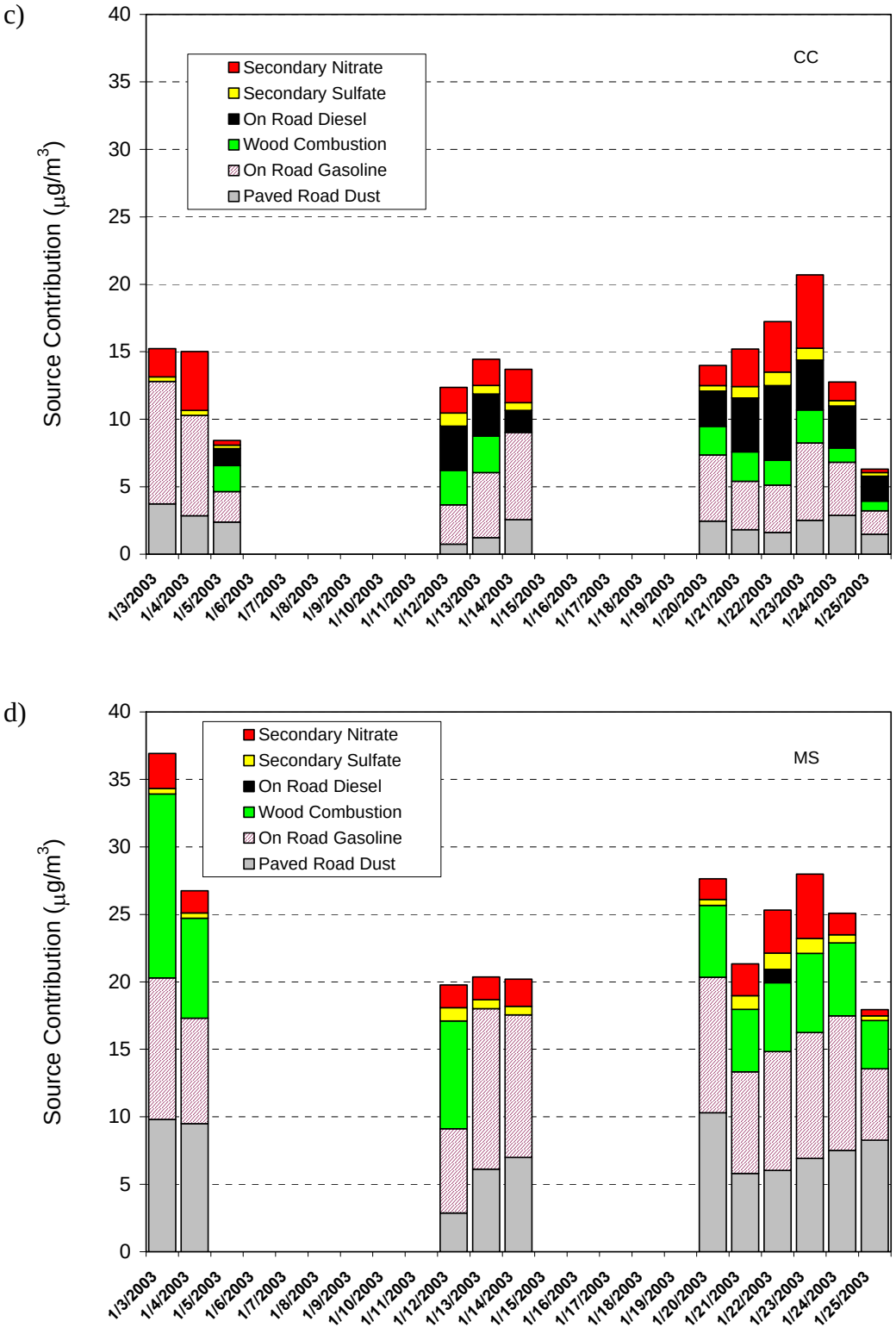

Figure 6-2. Source contributions to $PM_{2.5}$ mass as a function of time at a) OR b) JD c) CC and d) MS. One sample from JD (1/12/2003) is marked suspicious since the $PM_{2.5}$ mass closure is >>100%.

Despite the proximity to the highway, the contribution from road dust is lower at CC, which might be related to different road conditions and traffic patterns. MS is the opposite of CC, having many vehicles running at a low and unsteady speed, and MS measures the highest dust contributions. The secondary aerosol is mostly NH_4NO_3. The contribution and variation of NH_4NO_3 is consistent across the four sites. This spatial uniformity is commonly observed for secondary aerosol, which is formed in the atmosphere.

Figures 6-3 and 6-4 present the contribution of paved road dust, on-road gasoline, on-road diesel, and wood combustion to the ambient OC and EC concentrations, respectively. At OR, the EC is almost exclusively from on-road gasoline emission, except for 1/22/2003. Paved road dust and wood combustion contribute ~10% of OC. A similar pattern is found at MS, with a slightly higher contribution of wood combustion to OC. At JD and CC, more diesel contribution to carbonaceous aerosol is observed during the second and third episodes. Diesel trucks running on the nearby highways are believed to be the major source. At the CC site, diesel commonly contributes ~50% of EC and 30–40% of OC. The wood burning contribution is at negligible levels at the two sites.

a)

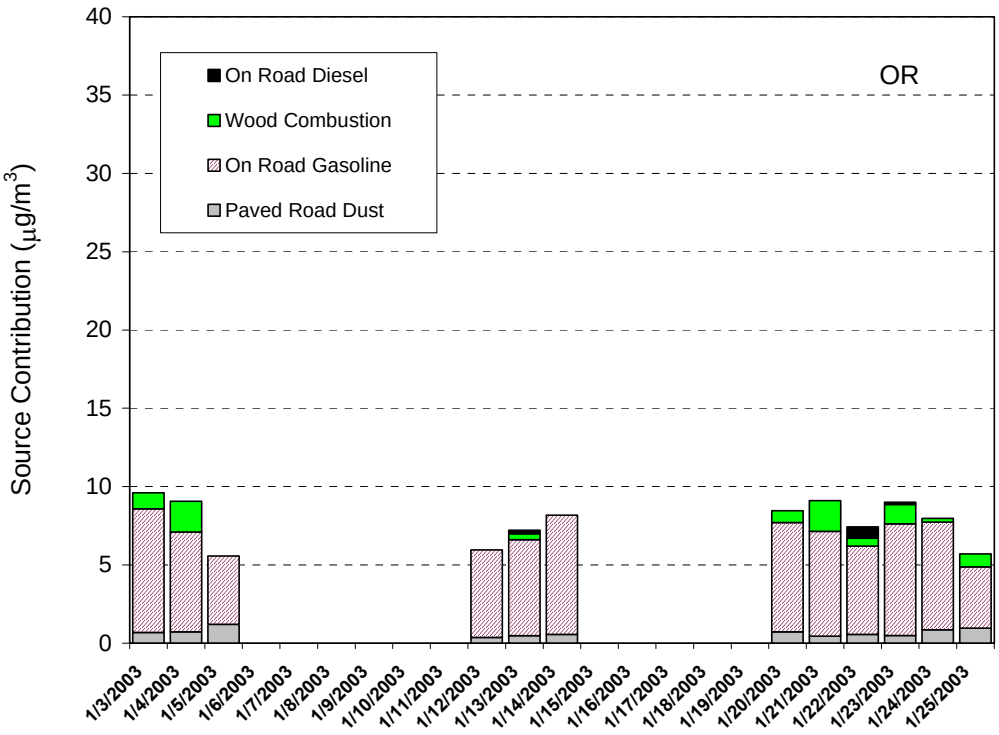
On Road Diesel
Wood Combustion
On Road Gasoline
Paved Road Dust
OR
Source Contribution (μg/m3)
0
5
10
15
20
25
30
35
40
1/3/2003
1/4/2003
1/5/2003
1/6/2003
1/7/2003
1/8/2003
1/9/2003
1/10/2003
1/11/2003
1/12/2003
1/13/2003
1/14/2003
1/15/2003
1/16/2003
1/17/2003
1/18/2003
1/19/2003
1/20/2003
1/21/2003
1/22/2003
1/23/2003
1/24/2003
1/25/2003

b)

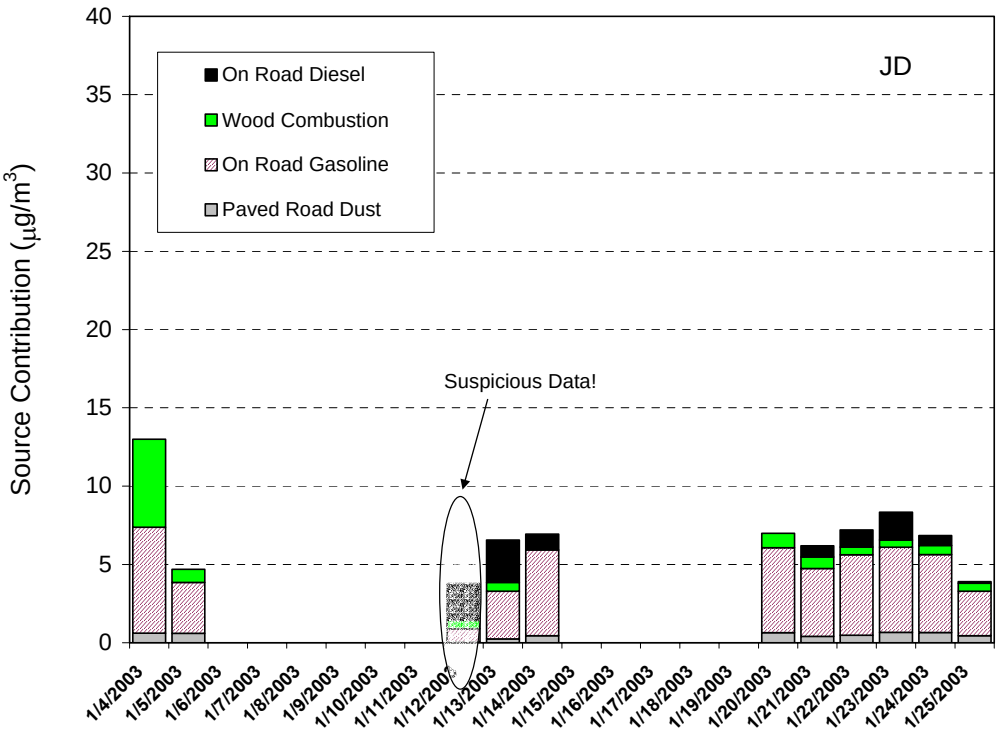
On Road Diesel
Wood Combustion
On Road Gasoline
Paved Road Dust
JD
Suspicious Data!
Source Contribution (μg/m3)
0
5
10
15
20
25
30
35
40
1/4/2003
1/5/2003
1/6/2003
1/7/2003
1/8/2003
1/9/2003
1/10/2003
1/11/2003
1/12/2003
1/13/2003
1/14/2003
1/15/2003
1/16/2003
1/17/2003
1/18/2003
1/19/2003
1/20/2003
1/21/2003
1/22/2003
1/23/2003
1/24/2003
1/25/2003

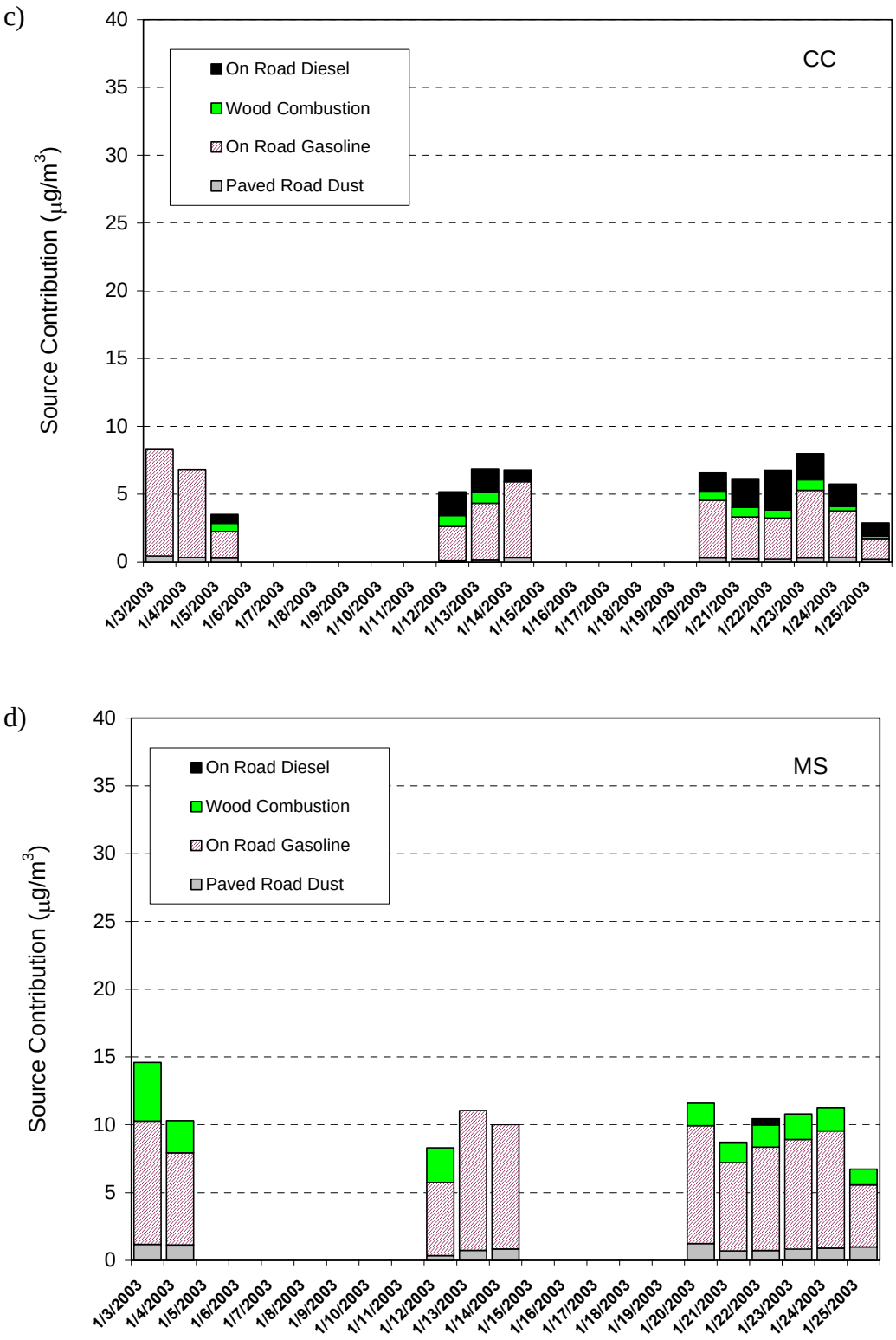

Figure 6-3. Source contributions to OC mass as a function of time at a) ORR b) JD c) CC and d)MS. One sample from JDS (1/12/2003) is marked suspicious since the $PM_{2.5}$ mass closure is >>100%.

a)

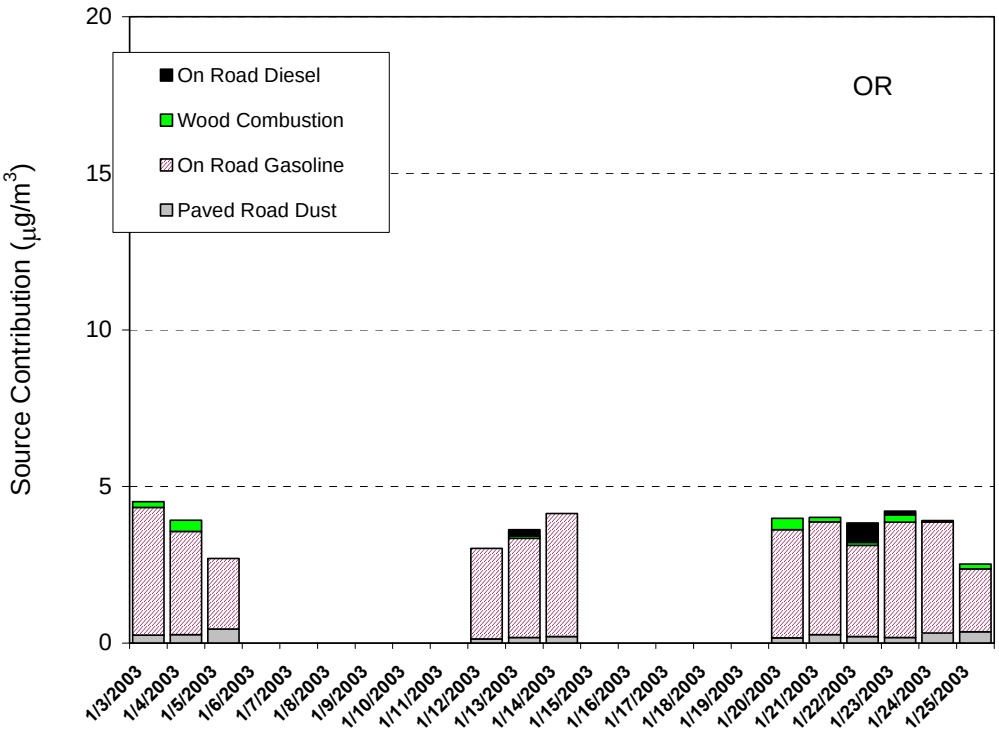
On Road Diesel
Wood Combustion
On Road Gasoline
Paved Road Dust
OR
Source Contribution (μg/m3)
20
15
10
5
0
1/3/2003
1/4/2003
1/5/2003
1/6/2003
1/7/2003
1/8/2003
1/9/2003
1/10/2003
1/11/2003
1/12/2003
1/13/2003
1/14/2003
1/15/2003
1/16/2003
1/17/2003
1/18/2003
1/19/2003
1/20/2003
1/21/2003
1/22/2003
1/23/2003
1/24/2003
1/25/2003

b)

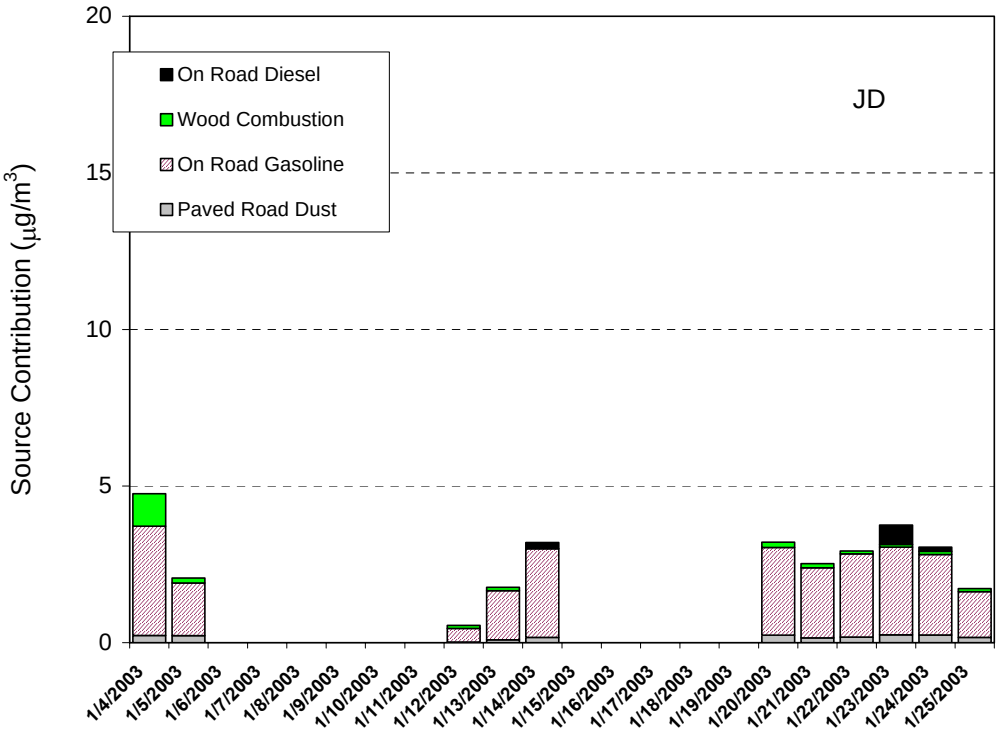
On Road Diesel
Wood Combustion
On Road Gasoline
Paved Road Dust
JD
Source Contribution (μg/m3)
20
15
10
5
0
1/4/2003
1/5/2003
1/6/2003
1/7/2003
1/8/2003
1/9/2003
1/10/2003
1/11/2003
1/12/2003
1/13/2003
1/14/2003
1/15/2003
1/16/2003
1/17/2003
1/18/2003
1/19/2003
1/20/2003
1/21/2003
1/22/2003
1/23/2003
1/24/2003
1/25/2003

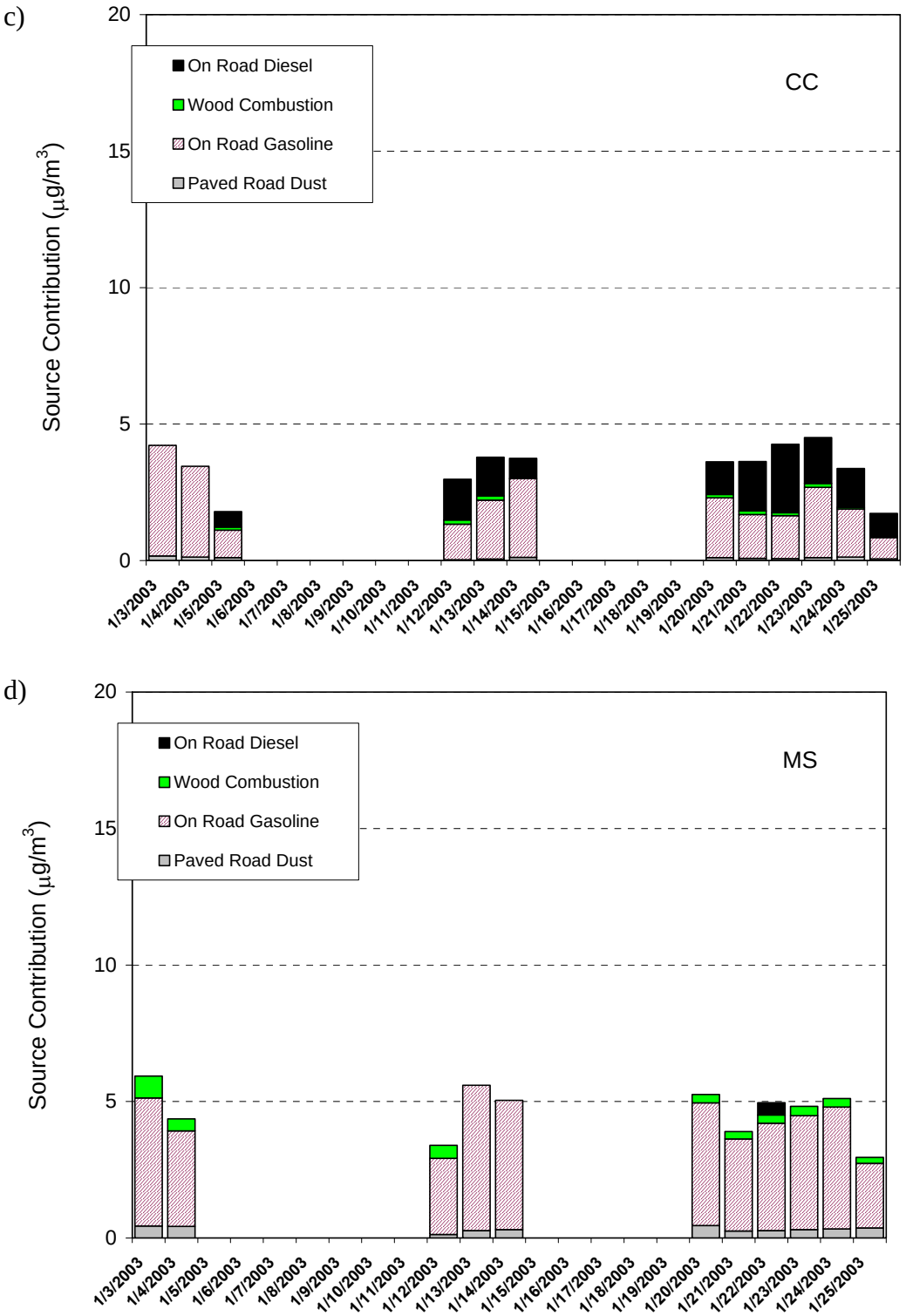

Figure 6-4. Source contributions to EC mass as a function of time at a) ORR b) JD c) CC and d) MS.

The spatial and temporal variations of contributions from these six sources to the ambient concentration agree with the site specification and sampling timeline for the most part. This again confirms the validity of the CMB source apportionment. Table 6-4 summarizes the overall average contribution from each source to each site in terms of

percentage of $PM_{2.5}$ mass, OC, and EC, respectively. On-road mixed fleet gasoline vehicle emission is the most dominant source, accounting for 32.6–40.0% of the $PM_{2.5}$ mass. Most of the gasoline emission is OC. At residential sites such as OR and MS on-road diesel vehicle emission seems less common (<2%) and CMB estimates on-road gasoline vehicle contributes to ~ 80% of OC and EC. The surprisingly low contributions of on-road diesel vehicle emissions to PM at MS and OR might be explained by the older automobile fleet in the neighborhood of MS and OR, emission characteristics of which are more similar to that of on-road diesel vehicles. Diesel trucks appear to be a significant portion of highway traffic. At JD and CC, diesel emission accounts for 17.6–34.1% of EC. Wood combustion accounts for ~10% of OC and only ~5% of EC on average. It is noted that wood combustion contribution varies substantially with time. The frequency of utilizing residential heating facilities depends on the ambient temperature.

Table 6-4. Average contribution from sources to receptor sites for (a) $PM_{2.5}$, (b) OC, and (c) EC.

a)

$PM_{2.5}$ Mass	**ORR (12 d)**	**JDH (10 d)**	**CIC (12 d)**	**ECH (11 d)**
Paved Road Dust	31.8 ± 13.9%	27.5 ± 9.7%	16.8 ± 7.2%	30.0 ± 8.3%
On-road Gasoline	40.0 ± 8.2%	32.6 ± 6.5%	33.7 ± 12.1%	37.2 ± 9.7%
Wood Combustion	11.3 ± 9.8%	15.9 ± 12.9%	11.1 ± 8.0%	20.8 ± 12.5%
On-road Diesel	1.0 ± 2.2%	9.5 ± 10.8%	18.6 ± 10.5%	0.4 ± 1.2%
Secondary Sulfate	3.9 ± 2.2%	3.4 ± 1.5%	4.2 ± 1.6%	3.0 ± 1.4%
Secondary Nitrate	12.0 ± 6.9%	11.2 ± 5.1%	15.5 ± 7.8%	8.6 ± 3.9%

b)

Organic Carbon	**ORR (12 d)**	**JDH (10 d)**	**CIC (12 d)**	**ECH (11 d)**
Paved Road Dust	9.2 ± 5.1%	7.9 ± 2.9%	4.5 ± 1.8%	8.6 ± 2.8%
On-road Gasoline	80.7 ± 8.1%	67.7 ± 10.6%	64.3 ± 17.2%	74.6 ± 10.0%
Wood Combustion	8.8 ± 7.8%	12.8 ± 11.7%	8.3 ± 6.0%	16.4 ± 9.9%
On-road Diesel	1.2 ± 2.9%	11.6 ± 12.9%	22.9 ± 13.5%	0.5 ± 1.5%

c)

Elemental Carbon	**ORR (12 d)**	**JDH (10 d)**	**CIC (12 d)**	**ECH (11 d)**
Paved Road Dust	7.3 ± 4.1%	6.1 ± 2.6%	3.0 ± 1.3%	7.1 ± 2.4%
On-road Gasoline	87.1 ± 5.8%	70.9 ± 13.7%	60.2 ± 19.7%	85.1 ± 5.5%
Wood Combustion	3.6 ± 3.3%	5.4 ± 6.1%	2.7 ± 2.0%	7.0 ± 4.5%
On-road Diesel	2.1 ± 4.8%	17.6 ± 18.1%	34.1 ± 19.0%	0.8 ± 2.7%

7. CONCLUSION AND RECOMMENDATIONS FOR ADDITIONAL WORK

This section summarizes the findings and observations of this report. Additional studies are recommended that may lead to a better understanding of source emissions within the Las Vegas Valley and help develop proper control and monitoring strategies to reduce the impact of source emissions on ambient air quality.

7.1. CONCLUSION AND SUMMARY

The primary objective of this study was to quantify contributions of source types to carbon $PM_{2.5}$ and haze within the Las Vegas Valley. A mini-intensive winter study was conducted to collect 24-hour ambient air samples, representing "air pollution episodes", at four locations: East Charleston, Orr Middle School, City Center, and J.D. Smith Elementary School. At the same time, suspected main carbonaceous PM sources of on-road gasoline vehicles, on-road diesel vehicles, and non-road diesel vehicles were characterized with their chemical abundance, as well as fuel-based emission factors. Using the "weight of evidence" approach, the CMB source apportionment model was applied to the ambient samples collected, using source profiles collected in this study as well as profiles from other studies.

The 24-hour average ambient samples were collected for mass, ions, elements, OC, EC, and trace organic compounds analysis. Comparisons of reconstructed mass and measured mass show a significant intercept of 5.4 $\mu g/m^3$ due to the adsorption of volatile organic compounds onto quartz-fiber filters for sample collection. This positive sampling artifact is often observed when $PM_{2.5}$ concentration is low and the OC fraction in $PM_{2.5}$ is relatively high. A backup quartz-fiber filter behind a PTFE Teflon filter can be used to correct for the positive sampling artifact.

Average 24-hour $PM_{2.5}$ concentrations for the winter stagnant meteorological condition (slow mixing) were observed to be 40% higher than the annual $PM_{2.5}$ average in 2001, and were the highest at East Charleston among the four sites. The most abundant chemical species were total carbonaceous compounds (organic matter [OC x 1.4] + EC), which comprises more than 80% of $PM_{2.5}$. The highest concentrations of organic matter and EC were observed at East Charleston. However, the relative contribution of total carbonaceous compounds to $PM_{2.5}$ and the EC/OC ratio were highest at City Center. This is probably because the City Center site is the immediate "receptor" site of PM emitted from vehicles on US-95.

The distributions of average fractional particle cross-section area in East Charleston in January 2003 show that about 45% of particle area is from particles less than 1.0 μm in diameter (from combustion processes or secondary gas-to-particle conversion) and 40% of the particle area is from particles with diameter greater than 2.5 μm (mechanical processes, such as wind erosion, road dust, mineral processing). Both small and large particles contribute significantly to haze at the East Charleston site. Thus, combustion particles from motor vehicles, wood smoke, and dust are important in the winter haze at East Charleston.

Diurnal variations of EC concentrations determined by aethalometer show a trend of peak concentrations from 6 to 8 a.m., are lowest at noon, and rise to another peak from 4 to 7 p.m. at East Charleston, City Center, and Orr Middle School, following daily traffic patterns. An elevated EC concentration at East Charleston was probably due to the adjacent residential neighborhood, which has higher levels of residential wood combustion and cooking. The diurnal pattern of CO concentration, CO_2 concentration, EC concentration derived from photoacoustic instrument, OC and EC concentrations by Sunset Field Carbon Analyzer, light scattering and light absorption by NO_2, and soot track each other closely at East Charleston.

Source profiles collected within the Las Vegas Valley include: 1) on-road mixed fleet gasoline vehicles at summer, 2) on-road mixed fleet gasoline vehicles at winter, 3) on-road diesel vehicles at summer, 4) on-road diesel vehicles at winter, and 5) non-road diesel engines. The most abundant chemical species in these sources is carbonaceous compounds, which comprise more than 80% of $PM_{2.5}$ for all source types. Higher EC/high-temperature to OC (OC-OC1-OC2) ratios were found in the on-road diesel vehicle source profile (>3) than for on-road mixed fleet gasoline vehicles (<1.1). Although on-road and non-road diesel fuels are very much the same (except for a red dye added to non-road fuel), the EC/high-temperature to OC ratio for non-road diesel engines is similar to that of on-road mixed fleet gasoline vehicles. This is probably due to different types and uses between engines used for on-road and non-road purposes.

Fuel-based emission factors for the sources were measured and calculated with DRI In-Plume Sampling System. Average emission factors for gaseous species and PM for on-road mixed fleet gasoline vehicles developed by the In-Plume system show very good agreement to those by VERSS during 2001-2002 in the Las Vegas Valley. CO emission factors for on-road mixed fleet gasoline vehicles were twice of those for on-road diesel vehicles. The CO emission factors was reduced 31% in winter than in summer, probably attributable to better combustion efficiency for vehicle engines when the Oxygenated Fuel Program (Clark County Air Quality Regulations, Section 53) was enforced for winter gasoline fuel. NH_3 , NO_x, and THC emission factors were higher for on-road mixed fleet gasoline vehicles than for on-road diesel vehicles, probably due to late-model gasoline vehicles. The largest $PM_{2.5}$ emission factor was found for non-road diesel engines and they are generally higher 50% in summer than in winter. The emission factor for ultrafine particles (particles with aerodynamic diameter less than 0.1 μm) is very low.

The CMB source apportionment model identified four main sources contributing to $PM_{2.5}$ carbon within the Las Vegas Valley: 1) paved road dust, 2) on-road gasoline vehicles, 3) residential wood combustion, and 4) on-road diesel vehicles. Collinearity was observed between on-road and non-road diesel sources in CMB model. This is due to the very similar fuel compositions for these two sources, which is against the model assumption. CMB estimates that on-road mixed fleet gasoline vehicles are the largest source for OC and EC at all the sites. The contribution of paved road dust to both OC and EC was 5% to 10% at the four sites. On-road diesel vehicles contribute 22% of the OC and 34% of the EC at City Center, which is located immediately downwind of US-95. The contribution of on-road diesel vehicles to haze decreases 50% as the distance between the source (US-95) and receptor increases (i.e., from the City Center site to the J.D. Smith Elementary

School site). Residential wood combustion is a more significant source for the East Charleston and Orr Middle School sites than on-road diesel vehicles, probably due to the residential neighborhood.

7.2. Recommendations

With the rapid growth and development of the Las Vegas Valley, emissions from mobile sources and construction exhausts are increasing, which adversely affects the ambient air quality. The worsening air quality can result in reduced visibility, elevated $PM_{2.5}$, and adverse public health effects. A better understanding of the emission sources within the valley will allow the county to develop effective planning, control, and monitoring strategies for air quality.

The CMB source apportionment model reasonably quantified contributions of different sources to $PM_{2.5}$, OC, and EC at the four ambient monitoring sites. Based on this knowledge of emission sources in the valley, the very low contribution from on-road diesel vehicles at East Charleston seems to be an artifact from the high gasoline vehicle emitters. These emitters also result in the skewness of higher average emission factors for on-road gasoline vehicles. Identification of these high gasoline emitters is critical to the effective reduction of PM. With the addition of tube counters and video cameras to the DRI In-Plume and remote sensing systems, these high emitters can be identified and the emission factors can also be properly classified as light-duty gasoline vehicles, heavy-duty gasoline vehicles, light-duty diesel vehicles, and heavy-duty diesel vehicles by applying proper statistics.

The average emission factors for gases and PM for on-road mixed fleet gasoline vehicles can be affected by driver habits, road conditions, meteorological conditions, and vehicle age. The differences in the median and average emission factors and a high range of standard deviation of the emission factors can be expected in on-road gasoline vehicles, on-road diesel vehicles, and non-road diesel engines. Increasing the number of such measurements and in-depth statistics analysis can increase the confidence of quantifying emission factors from these sources.

The collinearity of on-road diesel vehicle and non-road engine profiles in CMB modeling make it difficult to distinguish the contributions of the two sources. The Las Vegas Valley Visibility and $PM_{2.5}$ study in 2001 showed how the diurnal variation of light absorption in Palos Verde was impacted by the use of off-road diesel engines at a construction site. Markers for these sources are needed.

Recent toxicological and exposure studies show increasing evidence of a link between other PM properties, in addition to PM mass, and adverse public health effects. These studies suggest that PM number, surface concentration, and particle size are also important measurements. PM emissions from mobile sources are usually less than 1µm and their number and surface concentrations depend on fuel types. The mass median diameter, count median diameter, number concentration, and surface concentrations should be quantified in future studies.

8. REFERENCES

Allen, J.O.; Mayo, P.R.; Hughes, L.S.; Salmon, L.G.; and Cass, G.R., (2001). Emissions of size-segregated aerosols from on-road vehicles in the Caldecott Tunnel. *Environmental Science & Technology* **35** (21), 4189-4197.

Arnott, W.P.; Moosmüller, H.; Rogers, C.F.; Jin, T.; and Bruch, R., (1999). Photoacoustic spectrometer for measuring light absorption by aerosol: Instrument description. *Atmospheric Environment* **33** (17), 2845-2852

Baum, M.M.; Kiyomiya, E.S.; Kumar, S.; Lappas, A.M.; Kapinus, V.A.; and Lord, H.C., III, (2001). Multicomponent remote sensing of vehicle exhaust by dispersive absorption spectroscopy – 2. Direct on-road ammonia measurements. *Environmental Science & Technology* **35** (18), 3735-3741.

Bevington, P.R., (1969). *Data Reduction and Error Analysis for the Physical Sciences*. McGraw Hill, New York, NY.

Brown, J.E.; Clayton, M.J.; Harris, D.B.; and King, F.G., Jr., (2000). Comparison of particle size distribution of heavy diesel exhaust using a dilution tailpipe sampler and an in-plume sampler during on-road operations. *Journal of the Air & Waste Management Association* **50** (8), 1407-1416.

Chow, J.C. and Watson, J.G., (1989). Summary of particulate data bases for receptor modeling in the United States. In *Transactions, Receptor Models in Air Resources Management*, Watson, J.G., editor. Air & Waste Management Association, Pittsburgh, PA, pp. 108-133.

Chow, J.C.; Watson, J.G.; Pritchett, L.C.; Pierson, W.R.; Frazier, C.A.; and Purcell, R.G., (1993). The DRI Thermal/Optical Reflectance carbon analysis system: Description, evaluation and applications in U.S. air quality studies. *Atmospheric Environment* **27A** (8), 1185-1201.

Chow, J.C. and Watson, J.G., (1994). Guidelines for PM_{10} sampling and analysis applicable to receptor modeling. Report No. EPA-452/R-94-009. Prepared for U.S. EPA, Office of Air Quality Planning and Standards, Research Triangle Park, NC, by Desert Research Institute, Reno, NV.

Chow, J.C.; Watson, J.G.; Fujita, E.M.; Lu, Z.; Lawson, D.R.; and Ashbaugh, L.L., (1994a). Temporal and spatial variations of $PM_{2.5}$ and PM_{10} aerosol in the Southern California Air Quality Study. *Atmospheric Environment* **28** (12), 2061-2080.

Chow, J.C.; Watson, J.G.; Lowenthal, D.H.; Solomon, P.A.; Magliano, K.L.; Ziman, S.D.; and Richards, L.W., (1994b). PM_{10} and $PM_{2.5}$ chemical characteristics and source apportionment in the San Joaquin Valley. In *Planning and Managing Regional Air Quality, Modeling and Measurement Studies*, Solomon, P.A., editor. CRC Press, Inc., Boca Raton, FL, pp. 687-698.

Chow, J.C., (1995). Critical review: Measurement methods to determine compliance with ambient air quality standards for suspended particles. *Journal of the Air & Waste Management Association* **45** (5), 320-382.

Chow, J.C.; Watson, J.G.; and Divita, F., Jr., (1996). Particulate matter with aerodynamic diameters smaller than 10 mm: Measurement methods and sampling strategies. In *Principles of Environmental Sampling, 2nd Ed., 2nd Edition*, Keith, L.H., editor. American Chemical Society, Washington, DC, pp. 539-573.

Chow, J.C. and Watson, J.G., (1999a). Ion chromatography in elemental analysis of airborne particles. In *Elemental Analysis of Airborne Particles, Vol. 1*, Landsberger, S., Creatchman, M., editors. Gordon and Breach Science, Amsterdam, pp. 97-137.

Chow, J.C.; Watson, J.G.; Green, M.C.; Lowenthal, D.H.; DuBois, D.W.; Kohl, S.D.; Egami, R.T.; Gillies, J.; Rogers, F.C.; Frazier, C.A.; and Cates, W. (1999b). Middle- and Neighborhood-Scale variations of PM_{10} source contributions in Las Vegas, Nevada. *Journal of the Air & Waste Management Association* **49,** 641-654.

Chow, J.C.; Watson, J.G.; Crow, D.; Lowenthal, D.H.; and Merrifield, T., (2001). Comparison of IMPROVE and NIOSH carbon measurements. *Aerosol Science & Technology* **34** (1), 23-34.

Eatough, D.J.; Aghdaie, N.; Cottam, M.; Gammon, T.; Hansen, L.D.; Lewis, E.A.; and Farber, R.J., (1990). Loss of semi-volatile organic compounds from particles during sampling on filters. In *Transactions, Visibility and Fine Particles*, Mathai, C.V., editor. Air & Waste Management Association, Pittsburgh, PA, pp. 146-156.

Faxvog, F.R. and Roessler, D.M., (1979). Optoacoustic measurements of diesel particulate emissions. *Journal of Applied Physics* **50**, 7880-7882

Faxvog, F.R. and Roessler, D.M., (1982). Mass concentration of diesel particle emissions from photoacoustic and opacity measurements. *Aerosol Science & Technology* **1,** 225-234

Fraser, M.P. and Cass, G.R., (1998). Detection of excess ammonia emissions from in-use vehicles and the implications for fine particle control. *Environmental Science & Technology* **32** (8), 1053-1057.

Fraser, M.P.; Cass, G.R.; and Simoneit, B.R.T., (1998). Gas-phase and particle-phase organic compounds emitted from motor vehicle traffic in a Los Angeles roadway tunnel. *Environmental Science & Technology* **32** (14), 2051-2060.

Green, M.C.; Chow, J.C.; Hecobian, A.; Etyemezian, V.; Kuhns, H.D.; and Watson, J.G., (2002). Las Vegas Valley visibility and $PM_{2.5}$ study – final report. Prepared for Clark County Department of Air Quality Management, Las Vegas, NV, by Desert Research Institute, Reno, NV.

Hansen, L.A.; Frandsen, F.J.; Dam-Johansen, K.; Sorensen, H.S.; and Skrifvars, B.J., (1999). Characterization of ashes and deposits from high-temperature coal-straw co-firing. *Energy & Fuels* **13** (4), 803-816.

Henry, R.C., (1992). Dealing with near collinearity in chemical mass balance receptor models. *Atmospheric Environment* **26A** (5), 933-938.

Henry, R.C., (1984). Fundamental limitations of factor analysis receptor models. In *Aerosols: Science, Technology and Industrial Applications of Airborne Particles*, Liu, B.Y.H., Pui, D.Y.H., and Fissan, H.J., editors. Elsevier Press, New York, NY, pp. 359-362.

Henry, R.C., (1982). Stability analysis of receptor models that use least squares fitting. In *Proceedings, Receptor Models Applied to Contemporary Air Pollution Problems*, Hopke, P.K. and Dattner, S.L., editors. Air Pollution Control Association, Pittsburgh, PA, pp. 141-162.

Henry, R.C.; Lewis, C.W.; and Collins, J.F., (1994). Vehicle-related hydrocarbon source compositions from ambient data: The GRACE/SAFER method. *Environmental Science & Technology* **28** (5), 823-832.

Hidy, G.M., (1985). Jekyll Island meeting report: George Hidy reports on the acquisition of reliable atmospheric data. *Environmental Science & Technology* **19** (11), 1032-1033.

Huai, T.; Durbin, T.D.; Miller, J.W.; Pisano, J.T.; Sauer, C.G.; Rhee, S.H.; and Norbeck, J.M., (2003). Investigation of NH3 emissions from new technology vehicles as a function of vehicle operating conditions. *Environmental Science & Technology* **37** (21), 4841-4847.

Japar, S.M. and Szkarlat, A.C., (1981). Measurement of diesel exhaust particulate using photoacoustic spectroscopy. *Combustion Science & Technology* **24**, 215-219

Japar, S.M. and Szkarlat, A.C. Real-time measurements of diesel vehicle exhaust particulate using photo-acoustic spectroscopy and total light extinction (technical paper 811184), 1981; Warrendale, PA.

Japar, S.M.; Moore, J.; Killinger, D.K.; and Szkarlat, A.C., (1982). Spectrophone measurements of diesel vehicle particulate material. In *Light Absorption by Aerosol Particles*, Gerber, H.E. and Hindman, E.E., editors. Spectrum Press, Hampton, VA, pp. 275-278.

Japar, S.M.; Szkarlat, A.C.; Gorse, R.A., Jr.; Heyerdahl, E.K.; Johnson, R.L.; Rau, J.A.; and Huntzicker, J.J., (1984). Comparison of solvent extraction and thermal-optical carbon analysis methods: Application to diesel vehicle exhaust aerosol. *Environmental Science & Technology* **18** (4), 231-234

Killinger, D.K.; Moore, J.; and Japar, S.M., (1980). The use of photoacoustic spectroscopy to characterize and monitor soot in combustion processes. In *ACS Symposium Series No. 134: Laser Probes for Combustion Chemistry*. Crosley, D.R., editor. American Chemical Society, Washington, DC, pp. 457-462.

Kittelson, D.B.; McKenzie, R.L.; Vermeersch, M.; Dorman, F.; Pui, D.Y.H.; Linne, M.; Liu, B.Y.H.; and Whitby, K.T., (1978). Total sulfur aerosol concentration with an electrostatically pulsed flame photometric detector system. *Atmospheric Environment* **12,** 105-111.

Kleeman, M.J.; Schauer, J.J.; and Cass, G.R., (2000). Size and composition distribution of fine particulate matter emitted from motor vehicles. *Environmental Science & Technology* **34** (7), 1132-1142.

Kuhns, H.D.; Green, M.C.; Etyemezian, V.; Watson, J.G.; and Pitchford, M.L. Big Bend Regional Aerosol and Visibility Observational (BRAVO) Study Emissions Inventory. (2001). Pittsburgh, PA/Washington, DC.

Lee, K.W. and Ramamurthi, M., (1993). Filter collection. In *Aerosol Measurement: Principles, Techniques and Applications*. Willeke, K and Baron, P.A., editors. Van Nostrand, Reinhold, New York, NY, pp. 179-205.

Lioy, P.J.; Mallon, R.P.; and Kneip, T.J., (1980). Long-term trends in total suspended particulates, vanadium, manganese, and lead at near street level and elevated sites in New York City. *Journal of the Air Pollution Control Association* **30** (2), 153-156.

Lippmann, M., (1989). Sampling aerosols by filtration. In *Air Sampling Instruments for Evaluation of Atmospheric Contaminants*, Hering, S.V., editor. American Conference of Governmental Industrial Hygienists, Cincinnati, OH, pp. 305-336.

Lowenthal, D.H.; Chow, J.C.; Watson, J.G.; Neuroth, G.R.; Robbins, R.B.; Shafritz, B.P.; and Countess, R.J., 1992. The effects of collinearity on the ability to determine aerosol contributions from diesel- and gasoline-powered vehicles using the chemical mass balance model. *Atmospheric Environment* **26A** (13), 2341-2351.

NIOSH (1996). Elemental Carbon (diesel exhaust). In *NIOSH Manual of Analytical Method*. National Institute of Occupational Safety and Health.

NIOSH (1999). Method 5040 Issue 3 (Interim): Elemental Carbon (diesel exhaust). In *NIOSH Manual of Analytical Method*. National Institute of Occupational Safety and Health.

Ristimaki, J.; Virtanen, A.; Marjamaki, M.; Rostedt, A.; and Keskinen, J., (2002). On-line measurement of size distribution and effective density of submicron aerosol particles. *Journal of Aerosol Science* **33** (11), 1541-1557.

McDow, S.R. and Huntzicker, J.J., (1990). Vapor adsorption artifact in the sampling of organic aerosol: Face velocity effects. *Atmospheric Environment* **24A** (10), 2563-2571.

Moosmüller, H.; Arnott, W.P.; Rogers, C.F.; Bowen, J.L.; Gillies, J.A.; Pierson, W.R.; Collins, J.F.; Durbin, T.D.; and Norbeck, J.M., (2001). Time resolved characterization of diesel particulate emissions 1. Instruments for particle mass measurements. *Environmental Science & Technology* **35** (4), 781-787.

Moosmüller, H.; Arnott, W.P.; Rogers, C.F.; Bowen, J.L.; Gillies, J.A.; Pierson, W.R.; Collins, J.F.; Durbin, T.D.; and Norbeck, J.M., (2001). Time resolved characterization of diesel particulate emissions 2. Instruments for elemental and organic carbon measurements. *Environmental Science & Technology* **35**(10):1935-1942.

Moosmüller, H.; Mazzoleni, C.; Barber, P.W.; Kuhns, H.D.; Keislar, R.E.; and Watson, J.G., (2003). On-road measurement of automotive particle emissions by ultraviolet lidar and transmissometer: Instrument. *Environmental Science & Technology* **37** (21), 4971-4978.

Pokharel, S.S.; Bishop, G.A.; and Stedman, D.H., (2002). An on-road motor vehicle emissions inventory for Denver: An efficient alternative to modeling. *Atmospheric Environment* **36**(33):5177-5184.

Roessler, D.M., (1982). Diesel particle mass concentration by optical techniques. *Applied Optics* **21,** 4077-4086.

Roessler, D.M., (1984). Photoacoustic insights on diesel exhaust particles. *Applied Optics* **23**(8), 1148-1155.

Shi, J.P.; Mark, D.; and Harrison, R.M., (2000). Characterization of particles from a current technology heavy-duty diesel engine. *Environmental Science & Technology* **34** (5), 748-755.

Tang, H.; Lewis, E.A.; Eatough, D.J.; Burton, R.M.; and Farber, R.J., (1994). Determination of the particle size distribution and chemical composition of semi-volatile organic compounds in atmospheric fine particles with a diffusion denuder system. *Atmospheric Environment* **28** (5), 939-947.

Truex, T.J. and Anderson, J.E., (1979). Mass monitoring of carbonaceous aerosols with a spectrophone. *Atmospheric Environment* **13,** 507-509.

Turpin, B.J.; Huntzicker, J.J.; and Hering, S.V., (1994). Investigation of organic aerosol sampling artifacts in the Los Angeles Basin. *Atmospheric Environment* **28** (19), 3061-3071.

van Gulijk, C.; Schouten, J.M.; Marijnissen, J.C.M, Makkee, M.; and Moulijn, J.A.; (2001). Restriction for the ELPI in diesel particulate measurements. *Journal of Aerosol Science* **32** (9), 1117-1130.

van Gulijk, C.; Marijnissen, J.C.M.; Makkee, M.; and Moulijn, J.A., (2003). Oil-soaked sintered impactors for the ELPI in diesel particulate measurements. *Journal of Aerosol Science* **34,** 635-640.

Watson, J.G. (1979) Chemical element balance receptor model methodology for assessing the sources of fine and total suspended particulate matter in Portland, Oregon. Ph.D. Dissertation, Oregon Graduate Center, Beaverton, OR

Watson, J.G.; Cooper, J.A., and Huntzicker, J.J., (1984). The effective variance weighting for least squares calculations applied to the mass balance receptor model. *Atmospheric Environment* **18** (7), 1347-1355.

Watson, J.G.; Lioy, P.J.; and Mueller, P.K., (1989). The measurement process: Precision, accuracy, and validity. In *Air Sampling Instruments for Evaluation of Atmospheric Contaminants, Seventh Edition*, Hering, S.V., editor. American Conference of Governmental Industrial Hygienists, Cincinnati, OH, pp. 51-57.

Watson, J.G.; Chow, J.C.; and Stevens, R.K., (1990a). Survey of fine particle sampling systems used in visibility studies. In *Transactions, Visibility and Fine Particles*, Mathai, C.V., editor. Air & Waste Management Association, Pittsburgh, PA, pp. 109-121.

Watson, J.G.; Rogers, C.F.; Chow, J.C.; Mathai, C.V.; Tombach, I.H.; and Zwicker, J.O., (1990b). An intercomparison of aerosol samplers used in western visibility studies. Prepared for Electric Power Research Institute, Palo Alto, CA, by Desert Research Institute, Reno, NV.

Watson, J.G.; Chow, J.C.; Richards, L.W.; Haase, D.L.; McDade, C.; Dietrich, D.L.; Moon, D.; Chinkin, L.R.; and Sloane, C.S., (1991). The 1989-90 Phoenix, AZ PM10 Study. Volume II: The apportionment of light extinction to sources. Prepared for Arizona Department of Environmental Quality. Phoenix, AZ by Desert Research Institute, Reno, NV.

Watson, J.G. and Chow, J.C., (1992). Data bases for PM_{10} and $PM_{2.5}$ chemical compositions and source profiles. In *Transactions, PM_{10} Standards and Nontraditional Particulate Source Controls*, Chow, J.C. and Ono, D.M., editors. Air & Waste Management Association, Pittsburgh, PA, pp. 61-91.

Watson, J.G. and Chow, J.C., (1993). Ambient air sampling. In *Aerosol Measurement: Principles, Techniques and Applications*, Willeke, K. and Baron, P.A., editors. Van Nostrand, Reinhold, New York, NY, pp. 622-639.

Watson, J.G. and Chow, J.C., (1994). Particle and gas measurements on filters. In *Environmental Sampling for Trace Analysis*, Markert, B., editor. VCH, New York, NY, pp. 125-161.

Watson, J.G.; Lioy, P.J.; and Mueller, P.K., (1995). The measurement process: Precision, accuracy, and validity. In *Air Sampling Instruments for Evaluation of Atmospheric Contaminants*, Cohen, B.S. and Hering, S.V., editors. American Conference of Governmental Industrial Hygienists, Cincinnati, OH, pp. 187-194.

Watson, J.G.; Chow, J.C.; and Frazier, C.A., (1999). X-ray fluorescence analysis of ambient air samples. In *Elemental Analysis of Airborne Particles, Vol. 1*, Landsberger, S. and Creatchman, M., editors. Gordon and Breach Science, Amsterdam, pp. 67-96.

Watson, J.G.; Turpin, B.J.; and Chow, J.C., (2001). The measurement process: Precision, accuracy, and validity. In *Air Sampling Instruments for Evaluation of Atmospheric Contaminants, Ninth Edition*, Cohen, B.S. and McCammon, C.S., Jr., editors. American Conference of Governmental Industrial Hygienists, Cincinnati, OH, pp. 201-216.

APPENDIX A

$PM_{2.5}$ organic speciation profiles for the following emission sources: 1) mixed fleet on-road vehicles in summer 2003; 2) mixed fleet on-road vehicles in winter 2003; 3) on-road diesel vehicles in summer 2003; 4) on-road diesel vehicles in winter 2003; and 5) non-road engine exhaust in 2003, obtained in the Las Vegas Basin.

Emission profiles of different vehicle exhausts during winter and summer 2003.

	On-Road Vehicle, mixed fleet, August 2003	On-Road Vehicle, mixed fleet, December 2003	On-Road Diesel Bus, August 2003	On-Road Diesel Bus, December 2003	Off-Road Diesel Engine, December 2003
Chloride (Cl–)	0.0014 ± 0.0055	0.0092 ± 0.0124	0.0006 ± 0.0028	0.0000 ± 0.0018	0.0000 ± 0.0006
Nitrate (NO3–)	0.0000 ± 0.0056	0.0041 ± 0.0082	0.0033 ± 0.0048	0.0093 ± 0.0030	0.0020 ± 0.0014
Sulfate (SO4=)	0.0000 ± 0.0187	0.0008 ± 0.0076	0.0198 ± 0.0207	0.0114 ± 0.0027	0.0050 ± 0.0030
Ammonium (NH4+)	0.0497 ± 0.0211	0.0017 ± 0.0048	0.0124 ± 0.0107	0.0067 ± 0.0017	0.0025 ± 0.0013
Soluble Sodium (Na+)	0.0110 ± 0.0062	0.0041 ± 0.0010	0.0014 ± 0.0018	0.0003 ± 0.0002	0.0001 ± 0.0001
Soluble Potassium (K+)	0.0006 ± 0.0019	0.0032 ± 0.0009	0.0007 ± 0.0012	0.0004 ± 0.0003	0.0001 ± 0.0001
OC1 (IMPROVE)	0.0738 ± 0.0447	0.2879 ± 0.0809	0.0961 ± 0.0514	0.2564 ± 0.1214	0.3630 ± 0.0927
OC2 (IMPROVE)	0.2494 ± 0.1307	0.1942 ± 0.0360	0.0885 ± 0.0523	0.1176 ± 0.0209	0.0877 ± 0.0406
OC3 (IMPROVE)	0.4318 ± 0.2375	0.2688 ± 0.0776	0.1190 ± 0.0658	0.1056 ± 0.0275	0.1028 ± 0.0517
OC4 (IMPROVE)	0.1302 ± 0.0570	0.1474 ± 0.0525	0.0589 ± 0.0288	0.0436 ± 0.0126	0.0468 ± 0.0363
OPC (IMPROVE)	0.0000 ± 0.0172	0.0000 ± 0.0076	0.0050 ± 0.0051	0.0049 ± 0.0094	0.0426 ± 0.0681
Total OC (IMPROVE)	0.7716 ± 0.3735	0.8666 ± 0.1584	0.3648 ± 0.1565	0.5282 ± 0.1420	0.6430 ± 0.1956
EC1 (IMPROVE)	0.0838 ± 0.1093	0.2611 ± 0.0911	0.0621 ± 0.0303	0.1486 ± 0.0346	0.0911 ± 0.0504
EC2 IMPROVE)	0.1258 ± 0.0485	0.1451 ± 0.0657	0.5215 ± 0.2662	0.3095 ± 0.1268	0.1883 ± 0.1211
EC3 (IMPROVE)	0.0164 ± 0.0124	0.0086 ± 0.0032	0.0040 ± 0.0046	0.0009 ± 0.0010	0.0004 ± 0.0006
EC (IMPROVE)	0.3355 ± 0.1316	0.4473 ± 0.0949	0.5826 ± 0.2818	0.4541 ± 0.1291	0.2372 ± 0.1189
Total Carbon	1.1072 ± 0.4978	1.3138 ± 0.2143	0.9473 ± 0.3203	0.9822 ± 0.1805	0.8803 ± 0.3085
Sodium (Na)	0.0077 ± 0.0562	0.0089 ± 0.0378	0.0123 ± 0.0164	0.0094 ± 0.0078	0.0033 ± 0.0032
Magnesium (Mg)	0.0000 ± 0.0165	0.0000 ± 0.0075	0.0067 ± 0.0040	0.0002 ± 0.0027	0.0003 ± 0.0008
Aluminum (Al)	0.0000 ± 0.0186	0.0000 ± 0.0046	0.0034 ± 0.0024	0.0004 ± 0.0007	0.0000 ± 0.0002
Silicon (Si)	0.0007 ± 0.0657	0.0000 ± 0.0155	0.0148 ± 0.0081	0.0023 ± 0.0009	0.0005 ± 0.0003
Phosphorus (P)	0.0000 ± 0.0018	0.0001 ± 0.0010	0.0002 ± 0.0005	0.0005 ± 0.0002	0.0003 ± 0.0002
Sulfur (S)	0.0829 ± 0.0451	0.0031 ± 0.0032	0.0137 ± 0.0098	0.0047 ± 0.0007	0.0029 ± 0.0010
Chlorine (Cl)	0.0034 ± 0.0031	0.0031 ± 0.0010	0.0009 ± 0.0005	0.0000 ± 0.0004	0.0000 ± 0.0001
Potassium (K)	0.0001 ± 0.0094	0.0003 ± 0.0023	0.0025 ± 0.0022	0.0005 ± 0.0004	0.0001 ± 0.0001
Calcium (Ca)	0.0245 ± 0.0617	0.0056 ± 0.0130	0.0147 ± 0.0099	0.0055 ± 0.0016	0.0014 ± 0.0006
Titanium (Ti)	0.0002 ± 0.0035	0.0000 ± 0.0038	0.0002 ± 0.0020	0.0001 ± 0.0012	0.0000 ± 0.0004
Vanadium (V)	0.0000 ± 0.0019	0.0000 ± 0.0016	0.0000 ± 0.0009	0.0000 ± 0.0005	0.0000 ± 0.0002
Chromium (Cr)	0.0002 ± 0.0005	0.0001 ± 0.0003	0.0002 ± 0.0002	0.0000 ± 0.0001	0.0000 ± 0.0000
Manganese (Mn)	0.0002 ± 0.0004	0.0002 ± 0.0002	0.0001 ± 0.0001	0.0000 ± 0.0001	0.0000 ± 0.0000
Iron (Fe)	0.0292 ± 0.0207	0.0271 ± 0.0060	0.0054 ± 0.0040	0.0013 ± 0.0007	0.0004 ± 0.0002
Cobalt (Co)	0.0004 ± 0.0013	0.0000 ± 0.0006	0.0000 ± 0.0001	0.0000 ± 0.0000	0.0000 ± 0.0000
Nickel (Ni)	0.0001 ± 0.0001	0.0000 ± 0.0001	0.0001 ± 0.0001	0.0000 ± 0.0000	0.0000 ± 0.0000
Copper (Cu)	0.0270 ± 0.0222	0.0163 ± 0.0077	0.0008 ± 0.0008	0.0002 ± 0.0002	0.0000 ± 0.0000
Zinc (Zn)	0.0078 ± 0.0039	0.0039 ± 0.0007	0.0039 ± 0.0036	0.0018 ± 0.0005	0.0007 ± 0.0004
Gallium (Ga)	0.0001 ± 0.0004	0.0000 ± 0.0005	0.0000 ± 0.0002	0.0000 ± 0.0001	0.0000 ± 0.0000
Arsenic (As)	0.0000 ± 0.0004	0.0000 ± 0.0004	0.0000 ± 0.0002	0.0000 ± 0.0001	0.0000 ± 0.0000
Selenium (Se)	0.0000 ± 0.0001	0.0000 ± 0.0001	0.0000 ± 0.0001	0.0000 ± 0.0000	0.0000 ± 0.0000
Bromine (Br)	0.0004 ± 0.0002	0.0001 ± 0.0001	0.0000 ± 0.0001	0.0000 ± 0.0001	0.0000 ± 0.0000
Rubidium (Rb)	0.0000 ± 0.0002	0.0000 ± 0.0002	0.0000 ± 0.0001	0.0000 ± 0.0001	0.0000 ± 0.0000
Strontium (Sr)	0.0000 ± 0.0006	0.0000 ± 0.0002	0.0001 ± 0.0001	0.0000 ± 0.0001	0.0000 ± 0.0000
Yttrium (Y)	0.0000 ± 0.0002	0.0001 ± 0.0002	0.0000 ± 0.0001	0.0000 ± 0.0001	0.0000 ± 0.0000
Zerconium (Zr)	0.0001 ± 0.0002	0.0001 ± 0.0003	0.0000 ± 0.0001	0.0000 ± 0.0001	0.0000 ± 0.0000
Molybdenum (Mo)	0.0001 ± 0.0005	0.0000 ± 0.0005	0.0000 ± 0.0003	0.0000 ± 0.0002	0.0000 ± 0.0000
Palladium (Pd)	0.0001 ± 0.0005	0.0001 ± 0.0005	0.0000 ± 0.0003	0.0000 ± 0.0002	0.0000 ± 0.0000
Silver (Ag)	0.0001 ± 0.0006	0.0004 ± 0.0005	0.0000 ± 0.0003	0.0000 ± 0.0002	0.0000 ± 0.0001
Cadmium (Cd)	0.0000 ± 0.0006	0.0001 ± 0.0006	0.0000 ± 0.0003	0.0000 ± 0.0002	0.0000 ± 0.0001
Indium (In)	0.0000 ± 0.0008	0.0000 ± 0.0007	0.0000 ± 0.0004	0.0000 ± 0.0002	0.0000 ± 0.0001
Tin (Sn)	0.0002 ± 0.0011	0.0005 ± 0.0010	0.0000 ± 0.0006	0.0001 ± 0.0004	0.0000 ± 0.0001
Antimony (Sb)	0.0002 ± 0.0013	0.0005 ± 0.0013	0.0001 ± 0.0007	0.0001 ± 0.0004	0.0000 ± 0.0001
Barium (Ba)	0.0047 ± 0.0051	0.0034 ± 0.0061	0.0011 ± 0.0030	0.0004 ± 0.0019	0.0000 ± 0.0006
Lanthanum (La)	0.0013 ± 0.0077	0.0009 ± 0.0077	0.0000 ± 0.0042	0.0002 ± 0.0025	0.0001 ± 0.0008
Gold (Au)	0.0001 ± 0.0005	0.0000 ± 0.0005	0.0000 ± 0.0003	0.0000 ± 0.0002	0.0000 ± 0.0001
Mercury (Hg)	0.0000 ± 0.0003	0.0000 ± 0.0003	0.0000 ± 0.0001	0.0000 ± 0.0001	0.0000 ± 0.0000
Thallium (Tl)	0.0000 ± 0.0002	0.0000 ± 0.0002	0.0000 ± 0.0001	0.0000 ± 0.0001	0.0000 ± 0.0000
Lead (Pb)	0.0003 ± 0.0004	0.0001 ± 0.0005	0.0002 ± 0.0002	0.0001 ± 0.0002	0.0000 ± 0.0000
Uranium (U)	0.0001 ± 0.0003	0.0001 ± 0.0004	0.0000 ± 0.0002	0.0000 ± 0.0001	0.0000 ± 0.0000

Emission factors for polycyclic aromatic hydrocarbons (PAHs).

PAHs	On-Road Vehicle, mixed fleet, August 2003	On-Road Vehicle, mixed fleet, December 2003	On-Road Diesel Bus, August 2003	On-Road Diesel Bus, December 2003	Off-Road Diesel Engine, December 2003
Naphthalene	0.36136 ± 0.20225	0.40281 ± 0.27925	0.01873 ± 0.02500	0.00672 ± 0.00538	0.01062 ± 0.00526
2-methylnaphthalene	0.05323 ± 0.04952	0.06922 ± 0.05050	0.00056 ± 0.00073	0.00269 ± 0.00216	0.00293 ± 0.00083
1-methylnaphthalene	0.00000 ± 0.00014	0.04182 ± 0.03146	0.00004 ± 0.00007	0.00124 ± 0.00113	0.00181 ± 0.00051
Biphenyl	0.01772 ± 0.03544	0.00281 ± 0.00179	0.00577 ± 0.00888	0.00029 ± 0.00058	0.00033 ± 0.00017
1+2ethylnaphthalene	0.01047 ± 0.02095	0.00484 ± 0.00348	0.00007 ± 0.00014	0.00056 ± 0.00051	0.00084 ± 0.00011
2,6+2,7-dimethylnaphthalene	0.00101 ± 0.00060	0.00187 ± 0.00129	0.00012 ± 0.00016	0.00021 ± 0.00020	0.00029 ± 0.00007
1,3+1,6+1,7dimethylnaphth	0.00088 ± 0.00113	0.00289 ± 0.00205	0.00000 ± 0.00019	0.00057 ± 0.00062	0.00147 ± 0.00046
1,4+1,5+2,3-dimethylnaphth	0.00258 ± 0.00336	0.00121 ± 0.00087	0.00001 ± 0.00027	0.00018 ± 0.00025	0.00050 ± 0.00018
1,2-dimethylnaphthalene	0.00046 ± 0.00059	0.00051 ± 0.00042	0.00000 ± 0.00017	0.00003 ± 0.00015	0.00021 ± 0.00009
2-Methylbiphenyl	0.01280 ± 0.01100	0.00370 ± 0.00459	0.00539 ± 0.01078	0.00036 ± 0.00072	0.00229 ± 0.00144
3-Methylbiphenyl	0.01636 ± 0.02058	0.00000 ± 0.00008	0.00090 ± 0.00180	0.00000 ± 0.00003	0.00096 ± 0.00038
4-Methylbiphenyl	0.03557 ± 0.02529	0.00000 ± 0.00008	0.00438 ± 0.00877	0.00000 ± 0.00003	0.00045 ± 0.00017
Dibenzofuran	0.00144 ± 0.00125	0.00045 ± 0.00030	0.00004 ± 0.00004	0.00006 ± 0.00002	0.00008 ± 0.00001
Bibenzyl	0.00095 ± 0.00165	0.00000 ± 0.00008	0.00000 ± 0.00004	0.00000 ± 0.00003	0.00000 ± 0.00001
A-trimethylnaphthalene	0.01016 ± 0.00989	0.00000 ± 0.00009	0.00370 ± 0.00436	0.00203 ± 0.00274	0.00099 ± 0.00067
B-trimethylnaphthalene	0.00077 ± 0.00130	0.00006 ± 0.00006	0.00000 ± 0.00003	0.00008 ± 0.00006	0.00043 ± 0.00009
C-trimethylnaphthalene	0.00436 ± 0.00776	0.00030 ± 0.00029	0.00005 ± 0.00005	0.00009 ± 0.00004	0.00052 ± 0.00015
E-trimethylnaphthalene	0.00032 ± 0.00048	0.00011 ± 0.00013	0.00000 ± 0.00003	0.00004 ± 0.00003	0.00033 ± 0.00007
F-trimethylnaphthalene	0.00033 ± 0.00047	0.00065 ± 0.00074	0.00002 ± 0.00003	0.00050 ± 0.00040	0.00030 ± 0.00004
2,3,5+I-trimethylnaphthalene	0.00081 ± 0.00074	0.00015 ± 0.00011	0.00002 ± 0.00004	0.00006 ± 0.00003	0.00034 ± 0.00006
J-trimethylnaphthalene	0.02584 ± 0.01459	0.00005 ± 0.00006	0.00000 ± 0.00003	0.00001 ± 0.00002	0.00014 ± 0.00005
1,4,5-trimethylnaphthalene	0.00050 ± 0.00028	0.00001 ± 0.00006	0.00000 ± 0.00003	0.00000 ± 0.00002	0.00006 ± 0.00001
Acenaphthylene	0.00021 ± 0.00042	0.00281 ± 0.00239	0.00007 ± 0.00017	0.00002 ± 0.00015	0.00010 ± 0.00004
Acenaphthene	0.00177 ± 0.00104	0.00030 ± 0.00025	0.00073 ± 0.00147	0.00000 ± 0.00007	0.00003 ± 0.00002
Fluorene	0.00007 ± 0.00014	0.00001 ± 0.00009	0.00007 ± 0.00012	0.00000 ± 0.00004	0.00014 ± 0.00005
Phenanthrene	0.00000 ± 0.00004	0.00512 ± 0.00436	0.00008 ± 0.00011	0.00000 ± 0.00002	0.00103 ± 0.00054
A-methylfluorene	0.00006 ± 0.00009	0.00063 ± 0.00053	0.00015 ± 0.00011	0.00001 ± 0.00003	0.00018 ± 0.00004
1-methylfluorene	0.00000 ± 0.00007	0.00000 ± 0.00006	0.00000 ± 0.00003	0.00000 ± 0.00002	0.00006 ± 0.00012
B-methylfluorene	0.00000 ± 0.00010	0.00010 ± 0.00009	0.00000 ± 0.00003	0.00000 ± 0.00002	0.00002 ± 0.00005
9-fluorenone	0.00000 ± 0.00006	0.00006 ± 0.00012	0.00000 ± 0.00003	0.00000 ± 0.00002	0.00000 ± 0.00001
Xanthone	0.00000 ± 0.00029	0.00001 ± 0.00006	0.00000 ± 0.00003	0.00001 ± 0.00002	0.00005 ± 0.00006
Acenaphthenequinone	0.00001 ± 0.00011	0.00000 ± 0.00007	0.00001 ± 0.00006	0.00000 ± 0.00003	0.00000 ± 0.00001
Perinaphthenone	0.00002 ± 0.00010	0.00000 ± 0.00007	0.00004 ± 0.00005	0.00000 ± 0.00002	0.00003 ± 0.00004
A-methylphenanthrene	0.02223 ± 0.01530	0.00059 ± 0.00042	0.00110 ± 0.00112	0.00004 ± 0.00003	0.00076 ± 0.00042
2-methylphenanthrene	0.00014 ± 0.00017	0.00069 ± 0.00052	0.00019 ± 0.00022	0.00003 ± 0.00004	0.00085 ± 0.00045
B-methylphenanthrene	0.00000 ± 0.00006	0.00013 ± 0.00021	0.00000 ± 0.00003	0.00000 ± 0.00002	0.00008 ± 0.00004
C-methylphenanthrene	0.00011 ± 0.00010	0.00050 ± 0.00043	0.00006 ± 0.00006	0.00001 ± 0.00002	0.00041 ± 0.00020
1-methylphenanthrene	0.00000 ± 0.00031	0.00403 ± 0.00289	0.00019 ± 0.00037	0.00004 ± 0.00002	0.00003 ± 0.00006
Anthrone	0.00017 ± 0.00013	0.00007 ± 0.00006	0.00035 ± 0.00061	0.00002 ± 0.00002	0.00007 ± 0.00004
Anthraquinone	0.00034 ± 0.00023	0.00013 ± 0.00008	0.00020 ± 0.00011	0.00002 ± 0.00002	0.00002 ± 0.00003
3,6-dimethylphenanthrene	0.00000 ± 0.00007	0.00013 ± 0.00008	0.00000 ± 0.00004	0.00002 ± 0.00003	0.00011 ± 0.00005
A-dimethylphenanthrene	0.00000 ± 0.00006	0.00000 ± 0.00006	0.00002 ± 0.00004	0.00000 ± 0.00002	0.00021 ± 0.00010
B-dimethylphenanthrene	0.00005 ± 0.00008	0.00003 ± 0.00006	0.00003 ± 0.00003	0.00000 ± 0.00002	0.00009 ± 0.00004
C-dimethylphenanthrene	0.00005 ± 0.00011	0.00017 ± 0.00010	0.00004 ± 0.00008	0.00003 ± 0.00003	0.00020 ± 0.00008
1,7-dimethylphenanthrene	0.00004 ± 0.00007	0.00012 ± 0.00010	0.00003 ± 0.00004	0.00001 ± 0.00002	0.00011 ± 0.00004
D-dimethylphenanthrene	0.00009 ± 0.00008	0.00019 ± 0.00019	0.00004 ± 0.00003	0.00000 ± 0.00002	0.00003 ± 0.00002
E-dimethylphenanthrene	0.00000 ± 0.00006	0.00000 ± 0.00006	0.00029 ± 0.00058	0.00000 ± 0.00002	0.00016 ± 0.00017
Anthracene	0.00000 ± 0.00008	0.00073 ± 0.00084	0.00000 ± 0.00002	0.00000 ± 0.00002	0.00004 ± 0.00004
9-methylanthracene	0.00003 ± 0.00007	0.00001 ± 0.00006	0.00000 ± 0.00003	0.00000 ± 0.00002	0.00000 ± 0.00001
Fluoranthene	0.00000 ± 0.00012	0.00030 ± 0.00049	0.00000 ± 0.00005	0.00000 ± 0.00004	0.00004 ± 0.00002
Pyrene	0.00000 ± 0.00007	0.00000 ± 0.00007	0.00000 ± 0.00003	0.00000 ± 0.00003	0.00011 ± 0.00006
9-Anthraaldehyde	0.00000 ± 0.00006	0.00000 ± 0.00006	0.00000 ± 0.00003	0.00000 ± 0.00003	0.00024 ± 0.00026
Retene	0.00000 ± 0.00009	0.00000 ± 0.00008	0.00000 ± 0.00004	0.00000 ± 0.00003	0.00000 ± 0.00001
Benzonaphthothiophene	0.00000 ± 0.00012	0.00000 ± 0.00012	0.00003 ± 0.00006	0.00000 ± 0.00005	0.00000 ± 0.00001
1-MeFl+C-MeFl/Py	0.00000 ± 0.00006	0.00000 ± 0.00007	0.00000 ± 0.00003	0.00000 ± 0.00002	0.00000 ± 0.00001
B-MePy/MeFl	0.00000 ± 0.00006	0.00005 ± 0.00008	0.00000 ± 0.00003	0.00000 ± 0.00002	0.00000 ± 0.00001
C-MePy/MeFl	0.00000 ± 0.00006	0.00002 ± 0.00006	0.00001 ± 0.00003	0.00000 ± 0.00002	0.00000 ± 0.00001
D-MePy/MeFl	0.00000 ± 0.00006	0.00000 ± 0.00007	0.00001 ± 0.00003	0.00000 ± 0.00002	0.00002 ± 0.00001
4-methylpyrene	0.00000 ± 0.00006	0.00000 ± 0.00006	0.00000 ± 0.00003	0.00000 ± 0.00002	0.00001 ± 0.00001
1-methylpyrene	0.00000 ± 0.00006	0.00000 ± 0.00006	0.00000 ± 0.00003	0.00000 ± 0.00002	0.00000 ± 0.00001
Benzo(c)phenanthrene	0.00000 ± 0.00006	0.00000 ± 0.00006	0.00004 ± 0.00008	0.00000 ± 0.00002	0.00020 ± 0.00030
Benz(a)anthracene	0.00000 ± 0.00018	0.00000 ± 0.00017	0.00000 ± 0.00007	0.00000 ± 0.00007	0.00000 ± 0.00002
7-methylbenz(a)anthracene	0.00000 ± 0.00006	0.00000 ± 0.00006	0.00000 ± 0.00003	0.00000 ± 0.00002	0.00000 ± 0.00001
Chrysene	0.00000 ± 0.00009	0.00000 ± 0.00009	0.00000 ± 0.00004	0.00000 ± 0.00003	0.00000 ± 0.00001
Benzanthrone	0.00002 ± 0.00006	0.00002 ± 0.00006	0.00004 ± 0.00003	0.00001 ± 0.00002	0.00001 ± 0.00001
Benz(a)anthracene-7,12-dione	0.00000 ± 0.00006	0.00000 ± 0.00006	0.00003 ± 0.00004	0.00000 ± 0.00002	0.00001 ± 0.00001
5+6-methylchrysene	0.00000 ± 0.00006	0.00000 ± 0.00006	0.00000 ± 0.00003	0.00001 ± 0.00002	0.00000 ± 0.00001
Benzo(b+j+k)fluoranthene	0.00000 ± 0.00010	0.00000 ± 0.00009	0.00000 ± 0.00004	0.00000 ± 0.00004	0.00001 ± 0.00002
7-methylbenzo(a)pyrene	0.00000 ± 0.00006	0.00000 ± 0.00006	0.00000 ± 0.00003	0.00000 ± 0.00002	0.00000 ± 0.00001
BeP	0.00000 ± 0.00006	0.00000 ± 0.00006	0.00000 ± 0.00003	0.00000 ± 0.00002	0.00001 ± 0.00001
Perylene	0.00000 ± 0.00006	0.00000 ± 0.00006	0.00000 ± 0.00003	0.00000 ± 0.00002	0.00000 ± 0.00001
BaP	0.00000 ± 0.00020	0.00000 ± 0.00019	0.00000 ± 0.00008	0.00000 ± 0.00007	0.00003 ± 0.00003
Indeno[123-cd]pyrene	0.00000 ± 0.00017	0.00000 ± 0.00016	0.00000 ± 0.00007	0.00000 ± 0.00006	0.00001 ± 0.00002
Benzo(ghi)perylene	0.00000 ± 0.00022	0.00000 ± 0.00020	0.00002 ± 0.00010	0.00000 ± 0.00008	0.00011 ± 0.00008
Dibenzo(ah+ac)anthracene	0.00000 ± 0.00024	0.00001 ± 0.00022	0.00000 ± 0.00010	0.00002 ± 0.00009	0.00000 ± 0.00002
Coronene	0.00000 ± 0.00006	0.00005 ± 0.00006	0.00000 ± 0.00003	0.00000 ± 0.00002	0.00000 ± 0.00001

Emission factors for polar organic compounds.

Organic Polar Compounds	On-Road Vehicle, mixed fleet, August 2003	On-Road Vehicle, mixed fleet, December 2003	On-Road Diesel Bus, August 2003	On-Road Diesel Bus, December 2003	Off-Road Diesel Engine, December 2003
hexanoic acid (c6)	0.09931 ± 0.13485	0.08385 ± 0.05852	0.01400 ± 0.02800	0.00659 ± 0.00519	0.00033 ± 0.00073
heptanoic acid (c7)	0.02770 ± 0.03285	0.02951 ± 0.02024	0.00000 ± 0.00078	0.00205 ± 0.00137	0.00019 ± 0.00043
guaiacol	0.00113 ± 0.00145	0.03110 ± 0.02709	0.00026 ± 0.00033	0.00044 ± 0.00043	0.00013 ± 0.00007
benzoic acid	0.24257 ± 0.48514	0.05059 ± 0.10118	0.00000 ± 0.01756	0.00000 ± 0.01134	0.00000 ± 0.00427
octanoic acid (c8)	0.05400 ± 0.05464	0.04557 ± 0.03058	0.00000 ± 0.00101	0.00212 ± 0.00115	0.00011 ± 0.00027
glycerol	0.00850 ± 0.01700	0.00000 ± 0.00181	0.00911 ± 0.01690	0.00000 ± 0.00083	0.00094 ± 0.00070
phenylacetic acid	0.00880 ± 0.01761	0.01160 ± 0.02074	0.00105 ± 0.00209	0.00000 ± 0.00003	0.00479 ± 0.00436
maleic acid	0.00090 ± 0.00180	0.00216 ± 0.00431	0.00000 ± 0.00003	0.00057 ± 0.00060	0.00070 ± 0.00078
succinic acid (d-c4)	0.00000 ± 0.00006	0.00000 ± 0.00013	0.00000 ± 0.00009	0.00000 ± 0.00003	0.00002 ± 0.00012
4-me-guaiacol	0.00000 ± 0.00006	0.04768 ± 0.04104	0.00000 ± 0.00003	0.00016 ± 0.00015	0.00001 ± 0.00002
me-succinic acid (d-c4)	0.00000 ± 0.00005	0.00001 ± 0.00006	0.00000 ± 0.00003	0.00000 ± 0.00002	0.00001 ± 0.00002
o-toluic	0.00044 ± 0.00089	0.00230 ± 0.00081	0.00000 ± 0.00004	0.00007 ± 0.00006	0.00005 ± 0.00011
picolinic acid	0.00000 ± 0.00006	0.03025 ± 0.02697	0.00000 ± 0.00003	0.00000 ± 0.00002	0.00001 ± 0.00001
m-toluic	0.00049 ± 0.00099	0.00162 ± 0.00069	0.00000 ± 0.00006	0.00029 ± 0.00021	0.00005 ± 0.00012
nonanoic acid (c9)	0.01504 ± 0.03007	0.04218 ± 0.02341	0.00000 ± 0.00103	0.00480 ± 0.00226	0.00008 ± 0.00031
p-toluic	0.00195 ± 0.00391	0.00122 ± 0.00091	0.00000 ± 0.00009	0.00007 ± 0.00009	0.00002 ± 0.00005
4-ethyl-guaiacol	0.00079 ± 0.00108	0.03531 ± 0.03023	0.00001 ± 0.00003	0.00010 ± 0.00008	0.00001 ± 0.00001
glutaric acid (d-c5)	0.00007 ± 0.00014	0.01187 ± 0.01970	0.00004 ± 0.00008	0.00045 ± 0.00036	0.00001 ± 0.00002
syringol	0.00087 ± 0.00173	0.02040 ± 0.02684	0.00009 ± 0.00012	0.00004 ± 0.00004	0.00004 ± 0.00006
2,5-dimethylbenzoic acid	0.01376 ± 0.01987	0.00201 ± 0.00236	0.00043 ± 0.00051	0.00000 ± 0.00003	0.00000 ± 0.00003
2,4-dimethylbenzoic acid	0.09744 ± 0.08476	0.00000 ± 0.00516	0.03299 ± 0.02830	0.00000 ± 0.00134	0.00000 ± 0.00115
2,3- and 3,5- dimethylbenzoic acid	0.00000 ± 0.00012	0.00000 ± 0.00007	0.00000 ± 0.00003	0.00000 ± 0.00003	0.00194 ± 0.00434
decanoic acid (c10)	0.00242 ± 0.00483	0.00422 ± 0.00338	0.00000 ± 0.00032	0.00015 ± 0.00021	0.00001 ± 0.00017
4-allyl-guaiacol (eugenol)	0.00000 ± 0.00006	0.00558 ± 0.00414	0.00000 ± 0.00003	0.00036 ± 0.00026	0.00001 ± 0.00001
4-methyl-syringol	0.00000 ± 0.00006	0.00564 ± 0.00615	0.00000 ± 0.00003	0.00012 ± 0.00007	0.00001 ± 0.00001
3,4-dimethylbenzoic acid	0.00234 ± 0.00342	0.00149 ± 0.00135	0.00000 ± 0.00005	0.00001 ± 0.00003	0.00001 ± 0.00003
hexanedioic (adipic) acid (d-c6)	0.04019 ± 0.04794	0.01848 ± 0.02283	0.00137 ± 0.00274	0.00007 ± 0.00014	0.00000 ± 0.00005
salcylic acid	0.00002 ± 0.00010	0.00000 ± 0.00012	0.00000 ± 0.00008	0.00000 ± 0.00003	0.00049 ± 0.00058
trans-2-decenoic acid	0.00000 ± 0.00006	0.00046 ± 0.00028	0.00000 ± 0.00007	0.00006 ± 0.00003	0.00000 ± 0.00005
3-methyladipic acid (d-c6)	0.00000 ± 0.00006	0.00030 ± 0.00059	0.00000 ± 0.00003	0.00016 ± 0.00031	0.00032 ± 0.00033
4-formyl-guaiacol (vanillin)	0.00105 ± 0.00121	0.00167 ± 0.00334	0.00162 ± 0.00271	0.00000 ± 0.00002	0.00028 ± 0.00028
undecanoic acid (c11)	0.00145 ± 0.00290	0.00244 ± 0.00096	0.00000 ± 0.00036	0.00042 ± 0.00025	0.00001 ± 0.00032
isoeugenol	0.00324 ± 0.00346	0.00083 ± 0.00120	0.00000 ± 0.00003	0.00000 ± 0.00002	0.00000 ± 0.00001
heptanedioic (pimelic) acid (d-c7)	0.22441 ± 0.31735	0.23792 ± 0.19230	0.09481 ± 0.15332	0.00460 ± 0.00239	0.00267 ± 0.00305
acetovanillone	0.00000 ± 0.00006	0.00106 ± 0.00211	0.00000 ± 0.00004	0.00000 ± 0.00002	0.00004 ± 0.00009
dodecanoic (lauric) acid (c12)	0.02120 ± 0.01629	0.00802 ± 0.00785	0.00567 ± 0.00592	0.00129 ± 0.00144	0.01934 ± 0.01899
phthalic acid	0.63043 ± 0.63335	0.01395 ± 0.01275	0.00345 ± 0.00426	0.00051 ± 0.00064	0.00007 ± 0.00015
suberic acid (d-c8)	0.00000 ± 0.00006	0.00000 ± 0.00006	0.00000 ± 0.00003	0.00000 ± 0.00002	0.00000 ± 0.00001
levoglucosan	0.00072 ± 0.00143	0.00261 ± 0.00193	0.00000 ± 0.00015	0.00009 ± 0.00017	0.00018 ± 0.00027
syringaldehyde	0.00000 ± 0.00006	0.00087 ± 0.00127	0.00000 ± 0.00003	0.00002 ± 0.00002	0.00000 ± 0.00001
3,4-dimethoxybenzoic acid	0.00000 ± 0.00006	0.00002 ± 0.00006	0.00000 ± 0.00003	0.00000 ± 0.00002	0.00000 ± 0.00001
tridecanoic acid (c13)	0.00078 ± 0.00156	0.00091 ± 0.00071	0.00000 ± 0.00024	0.00006 ± 0.00005	0.00001 ± 0.00018
isophthalic acid	0.01769 ± 0.03538	0.00000 ± 0.00014	0.00000 ± 0.00216	0.00000 ± 0.00007	0.00000 ± 0.00063
vanillic acid	0.00863 ± 0.00638	0.00067 ± 0.00050	0.00000 ± 0.00003	0.00003 ± 0.00003	0.00000 ± 0.00006
homovanillic acid	0.04374 ± 0.08749	0.01733 ± 0.02109	0.01102 ± 0.01006	0.00011 ± 0.00014	0.00009 ± 0.00011
azelaic acid (d-c9)	0.00050 ± 0.00100	0.00010 ± 0.00015	0.00000 ± 0.00010	0.00003 ± 0.00005	0.00000 ± 0.00001
myristic acid (c14)	0.01430 ± 0.00825	0.00694 ± 0.00560	0.00348 ± 0.00392	0.00134 ± 0.00111	0.00184 ± 0.00348
sebacic acid (d-c10)	0.00020 ± 0.00026	0.00021 ± 0.00017	0.00000 ± 0.00004	0.00002 ± 0.00003	0.00000 ± 0.00001
syringic acid	0.00142 ± 0.00172	0.00003 ± 0.00006	0.00000 ± 0.00003	0.00002 ± 0.00002	0.00000 ± 0.00001
pentadecanoic acid (c15)	0.00386 ± 0.00273	0.00347 ± 0.00234	0.00054 ± 0.00062	0.00056 ± 0.00036	0.00022 ± 0.00049
undecanedioic acid (d-c11)	0.00000 ± 0.00006	0.00040 ± 0.00071	0.00142 ± 0.00277	0.00039 ± 0.00029	0.00000 ± 0.00001
palmitoleic acid	0.00355 ± 0.00205	0.00130 ± 0.00192	0.00053 ± 0.00062	0.00122 ± 0.00159	0.00130 ± 0.00100
palmitic acid (c16)	0.03221 ± 0.02873	0.03775 ± 0.01982	0.00946 ± 0.01844	0.01133 ± 0.00531	0.00005 ± 0.00025
dodecanedioic acid (d-c12)	0.00000 ± 0.00008	0.00005 ± 0.00008	0.00000 ± 0.00003	0.00001 ± 0.00002	0.00172 ± 0.00289
traumatic acid	0.00278 ± 0.00221	0.00025 ± 0.00011	0.00000 ± 0.00005	0.00010 ± 0.00005	0.00000 ± 0.00002
heptadecanoic acid (c17)	0.00221 ± 0.00099	0.00214 ± 0.00117	0.00026 ± 0.00034	0.00068 ± 0.00029	0.00006 ± 0.00009
1,11-undecanedicarboxylic acid (d-c13)	0.00002 ± 0.00007	0.00014 ± 0.00013	0.00000 ± 0.00003	0.00004 ± 0.00005	0.00002 ± 0.00002
oleic acid	0.00461 ± 0.00659	0.01104 ± 0.00437	0.00548 ± 0.00659	0.01076 ± 0.00918	0.02499 ± 0.01991
elaidic acid	0.00393 ± 0.00186	0.00730 ± 0.00612	0.00152 ± 0.00158	0.00250 ± 0.00331	0.00288 ± 0.00238
stearic acid (c18)	0.00000 ± 0.00293	0.02294 ± 0.01195	0.00000 ± 0.00210	0.00752 ± 0.00354	0.00005 ± 0.00059
1,12-dodecanedicarboxylic acid (d-c14)	0.00005 ± 0.00009	0.00001 ± 0.00006	0.00000 ± 0.00003	0.00003 ± 0.00005	0.00000 ± 0.00001
8,15-pimaradien-18-oic acd	0.00000 ± 0.00006	0.00011 ± 0.00012	0.00008 ± 0.00017	0.00005 ± 0.00007	0.00010 ± 0.00007
pimaric acid	0.00000 ± 0.00006	0.00007 ± 0.00008	0.00000 ± 0.00003	0.00004 ± 0.00009	0.00001 ± 0.00001
nonadecanoic acid (c19)	0.00022 ± 0.00043	0.00415 ± 0.00484	0.00000 ± 0.00006	0.00064 ± 0.00074	0.00000 ± 0.00002
sandaracopimaric acid	0.00000 ± 0.00006	0.00012 ± 0.00025	0.00000 ± 0.00003	0.00002 ± 0.00004	0.00026 ± 0.00058
isopimaric acid	0.00004 ± 0.00009	0.00049 ± 0.00018	0.00011 ± 0.00022	0.00015 ± 0.00003	0.00000 ± 0.00001
dihydroisopimaric acid	0.00087 ± 0.00038	0.00000 ± 0.00006	0.00028 ± 0.00033	0.00000 ± 0.00002	0.00005 ± 0.00005
8-abietic acid	0.00152 ± 0.00065	0.00000 ± 0.00006	0.00032 ± 0.00041	0.00000 ± 0.00002	0.00009 ± 0.00013
dehydroabietic acid	0.00099 ± 0.00119	0.00139 ± 0.00055	0.00000 ± 0.00027	0.00041 ± 0.00037	0.00018 ± 0.00026
8,14-abietenic acid	0.00050 ± 0.00059	0.00000 ± 0.00006	0.00018 ± 0.00035	0.00000 ± 0.00002	0.00013 ± 0.00030
eicosanoic acid (c20)	0.00018 ± 0.00036	0.00006 ± 0.00016	0.00007 ± 0.00016	0.00003 ± 0.00007	0.00036 ± 0.00028
abietic acid	0.00977 ± 0.00710	0.00393 ± 0.00187	0.01028 ± 0.01119	0.00302 ± 0.00313	0.01628 ± 0.01332
levopimaric acid	0.00000 ± 0.00006	0.00000 ± 0.00006	0.00000 ± 0.00003	0.00000 ± 0.00002	0.00000 ± 0.00001
heneicosanoic acid (c21)	0.00108 ± 0.00216	0.00134 ± 0.00107	0.00093 ± 0.00118	0.00000 ± 0.00003	0.00021 ± 0.00029
7-oxodehydroabietic acid	0.00016 ± 0.00031	0.00056 ± 0.00041	0.00012 ± 0.00024	0.00003 ± 0.00005	0.00004 ± 0.00009
docosanoic acid (c22)	0.00070 ± 0.00103	0.00024 ± 0.00042	0.00079 ± 0.00092	0.00007 ± 0.00015	0.00320 ± 0.00388
tricosanoic acid (c23)	0.00103 ± 0.00140	0.00000 ± 0.00011	0.00553 ± 0.01073	0.00000 ± 0.00005	0.04099 ± 0.03082
tetracosanoic acid (c24)	0.01704 ± 0.02392	0.00002 ± 0.00063	0.00889 ± 0.01298	0.00001 ± 0.00026	0.05469 ± 0.06192
cholesterol	0.00492 ± 0.00393	0.00304 ± 0.00168	0.00188 ± 0.00169	0.00128 ± 0.00074	0.00102 ± 0.00089
cholestanol	0.00014 ± 0.00029	0.00006 ± 0.00011	0.00000 ± 0.00004	0.00002 ± 0.00005	0.00001 ± 0.00002
ergosterol	0.00005 ± 0.00010	0.00000 ± 0.00006	0.00000 ± 0.00003	0.00000 ± 0.00002	0.00004 ± 0.00010
stigmasterol	0.00016 ± 0.00032	0.00003 ± 0.00009	0.00000 ± 0.00007	0.00172 ± 0.00344	0.00000 ± 0.00001
sitosterol	0.00000 ± 0.00141	0.00000 ± 0.00144	0.00000 ± 0.00035	0.02325 ± 0.04650	0.00027 ± 0.00061

Emission factors for hopsters and steranes.

Hopsters and Steranes	On-Road Vehicle, mixed fleet, August 2003	On-Road Vehicle, mixed fleet, December 2003	On-Road Diesel Bus, August 2003	On-Road Diesel Bus, December 2003	Off-Road Diesel Engine, December 2003
C27-20S-13ß(H),17a(H)-diasterane	0.00015 ± 0.00018	0.00088 ± 0.00038	0.00031 ± 0.00062	0.00029 ± 0.00013	0.00092 ± 0.00124
C27-20R-13ß(H),17a(H)-diasterane	0.00069 ± 0.00042	0.00050 ± 0.00029	0.00088 ± 0.00174	0.00022 ± 0.00018	0.00286 ± 0.00409
C27-20S-13a(H),17ß(H)-diasterane	0.00024 ± 0.00016	0.00003 ± 0.00006	0.00004 ± 0.00009	0.00014 ± 0.00012	0.00023 ± 0.00024
C27-20R-13a(H),17ß(H)-diasterane	0.00023 ± 0.00013	0.00041 ± 0.00046	0.00012 ± 0.00025	0.00013 ± 0.00009	0.00024 ± 0.00028
C28-20S-13ß(H),17a(H)-diasterane	0.00013 ± 0.00010	0.00036 ± 0.00034	0.00022 ± 0.00045	0.00020 ± 0.00026	0.00102 ± 0.00194
C27-20S5a(H),14a(H)-cholestane	0.00062 ± 0.00035	0.00037 ± 0.00029	0.00001 ± 0.00003	0.00012 ± 0.00014	0.00023 ± 0.00025
C27-20R5a(H),14ß(H)-cholestane	0.00080 ± 0.00044	0.00051 ± 0.00020	0.00041 ± 0.00074	0.00594 ± 0.01166	0.00143 ± 0.00202
C27-20S5a(H),14ß(H),17ß(H)-cholestane	0.00015 ± 0.00011	0.00013 ± 0.00026	0.00011 ± 0.00018	0.00007 ± 0.00008	0.00099 ± 0.00183
C27-20R5a(H),14a(H),17a(H)-cholestane&C29-20S13ß(H),17a(H)-diasterane	0.00016 ± 0.00011	0.00053 ± 0.00014	0.00028 ± 0.00041	0.00074 ± 0.00115	0.00095 ± 0.00105
C28-20S5a(H),14a(H),17a(H)-ergostane	0.00052 ± 0.00040	0.00005 ± 0.00010	0.00053 ± 0.00107	0.00012 ± 0.00019	0.00000 ± 0.00001
C28-20R5a(H),14ß(H),17ß(H)-ergostane	0.00007 ± 0.00008	0.00025 ± 0.00032	0.00010 ± 0.00020	0.00053 ± 0.00085	0.00015 ± 0.00022
C28-20S5a(H),14ß(H),17ß(H)-ergostane	0.00000 ± 0.00006	0.00009 ± 0.00011	0.00004 ± 0.00008	0.00024 ± 0.00028	0.00026 ± 0.00046
C29-20R-13a(H),17ß(H)-diasterane	0.00000 ± 0.00006	0.00005 ± 0.00010	0.00011 ± 0.00021	0.00004 ± 0.00004	0.00052 ± 0.00101
C27-tetracyclic terpane	0.00028 ± 0.00032	0.00101 ± 0.00093	0.00040 ± 0.00057	0.00017 ± 0.00018	0.00074 ± 0.00088
C28-20R5a(H),14a(H),17a(H)-ergostane	0.00002 ± 0.00006	0.00026 ± 0.00032	0.00000 ± 0.00003	0.00003 ± 0.00005	0.00038 ± 0.00068
C27-tetracyclic terpane	0.00086 ± 0.00049	0.00024 ± 0.00028	0.00001 ± 0.00003	0.00011 ± 0.00019	0.00040 ± 0.00040
C28-tetracyclic terpane	0.00087 ± 0.00173	0.00019 ± 0.00024	0.00000 ± 0.00003	0.00006 ± 0.00007	0.00009 ± 0.00015
C29-20S5a(H),14a(H),17a(H)-stigmastane	0.00011 ± 0.00023	0.00013 ± 0.00017	0.00000 ± 0.00003	0.00008 ± 0.00010	0.00016 ± 0.00015
C28-tetracyclic terpane	0.00073 ± 0.00140	0.00023 ± 0.00027	0.00055 ± 0.00075	0.00003 ± 0.00006	0.00022 ± 0.00029
C29-20R5a(H),14ß(H),17ß(H)-stigmastane	0.00009 ± 0.00016	0.00012 ± 0.00017	0.00000 ± 0.00003	0.00002 ± 0.00005	0.00044 ± 0.00059
C29-20S5a(H),14ß(H),17ß(H)-stigmastane	0.00005 ± 0.00010	0.00004 ± 0.00007	0.00032 ± 0.00065	0.00002 ± 0.00005	0.00011 ± 0.00023
18a(H),21ß(H)-22,29,30-Trisnorhopane	0.00228 ± 0.00289	0.00046 ± 0.00019	0.00158 ± 0.00225	0.00014 ± 0.00017	0.00139 ± 0.00151
17a(H),18a(H),21ß(H)-25,28,30-Trisnorhopane	0.00049 ± 0.00035	0.00016 ± 0.00032	0.00007 ± 0.00013	0.00005 ± 0.00010	0.00027 ± 0.00042
C29-20R5a(H),14a(H),17a(H)-stigmastane	0.00002 ± 0.00007	0.00014 ± 0.00019	0.00000 ± 0.00003	0.00009 ± 0.00019	0.00014 ± 0.00030
17a(H),21ß(H)-22,29,30-Trisnorhopane	0.00000 ± 0.00006	0.00000 ± 0.00006	0.00000 ± 0.00003	0.00006 ± 0.00012	0.00003 ± 0.00005
17a(H),18a(H),21ß(H)-28,30-Bisnorhopane	0.00000 ± 0.00006	0.00000 ± 0.00006	0.00000 ± 0.00003	0.00000 ± 0.00002	0.00028 ± 0.00061
17a(H),21ß(H)-30-Norhopane	0.00226 ± 0.00111	0.00251 ± 0.00093	0.00042 ± 0.00046	0.00042 ± 0.00040	0.00064 ± 0.00030
18a(H),21ß(H)-30-Norneohopane	0.00000 ± 0.00006	0.00000 ± 0.00006	0.00000 ± 0.00003	0.00006 ± 0.00012	0.00001 ± 0.00001
17a(H),21ß(H)-Hopane	0.00229 ± 0.00119	0.00338 ± 0.00176	0.00047 ± 0.00041	0.00093 ± 0.00089	0.00092 ± 0.00033
17ß(H),21a(H)-hopane	0.00000 ± 0.00006	0.00000 ± 0.00006	0.00000 ± 0.00003	0.00005 ± 0.00011	0.00000 ± 0.00001
22S-17a(H),21ß(H)-30-Homohopane	0.00000 ± 0.00006	0.00031 ± 0.00062	0.00000 ± 0.00003	0.00007 ± 0.00014	0.00006 ± 0.00008
22R-17a(H),21ß(H)-30-Homohopane	0.00000 ± 0.00006	0.00033 ± 0.00066	0.00000 ± 0.00003	0.00000 ± 0.00002	0.00000 ± 0.00001
17ß(H),21ß(H)-Hopane	0.00000 ± 0.00006	0.00000 ± 0.00006	0.00000 ± 0.00003	0.00000 ± 0.00002	0.00000 ± 0.00001
22S-17a(H),21ß(H)-30,31-Bishomohopane	0.00000 ± 0.00006	0.00011 ± 0.00022	0.00000 ± 0.00003	0.00000 ± 0.00002	0.00000 ± 0.00001
22R-17a(H),21ß(H)-30,31-Bishomohopane	0.00000 ± 0.00006	0.00000 ± 0.00006	0.00000 ± 0.00003	0.00000 ± 0.00002	0.00000 ± 0.00001
22S-17a(H),21ß(H)-30,31,32-Trisomohopane	0.00000 ± 0.00006	0.00000 ± 0.00006	0.00037 ± 0.00071	0.00000 ± 0.00002	0.00000 ± 0.00001
22R-17a(H),21ß(H)-30,31,32-Trishomohopane	0.00015 ± 0.00030	0.00000 ± 0.00006	0.00000 ± 0.00003	0.00000 ± 0.00002	0.00000 ± 0.00001

APPENDIX B: SOURCE PROFILES USED IN CMB MODELING IN ADDITION TO THOSE OBTAINED IN THE LAS VEGAS BASIN IN 2003.

Source profiles of inorganic species for: 1) ammonium bisulfate, 2) ammonium sulfate, 3) ammonium nitrate, 4) woodstove with almond hardwood (residential wood combustion), and 5) composite paved road dust (Las Vegas, 1995).

Species_Name	Ammonia Bisulfate	Ammonia Sulfate	Ammonia Nitrate	Woodstove/Almond	Pave Road Dust
Chloride (Cl–)	0.0000 ± 0.0000	0.0000 ± 0.0000	0.0000 ± 0.0000	0.0028 ± 0.0014	0.0012 ± 0.0006
Nitrate (NO3–)	0.0000 ± 0.0000	0.0000 ± 0.0000	0.7750 ± 0.0780	0.0010 ± 0.0014	0.0019 ± 0.0009
Sulfate (SO4=)	0.8530 ± 0.0830	0.7270 ± 0.0727	0.0000 ± 0.0000	0.0026 ± 0.0022	0.0150 ± 0.0080
Ammonium (NH4+)	0.1570 ± 0.0160	0.2730 ± 0.0273	0.2260 ± 0.0230	0.0010 ± 0.0005	0.0016 ± 0.0005
Soluble Sodium (Na+)	0.0000 ± 0.0000	0.0000 ± 0.0000	0.0000 ± 0.0000	0.0002 ± 0.0002	-99.0000 ± -99.0000
Soluble Potassium (K+)	0.0000 ± 0.0000	0.0000 ± 0.0000	0.0000 ± 0.0000	0.0057 ± 0.0048	0.0018 ± 0.0006
OC1 (IMPROVE)	0.0000 ± 0.0000	0.0000 ± 0.0000	0.0000 ± 0.0000	0.1241 ± 0.0879	0.0035 ± 0.0006
OC2 (IMPROVE)	0.0000 ± 0.0000	0.0000 ± 0.0000	0.0000 ± 0.0000	0.0549 ± 0.0053	0.0117 ± 0.0015
OC3 (IMPROVE)	0.0000 ± 0.0000	0.0000 ± 0.0000	0.0000 ± 0.0000	0.0832 ± 0.0632	0.0361 ± 0.0068
OC4 (IMPROVE)	0.0000 ± 0.0000	0.0000 ± 0.0000	0.0000 ± 0.0000	0.0335 ± 0.0099	0.0569 ± 0.0051
OPC (IMPROVE)	0.0000 ± 0.0000	0.0000 ± 0.0000	0.0000 ± 0.0000	0.0234 ± 0.0164	0.0134 ± 0.0015
Total OC (IMPROVE)	0.0000 ± 0.0000	0.0000 ± 0.0000	0.0000 ± 0.0000	0.3191 ± 0.0417	0.1197 ± 0.0395
EC1 (IMPROVE)	0.0000 ± 0.0000	0.0000 ± 0.0000	0.0000 ± 0.0000	0.0769 ± 0.0687	0.0263 ± 0.0023
EC2 IMPROVE)	0.0000 ± 0.0000	0.0000 ± 0.0000	0.0000 ± 0.0000	0.0042 ± 0.0039	0.0305 ± 0.0037
EC3 (IMPROVE)	0.0000 ± 0.0000	0.0000 ± 0.0000	0.0000 ± 0.0000	0.0011 ± 0.0007	0.0014 ± 0.0002
EC (IMPROVE)	0.0000 ± 0.0000	0.0000 ± 0.0000	0.0000 ± 0.0000	0.0588 ± 0.0486	0.0447 ± 0.0235
Total Carbon	0.0000 ± 0.0000	0.0000 ± 0.0000	0.0000 ± 0.0000	0.3779 ± 0.0800	0.1645 ± 0.0597
Sodium (Na)	0.0000 ± 0.0000	0.0000 ± 0.0000	0.0000 ± 0.0000	0.0001 ± 0.0020	0.0002 ± 0.0010
Magnesium (Mg)	0.0000 ± 0.0000	0.0000 ± 0.0000	0.0000 ± 0.0000	0.0000 ± 0.0003	0.0269 ± 0.0041
Aluminum (Al)	0.0000 ± 0.0000	0.0000 ± 0.0000	0.0000 ± 0.0000	0.0002 ± 0.0002	0.0162 ± 0.0014
Silicon (Si)	0.0000 ± 0.0000	0.0000 ± 0.0000	0.0000 ± 0.0000	0.0001 ± 0.0001	0.0844 ± 0.0077
Phosphorus (P)	0.0000 ± 0.0000	0.0000 ± 0.0000	0.0000 ± 0.0000	0.0000 ± 0.0000	0.0003 ± 0.0002
Sulfur (S)	0.2790 ± 0.0280	0.2430 ± 0.0243	0.0000 ± 0.0000	0.0015 ± 0.0008	0.0047 ± 0.0008
Chlorine (Cl)	0.0000 ± 0.0000	0.0000 ± 0.0000	0.0000 ± 0.0000	0.0064 ± 0.0006	0.0008 ± 0.0004
Potassium (K)	0.0000 ± 0.0000	0.0000 ± 0.0000	0.0000 ± 0.0000	0.0122 ± 0.0072	0.0109 ± 0.0013
Calcium (Ca)	0.0000 ± 0.0000	0.0000 ± 0.0000	0.0000 ± 0.0000	0.0001 ± 0.0002	0.1496 ± 0.0267
Titanium (Ti)	0.0000 ± 0.0000	0.0000 ± 0.0000	0.0000 ± 0.0000	0.0000 ± 0.0002	0.0019 ± 0.0002
Vanadium (V)	0.0000 ± 0.0000	0.0000 ± 0.0000	0.0000 ± 0.0000	0.0000 ± 0.0001	0.0001 ± 0.0001
Chromium (Cr)	0.0000 ± 0.0000	0.0000 ± 0.0000	0.0000 ± 0.0000	0.0000 ± 0.0000	0.0001 ± 0.0000
Manganese (Mn)	0.0000 ± 0.0000	0.0000 ± 0.0000	0.0000 ± 0.0000	0.0000 ± 0.0000	0.0004 ± 0.0001
Iron (Fe)	0.0000 ± 0.0000	0.0000 ± 0.0000	0.0000 ± 0.0000	0.0000 ± 0.0000	0.0222 ± 0.0029
Cobalt (Co)	0.0000 ± 0.0000	0.0000 ± 0.0000	0.0000 ± 0.0000	0.0000 ± 0.0000	0.0000 ± 0.0001
Nickel (Ni)	0.0000 ± 0.0000	0.0000 ± 0.0000	0.0000 ± 0.0000	0.0000 ± 0.0000	0.0000 ± 0.0000
Copper (Cu)	0.0000 ± 0.0000	0.0000 ± 0.0000	0.0000 ± 0.0000	0.0000 ± 0.0000	0.0001 ± 0.0000
Zinc (Zn)	0.0000 ± 0.0000	0.0000 ± 0.0000	0.0000 ± 0.0000	0.0006 ± 0.0006	0.0009 ± 0.0003
Gallium (Ga)	0.0000 ± 0.0000	0.0000 ± 0.0000	0.0000 ± 0.0000	0.0000 ± 0.0000	0.0000 ± 0.0000
Arsenic (As)	0.0000 ± 0.0000	0.0000 ± 0.0000	0.0000 ± 0.0000	0.0000 ± 0.0000	0.0000 ± 0.0000
Selenium (Se)	0.0000 ± 0.0000	0.0000 ± 0.0000	0.0000 ± 0.0000	0.0000 ± 0.0000	0.0000 ± 0.0000
Bromine (Br)	0.0000 ± 0.0000	0.0000 ± 0.0000	0.0000 ± 0.0000	0.0000 ± 0.0000	0.0000 ± 0.0000
Rubidium (Rb)	0.0000 ± 0.0000	0.0000 ± 0.0000	0.0000 ± 0.0000	0.0000 ± 0.0000	0.0000 ± 0.0000
Strontium (Sr)	0.0000 ± 0.0000	0.0000 ± 0.0000	0.0000 ± 0.0000	0.0000 ± 0.0000	0.0012 ± 0.0005
Yttrium (Y)	0.0000 ± 0.0000	0.0000 ± 0.0000	0.0000 ± 0.0000	0.0000 ± 0.0000	0.0000 ± 0.0000
Zerconium (Zr)	0.0000 ± 0.0000	0.0000 ± 0.0000	0.0000 ± 0.0000	0.0000 ± 0.0000	0.0001 ± 0.0000
Molybdenum (Mo)	0.0000 ± 0.0000	0.0000 ± 0.0000	0.0000 ± 0.0000	0.0000 ± 0.0000	0.0000 ± 0.0000
Palladium (Pd)	0.0000 ± 0.0000	0.0000 ± 0.0000	0.0000 ± 0.0000	0.0000 ± 0.0000	0.0001 ± 0.0001
Silver (Ag)	0.0000 ± 0.0000	0.0000 ± 0.0000	0.0000 ± 0.0000	0.0000 ± 0.0000	0.0001 ± 0.0001
Cadmium (Cd)	0.0000 ± 0.0000	0.0000 ± 0.0000	0.0000 ± 0.0000	0.0000 ± 0.0000	0.0001 ± 0.0001
Indium (In)	0.0000 ± 0.0000	0.0000 ± 0.0000	0.0000 ± 0.0000	0.0000 ± 0.0000	0.0000 ± 0.0001
Tin (Sn)	0.0000 ± 0.0000	0.0000 ± 0.0000	0.0000 ± 0.0000	0.0000 ± 0.0001	0.0001 ± 0.0002
Antimony (Sb)	0.0000 ± 0.0000	0.0000 ± 0.0000	0.0000 ± 0.0000	0.0000 ± 0.0001	0.0000 ± 0.0002
Barium (Ba)	0.0000 ± 0.0000	0.0000 ± 0.0000	0.0000 ± 0.0000	0.0000 ± 0.0003	0.0003 ± 0.0006
Lanthanum (La)	0.0000 ± 0.0000	0.0000 ± 0.0000	0.0000 ± 0.0000	0.0001 ± 0.0004	0.0000 ± 0.0008
Gold (Au)	0.0000 ± 0.0000	0.0000 ± 0.0000	0.0000 ± 0.0000	0.0000 ± 0.0000	0.0000 ± 0.0000
Mercury (Hg)	0.0000 ± 0.0000	0.0000 ± 0.0000	0.0000 ± 0.0000	0.0000 ± 0.0000	0.0000 ± 0.0000
Thallium (Tl)	0.0000 ± 0.0000	0.0000 ± 0.0000	0.0000 ± 0.0000	0.0000 ± 0.0000	0.0000 ± 0.0000
Lead (Pb)	0.0000 ± 0.0000	0.0000 ± 0.0000	0.0000 ± 0.0000	0.0000 ± 0.0000	0.0002 ± 0.0001
Uranium (U)	0.0000 ± 0.0000	0.0000 ± 0.0000	0.0000 ± 0.0000	0.0000 ± 0.0000	0.0000 ± 0.0000

* -99, not available